UAB
Universitat Autònoma de Barcelona

Novel Approaches in Aptamer-Based Diagnostics: Design, Stability, and Targeted SELEX Protocols

Celia Fuentes Chust

ADVERTIMENT. L'accés als continguts d'aquesta tesi queda condicionat a l'acceptació de les condicions d'ús establertes per la següent llicència Creative Commons: https://creativecommons.org/licenses/?lang=ca

ADVERTENCIA. El acceso a los contenidos de esta tesis queda condicionado a la aceptación de las condiciones de uso establecidas por la siguiente licencia Creative Commons: https://creativecommons.org/licenses/?lang=es

WARNING. The access to the contents of this doctoral thesis it is limited to the acceptance of the use conditions set by the following Creative Commons license: https://creativecommons.org/licenses/?lang=en

UAB
Universitat Autònoma de Barcelona

Novel Approaches in Aptamer-Based Diagnostics: Design, Stability, and Targeted SELEX Protocols

Celia Fuentes Chust

PhD Thesis

PhD in Biotechnology

Directors:

Prof. Arben Merkoçi, Dr. Claudio Parolo, Dr. Andrew Piper

Catalan Institute of Nanoscience and Nanotechnology

Department of Chemical, Biological and Environmental Engineering

The present thesis, entitled “Novel Approaches in Aptamer-Based Diagnostics: Design, Stability, and Targeted SELEX Protocols”, is presented by Celia Fuentes Chust to obtain the degree of doctor by the Universitat Autònoma de Barcelona. This work was performed at the Nanobioelectronics and Biosensors Group at the Institut Català de Nanociència i Nanotecnologia (ICN2), under the supervision of Prof. Arben Merkoçi, ICREA Professor and Group Leader, Dr. Claudio Parolo and Dr. Andrew Piper.

The author:

Celia Fuentes Chust

The supervisors:

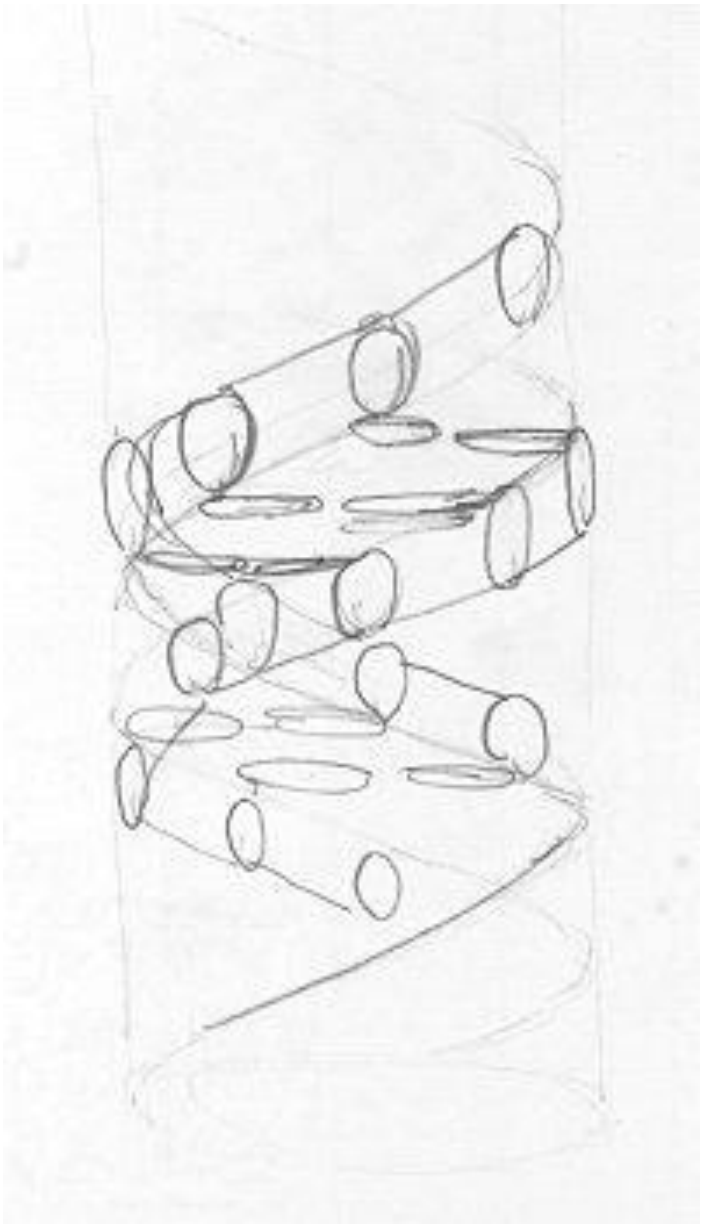
Prof. Arben Merkoçi Dr. Claudio Parolo Dr. Andrew Piper

The present thesis was performed also under the doctoral program studies “Doctorat en Biotecnologia” at the Faculty of Chemical Engineering, Universitat Autònoma de Barcelona, under the tutorship of Professor Francesc Gòdia.

The tutor:

Prof. Francesc Gòdia

Bellaterra, July 2024



-DNA double helix, by Prof. Francis Crick, 1953.

PREFACE

The research performed in this PhD resulted in several publications and manuscripts that were submitted to international peer-reviewed scientific journals.

The state-of-the-art studies led to a review article publication:
1) Fuentes-Chust C, Parolo C, Rosati G, Rivas L, Perez-Toralla K, Simon S, de Lecuona I, Junot C, Trebicka J, Merkoçi A. The Microbiome Meets Nanotechnology: Opportunities and Challenges in Developing New Diagnostic Devices. *Adv Mater*. (2021).

As a result of the experimental work performed, several articles have been either published or, as of thesis submission date, submitted to high impact scientific journals:

1) Fuentes-Chust, C.; Parolo, P.; Piper, A.; Merkoçi, A. Stability Matters: Evaluating the Long-Term Performance of AuNP-DNA Conjugates in Lateral Flow Assays through Varied Conjugation Methods and Storage Buffers. Submitted to Nanoscale.

2) Hu, L.; Calucho, E.; Fuentes-Chust, C.; Parolo, C.; Idili, A.; Álvarez-Diduk, R.; Rivas, L.; Merkoçi, A. Selection and characterization of bioreceptors to develop nanoparticle-based lateral-flow immunoassays in the context of the SARS-CoV-2 outbreak. *Lab Chip* (2022).

Additionally, the collaborations performed during the PhD resulted in the participation in several review publications not part of the thesis:

Parolo, C.; Sena-Torralba, A.; Bergua, J. F.; Calucho, E.; Fuentes-Chust, C.; Hu, L.; Rivas, L.; Álvarez-Diduk, R.; Nguyen, E. P.; Cinti, S.; Quesada-González, D.; Merkoçi, A. Tutorial: design and fabrication of nanoparticle-based lateral-flow immunoassays. *Nature Protocols* 2020, 15, 3788-3816.

Rosati, G.; Idili, A.; Parolo, C.; Fuentes-Chust, C.; Calucho, E.; Hu, L.; de Carvalho Castro e Silva, C.; Rivas, L.; Nguyen, E. P.; Bergua, J. F.; Álvarez-Diduk, R.; Muñoz, J.; Junot, C.; Penon, O.; Monferrer, D.; Delamarche, E.; Merkoçi, A. Nanodiagnostics to face SARS-CoV-2 and future pandemics: from an idea to the market and beyond. *ACS Nano*, 2021, 15, 11, 17137-17149.

Castelli, F.A., Rosati, G., Moguet, C., Fuentes-Chust, C., Marrugo-Ramírez, J., Lefebvre, T., Volland, H., Merkoçi, A., Simon, S., Fenaille, F., and Junot, C. Metabolomics for personalized medicine: the input of analytical chemistry from biomarker discovery to Point-of-Care tests. *Anal Bioanal Chem*, 2022, 414, 759–789.

ACKNOWLEDGEMENTS

Working on a PhD thesis has been quite a journey, and I couldn't have made it this far without the incredible support of my loved ones. I just want to take a moment to really express my heartfelt thanks for everything you've done for me over the years. My words may not fully capture the depth of my gratitude, but please know that you mean the world to me.

Al meu amor, Gerard, ets la llum de la meva vida. No hagués pogut acabar aquesta travessa sense la teva llum indicant-me el camí, ni sense la teva mà a cada caiguda. Després de tot el que t'he fet patir en aquest viatge la teva mirada encara m'acompanya amb l'amor més sincer, i em done compte de que no hi ha projecte, o tesi, que pugui crear més important que aquesta vida que estem creant junts.

Aquesta tesi ha sigut patrocinada pel Prof. Arben Merkoçi. Gràcies per veure en una inocent estudiant de màster el potencial de fer aquesta grandísima tasca que és el doctorat. Aquest viatge ha començat gràcies a la teva confiança en mi. M'has obert una gran finestra a la ciència, i a pràcticament tots els continents! Precisament per això, aquests agraïments estàn escrits en "cataspanglish" únic del nostre grup, i t'ho agraeixo molt, Arben.

To my supervisors, Dr. Claudio Parolo and Dr. Andrew Piper, thank you for your trust and advice. You have helped me improve and be the best researcher I could be and believed in me more than I sometimes did. Thank you to both for making me see the reality when I struggled with my data and thought that it wasn't just enough. That data are data, no matter what. For all of that and for your enormous patience, thank you! Andrew, thank you for your friendship, and all of our sandwich, Eurovision and Blackpink discussions! And the ones left for the future!

When I arrived at the group, I had the luck to meet people from so many places! You guys welcomed me with open arms, and I am so grateful for that. This is what I experienced when I started my master period in the group:

Una mención especial es para mi primer amigo y mentor en el grupo, José Fran, Dr. Bergua, por enseñarme todo lo que podías y más, científica y personalmente. Eres la persona que me guió por la ciencia por primera vez de verdad, animándome a tomar mis propias decisiones y seguir mis ideas. Te he echado un montón de menos en el grupo, y me has hecho suspirar cada ver que me he encontrado material con tu nombre escrito por el laboratorio. Siempre intento devolver a mis estudiantes todo lo que tú me diste. Guardo nuestros recuerdos en un lugar muy especial de mi corazón. Simplemente gracias, José Fran. Enriquet, començarem aquesta història al mateix temps i hem rigut, patit i comparat els nostres vocabularis de "Lleide" i "Valensia" tants cops! No he pogut

tenir millor company de laboratori, experiments, escritura, o editor assistant, entre tantes altres coses. Espere seguir compartint amb tu tot el que ens prepari la vida. Merci per tot, bonico!
Lei, thanks for our chats and laughs on the back patio of ICN2, and your trust in me. Qiuyue, you are so funny and close, I admire you so much! Anna and Caterina, we shared so many moments and I never imagined I would cry so much to say goodbye to you. Xin Yi and Amadeo, menudo par de liantes. Aún me río muchísimo con anécdotas vuestras. Ruslan, gracias por los bailes y las barbacoas. Sin tu salsa el grupo no es lo mismo. Dani, por los datos curiosos, chistes malos, juegos de palabras y tests de psicopatía y muletillas.... chan, chan, chan… Gracias! Os deseo lo mejor a ti y a Leyla. Anna Puig, *mamma mia* quina paciència! No sé quants emails t'he pogut enviar oblidant l'adjunt i no t'has enfadat! Has sigut advocada de tots nosaltres i ens has cuidat tant! T'estimo molt i espere seguir en contacte amb tu!

Me fui del grupo al terminar el máster, y volví para empezar el doctorado, un camino largo y exigente, que no podría haber recorrido sin mis compañeros de travesía:
Nerea, mi guerrera. Sabes que no se me da bien escribir estas cosas, pero tú te mereces todo mi corasonsito. ¡Gracias por tantas cosas! Me has enseñado lo que es la fuerza de verdad, aunque yo no sepa dar mortales. Tu compañía, tus abrazos, tu oído o tu hombro cuando lo necesitaba han sido mi salvación. Siempre he sabido que podía contar contigo y eso me emociona. Aquí me tienes, llorando. Un saludito a Alan que puede estar leyendo esto, y no, no me olvido de ti porque eres una maravilla. ¡Os quiero mucho a los dos, rebonicos!

José, a ti qué te voy a decir... Fuiste el único que me contagió la pasión e hizo que me planteara un postdoc, y lo sabes. He tenido una suerte enorme de poder trabajar contigo y concocerte como te he conocido. Hemos compartido muchas cosas, lo bueno, lo malo, lo feo, lo bonito, y espero que lo que está por llegar. El apoyo que nos hemos dado ha sido la clave para todo, y esta tesis no exisistiría sin la "SELEX crew". El equipo Panda que hemos creado, y nuestra baby Panda Laura Patricia Mercury Matcha, es más de lo que podría pedir. Laura, eres la mejor estudiante que una podría pedir. Inteligentísima, luchadora, apasionada, meticulosa, empática y aún mejor amiga. Sé que la vida te prepara cosas alucinantes, gracias a todo lo que tú eres. Éxitos baby Panda!

Gabriel, xiki. Me hace muy feliz haberte visto conseguir tantas cosas estos años ¡y que siga siendo así! Gracias por enseñarme a bailar cuarteto, a imprimir en 3D, a pensar como lo haría un verdadero showman, y a pronunciar correctamente "gashetita". Aunque nuestro debate sobre los Simpson sigue y seguirá abierto, para que podamos seguir discutiéndolo durante años.

ACKNOWLEDGEMENTS

Anna G., qui m'anava a dir que una visiting podia causar un impacte tan gran a la meva vida! Ma que hem compartit coses aquests anys, des-de lateral flow o el covid, a viatges, rises, música i pijamades. La distància no ha pogut trencar la nostra amistat, i encara que no ens veiem molt, m'encanta que podem seguir contant-nos tot! T'estimo guapa!

Vernalyn, you are the sweetest, cutest, and loveliest person I have ever met. I am so proud of everything you have achieved these years. I hope I can come visit the Philippines and keep in touch for many years. Massimo, you are the most hard-worker person I know, and I admire your persistence and strong will. I know you will have a brilliant future and career, and I will be so happy to see you achieving everything! Andy, no pensé que te cogería tanto cariño en tan poco tiempo, y eso que al principio no te entendía y todo lo que te contestaba era "¿Qué?" Perdóname, porque me encanta como hablas y eres una persona preciosa. Te deseo lo mejor para ti y la familia tan linda que estás creando con Maite y Mae. Tú siempre tan oportuno, Bruno! ;) Giulio, thanks for the teachings and your guidance. I am grateful we got to do those work trips together! Marianna, thank you for your support and guidance when I was lost with my aptamer! Your advice was like fresh water to me. Can't forget to mention a lot of international friends that I am very fond of: Danilo, Matheus, Cecília, Emily, David, Greg, Sinan, José "from Brazil", Andrea "el presidente", Ele, Ane, Robert, and Manasi. I miss you guys! I am sure I am missing a lot of incredible people and I hope that our paths cross again in the future. Als amics nous i de tota la vida, Isis, Adri, Pablet, Aino, Aitoret, Joan, Juan, Laura, Glòria, Jana, i molts més que m'han soportat i han sigut ultra pacients, Gràcies!

Per últim, l'agraïment més gran del món es per a la meva familia, que no m'imaginava que anava a créixer tant durant aquest viatge. Al support incondicional dels meus pares i la meva germana, teta Ana, que han sentit tot el que he sentit fins i tot des-se la distància, ara se li suma el meu "cunyato" Manu. Vos vuic més del que puc expresar. Ana, Manu, no sé com ho feu, pero haveu portat a aquest món als dos nebodets més bonicos del món, Dries i Djim. Estic escrivint aquestes paraules durant el primer cumple de Djim, i no puc esperar a veure'ls i celebrar-ho com toca de veritat. Gràcies per fer-me la tia més orgullosa del món (i de Swan jeje). Als meus nous pares, Cristina i Magí, no pensava que al mudar-me a Barcelona trobaria un lloc on sentir-me tan protegida, acollida i estimada. I no imaginava que aquel lloc seria el vostre cor Us estimo! Gràcies als meus nous cunyats Adri i Dunya, pel seu carinyo i paciència per haver de posposar constantment el viatge de Falles. Janeth, muchas gracias por tu apoyo y tu cariño. Tú y tu familia sois preciosos, y te agradezco mucho todo lo que haces por todos nosotros. No puc oblidar esmentar als meus quadrúpeds Shaggy, Duna, i ara Darwin. Tinc molta sort de tenir-vos a tots a la meva vida.

Una abraçada a la meva awelita, que li hagués encantat dir-me doctora. Te vuic hasta el sol, aweli.

ACKNOWLEDGEMENTS FOR FINANCIAL AND LOGISTIC SUPPORT

















ABBREVIATION LIST

λ: Lambda

0D: zero-dimensional

1D: one-dimensional

2D: two-dimensional

3D: three-dimensional

6'FAM: 6-Carboxyfluorescein

ABAA: Apta-Bead Affinity Assay

AC: Aptamer Complementary

ACLF: Acute-on-Chronic Liver Failure

AD: Acute Decompensation

AFB1: Aflatoxin B1

AgNPs: Silver Nanoparticles

APAA: Apta-PCR Affinity Assay

A-PCR: Asymmetric PCR

AT: Adenine-Thymine

ATP: Adenine Triphosphate

AuNPs: Gold Nanoparticles

BB: Binding Buffer

BBB: Blood-Brain barrier

BH_4: tetrahydrobiopterin or sapropterin

BHQ-1: Black Hole Quencher

BIA: Bacterial Inhibition Assay

BSA: Bovine Serum Albumin

CCHF: Crimean-Congo Hemorrhagic Fever

CD: Circular Dichroism

cDNA: coding DNA or complementary DNA

CE-SELEX: Capillary Electrophoresis SELEX

CGMS: Continuous Glucose Monitor System

CHA: catalytic hairpin assembly

CL: Control Line

CLIF-C: Chronic Liver Failure Consortium

Cp*Rh(III): pentamethylcyclopentadienyl-rhodium (III)

CRP: C-reactive Protein

Da: Dalton

DBS: Dried Blood Spots

DLS: Dynamic Light Scattering

ABBREVIATION LIST

DNA: Deoxyribonucleic Acid

dsDNA: double-stranded Deoxyribonucleic Acid

E2: 17β-estradiol

EASL: European Association for the Study of the Liver

EDC: 1-Ethyl-3-(3-dimethylaminopropyl)carbodiimide

ELAA: Enzyme Linked Aptamer Assay

EMSA: Electrophoretic Mobility Shift Assay

Fe^{2+}: Ferrous anion

FET: Field-Effect Transistors

GAT: Gold Aggregation Test

GC: Guanine-Cytosine

GO: Graphene Oxide

GO-SELEX: Graphene Oxide SELEX

hCG: human Chorionic Gonadotropin

$HAuCl_4$: Tetrachloroauric(III) acid

HPA: Hyperphenylalaninaemia

HPL: human placental lactogen

INDEBT: Instant Dehydration by Butanol

ITC: Isothermal Titration Calorimetry

K^+: Potassium cation

KA: Kynurenic acid

K_D: Dissociation constant

KP: Kynurenine Pathway

L1: Line 1

L2: Line 2

LFA: Lateral Flow Assays

LFV: Lassa fever virus

Mag-SELEX: Magnetic bead SELEX

Mg^{2+}: Magnesium cation

$MgCl_2$: Magnesium Chloride

MIPs: Molecularly Imprinted Polymers

MQ water: Deionized Water

MRI: Magnetic Resonance Imaging

mRNA: messenger Ribonucleic acid

MST: Microscale Thermophoresis

mV: millivolt

ABBREVIATION LIST

Na^+: Sodium Cation

NaCl: Sodium Chloride

NALF: Nucleic Acid Lateral FLow

NALFIA: Nucleic Acid Lateral FLow Immuno Assay

NBS: Newborn Screening

NFC: Near-Field-Communication

NGS: Next Generation Sequencing

NHS: N-Hydroxysuccinimide

nm: nanometer

nt: nucleotide

O_2: molecular oxygen

PAH: Phenylalanine Hydroxylase enzyme

PB: Phosphate Buffer Non-saline

PBS: Phosphate Buffer Saline

PBST: Phosphate Buffer Saline Tween-20

PCR: Polymerase Chain reaction

PEG: Polyethylene Glycol

pH: Power of Hydrogen

Phe: Phenylalanine amino acid

PKU: Phenylketonuria

PoC: Point-of-Care

PolyT: poly-Thymine

PZT: Lead Zirconate Titanate

QA: Quinolinic Acid

QCM: Quartz Crystal Microbalance

QDs: Quantum Dots

REASSURED: Real-time connectivity, Ease of specimen collection, Affordability, Sensitivity, Specificity, User-friendliness, Rapid & robust operation, Equipment-free, and Deliverability

RNA: Ribonucleic acid

RPA: Recombinase Polymerase Amplification

rpm: Revolutions per minute

rRNA: ribosomal Ribonucleic acid

RSV: Respiratory Syncytial Virus

SA: Salt-Aging

SA-pH: Salt-Aging pH assisted

SA-LF: Salt Aging Lateral Flow optimized

ABBREVIATION LIST

SAW: Surface Acoustic Wave

SELEX: Systematic Evolution of Ligands by Exponential Enrichment

SERS: Surface-Enhanced Raman Scattering

SNA: Spherical Nucleic Acid

SPR: Surface Plasmon Resonance

ssDNA: single stranded Deoxyribonucleic Acid

Str: Streptavidin

Taq: Thermus aquaticus

TBE: Tris-Borate-EDTA buffer

TCEP: Tris(2-carboxyethyl)phosphine hydrochloride

TL: Test Line

TMB: 3,3′,5,5′-Tetramethylbenzidine

Tris: tris(hydroxymethyl)aminomethane

Trp: Tryptophan

FETs: Field-effect Transistors

UPTs: Upconverting nanoparticles

UV: Ultraviolet

UV-Vis: Ultraviolet-Visible

WHO: World Health Organization

TABLE OF CONTENTS

THESIS OVERVIEW *23*

CHAPTER 1. INTRODUCTION *27*

1.1. Biosensors for Point-of-Care Diagnostics and Monitoring **29**

1.1.1. Definition of a Biosensor 29

1.1.2. Biosensors for Point-of-care Testing Applications 30

1.1.3. Nanomaterials and Nanobiosensors 32

1.2. Biomarkers for Precision and Personalized Medicine **34**

1.2.1. Microbiome-related Biomarkers 35

1.2.2. Small Molecules and Acute-on-Chronic Liver Failure 37

1.2.3 Acute-on-Chronic Liver Failure 39

1.2.4. Phenylketonuria 41

1.3. Biorecognition Elements **44**

1.3.1. Small Molecule Detection Challenges 45

1.3.2. Aptamers for Small Molecule Detection 46

1.3.3. Systematic Evolution of Ligands by Exponential Enrichment 47

1.3.3.1. Components and Workflow 48

1.3.3.1.1. Oligonucleotide Library 48

1.3.3.1.2. Selection Conditions 49

1.3.3.1.3. Library Amplification and Conditioning 50

1.3.3.1.4. Next Generation Sequencing Analysis 52

1.3.3.1.5. Binding Assays 53

1.3.3.2. Types of Systematic Evolution of Ligands by Exponential Enrichment 53

1.4. PoC Nanobiosensing Platforms **55**

1.4.1. Lateral Flow Assays 56

1.4.1.1. Aptamer Lateral Flow Assays for Small Molecule Detection 58

1.4.1.2. Historical Background and Impact of AuNP-DNA Conjugates 61

1.5. References **64**

CHAPTER 2. OBJECTIVES *87*

CHAPTER 3. Development and Performance Evaluation of Aptamer-Based Lateral Flow Assays for Phenylalanine Detection *91*

3.1. Aptamer Lateral Flow Assay proof-of-concept for Phe monitoring **93**

3.1.1. Overview of Aptamer Research for Phe Detection 93

3.1.1.1. Hypothesis 94

3.1.1.2. Probe design 94

3.1.1.2.1. Method 1: The Displacement Assay 98

3.1.1.2.2. Method 2: The competitive assay 99

3.2. Objectives 102

3.3. Materials and Methods 103

3.3.1. Materials 103

3.3.2. AuNPs synthesis and conjugation 103

3.3.3. Lateral Flow preparation 104

3.3.4. Conjugate and sequence characterization 104

3.3.5. Binding studies 105

3.4. Results 106

3.4.1. Conjugate characterization and Control Line optimization. 106

3.4.2. Nucleic Acid Characterization 109

3.4.3. Binding studies 110

3.4.4. Phenylalanine Detection strategies 112

3.4.4.1. Displacement assays 113

3.4.4.1.1. Specificity tests 115

3.4.4.1.2. Screening tests 118

3.4.4.2. Competitive assays 121

3.4.4.2.1. Printed aptamer 121

3.4.4.2.2. Printed Streptavidin 124

3.4.5. Strategies for Enhancing Lateral Flow Assay Performance 127

3.4.5.1. Lateral Flow optimization strategies for signal modulation 127

3.4.5.2. Substituting Nucleic Acid System Elements: Evaluating Alternatives 130

3.5. Discussion 134

3.6. Conclusions 137

3.7. References 138

3.8. ANNEX 141

CHAPTER 4. Effects of Conjugation Methods and Storage Conditions on AuNP-DNA Conjugates for Long-Term Stability in Lateral Flow Sensors 143

4.1. Complexities in the Selection of Optimal AuNP-DNA Methods 145

4.1.1. Design of a AuNP-DNA Stability Study for Lateral Flow Applications 146

4.1.1.1. Conjugation techniques 147

4.1.1.2. Storage buffer 149

4.1.1.3. Characterization techniques 150

4.2. Objectives 153

4.3. Materials and Methods 154
4.3.1. Materials 154
4.3.2. Methods 154
4.3.2.1. Conjugate preparation 154
4.3.2.2. Lateral Flow Tests 156
4.3.2.3. Electrophoretic Mobility Shift Assay 157
4.3.2.4. UV-Vis 157
4.3.2.5. DLS and Z-potential 157
4.4. Results 158
4.4.1. Electrophoretic Mobility Shift Assay 158
4.4.1.1. Variation between conjugation methods 158
4.4.1.2. Variation between buffers 159
4.4.1.3. Stability over time. 159
4.4.1.4. Electrophoretic Mobility Shift Assay General conclusions 161
4.4.2. UV-Vis 162
4.4.2.1. Variation between conjugation methods 162
4.4.2.2. Variation between storage buffers 163
4.4.2.3. Stability over time 164
4.4.2.4. UV-Vis general conclusions 166
4.4.3. Z-potential and Dynamic Light Scattering 166
4.4.3.1. Variation between conjugation methods 167
4.4.3.2. Variation between storage buffers 168
4.4.3.3. Stability over time 169
4.4.3.4. Z-potential and Dynamic Light Scattering General conclusions 170
4.4.4. Lateral Flow 171
4.4.4.1. Variations between conjugation methods 172
4.4.4.2. Variations between storage buffers 173
4.4.4.3. Stability over time 174
4.4.4.4. Lateral Flow general conclusions 177
4.5. Discussion 179
4.6. Conclusions 181
4.7. References 183
CHAPTER 5. Tailored SELEX Protocols for the Identification of ACLF Biomarker Aptamers 1
5.1. Acute-on-Chronic Liver Failure Biomarkers. 189
5.1.1. Systematic Evolution of Ligands by Exponential Enrichment for Small Molecule biomarkers. 190
5.1.2. Strategy for Multiplexed Aptamer Selection 192

5.2. Objectives 197

5.3. Materials and Methods 198

5.3.1. Materials 198

5.3.2. Methods 198

5.3.2.1. Target immobilization 198

5.3.2.2. Target verification 199

5.3.2.3. Selection Conditions and Round Progress 200

5.3.2.4. Library amplification and conditioning 202

5.3.2.5. Next Generation Sequencing 203

5.4. Results and Discussion 204

5.4.1. Target conjugation verification 204

5.4.2. SELEX round progression 205

5.4.3. Enrichment monitoring 213

5.4.4. Next-generation sequencing 215

5.5. Conclusions and Future Perspectives 219

5.6. References 222

CHAPTER 6. GENERAL CONCLUSIONS 225

THESIS OVERVIEW

This Thesis is divided into five chapters, followed by a general conclusion section. A brief explanation of each chapter is given below:

Chapter 1. Introduction. This chapter starts with a general introduction to the concepts of biosensors and point-of-care (PoC) biosensing for precision and personalized medicine. Then, the focus is given to biomarkers and biorecognition elements, placing emphasis on the case of small molecules and the related detection challenges. In particular, focus is given to microbiome-related biomarkers and conditions such as Acute-on-Chronic Liver Failure (ACLF), and metabolic disorders such as Phenylketonuria (PKU). Aptamers are presented as an adequate alternative to antibodies for the detection of small molecules, and aptamer isolation and development by Systematic Evolution of Ligands by Exponential Enrichment (SELEX) is discussed. The chapter continues with an overview of the state of the art of aptamer-based Lateral Flow Assay (LFA) technologies for small molecule detection and finalizes with a historical review of the application of gold nanoparticles (AuNPs) coupled to nucleic acids as LFA optical reporter.

Chapter 2. Objectives of the thesis. This chapter briefly describes the objectives that motivated this work.

Chapter 3. Development and Performance Evaluation of Aptamer-Based Lateral Flow Assays for Phenylalanine detection. This chapter presents different aptamer-based LFA formats for the detection of Phenylalanine (Phe), an amino acid used as a PKU and ACLF biomarker. Characterization of the aptamer in solution and paper format are presented, displacement and competitive formats are implemented, and specificity and screening tests are performed to evaluate the effect of the immobilization directionality of the different nucleic acids used in this work. Finally, optimization strategies and alternative methods for enhancement of the aptamer performance in paper format are attempted.

Chapter 4. Effects of Conjugation Methods and Storage Conditions on AuNP-DNA Conjugates for Long-Term Stability in Lateral Flow Assays. In this chapter, a stability study of AuNP-DNA conjugates in LFA over a period of three weeks is presented. The study evaluates various conjugation methods based on different principles and conditions, as well as different storage buffers, using LFA, UV-Vis spectroscopy, Electrophoretic Mobility Shift Assays, and Dynamic Light Scattering techniques over the course of 21 days.

Chapter 5. Tailored SELEX Protocols for the Identification of ACLF Biomarker Aptamers. This chapter presents two SELEX strategies for the isolation of ACLF biomarkers, including a novel

multiplexed SELEX variation termed Joint One-Pot SELEX. Next-Generation Sequencing (NGS) analysis, facilitated by custom MATLAB code, to address limitations related to the number of SELEX rounds and low enrichment levels, is performed.

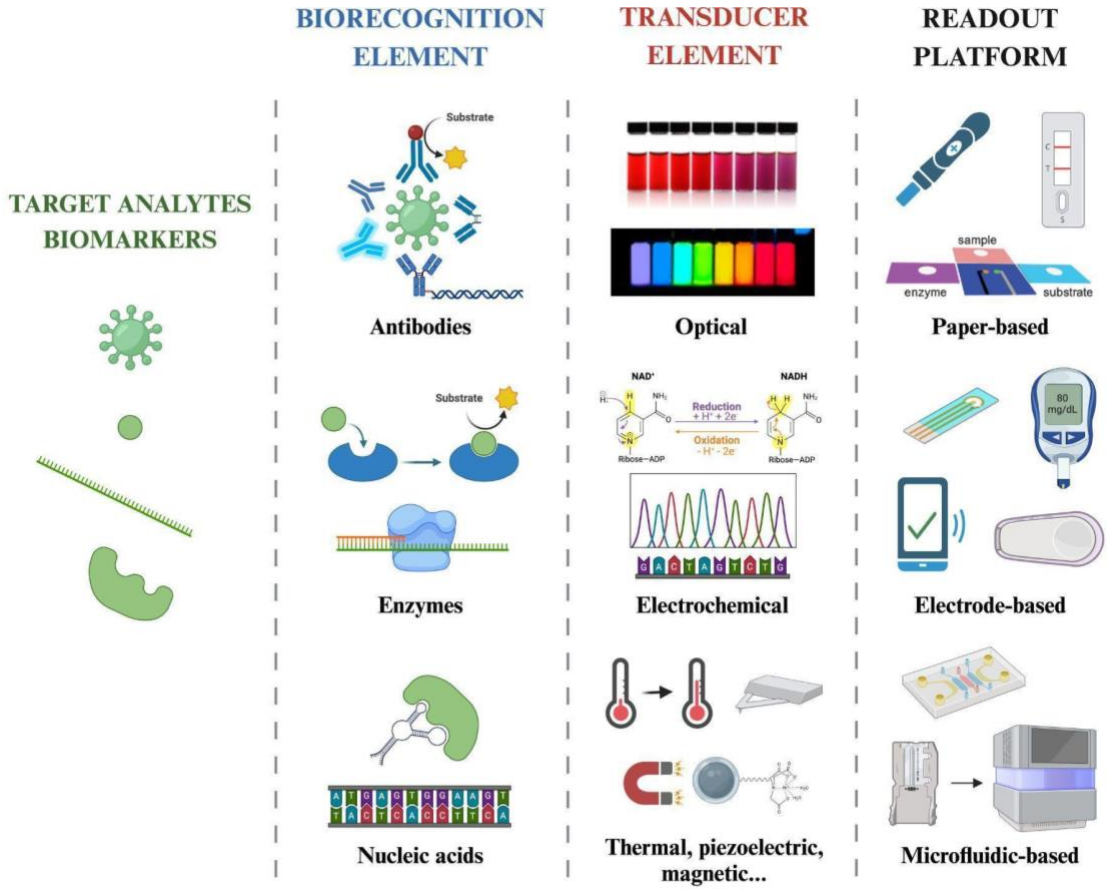
Chapter 6. General Conclusions. A summary of objectives achieved, conclusion remarks, future perspectives, and work to be done are given in this section.

CHAPTER 1. INTRODUCTION

1.1. Biosensors for Point-of-Care Diagnostics and Monitoring

1.1.1. Definition of a Biosensor

The emergence of biosensors has revolutionized our day-to-day interactions with biological samples, providing efficient, precise, and easy-to-use solutions for a range of diagnostic and monitoring requirements.[1] These miniature diagnostic instruments incorporate advanced biosensing technologies that enable the detection and quantification of specific analytes in complex samples, empowering individuals and experts alike to make informed judgments on health, safety, and environmental matters. Biosensors are composed of three essential components: a biorecognition element, a transduction element, and a signal readout platform (Scheme 1).[2,3]



Scheme 1: Schematic representation of the different possible components of Biosensors. Created with Biorender.

Biorecognition elements are the key component of biosensors that differentiate them from other sensors.[4,5] Biorecognition elements, or bioreceptors, are biomolecules ranging from antibodies to enzymes, antigens, nucleic acids, etc. They are selective, specific, and sensitive to a particular target by affinity. These bioreceptors must be stable, have strong binding affinities, and fast association kinetics.[6] Biosensors, particularly nanobiosensors, harness the properties of nanomaterials (i.e., biocompatibility, fluorescence, electrical and thermal conductivity, or magnetism) to transduce the

biorecognition event into a measurable signal, which can be optical, electrochemical, thermal, or piezoelectric, amongst others. The final main element of nanobiosensors is the platform. This platform must contain the miniaturized assay, be able to process an input biological sample and display an output signal in an interpretable and friendly way for the end user. Indeed, the platform of choice depends on the requirements of the type of processed sample, the nature and type of signal generated by the biorecognition element along with the transducer, and the intended use of the final device. Good examples of platforms are paper-based or electrode-based, which are widely used as pregnancy tests or glucometers, respectively.[7]

1.1.2. Biosensors for Point-of-care Testing Applications

Point-of-Care (PoC) tests refer to medical diagnostic devices deployable at or near the site where a patient is located.[6] This type of testing allows for immediate results, enabling rapid clinical decisions without the need to send samples to specialized laboratories. PoC tests are commonly used in various settings, including hospitals, clinics, and in the field or at home, particularly for urgent care, primary care, and in areas with limited access to healthcare facilities. For a nanobiosensor to be considered a PoC device, it needs to meet the World Health Organization (WHO) guidelines known as REASSURED criteria (Real-time connectivity, Ease of specimen collection, Affordability, Sensitivity, Specificity, User-friendliness, Rapid & robust operation, Equipment-free, and Deliverability).[8] The WHO sets these criteria to facilitate access to these devices and their use in developing and developed countries. This is especially important in developing countries or remote settings, where there is poor to no access to healthcare or laboratory facilities.[9]

PoC biosensors have become essential tools, revolutionizing the field of diagnostics and healthcare worldwide and significantly improving the lives of millions of people. These innovative devices represent a novel medical technology paradigm, transforming healthcare delivery. From commonly used applications like pregnancy tests and glucometers to recent advancements in SARS-CoV-2 antigen tests, PoC nanobiosensors have expanded their reach across various health domains. They work by detecting and in some cases quantifying vital analytes that play crucial roles in our daily lives. They can detect hormones, glucose levels, antigens, antibodies, and toxins, amongst others, providing a comprehensive diagnostic toolkit for patients and healthcare professionals.[10,11]

The ability to quickly detect these analytes facilitates rapid decision-making at the PoC, significantly reducing the time required for critical results and improving patient outcomes. In addition to their immediate impact on patient care, PoC nanobiosensors help alleviate the burden on centralized laboratories, contributing to the broader healthcare ecosystem. The decentralization of diagnostic processes enables individuals to receive timely results without extensive laboratory analysis. This

simplifies the diagnostic workflow and optimizes resource utilization, leading to a more efficient and cost-effective healthcare model.[12–15] Moreover, they help emphasize the importance of preventive strategies. By enabling the rapid detection of biomarkers associated with various health conditions, these sensors empower individuals and healthcare professionals to take proactive measures. Early identification of health issues allows for timely interventions, potentially preventing the progression of diseases and improving overall health outcomes.[1617]

Good examples of these advantages are the previously mentioned devices. Diabetic patients have been familiar with electrochemical glucometers since the 1970s, improving the patient's quality of life.[18] Glucometers consist of single-use strips impregnated with glucose oxidase enzymes that catalyze glucose oxidation. These strips are inserted in an electronic device that converts the enzymatic reaction to a quantifiable glucose concentration, giving a numeric value as an output. Being able to monitor glucose levels in real-time enables rapid decision-making (i.e., intake of glucose or insulin injection) and allows independence from trained personnel and laboratories.[19] Recent development of CGMSs (Continuous Glucose Monitor Systems), wearable devices that are connected to insulin pumps and have Near-Field-Communication (NFC) connections with smartphones for real-time connectivity, show how biosensors can be turned into theranostic devices.[20,21]

Another example is the standard pregnancy test based on a Lateral Flow Assay (LFA) format.[22,23] It is commercially available since 1971 (in Canada, in 1977 in EEUU). It targets the beta subunit of human chorionic gonadotropin (hCG) levels in urine, which rise quickly in the first few weeks of pregnancy, thanks to the discovery of monoclonal antibodies.[22] As opposed to the glucometer, pregnancy tests offer a binary response (yes/no). It is recommended that these results be validated by a quantitative blood test performed by a physician due to the possibility of false positive or negative cases. However, it is a potent tool that allows earlier detection of pregnancy in remote settings without access to healthcare centers. Besides, it is also used for pregnancy prognosis and confirmation of induced abortions. Nowadays, there are semi-quantitative tests available, as well as digitalized options, that display results in alphanumeric values, which is helpful for people with impaired vision.[24]

Since the SARS-CoV-2 outbreak in 2020, we have become accustomed to antigen LFA tests for early screening and assessment before or after symptoms were present and helped reduce the burden of healthcare facilities.[13,25–28] Furthermore, antigen LFA and Polymer Chain Reaction (PCR) tests became required for specific administrative and travel procedures worldwide.[29,30] Due to the significant presence of these in our lives, we have reached a point where society as a whole is familiar with the use of these tests and, although they are limited in sensitivity in some cases (i.e., too early testing or too low concentrations of analyte that lead to false negative results), the general public is

acquainted with this risk.[31,32] At the time of writing, 2024, triple LF tests are commercially available that include SARS-CoV-2, Influenza A/B, and RSV (Respiratory Syncytial Virus) antigen tests in a single cartridge for PoC assessment in the flu season.[31] Other commercial lateral flow tests used in epidemic situations target biomarkers related to Zika virus, Ebola virus, Lassa Fever Virus (LFV), or Crimean-Congo Hemorrhagic Fever (CCHF).[33–35]

1.1.3. Nanomaterials and Nanobiosensors

Nanomaterials are materials with dimensions on the nanoscale, typically ranging from 1 to 100 nanometers (nm).[36–40] Due to their small size, they exhibit unique properties not observed in their bulk counterparts, including optical, electric, magnetic, and catalytic properties.[35–38] Their scale facilitates interaction with biological systems at the molecular level, enhancing their usefulness in medical diagnostics and therapeutic interventions.[41–43] Furthermore, the capacity to customize nanomaterials' size, shape, and surface properties expands their versatility, allowing for the creation of precise and effective tools for a wide range of applications. In nanobiosensors, nanomaterials are used as transducer elements by harnessing their unique properties. As we saw, the transducer in a biosensor is the element responsible for converting biorecognition events into measurable signals. Therefore, by employing different types of nanomaterials it is possible to transduce the biorecognition event into different types of signals, such optical and electrochemical.[38,44,45]

Nanomaterials can be classified into several types based on their dimensions, composition, and properties.[46,47] They can be categorized as zero-dimensional (0D), one-dimensional (1D), two-dimensional (2D), and three-dimensional (3D) nanomaterials. Zero-dimensional nanomaterials include nanoparticles, which are spherical or nearly spherical particles like gold nanoparticles (AuNPs) or quantum dots (QDs).[48,49] 1D nanomaterials consist of nanotubes, nanorods, and nanowires, which are cylindrical or wire-like structures.[50–52] 2D nanomaterials are represented by nanosheets and nanoplates, which are flat, thin layers or plate-like structures.[53] 3D nanomaterials include nanocomposites and nanoporous materials, which are made from combining nanoparticles with bulk materials to enhance properties or structures with nanopores, respectively.[54,55]

Nanomaterials can also be classified by their composition, such as carbon-based nanomaterials like fullerenes, graphene, and carbon nanotubes, as well as metal-based nanomaterials like metal nanoparticles and metal oxide nanoparticles.[5657] Another example are QDs, made up of a semiconductor core composed of heavy metals such as cadmium selenide (CdSe), lead selenide (PbSe), or indium arsenide (InAs), and a protective outer shell made of zinc sulfide (ZnS) or cadmium sulfide (CdS) to prevent toxicity.[58,59] Ceramic-based nanomaterials, polymeric nanomaterials, and composite nanomaterials are also part of this classification. [60–64]

Nanomaterials can also be classified based on their properties, such as magnetic, optical, electronic, or catalytic properties.[44,65–69] These materials often exhibit multiple properties, which can be utilized in various biosensing approaches. For example, AuNPs can serve as an optical transducer because of their surface plasmon resonance (SPR) properties and as electrochemical transducer due to their catalytic and electrochemical properties.[70–72] The main property utilized in developing a biosensor typically determines its nomenclature and classification (e.g., optical, electrochemical nanobiosensors, etc.), although these criteria are fairly flexible depending on the combination of nanomaterials, platforms, etc.[73–75]

For example, optical nanobiosensors make use of the optical properties of nanomaterials, offering unique optical characteristics suitable for colorimetric or fluorescent detection. Notably, nanoparticles hold significant importance due to their high surface-volume ratio and high tunability.[76,77] As mentioned AuNPs display unique optical characteristics, such as localized SPR, capable of inducing noticeable color changes in the presence of target analytes, rendering them exceptionally effective for visual detection techniques.[78,79] QDs demonstrate size-dependent fluorescence, which can be utilized for highly sensitive and multiplexed detection purposes. [80]

Electrochemical nanobiosensors utilize nanomaterials' electric and catalytic properties to detect target molecules.[44,81] The high surface area of nanomaterials, such as carbon nanotubes and graphene, facilitates enhanced electron transfer rates and provides a conducive environment for catalytic reactions when employed for the fabrication of working electrodes.[82–85] This results in improved sensitivity and lower detection limits for electrochemical biosensors, making them suitable for detecting low concentrations of biomolecules in complex biological samples. Besides, certain nanoparticles have redox characteristics which enable them to be directly identified using electrochemical methods without requiring further steps or reactions post the immunoreaction in which they serve as markers. Included in this category are AuNPs, silver nanoparticles (AgNPs), and QDs.[45]

Gravimetric biosensors, which include piezoelectric and magnetic biosensors, utilize nanomaterials to detect alterations in mass or mechanical properties resulting from biorecognition events.[86,87] Piezoelectric biosensors make use of nanomaterials such as zinc oxide nanowires or lead zirconate titanate (PZT) nanoparticles, which can effectively convert mechanical energy into electrical signals.[88] This capability enables the detection of minute mass changes on the sensor surface, making it valuable for tasks such as pathogen detection or monitoring biomolecular interactions.

On the other hand, magnetic biosensors employ magnetic nanoparticles that modify their magnetic properties upon binding with target molecules, enabling highly sensitive detection methods, especially in applications requiring rapid and specific target identification.[73,74] Common magnetic

nanoparticles include metallic nanoparticles, metal oxide nanoparticles, and steel alloy nanoparticles. Examples of commonly used magnetic nanoparticles are iron, cobalt, nickel, silver, and gold. [89–91]

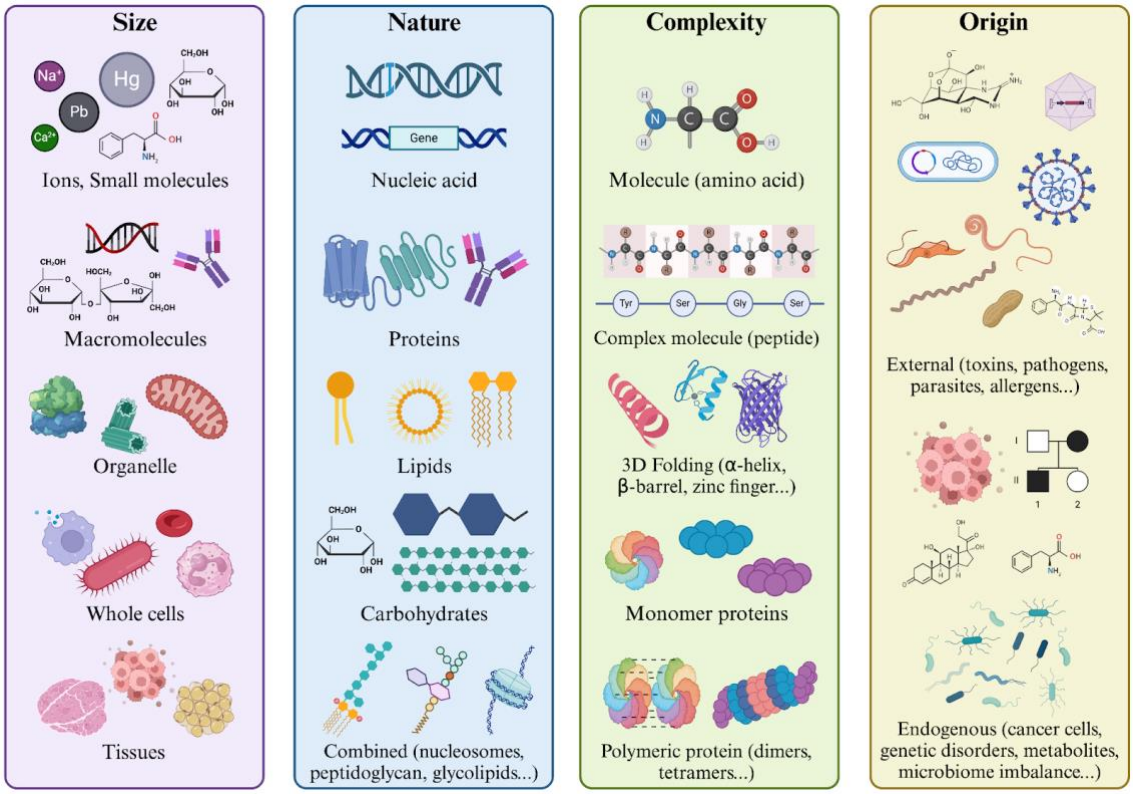
Acoustic biosensors can be significantly improved by incorporating nanomaterials to enhance their capacity to detect changes in acoustic wave properties resulting from biorecognition events.[92] Examples of acoustic biosensors include surface acoustic wave (SAW) and quartz crystal microbalance (QCM) sensors, which are capable of measuring variations in the frequency or amplitude of acoustic waves traveling through or on the surface of a sensor material.[93] Nanomaterials, with their extensive surface area and functionalization capabilities, play a crucial role in enhancing the sensitivity and specificity of acoustic biosensors. Consequently, they are highly effective for diverse applications such as real-time monitoring of biomolecular interactions, detection of environmental pollutants, and medical diagnostics.[94]

Thermal biosensors utilize the thermal conductivity of nanomaterials, such as AuNPs and AgNPs, to detect temperature changes linked to biochemical reactions.[95] By quantifying the heat produced or absorbed during these reactions, thermal biosensors can swiftly and accurately identify target analytes.[96] This methodology is particularly beneficial in scenarios that necessitate real-time tracking of biochemical processes, such as in metabolic studies or enzymatic assays.[97]

1.2. Biomarkers for Precision and Personalized Medicine

Biomarkers are measurable biological indicators of a particular health state. As stated by the WHO, "*Biomarkers include almost any measurement reflecting an interaction between a biological system and a potential hazard, which may be chemical, physical, or biological. The measured response may be functional, physiological, or biochemical at the cellular level, or a molecular interaction*."[98] Biomarkers include any (bio)molecule or differential state that is measurable, either qualitatively or semi-quantitatively, whose presence, absence, or concentration range indicates a health or disease state. This can include ions, small or big, complex molecules, or complete cells, for instance.[10,99,100]

Some characteristics need to be considered regarding the potential use of biomarkers as targets for PoC nanobiosensors. Biomarkers must be present in a retrievable sample or body fluid for its processing and application to the final PoC device. Examples are blood, urine, saliva, sweat, or tears.[99,101,102] These different matrices are different in composition, density, and availability. PoC biosensors should ideally be capable of processing the matrix (i.e., diluting or concentrating the sample, filtering undesired components, adjusting the pH of the sample) or instead provide a user-friendly extra step for its treatment (i.e., nasal swab dipping in extraction and/or running buffer for SARS-CoV-2 testing). [103,104]



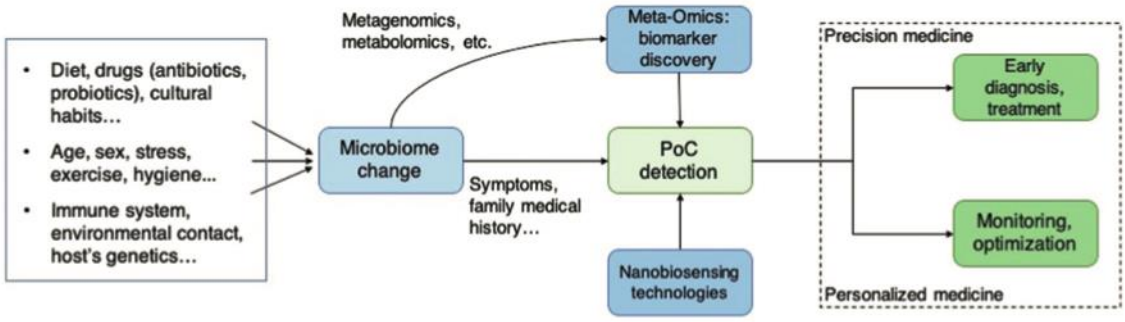
Scheme 2: Schematic illustration of different possible classifications of biomarkers. Created with Biorender.

Biomarkers can be classified in various ways based on their size, nature, complexity, or origin, amongst others (Scheme 2). When it comes to size, biomarkers can range from small molecules to cells or even tissues. In terms of nature, biomarkers can be categorized as small molecules, nucleic acids, proteins, ions, lipids, etc. Finally, when it comes to complexity, biomarkers can be further classified as ions, molecules, molecule complexes, organelles, cells, or tissues. Understanding these different classifications of biomarkers is important in developing effective PoC nanobiosensors that can accurately detect and diagnose diseases.[105,106]

1.2.1. Microbiome-related Biomarkers

At the time of writing, numerous research institutions, consortia, and organizations are dedicated to the discovery of biomarkers to detect and monitor a diverse range of conditions, diseases, and states affecting human health.[107–111] These biomarkers are particularly crucial in the fields of cancer, microbiome-related conditions, infectious diseases, or environmental pollution, with the ultimate aim of advancing personalized medicine.[112,113] In this way, **precision and personalized medicine** might establish a set of biomarkers for common metabolic conditions (e.g., phenylketonuria, propionic acidemia), infectious diseases (e.g., sexually transmitted infections, urinary tract infections), or

genetic disorders, streamlining and accelerating routine analyses.[114] Ultimately those biomarkers will be employed in either laboratory based analysis or in PoC diagnostic devices, depending on the specific application and required analytical sensitivity and specificity. [115,116]



Scheme 3: Nanobiosensing for detection of validated microbiome-related biomarkers based on multi-omics data. PoC devices based on nanobiosensors could enable prevention, early diagnosis, and monitoring of microbiome-related conditions according to diverse clinical parameters (e.g., symptoms, antibiotics use, age, family medical history) and lifestyle parameters (e.g., diet, stress, or drug use). Reprinted with Permission from Fuentes-Chust, C. et al. The Microbiome Meets Nanotechnology: Opportunities and Challenges in Developing New Diagnostic Devices. Adv. Mat., 33, 18 (2021).

The usual methods for microbiome analysis include metagenomic sequencing, which involves sequencing the genetic material from an environmental sample to identify the microbial species present.[117,118] Another method is 16S ribosomal RNA (rRNA) gene sequencing, which targets the 16S rRNA gene to identify and compare bacterial species in a sample.[119] Additionally, metabolomics involves analyzing the metabolites produced by the microbiome to understand its functional activity. Microbiome profiling techniques, such as PCR and DNA microarrays, are used to identify and quantify microbial species in a sample.[120,121] Finally, shotgun metagenomic sequencing sequences all the genetic material in a sample, providing a comprehensive view of the microbial community. These methods help researchers understand the composition, diversity, and functional potential of the microbiome in various environments, including the human body (Scheme 3).[105,122–124] The wealth of data produced by these approaches has facilitated the discovery of microbiome biomarkers linked to specific conditions and diseases (Table 1). This opens the door to innovative diagnostic strategies. It is conceivable that we could develop sensitive and rapid sensors for monitoring microbiome-related biomarkers in hospital or home settings. Such devices could potentially revolutionize the diagnosis and daily management of patients with various diseases.[125–138]

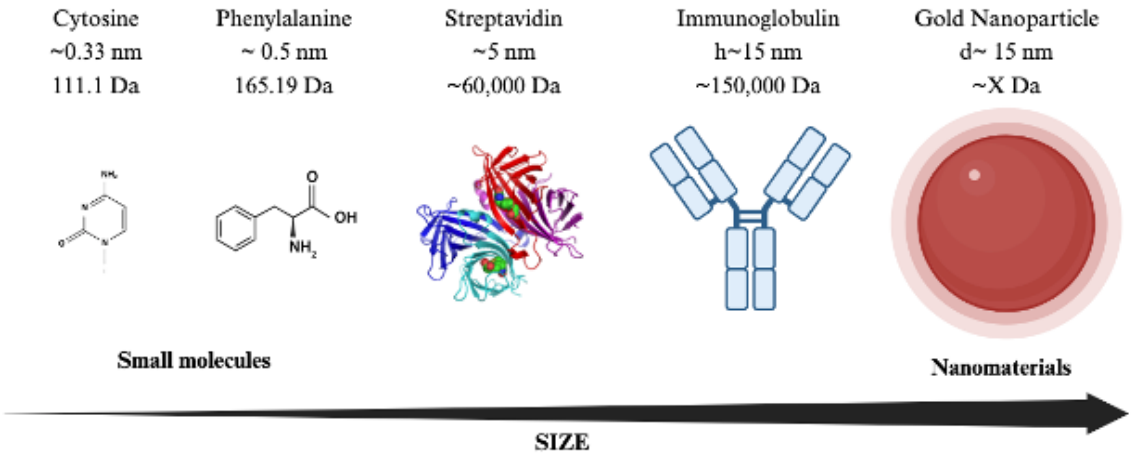
Table 1: Examples of microbiome-related biomarkers and availability of dedicated (nano)biosensors for the diagnosis of different diseases. The type of molecule and weight/size column serves to illustrate the different kinds of potential biomarkers. mRNA: Messenger RNA. Reprinted (Adapted) with Permission from Fuentes-Chust, C. et al. The Microbiome Meets Nanotechnology: Opportunities and Challenges in Developing New Diagnostic Devices. ***Adv. Mat., 33****, 18 (2021)*

PoC	Technology	Disease	Biomarker	Type of molecule	Weight / Size	Sample	Ref
Already exists	Lateral Flow	Intestinal Inflammation	Calprotectin	Zinc-binding Protein	35.6 kDa	Stool	128
Already exists	Lateral Flow	SARS-CoV-2	Human IgG/IgM	Immunoglobulin	150 kDa	Saliva	129
Optimizable	Lateral Flow	Tuberculosis	Mycobacterial lipoarabinomannan (LAM)	Lipoglycan	17.4 kDa	Urine	130, 131
Optimizable	Paper-based sensor	Clostridium Difficile Infection (CDI)	Calprotectin mRNA	Nucleic Acid	-	Stool	132
			CXCL5 mRNA		-		
			IL-8 mRNA		-		
Not available	-	Equine Grass Sickness (EGS)	4-cresyl-sulfate	Organic Compound	188.2 kDa	Urine	133
			Hippurate		179.2 kDa		
			TMAO		75.1 kDa		
			O-acetyl carnitine		203.2 kDa		
Not available	-	Colorectal Cancer (CRC)	Matrix-metalloproteinase-9 (MMP-9)	Enzyme	92 kDa	Stool	134
Not available	-	Multiple Sclerosis	Lipid 654	Lipopeptide	653.5 kDa	Stool	135
Not available	-	Lung Cancer	Capnocytophaga	Nucleic acid	-	Saliva	109
			Veillonella	Whole cell	0.3 µm to 0.5 µm		
Not available	-	Cirrhosis	Kynurenic acid / Quinolinic acid	Metabolites	<500 Da	Plasma	137

Given the dynamic nature of the microbiome, PoC sensors for microbiome biomarkers should incorporate additional monitoring and multiplexing capabilities.[139–141] Indeed, capturing clinically relevant information about a patient's condition may necessitate simultaneous, real-time monitoring of multiple biomarkers such as metabolites, sugars, lipids, nucleic acids, peptides and proteins (Table 1).[142]

1.2.2. Small Molecules and Acute-on-Chronic Liver Failure

There has been a notable emphasis on small molecules in recent years as they have been identified as biomarkers for several states, diseases, or conditions, thanks to the progress made in metabolomics and related fields.[115,143,144] Small molecules are a category of compounds distinguished by their low molecular weight, **typically below 1000 Dalton** (Da or g/mol) (Scheme 4). These molecules are highly significant due to their widespread presence in biological processes and critical roles in various physiological and biochemical functions, such as metabolism, signaling, and gene expression.[123,145,146]



Scheme 4. Size comparison reference for different elements used in this work. nm: nanometers, h: height, d: diameter, Da: Dalton. Figures not to scale. Created with Biorender.

Some small molecules can cross the blood-brain barrier (BBB), making them attractive drug targets for diagnosing and treating central nervous system disorders.[147,148] They have intrinsic properties in human anatomy and are essential for life. Any imbalance of these molecules can be of great interest in the diagnosis or prognosis of different diseases. For instance, the levels of certain small molecules in the blood or urine can be used as biomarkers for various diseases such as cancer, diabetes, and cardiovascular diseases.[107,149–154] The list of small molecules also includes harmful molecules such as toxins, carcinogens, mutagens, endocrine disruptors, secondary metabolites of other microorganisms, chemical agents, and more.[155–159] The body itself can produce these molecules or can acquire them through exposure to environmental toxins, pollutants, or drugs.[160–162] Some of these molecules can cause severe health effects such as cancer, birth defects, and developmental disorders.[163]

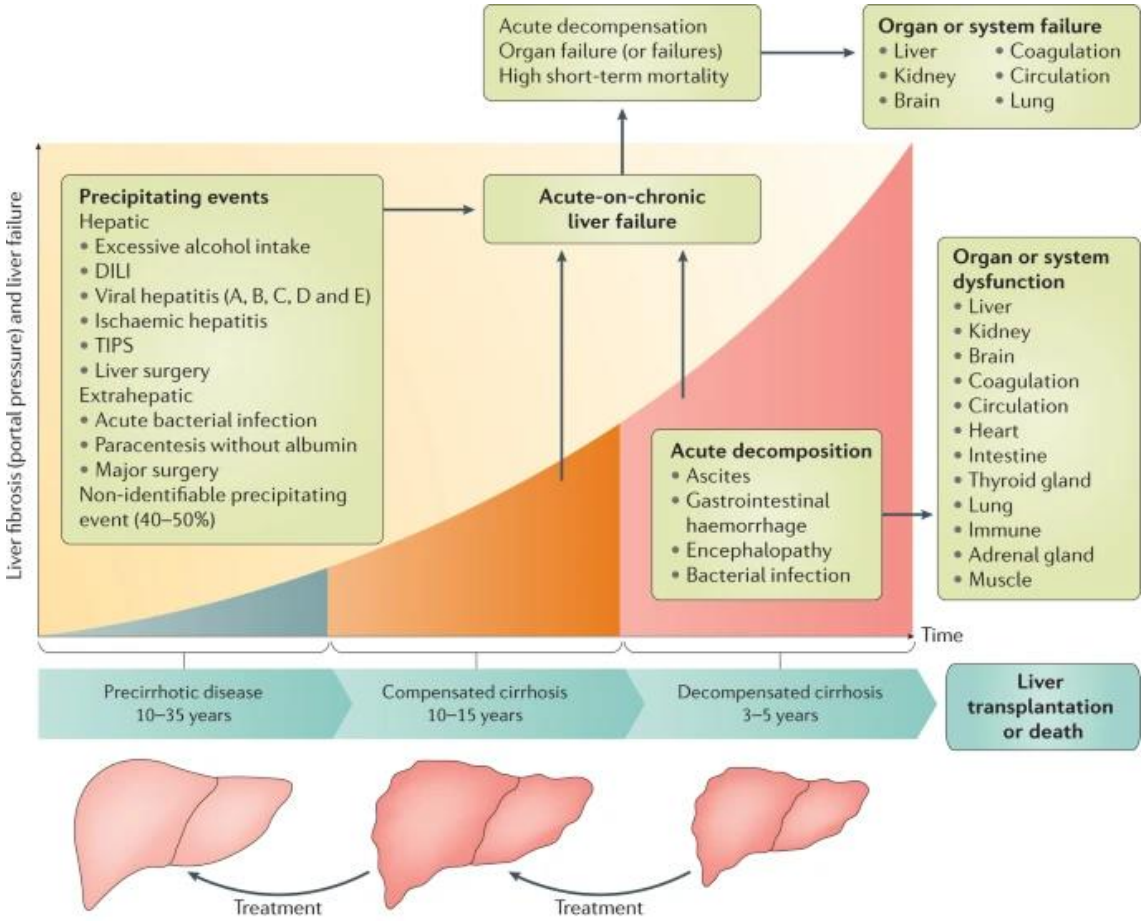
For instance, due to its size and structure (165.19 g/mol), the amino acid **phenylalanine (Phe)** is considered a small molecule (Scheme 4). It consists of an aromatic ring, or phenyl, attached to the base structure of every amino acid, which is a carboxylic acid and a primary amine.[110] Phe is omnipresent in the body, meaning that it does not trigger an immune response. However, Phe has been considered a biomarker for a series of different conditions such as Phenylketonuria metabolic disorder (PKU), Acute-on-Chronic Liver Failure (ACLF), Parkinson's disease, or amyotrophic lateral sclerosis, as well as being useful for tracking metabolic states during exercise, and for techniques such as cellular content estimation for cultured fibroblasts, or detection of cancerous breast tissues.[151,164–169] It needs to be noted that only the L-Phe enantiomer is an essential amino acid and building block for protein synthesis and, therefore, a biomarker since the D-Phe enantiomer's biological role is not currently understood.[170] Another two small molecules have been identified as ACLF biomarkers; **Quinolinic and Kynurenic acids** (QA, and KA, respectively).[171] These small metabolites (167.12 and 189.17 g/mol, respectively) are part of the kynurenine pathway (KP). The

KP plays a vital role in the development, progression, and outcome of acute decompensation (AD) and ACLF in cirrhosis.[165,172] KP activity is normal in compensated cirrhosis, increases in AD, and further rises in ACLF, in line with systemic inflammation. Short-term clinical outcomes of AD and ACLF closely correspond with changes in serum KP activity. Moreover, higher baseline KP activity is an independent predictor of mortality in patients with AD and ACLF. Reports suggest that KP activation emerges in patients with AD, peaks in patients with ACLF, and may contribute to the development, clinical progression, and mortality of ACLF.[173–175]

This project particularly focuses on the detection of L-Phe as a biomarker for PKU and ACLF, as well as Quinolinic and Kynurenic acids for ACLF monitoring.[171,172]

1.2.3 Acute-on-Chronic Liver Failure

ACLF is a severe and life-threatening condition that develops in individuals with existing chronic liver disease, such as cirrhosis. ACLF is characterized by a sudden deterioration in liver function, resulting in multiorgan failure and high mortality rates.[176–178] It is recognized as a separate condition from both acute liver failure and chronic liver disease alone. Various factors, including infection (such as bacterial infections or spontaneous bacterial peritonitis), alcohol abuse, drug-induced liver injury, ischemia, hepatitis flare-ups, or other forms of liver damage, typically trigger ACLF.[179–181] The underlying chronic liver disease, combined with the acute insult, sparks a systemic inflammatory response, and disrupts normal liver function. The symptoms of ACLF can include jaundice (yellowing of the skin and eyes), hepatic encephalopathy (impaired brain function due to liver failure), ascites (buildup of fluid in the abdomen), gastrointestinal bleeding, renal dysfunction, and coagulopathy (impaired blood clotting). Patients with ACLF often deteriorate rapidly and may require intensive care unit support (Scheme 5).[165,177]



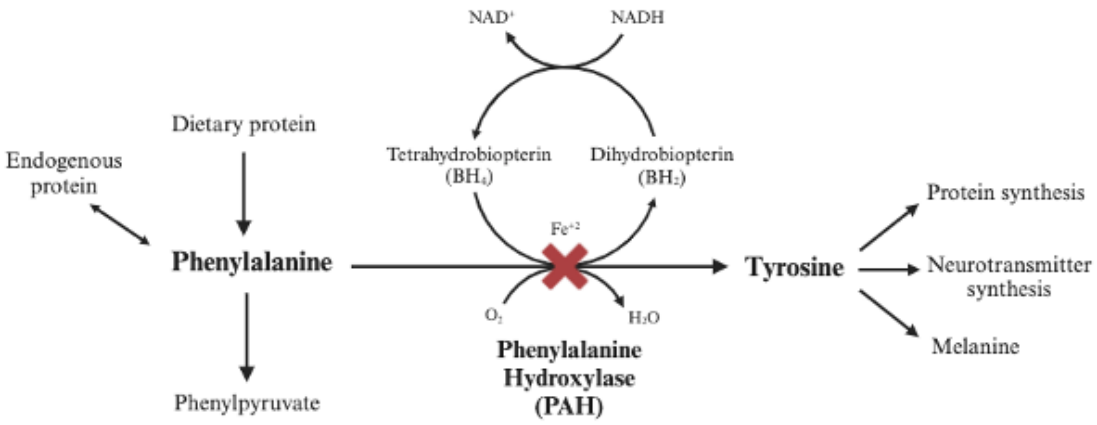
Scheme 5: Clinical course of cirrhosis and ACLF. Retrieved with permission from Arroyo, V., Moreau, R., Kamath, P. et al. Acute-on-chronic liver failure in cirrhosis. ***Nat Rev Dis Primers 2****, 16041 (2016).*

The prognosis of ACLF is generally poor, with high short-term mortality rates. The severity of ACLF is frequently evaluated using scoring systems such as the Chronic Liver Failure Consortium (CLIF-C) ACLF score or the European Association for the Study of the Liver-CLIF (EASL-CLIF) Consortium Organ Failure (CLIF-C OF) score, which take into account laboratory parameters, clinical features, and organ dysfunction to predict the risk of mortality.[165] Management of ACLF involves a multidisciplinary approach and emphasizes supportive care, addressing the underlying cause or triggers, and preventing complications. Interventions may involve infection control, hemodynamic support, nutritional support, management of hepatic encephalopathy, and close monitoring of vital functions and organ systems. Liver transplantation is widely regarded as the ultimate treatment for ACLF in specific cases. However, it may not be a viable option for all patients due to factors such as organ availability and patient suitability.[175] As a result, the prevention and early detection of ACLF triggers, coupled with proactive management, play a critical role in enhancing outcomes for individuals with chronic liver disease who are at risk of developing ACLF.[138] The MICROB-PREDICT project, which financed this PhD thesis, investigates the human microbiome to identify biomarkers and mechanisms related to the development and progression of

ACLF. By analyzing extensive data from 10,000 patients involved in prior European cirrhosis research (PREDICT, GALAXY, and LIVERSHOPE), the project aims to develop innovative diagnostic tools, including PoC tests and nanobiosensors.[182]

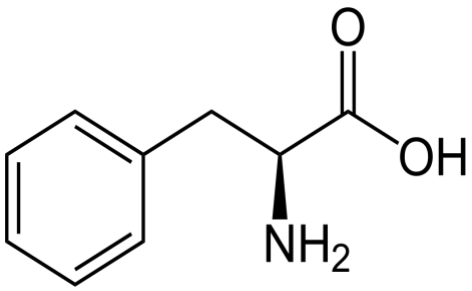
1.2.4. Phenylketonuria

PKU is an inborn autosomal-recessive metabolic disease caused by a series of mutations related to the phenylalanine hydroxylase (PAH) gene, found in chromosome 12, that leads to a deficiency in Phe amino acid metabolism.[183] The PAH enzyme, along with the cofactor tetrahydrobiopterin (BH_4 or sapropterin), molecular oxygen (O_2), and non-heme iron (Fe^{+2}), hydroxylates Phe to tyrosine. Tyrosine is one of the 20 standard amino acids, however it is not naturally occurring so must be synthesized in the body via the oxidation of Phe (Scheme 6).[164,170] While not strictly vital for life, neurotransmitters such as dopamine, noradrenaline, norepinephrine and melanin all contain tyrosine, hence it is important for correct bodily function.



Scheme 6. Phenylalanine metabolism. Total or partial inactivity of the Phenylalanine hydroxilase (PAH) creates a bottleneck for metabolic pathways involved in protein, neurotransmitter, and melanin synthesis. NAD^+ and NADH are nicotinamide adenine dinucleotide and its protonated form, cofactors for BH_4 regeneration. Created with Biorender.

Phe (165.19 g/mol) is an essential amino acid (Scheme 7). They are defined as the amino acids that can't be produced in the body; hence, they must be consumed in our diet for their further metabolism into other non-essential amino acids, in this case, tyrosine. Phe has the ability to cross the BBB, but excessive accumulation in the bloodstream can be toxic to the brain, causing seizures and progressive intellectual and motor disabilities.[147,184] Due to the genetic component of this disorder, and the rapid dangerous effects of Phe accumulation, newborn screening (NBS) is fundamental for early diagnosis of PKU within the first ten days of life.[185]



Scheme 7: Phenylalanine chemical structure.

PKU was first discovered in 1934 by Asbjørn Følling, who identified a biomarker, phenylpyruvic acid, a substance never found in nature before, in two children's urine.[186] They were showing signs of intellectual disabilities and a characteristic musty odor, known nowadays to be caused by phenylacetic acid, a by-product of Phe, in urine and sweat. This was inadvertently discovered by performing ferric chloride tests on the patient's urine in search of ketones. From that moment, ferric chloride tests would be performed on freshly wet diapers to diagnose and monitor children suspected of suffering from this disorder. In the 1950s, the concept of a low-Phe diet was introduced and tested with positive results, to some extent reverting some of the intellectual disabilities caused by the accumulation of Phe. However, at the time, most children affected by PKU remained undiagnosed and profoundly mentally disabled, mostly due to a general lack of awareness.[164]

It was not until 1963 when Robert Guthrie and Ada Susi developed the Guthrie test, allowing a more general screening of the population, progressively becoming compulsory in the NBS routine of almost every country of the world between the 1960s-1990s.[187] The Guthrie test or Bacterial Inhibition Assay (BIA) consists of the application of dried blood spots (DBS) previously obtained from capillary blood onto a *Bacillus subtilis* culture along with a growth inhibitor, B-2-thienyl-alanine, that is overcome by high Phe blood levels. Progressively, other techniques such as chromatography, enzymatic assays, the fluorometric method, and tandem mass spectroscopy substituted the Guthrie test due to their higher sensitivity and precision.[188,189]

Depending on the combination of mutations related to the PAH enzyme, there exist varying phenotypes that affect the residual PAH activity and blood Phe concentrations, ranging from mild to pronounced/severe hyperphenylalaninaemia (HPA). Normal Phe concentrations in the blood range from 50 to 110 μmol/L, 120-600 μmol/L are considered mild HPA, 600-1200 μmol/L are considered mild PKU and levels above 1200 μmol/L are considered classic PKU (Table 2).[190,191] Special attention is taken for mothers affected by PKU during pregnancy and for children during their developmental years (Table 3). It is estimated that globally, 0.45 million individuals have PKU, with a global prevalence of 1:23,930 live births with a global phenotype distribution of 62% classic PKU, 22% mild PKU, and 16% mild HPA.[192]

Individuals with PKU must follow a strict, age-appropriate diet after receiving an early diagnosis. This diet is necessary to prevent the accumulation of Phe in the bloodstream, which can lead to neurological problems.[193] Regular monitoring of Phe levels is also recommended to ensure the effectiveness of the diet. The recommended blood Phe levels range from 120 to 360 μmol/L for individuals aged 0-12 and 120 to 600 μmol/L for those above 12 years old. Optimal target ranges have also been recommended for women trying to conceive and during pregnancy (120–360 μmol/L) (Table 3)**.**[170,191] It is important that women with PKU who fall pregnant keep their Phe levels under control or the child can develop neurological deficits, microcephaly, and congenital heart defects. Therefore, PKU patients often rely on dietary supplements (i.e., tyrosine and vitamins) on a personalized regime, Phe-free amino acid formula as a substitution of protein source, and medications like the cofactor sapropterin (in BH_4-responsive patients) to supplement its deficiency and help metabolize ingested Phe.

Table 2: Diagnostic Phe levels in blood.

State	**Blood Phe levels**
Normal Phe levels	50-110 μmol/L
HPA	120-600 μmol/L
Mild PKU	600-1200 μmol/L
Classic PKU	>1200 μmol/L

Table 3: Recommended Phe blood levels for different population groups.

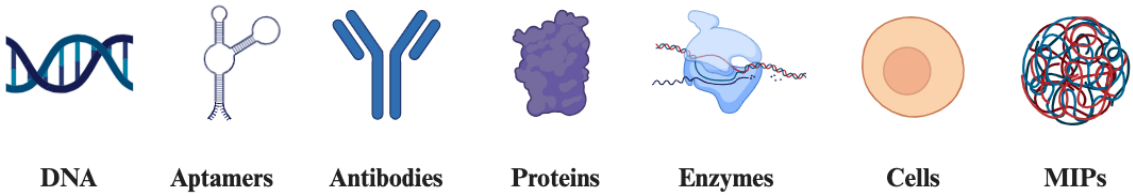
Population Groups	**Recommended Blood Phe levels**
Ages 0-12 y/o	120-360 μmol/L
> 12 y/o	120-600 μmol/L
Pregnant women	120-360 μmol/L

Although most countries have a well-established NBS system, patients with PKU must continue to monitor their Phe levels periodically throughout their lives. This is currently done by either visiting a PKU clinic or collecting DBS samples at home and mailing them to their associated laboratory. PKU patients typically maintain food records, nowadays opting for smartphone diet management apps, to assist in interpreting their blood test results.[190,194] While DBS tests are a simple and efficient way to collect, store, and send blood samples from home, it can be inconvenient, particularly during the first year of life when weekly monitoring tests are required, followed by fortnightly tests until the patient reaches 12 years of age. Additionally, the turnaround time for receiving test results is usually several days.

Therefore, accurate and reproducible monitoring of blood Phe concentrations is desirable for managing PKU.[189] To improve the quality of life for PKU patients, new technologies that can be used at home and allow real-time monitoring are necessary. This is similar to how diabetic patients have benefited from new technologies. To meet this need, it is important to develop specific biorecognition elements that can interact with PKU biomarkers with high sensitivity and selectivity.

1.3. Biorecognition Elements

The main difference between sensors and biosensors lies in the use of biorecognition elements.[4] These elements are derived from biological compounds, such as proteins, nucleic acids, or even entire cells, and they utilize naturally evolved physiological interactions to achieve high levels of specificity toward their target analytes. This specificity is achieved through highly specific molecular recognition events, such as antigen-antibody interactions or complementary base pairing between DNA strands.



Scheme 8: Schematic illustration of different biorecognition elements. MIPs: Molecularly Imprinted Polymers. Created with Biorender.

There are a variety of biorecognition elements that can be employed to identify particular biomarkers (Scheme 8). Antibodies, for instance, can be labeled in numerous ways, ranging from optical to electrochemical methods, to facilitate tracking.[88,195] Enzymes also possess high affinity and can catalyze reactions with their target analyte, enabling detection through the analysis of catalysis byproducts. Nucleic acids can recognize specific nucleic acid sequences via base complementarity, while aptamers have a powerful binding affinity to a target through the secondary structure conformation of a DNA or RNA sequence.[75,97,196,197] Proteins and peptides can also be used as biorecognition elements based on previously defined strong interactions between their amino acids, which can be utilized by immobilizing one of the pair on a transducer.[198] For instance, a specific disease biomarker, such as the nucleoprotein of SARS-Cov-2, can be immobilized and employed as a biorecognition element to detect antibodies produced against it, provided that there is a well-defined and robust interaction between them.[199]

A bioreceptor must have three main characteristics to be effective in a PoC nanobiosensor. These include stability, fast association kinetics, and a strong binding affinity to the target molecule over similar interferents found in the sample matrix.[4,102,200] The bioreceptor must maintain its structure and functionality in different environments, including varying temperatures, humidity percentages, and pressures. Additionally, it should retain its function after undergoing a cycle of drying and rewetting to ensure its stability. Fast target analyte binding kinetics are crucial, as the bioreceptors must bind to the target during very short incubation steps, to comply with the REASSURED criteria.[8] Besides, selective, and specific biorecognition elements must be available or possibly produced for the biomarker of interest. Reproducible and constant production of this element is essential to avoid

batch-to-batch variations that might hinder the assay's sensitivity, which can be the case with antibody production. Conversely, biorecognition elements such as aptamers or Molecularly Imprinted Polymers (MIPs) rely on robust and reproducible synthesis.[62] Another positive feature of biorecognition elements is the possibility of chemical modification (e.g., the addition of thiols or reporter molecules), which often enhances the assay's sensitivity, aids transducer conjugation, and increases the number of detection strategies.[201]

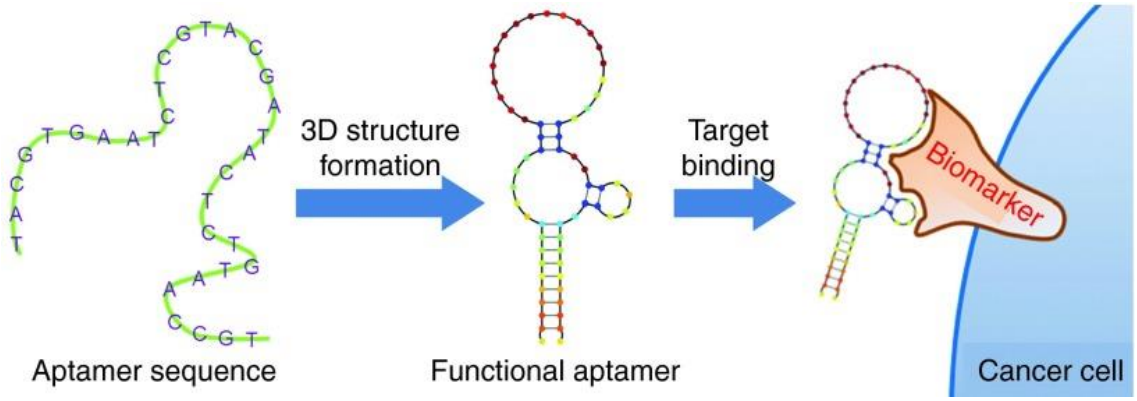
1.3.1. Small Molecule Detection Challenges

Detecting small molecules can be challenging due to their low abundance and mass. Producing biorecognition elements against small molecules is especially challenging as these molecules are difficult to isolate and purify.[202] Moreover, the small size of these molecules makes it challenging to design sensors and assays that can accurately detect them due to the difference in size with respect to the commonly used labels.[203] The scarcity of epitopes, combined with the non-immunogenic nature of many small molecules, makes antibody production a challenging task, often requiring the use of haptens. Haptens are low-molecular-weight chemical substances (typically below 10,000 Da) that exhibit specificity towards another molecule and are non-immunogenic.[204] When haptens form a complex a carrier molecule, typically a protein, the resulting structure becomes more prone to eliciting an immunogenic response, producing antibodies against the hapten/target complex. This often results in antibodies with very low selectivity since some may bind to haptens in the absence of a target.[205] Applying haptens can also be exploited to increase the number of available epitopes in synthesizing other biorecognition elements, such as aptamers or MIPs.

Another challenge that arises due to the reduced amount of epitopes is the difficulty in implementing sandwich detection formats or target immobilization in competitive formats.[206] This is because sandwich detection formats utilize two recognition elements that bind to different regions of the target molecule, creating a sandwich-like structure, which is problematic for small molecule targets with a low number of epitopes. Similarly, target immobilization in competitive formats on a platform or surface can lead to steric blocking of the epitopes required for biorecognition events. When detecting small molecules, competitive assays are suggested as they have higher sensitivity and specificity.[207] These assays utilize labeled analytes that compete with the target molecules for binding to a limited number of immobilized recognition elements. As a result, a signal is produced that is inversely proportional to the concentration of the target molecule. Despite these challenges, developing new technologies for detecting small molecules is crucial in advancing our understanding of their roles in health and disease.

1.3.2. Aptamers for Small Molecule Detection

Aptamers are nucleic acid sequences (either RNA or DNA) that can bind different targets (ranging from ions and small molecules to cells and tissues) thanks to their secondary structure, which is determined by the nucleic acid sequence.[75,196,208] The final 3D structures of aptamers exhibit high specificity in recognizing their targets through a combination of hydrogen bonds, van der Waals interactions, molecular shape complementarity, electrostatic interactions, hydrophobic interactions, and aromatic stacking of flat moieties (Scheme 9).[209]



Scheme 9: Schematic illustration of an aptamer binding to its target. I.e., cancer cell surface biomarker. Reproduced with permission from Sun H. et al. Oligonucleotide Aptamers: New Tools for Targeted Cancer Therapy. ***Mol. Ther. Nucleic Acids, 3****, e182 (2014).*

Aptamers have emerged as a promising alternative for the detection of small molecules due to their high specificity and affinity. They have unique advantages over other biorecognition elements, such as antibodies, including their size, ease of synthesis, reproducibility, recyclability, and stability, making them an attractive option for small molecule detection. [210]

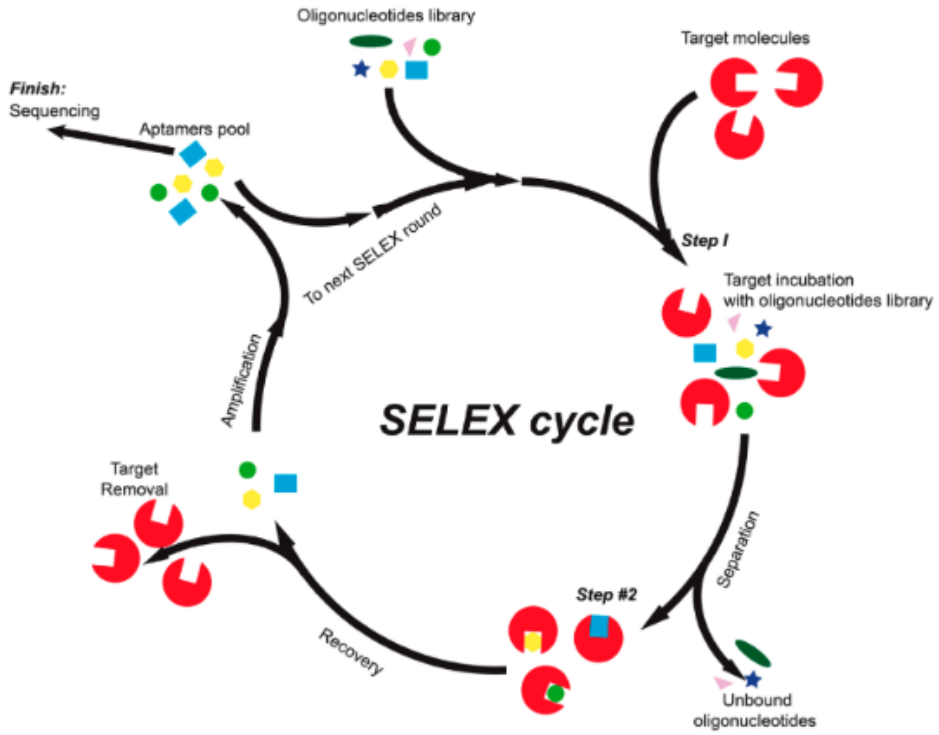
These advantages are mostly due to the aptamer development process, Systematic Evolution of Ligands by Exponential Enrichment (SELEX), compared to other biorecognition element production methods.[211,212] The isolation of aptamers is conducted *in vitro*, thereby avoiding the use of animals and cellular cultures. This approach enables the use of molecules of varying sizes and natures as targets for aptamer generation, which usually do not create immunogenicity, which is the case for many small molecule biomarkers.[213–215] Additionally, the isolation process can be directed towards a specific epitope or area of the target, which can be utilized in a variety of applications.[201]

Once aptamers are isolated and sequenced, they can be synthesized in large batches with high reproducibility and low cost, avoiding the typical variations seen in antibody production.[216] Aptamers offer greater flexibility as they can be chemically modified with a wide range of functional molecules (e.g. fluorescent molecules, redox reporters, magnetic particles) and can bind to a wider range of targets.[217–220] They can also be recycled and reused with high stability. Aptamers can be engineered

to match specific applications, for example, by truncating or elongating them to modulate the dissociation constant (K_D) or by splitting them into shorter portions for use in a sandwich format. K_D in the picomolar and nanomolar ranges have been reported. Unlike antibodies or enzymes, aptamers can withstand a wide temperature range, making storage more convenient until use.[221]

1.3.3. Systematic Evolution of Ligands by Exponential Enrichment

Aptamers are developed through SELEX, an *in vitro* process that involves multiple rounds of selection, amplification, and isolation of target-binding molecules.[212] During SELEX, a large pool of random oligonucleotides, or library, is exposed to the target of interest, and the molecules that bind to the target are separated from the non-binding ones. The bound molecules are then amplified using PCR, and the process is repeated several times to obtain a pool of highly specific and selective aptamers by periodic increases in stringency conditions (Scheme 10). Besides the positive selection, counter and negative selection steps are included to discard aptamers with affinity against the solid support of choice and against similar or antagonistic molecules, for instance.[222]



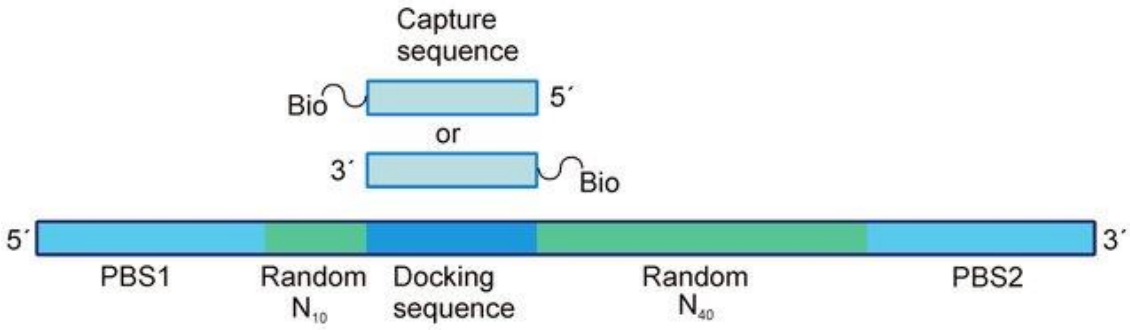
Scheme 10: Schematic representation of the SELEX procedure. Reprinted with permission from Buglak A. A. et al., Methods and Applications of In Silico Aptamer Design and Modeling. ***Int. J. Mol. Sci., 21****, 8420 (2020).*

1.3.3.1. Components and Workflow

The SELEX methodology consists of several key components, including an oligonucleotide library and a partitioning strategy. Additionally, SELEX involves a series of procedures for nucleic acid amplification and purification between rounds, which need to be carefully designed.

1.3.3.1.1. Oligonucleotide Library

In SELEX, a randomized oligonucleotide pool, or library is utilized in order to isolate sequences that bind the target of interest. The typical length of a library can vary from 40 to 100 nucleotides (nt), including the randomized region and a constant region.[223] The library can be presented to the target molecules in solution or immobilized on a surface or partition strategy, in which case the sequence can include a constant docking region complementary to an immobilized sequence, such as the case of Capture SELEX (Scheme 11).[224] Besides, library sequences are designed with flanking primers to perform PCR amplification of the isolated sequences, and primer regions are carefully designed to avoid dimer or hairpin formation.[225]



Scheme 11: A general scheme of library design for a capture-SELEX, containing a docking region and two Primer Binding Sites (PBS1 and 2). Retrieved with permission from Vorobyeva M. A. et al., Key Aspects of Nucleic Acid Library Design for in Vitro Selection. ***Int. J. Mol. Sci., 19****, 470 (2018).*

It is important to ensure that the library has a high level of diversity in order to maximize the chances of containing target-binding motifs in the initial pool.[222] It is important for the initial library to be significantly more diverse than the sequences used in the first selection round to guarantee complete heterogeneity. Increasing the length of the random region is key to introducing greater variability in the library. Additionally, generating the required target-binding motifs may be insufficient if the random region is too short. A library with 10^{25} unique sequences corresponding to a random region of 25 nucleotides ($4^{25} \sim 10^{15}$) is generally believed to be sufficient for successful aptamer isolation. While using larger libraries may be beneficial, it can present challenges in PCR amplification and single-stranded DNA (ssDNA) or RNA production.[225]

When choosing between a ssDNA library or an RNA library, various factors come into play, such as the specific application of the isolated aptamers. Both DNA and RNA aptamers have their own advantages and disadvantages.[226,227] In the past, RNA libraries were prioritized due to the belief that

RNA oligonucleotides presented higher structural complexity; however, it has been demonstrated that ssDNA libraries offer similar capabilities. The increasing preference for ssDNA libraries is due to their practicality and superior stability. DNA and RNA aptamers demonstrate comparable target affinities, shifting the selection process to focus on other practical considerations.[211]

1.3.3.1.2. Selection Conditions

In SELEX, the selection conditions encompass a variety of factors that influence the process of identifying aptamers with a high affinity for a specific target. These factors include selecting an appropriate binding buffer, determining stringency conditions to optimize the selection process, potentially using negative or counter-selection steps to enhance specificity, and considering any other variables that could impact the final affinity or K_D of the aptamer for its target.[228]

The binding buffer (BB) is the solution in which the incubation of the target and library will happen through the different rounds of SELEX, therefore determining the possible interactions and secondary structures that the aptamers can achieve. The ionic force, pH, and even the temperature of this buffer can greatly influence the generation of different target-binding populations. After isolating aptamers using a specific BB, they are expected to perform optimally in various applications, such as biosensing or imaging, when the same buffer solution is used.[42,43] Therefore, the choice of BB is typically made with the final application of the aptamer in mind. This often involves replicating the chemical composition of the sample matrix where the target is commonly present, such as urine or serum. Typical BB solutions used for aptamer selection include tris(hydroxymethyl)aminomethane (Tris) hydrochloride (Tric-HCl) and phosphate buffer solution (PBS). Aptamers selected in PBS generally demonstrate stronger affinity to their targets. Moreover, the presence of cations such as Na^+, Mg^{2+}, and K^+ can neutralize the negative charge of the DNA backbone, effectively reducing non-specific electrostatic interactions.[229] Additional components that may be included in the BB solution are surfactants like Tween-20 or Triton X-100, chelating agents, and, in the case of cell-SELEX, even nutritional components.[206,222]

In SELEX, the stringency conditions are adjusted to gradually isolate aptamers with higher binding affinity towards the target molecule. Tailoring the binding stringency is essential, starting with parameters that ensure some degree of binding and then gradually shifting toward harsher conditions as the SELEX rounds advance to increase the stringency[230,231]. The increase in stringency can be implemented in various ways. For instance, the concentration of the target can be gradually reduced to promote aptamer competition, and the incubation times can be decreased to prioritize faster binding kinetics. As a general rule, aptamer species with nanomolar dissociation constants may require minutes to compete and bind, while picomolar species usually require hours.[232] Increasing or extending washing steps discards weaker interactions, raising the temperature helps isolate aptamers

able to perform at biological organisms' temperatures, and gradually adding other components to the binding buffer mimics the final biologic matrix, such as increasing urea concentrations to mimic urine. The implementation of negative and counter-selection also affects the sensitivity, specificity, and selectivity of the isolated aptamer and must be carefully chosen depending on factors such as possible structurally similar competitors of the target molecule or the presence of other components in the final matrix or application.[222]

1.3.3.1.3. Library Amplification and Conditioning

During the intervals between incubation rounds with the target molecule, binding sequences are isolated from the non-binding sequences, amplified through PCR, and prepared for the next round of incubation.

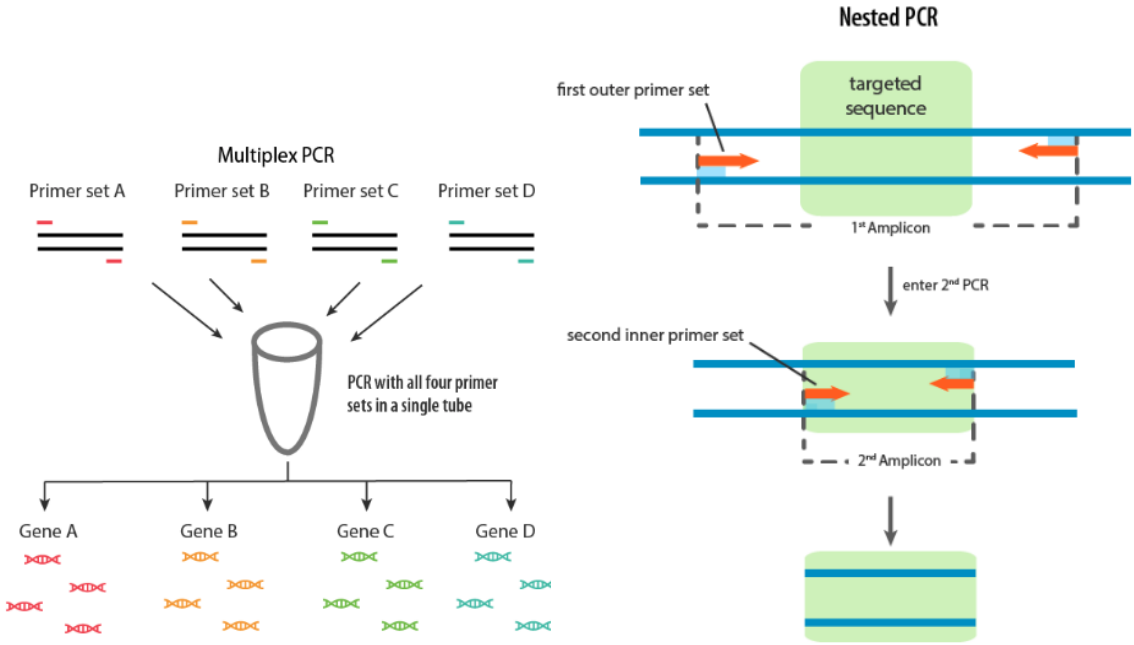
Various considerations are taken into account during the library design phase to address factors that can influence PCR amplification. This includes designing primers with compatible melting temperatures (Tm) to prevent non-specific annealing, avoiding GC-rich (Guanine/Cytosine) and AT-rich (Adenine/Thymine) regions, maintaining a GC content of approximately 40 to 60%, and preventing strong secondary structures or primer-dimer formation.[225,233–235]

The selection of a suitable polymerase is crucial and should align with the chosen PCR technique and the length of the product. Choosing a polymerase that does not compromise the amplification's fidelity and the polymerase's processivity is important. For instance, Hot-Start Taq polymerases are popular as they prevent nonspecific amplification during the reaction setup. Other polymerases are equipped with proofreading 3'-5' exonuclease activity, which helps reduce PCR biases, although they are generally recommended for longer product fragments.

It's important to note that PCR bias is unavoidable to some extent, but it can be minimized by reducing the number of amplification cycles, lowering the template amount, increasing primer concentrations, omitting the final elongation step, and/or carrying out emulsion PCR, for instance. While higher numbers of PCR cycles can theoretically result in greater yields, excessive amplification should be avoided to prevent the formation of by-products. This is particularly crucial in SELEX protocols, where the highly diverse templates can lead to undesired, nonspecific interactions in the form of product-product, product-primer, and primer-primer dimers. With exponential amplification, by-products may accumulate over multiple rounds, potentially dominating the library and resulting in SELEX failure. A common approach is to implement Pilot PCRs, testing different numbers of cycles for the selection of optimal amplification. Therefore, optimizing PCR conditions, using less-bias-prone DNA polymerase, and determining the appropriate number of

amplification cycles are essential to ensure the accurate generation of double-stranded DNA (dsDNA).[225]

When conducting SELEX, it is important to consider the PCR strategy. For RNA libraries, an additional step of reverse transcription to cDNA (complementary/coding DNA) is required before proceeding to PCR using standard primers, although nowadays, this can be done in a single step. Different PCR strategies, such as Real-Time PCR, Nested PCR, or Multiplexed PCR, each have their own advantages and disadvantages that can impact a specific SELEX process (Scheme 12). It is common to use modified primers, such as biotinylated or phosphorylated primers, to facilitate the subsequent step, which involves conditioning the library.[225]



Scheme 12: Schematic illustration of a Multiplex PCR (Left), and a Nested PCR (Right). Available at: https://old.abmgood.com/marketing/knowledge_base/polymerase_chain_variation_system.php.

The amplified oligonucleotide library should be converted to ssDNA for the subsequent incubation round. Various strategies can be employed for conditioning and purifying the library.[236] For example, one approach involves using streptavidin-coated magnetic beads and a biotinylated dsDNA library to denature and elute the non-biotinylated complementary sequence, preparing it for further use. Another popular option involves exonuclease digestion using T7 exonuclease or Lambda (λ) exonuclease for products amplified with phosphorothioate or phosphorylated primers, respectively.[237,238] This approach can be complemented with Asymmetric PCR (A-PCR) to reduce the population of dsDNA, thereby enhancing the efficiency of the process.

Subsequently, the purity and quantity of the ssDNA should be assessed before proceeding to the next round. This can be accomplished using agarose electrophoresis gels, spectrophotometry, or a combination of both methods.[239]

During SELEX, the accumulation of target-binding sequences occurs gradually over multiple rounds of selection. Initially, a varied pool of nucleic acid molecules is exposed to selective pressure, leading to the preferential retention of sequences with an affinity for the target molecule. Subsequent amplification steps through PCR concentrates these sequences. This process is referred to as enrichment. Saturation occurs when the pool of DNA molecules contains a significant proportion of high-affinity binders, and further rounds of selection do not notably increase the enrichment level, at which point the oligonucleotide pools are sent for sequencing. As a result, monitoring the enrichment process is essential to assess the success of the selection process and determine the end of the SELEX assay. The monitoring process can be adapted to the specific SELEX variation being performed. Generally, as the SELEX rounds progress, fewer PCR cycles are needed to optimally amplify the obtained pools from the positive selection. Conversely, more PCR cycles are required to achieve the same levels of amplification in negative selection pools. Hence, evaluating the decrease and increase in PCR cycles for positive and negative selection, respectively, assists in identifying saturation levels. This assessment of PCR cycle changes can be easily conducted through Pilot PCR or Real-Time PCR, for example.[222,240]

1.3.3.1.4. Next Generation Sequencing Analysis

Once successful enrichment is confirmed, samples from the resulting DNA pools are sequenced using Next-Generation Sequencing (NGS) technologies.[241] This method allows for the analysis of millions of sequences from a single sample, as opposed to other methods such as traditional cloning and Sanger sequencing, which can handle only hundreds of different sequences.[242]

The analysis of the obtained reads enables the determination of read quality and identification of overrepresented sequences within the pool, which are the most conserved sequences from the SELEX rounds. Subsequent bioinformatic analysis facilitates the identification of sequence families with similar sequences and minimal variations, known as motifs. Analysis of recurring motifs in overrepresented sequences or families of sequences can help in the identification of the binding regions with the target, which can be further confirmed through binding assays and exploited through further truncation studies, for instance.[243]

Sequencing and analyzing previous rounds of the SELEX process (or negative or counter discarded pools) allows for monitoring the evolution and appearance or disappearance of motifs, families, or subfamilies. Additionally, these data can be correlated with various parameters, such as the

implementation of counter-selection steps, increased stringency, or potential human errors. The NGS analysis concludes with the identification of aptamer candidates, which are then either ordered or synthesized for further characterization and validation as effective aptamers against the target.[244,245]

1.3.3.1.5. Binding Assays

Binding assays involve the measurement and characterization of the interactions between aptamers and their targets. These assays are crucial in understanding the specificity and affinity of the binding interaction. Similar to the SELEX technique, binding assays can be customized and tailored to specific binding requirements, SELEX strategies, or experimental conditions. The easy modification of oligonucleotides facilitates the immobilization of aptamer candidates or labeling for optical or chemical monitoring. Notable examples include the Apta-PCR Affinity Assay (APAA), Enzyme Linked Aptamer Assay (ELAA), and Apta-Bead Affinity Assays (ABAA). Other methods that do not require DNA modification include SPR, Electrophoretic Mobility Shift Assay (EMSA), Circular Dichroism (CD), Isothermal Titration Calorimetry (ITC), and Microscale Thermophoresis (MST).[246–248]

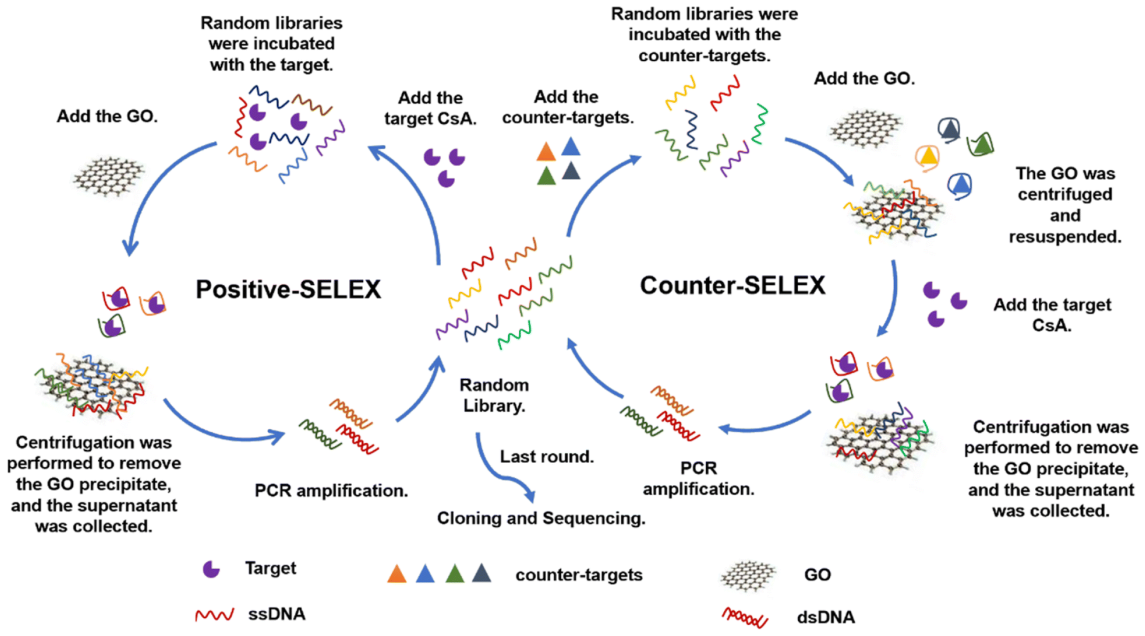
1.3.3.2. Types of Systematic Evolution of Ligands by Exponential Enrichment

Since its discovery in 1990 by Tuerk and Gold, many different SELEX variants have arisen in order to improve specificity, reduce selection time, enable high-throughput screening, adapt to different types of targets (e.g., cells, small molecules, proteins), and to enhance the stability and applicability of selected aptamers.[212,226] In the early stages of SELEX development, the incorporation of negative and counter selection techniques represented significant progress. These approaches were termed Negative-SELEX and Counter-SELEX, respectively. However, with the evolution of SELEX methodologies, the terms "Negative-SELEX" and "Counter-SELEX" are no longer commonly used. Instead, later SELEX variants are named based on other distinguishing features of their protocols, reflecting their unique methodologies and applications.[246,249]

For instance, different SELEX variations are characterized according to their nucleic acid immobilization strategy and separation methods used to separate binding from non-binding molecules. Classic-SELEX relies on the immobilization of the target molecule on a solid support, whereas Capture-SELEX relies on the immobilization of the oligonucleotide library in a solid support.[250–252] Capillary Electrophoresis SELEX (CE-SELEX) relies on both library and target molecules in solution thanks to the ability to separate binding from non-binding species by electrophoretic mobility patterns. CE-SELEX allows the isolation of high-affinity aptamers with a

reduced number of selection rounds, but requires expensive equipment.[253,254] Graphene Oxide SELEX (GO-SELEX) is a cheaper alternative where both, library and target in solution, are incubated with Graphene Oxide (GO) sheets, which has selective adsorption towards unbound sequences (Scheme 13).[255] An early version of this strategy used nitrocellulose filters instead of GO, to filter target-DNA complexes from the unbound sequences, to elute the complexes from the filter and continue the selection process. However, the efficiency of this SELEX version depends on the target nature and size, reportedly working better for protein targets.[256,257]

As observed with GO and nitrocellulose SELEX, SELEX variants can be classified depending on the partition method used. Mag-SELEX utilizes magnetic beads for the immobilization of either the target or library and therefore can be applied to Classic or Capture-SELEX.[251,258] Magnetic separation is a very efficient partitioning method and magnetic beads of different sizes are available with many functionalization chemistries, such as; streptavidin-coated, amine or maleimide coated. Some examples are conjugation reactions include biotin-streptavidin coupling, 1-Ethyl-3-(3-dimethylaminopropyl)carbodiimide and N-Hydroxysuccinimide (EDC/NHS) conjugation, or maleimide-thiol conjugation via click chemistry, for instance.[90,259] Agarose-based beads and resins, such as Sepharose, are frequently used as partition strategies due to its simplicity and wide availability for target immobilization. However, they can be challenging for small molecule targets. Microtiter plates can also be applied as a partition strategy, allowing easy immobilization of the well surfaces with fresh target for each round, although this option is specially advised for protein targets.[222]



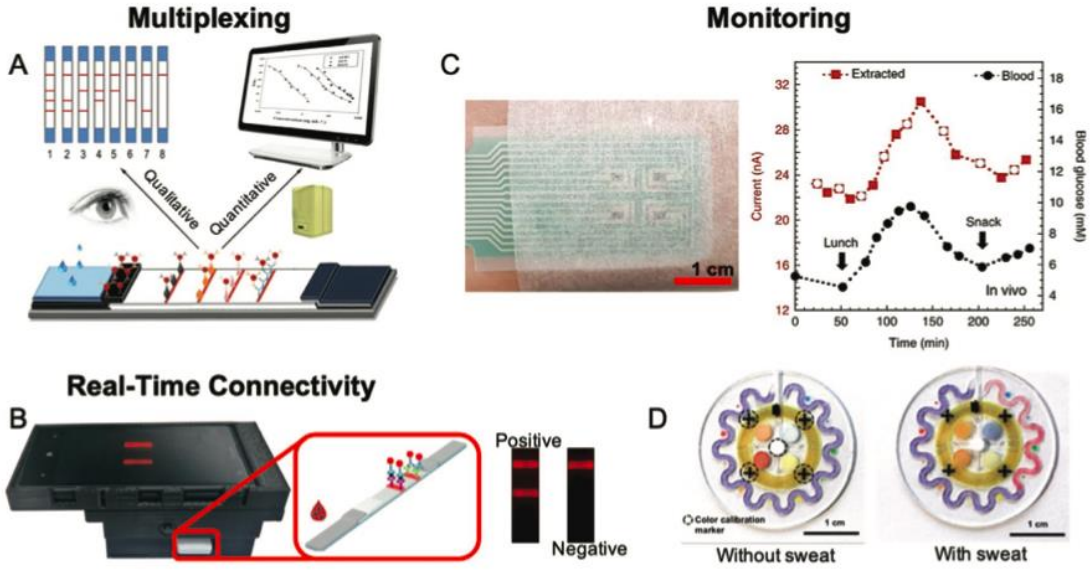
Scheme 13: Schematic representation of GO-SELEX with counter and positive selection steps. Reprinted with permission from Yang J. et al., Non-immobilized GO-SELEX screening of Aptamers Against Cyclosporine A and its Application in a AuNPs Colorimetric Aptasensor. ***Anal. Methods, 16****, 227, (2024).*

In the diverse landscape of SELEX methodologies, there are specialized approaches tailored to different objectives and applications. Cell-SELEX is a notable example of target-dependent SELEX, using whole cells as targets to select aptamers that can specifically recognize cell surface markers and employing flow cytometry as a partition strategy.[246] One-Pot SELEX is an instance of multiplexed SELEX, wherein multiple targets are immobilized and selected against simultaneously in a single process, enabling the efficient discovery of aptamers for complex biological systems with multiple interacting molecules.[258,260] On the other hand, Dual Aptamer SELEX is an application-driven SELEX technique that focuses on selecting aptamers capable of binding to different epitopes of the same target or to two distinct targets concurrently. This approach enhances binding affinity and specificity, proving especially useful in therapeutic and diagnostic contexts requiring multi-valent interactions.[261,262]

These techniques underscore the versatility and adaptability of SELEX in addressing a wide range of scientific and clinical challenges, therefore making the use of aptamers extremely beneficial for the creation of adaptable biosensing platforms, whose specificity and sensitivity can be quickly changed by employing a different aptamer sequence.

1.4. PoC Nanobiosensing Platforms

A PoC nanobiosensor needs to be contained, stored, and utilized within a platform, which serves as the medium for applying, adapting, and processing a biological sample. Additionally, the platform is where the biorecognition element detects a target in the sample, and a transducer element translates the biorecognition element into a signal. The platform displays and/or interprets this signal into an understandable result for the end user.[73,263] Furthermore, different nanomaterials can be utilized for various detection methods based on the chosen platform. Although the choice of the platform will mostly depend on the limitations or potentials of available biorecognition elements and compatible transducer elements, when considering the importance of platforms, it is crucial to consider the end user's perception and user-friendliness of the platform. Additionally, the platform needs to be able to contain a bioassay for an extended period of time and function effectively in any reasonable setting. It is possible to combine different platforms, such as microfluidics with electrochemistry (i.e., glucometer electrode strips) or LFA and smartphone use, depending on the user's specific needs (Scheme 14). This entails an evaluation of PoC and potential PoC platforms and nanomaterials that can be utilized for each, as well as the level of PoC standards that can be attained.[264,265]



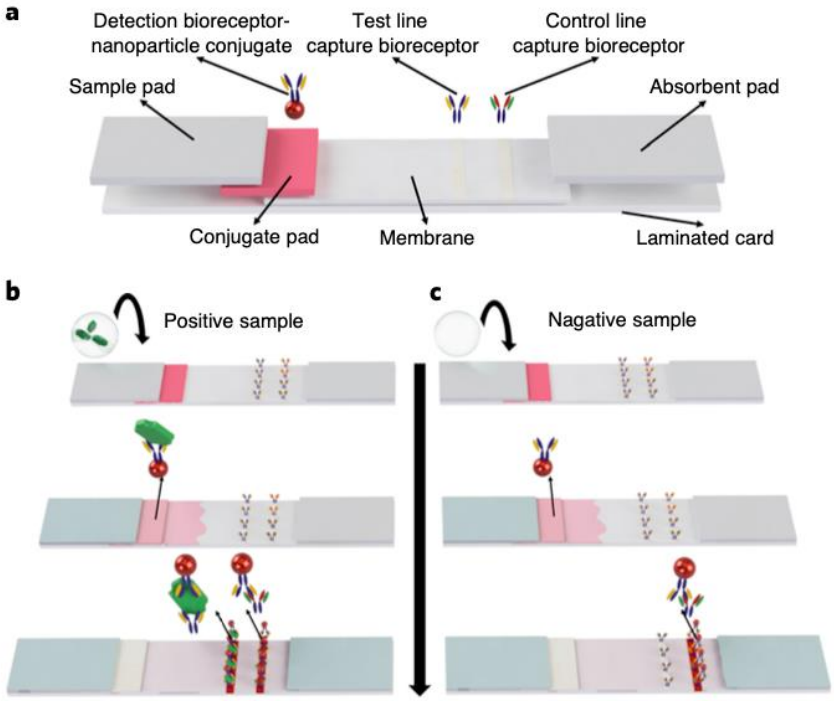
Scheme 14: PoC biosensing devices able to fulfill the REASSURED criteria. A) Multiplexing: Schematic of a multiplex LFA for multiple mycotoxins. B) Real-time connectivity: Smartphone-based fluorescent LFIA platform for highly sensitive PoC detection of Zika virus non-structural protein 1. C) Monitoring (C&D): In-vivo continuous glucose monitoring in healthy human subjects. Left: screen-printed array fixed onto a volunteer's forearm and connected to a potentiostat. Right: values of interstitial fluid-borne glucose as read from extracted blood (red) or through the skin (black). D) Epidermal microfluidic sweat-monitoring device before (left) and after (right) injection of artificial sweat. Lactate, glucose, creatinine, pH, and chloride ions in the sweat sample are monitored and integrated NFC electronics enabled smartphone-based analysis. Reprinted with Permission from Fuentes-Chust, C. et al. The Microbiome Meets Nanotechnology: Opportunities and Challenges in Developing New Diagnostic Devices. ***Adv. Mat., 33****, 18 (2021)*

1.4.1. Lateral Flow Assays

LFA are considered the platform that fits the REASSURED criteria the most, due to their simplicity and user-friendly nature, making them particularly advantageous in situations where rapid and straightforward testing is essential.[73,132,266] Their ability to deliver fast results without the need for specialized laboratory equipment makes them incredibly valuable for PoC diagnosis and monitoring of various health conditions. LFA stand out for their capability to detect a wide array of target analytes, including metal ions, drugs, proteins, pesticides, toxins, and pathogens.[102]

LFA comprise four essential components, each serving a distinct function (Scheme 15). The first component is the sample pad, typically constructed from cellulose, which processes and introduces the sample into the assay, it can also be functionalized to perform pH adjustments and provide an initial filtering of the sample to ensure its suitability for analysis. The second component is the conjugate pad, usually made from glass fiber, which is where the target analyte in the sample interacts with a functionalized nanomaterial. The third component is the detection pad, typically made of nitrocellulose, where the assay occurs, and the results are visually read. Finally, the absorption pad,

almost always constructed from cellulose, collects excess liquid and aids in fluid movement through capillarity, driving the assay to completion. Together, these components create a reliable and efficient diagnostic tool applicable to diverse analytical scenarios.[102,267–269]



Scheme 15: Schematic of the main components and operation of a typical LFA. a) A LFA strip is made of four main parts: the sample pad, the conjugate pad, the membrane, and the absorbent pad. They are mounted on a laminated card. The membrane binds to the capture bioreceptors that form the test and control lines. Panels b) and c) show the operation of an LFA based on immunosandwich recognition. b) The presence of the target analyte in the sample results in the accumulation of nanoparticles on the test and control lines, making the classical two red lines appear. c) In the absence of the target analyte, the nanoparticles accumulate only on the control line, giving a single-colored line output. Reprinted with permission from Parolo C. et al., Tutorial: design and fabrication of nanoparticle-based lateral Flow immunoassays. ***Nat Protoc 15****, 3788–3816 (2020).*

The effectiveness of LFA is significantly enhanced by exploiting the optical properties of nanomaterials.[50,270,271] AuNPs are the most frequently used labels due to their ease of functionalization and unique plasmonic properties, which confer a strong red color ideal for naked-eye detection.[37,272,273] Besides AuNPs, iridium oxide nanoparticles, dyed latex beads, carbon nanoparticles, and nanotubes have also been employed as colorimetric labels in LFA.[274–277] To further improve the sensitivity of LFA using standard AuNPs, developers have leveraged their catalytic properties, their capacity as carriers for enzymes, and their quenching properties in fluorescence-based measurements.[278] In situations requiring higher sensitivity, fluorescence signals are often utilized.[277,279] Semiconducting or carbon-based QDs, silica beads, and liposomes are among the most commonly used fluorescent nanoparticles. QDs, in particular, offer a higher quantum yield and

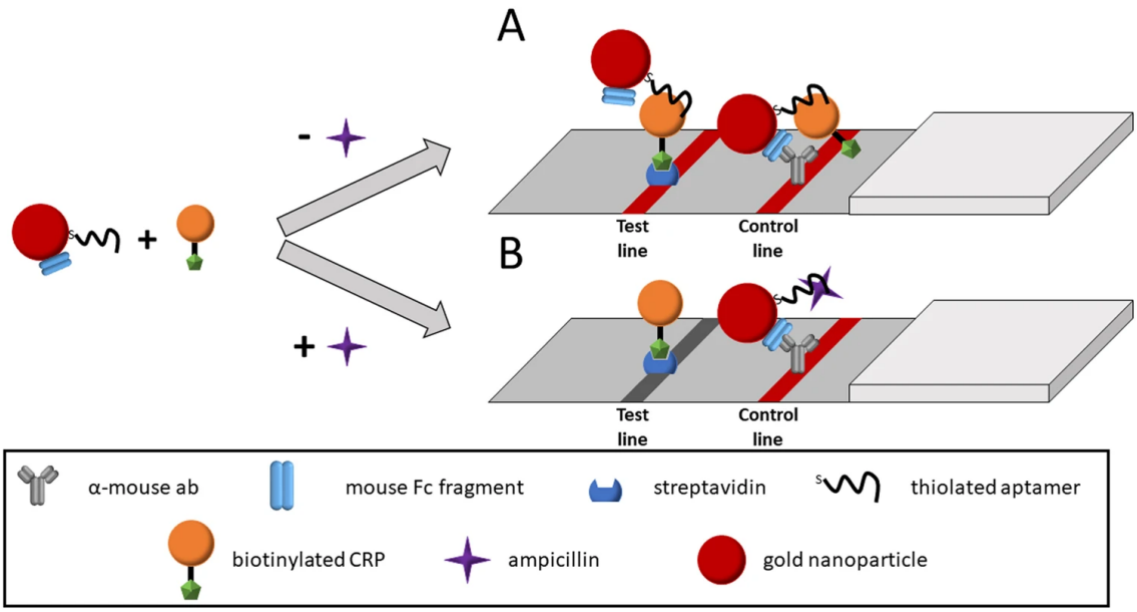
stability compared to traditional organic dyes, making them ideal for PoC applications despite the necessity of a fluorescence reader. Additionally, UV light can excite QDs to produce different emission spectra based on the type of QD utilized, making them suitable for multiplexed detection of biomarkers such as mycotoxins, food contaminants, and viruses.[15,280,281] Recently, upconverting nanoparticles (UPTs) have been employed to achieve even greater sensitivity, although their high cost may hinder widespread use.[282,283] Beyond their optical detection capabilities, nanomaterials play various roles in LFA, such as serving as signal generators to improve sensitivity in diverse readout strategies, including those that use chromophores and fluorescent dyes, like Surface-Enhanced Raman Spectroscopy (SERS).[79,284] Combining different nanomaterials can further enhance the sensitivity. For example, graphene has been used to quench QDs and act as a revealing agent in LFA for detecting bacteria, while magnetic nanoparticles have been utilized for pre concentrating and purifying samples.[159,285–287]

In summary, LFAs exemplify the effectiveness of PoC diagnostics by integrating various nanomaterials to enhance detection capabilities, thereby fulfilling critical roles in diverse applications.

1.4.1.1. Aptamer Lateral Flow Assays for Small Molecule Detection

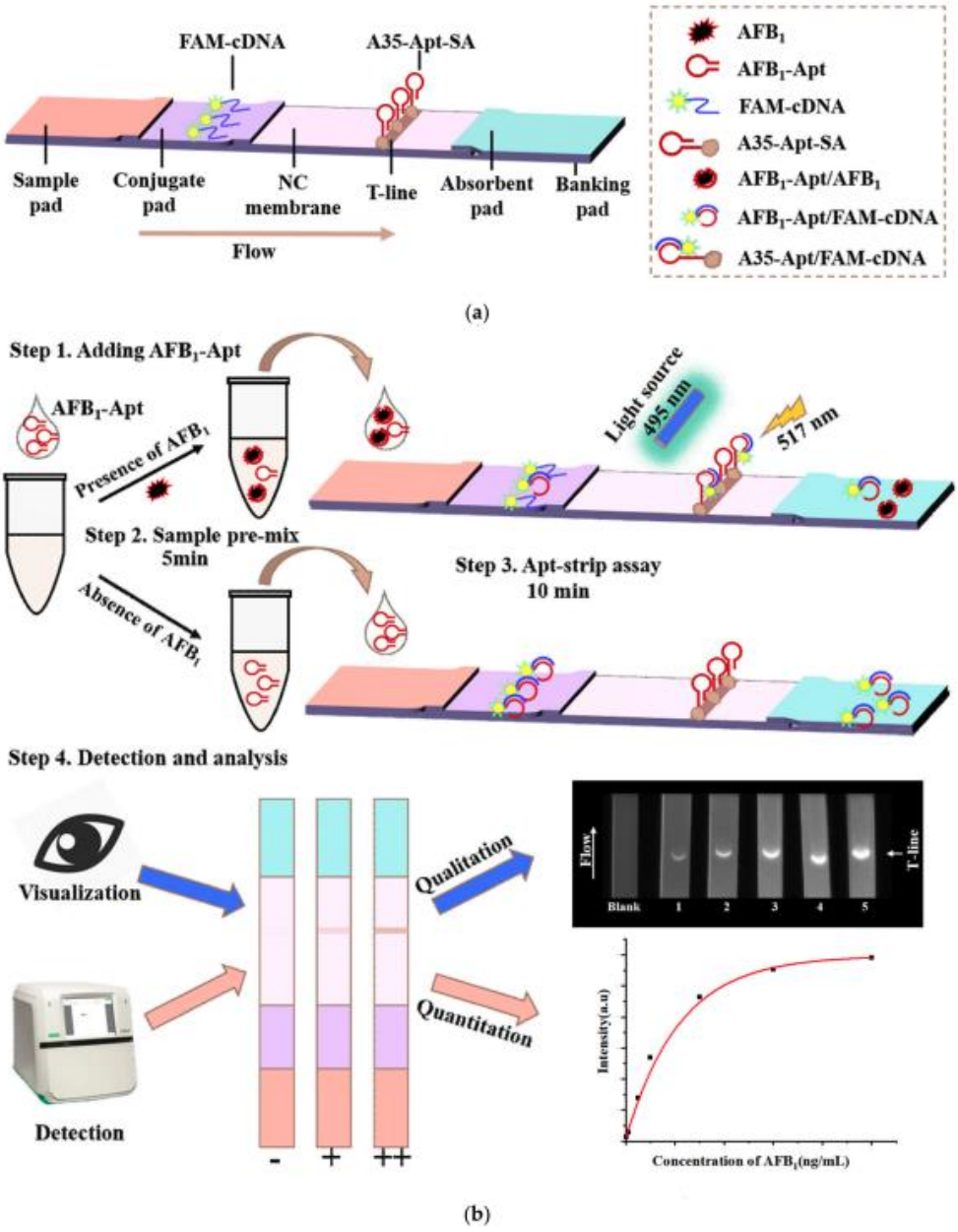
Detecting small molecules with aptamer-based LFA is considerably more challenging than detecting larger molecules like proteins, primarily due to the factors mentioned earlier and the difficulty in creating high-affinity and specific aptamers for small molecule identification. Besides, sandwich assays, which is the most preferred format for enhanced sensitivity, are hard to achieve for small molecule aptamers due to the lack of epitopes. Nonetheless, the scientific community is working diligently to address these obstacles and make it possible to detect these crucial molecules at the PoC.[75,219,288]

In response to the challenges in small molecule detection, strategies such as competitive assays have been explored. For instance, Kaiser *et al*. developed a competitive LFA for the detection of the antibiotic ampicillin using an aptamer capable of binding to both ampicillin and C-reactive protein (CRP), that is immobilized on the test line (Scheme 16).[289] This format exploits the competition between the target molecules in the sample and the target molecules immobilized on the membrane. It is crucial to experimentally test the binding capacity of the detection aptamer to the immobilized small molecules, as immobilizing small molecules on the LFA membrane can lead to conformational changes that affect aptamer-target recognition.



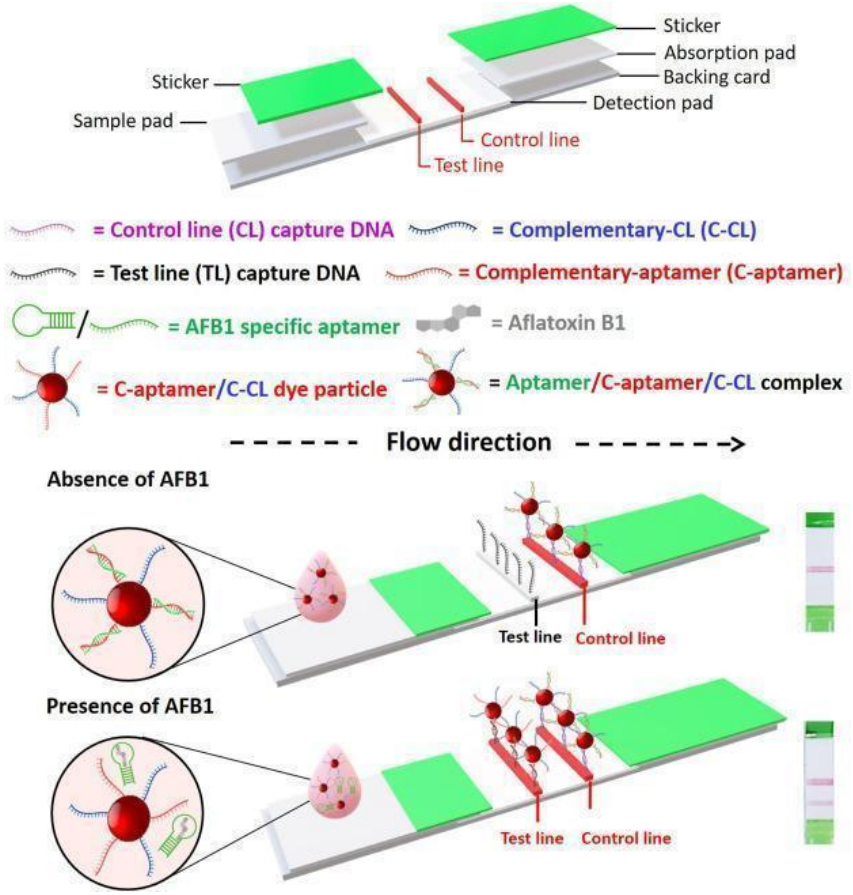
Scheme 16: Schematic representation of a competitive LFA for ampicillin detection. Aptamer-mFc-AuNP conjugates are incubated with biotinylated CRP in the presence or absence of ampicillin. If ampicillin is absent, the conjugates will bind towards biotinylated CRP and will be immobilized on the test line with streptavidin A). If ampicillin is present, CRP is displaced from the aptamer, leading to a signal decrease on the test line B). In both cases, the mFc on the conjugates leads to an immobilization on the control line via the α-mouse antibody, generating the control line. Reprinted with permission from Kaiser L. et al., Small molecule detection with aptamer-based lateral flow assays: Applying aptamer-CRP cross-recognition for ampicillin detection. Sci. Rep. 8, 5628 (2018).

Another example of a competitive LFA is the aptamer-based LFA strip for aflatoxin B1 (AFB1) detection, where AFB1 competes with 6-FAM (6-Carboxyfluorescein) labeled complementary DNA strands for binding to the AFB1-specific aptamer, resulting in increased fluorescence intensity at the test line proportional to the AFB1 concentration (Scheme 17).[290]



Scheme 17: Schematic representation of a competitive LFA for AFB1 detection. (b) Working principle and detection procedures of the LFA for AFB1 detection. Reproduced with permission from Shen K. et al., Development of a lateral flow strip with a positive readout for the on-site detection of aflatoxin B1. ***Molecules, 27****, 4949 (2022).*

Another strategy was simultaneously developed by another group for the detection of AFB1, who used a displacement LFA instead. In this work, dyed polystyrene nanoparticles serve as signal reporters and the presence of AFB1 displaces the aptamer-bound particles, leading to a colorimetric readout directly proportional to the AFB1 concentration (Scheme 18). Displacement assays are a good alternative to competitive assays when immobilization of the small molecule target is detrimental to the sensitivity of the assay and allows indirect signal generation by relying on robust interactions, such as the hybridization of complementary DNA sequences.[291]



Scheme 18: Schematic illustration of the LFA for the detection of AFB1. Reprinted with permission from Vijitvarasan P. et al., A Point-of-use lateral flow aptasensor for naked-eye detection ofaflatoxin B1. ***Food Control, 134,*** *108767, (2022).*

Aptamer-based LF assays for small molecule detection have been reported for 17β-estradiol (E2), bisphenol A, adenosine triphosphate (ATP), p-amino hippuric acid, Ochratoxin A, dopamine, cocaine, and mercury ion.[292–297] However, small molecule detection using aptamer-based LFA remains challenging and requires further investigation, particularly as there is a growing interest in using small endogenous metabolites for disease diagnosis.[298,299]

1.4.1.2. Historical Background and Impact of AuNP-DNA Conjugates

AuNPs have gained significant attention due to their unique optical, electronic, and chemical properties, which render them essential in the fabrication of advanced nanobiosensors. The synthesis of AuNPs was notably advanced in 1951 with the introduction of the Turkevich method.[300] This method involved the reduction of chloroauric acid with sodium citrate to produce nanoparticles with controlled size and shape, laying the foundation for the widespread utilization of AuNPs in diverse applications.[77,217,301–304]

In 1971, researchers Faulk and Taylor achieved a significant breakthrough by demonstrating the first successful conjugation of antibodies to AuNPs. They adsorbed anti-salmonella antibodies onto AuNPs, forming complexes capable of agglutinating salmonellae with remarkable specificity and selectivity.[305] Since then, AuNPs have been utilized in a wide range of applications, including imaging, drug delivery, gene therapy, and biosensing.

It was in 1980 when the first LF using AuNPs for the detection of human placental lactogen (HPL) and hCG was published by Leuvering *et al.*, which paved the way for the development of rapid and easy-to-use diagnostic tests.[23,306] Since then, LFA have become a popular tool for PoC testing for a variety of diseases and conditions, including infectious diseases, drug abuse, and pregnancy.

In 1996, Dr. Chad A. Mirkin and colleagues conjugated thiolated DNA to AuNPs for the first time, introducing the term "spherical nucleic acid" (SNA).[307] This was achieved by finding an equilibrium of ionic strength during the process. AuNPs are prone to aggregation in the presence of salt, yet ionic forces are needed to overcome the repulsion between AuNPs and DNA since both are negatively charged. An initial addition of salt promotes the conjugation of DNA, either via thiol-conjugation or nucleobase adsorption, which stabilizes AuNPs and increases their tolerance to ionic strength. Further additions of salt promote the conjugation of more nucleotides, which reach new repulsion equilibriums at every addition. The method is called salt-aging (SA), in which salts are slowly added to the AuNPs-DNA (thiolated) solution over three days.[308] Although the initial use of this new technique was the development of programmable colloidal crystals, the potential of these complexes was enormous for the development of molecular diagnostic tools.[66,309] Quickly, conjugations of DNA to QDs, carbon nanotubes, silicon nanowires, and many other nanomaterials followed this precedent.[310,311]

Since then, DNA-AuNP conjugates have been employed in various applications, including biosensing, drug delivery, gene therapy, and bioimaging.[312,313] In the field of biosensors, DNA-AuNPs are used in not only LFA but also electrochemistry, SPR biosensors, SERS Biosensors, and Field-Effect Transistor (FET) Biosensors, for instance.[79,314–317]

Another example of the application of DNA-AuNPs is in PCR, where the adsorption affinity of ssDNA over dsDNA on AuNPs is harnessed.[318] In these assays, PCR products are adsorbed to AuNPs, which prevents AuNPs aggregation and allows the colorimetric detection of specific DNA sequences in a sample. There exist several variations that involve A-PCR, covalent conjugation of product-complementary DNA probes to the AuNPs, or the formation of triplex DNA-mediated AuNP networks, for instance.[235,236,302]

In the LFAs field, DNA-AuNP conjugates have been exploited in many directions. DNA-AuNPs were combined with antibodies, creating Nucleic Acid Lateral FLow Immuno Assay (NALFIA)

devices and Nucleic Acid Lateral Flow (NALF) devices without the need for antibodies in the early 2000s.[71,318–320] Besides, these LFA approaches were quickly combined with techniques such as PCR, immuno-PCR, Isothermal amplification, or Recombinase Polymerase Amplification (RPA), for instance, to enhance sensitivity and allow PoC detection and diagnostic for a plethora of biomarkers. AuNPs can also be conjugated with aptamers for target binding by affinity.[321,322]

The continuous advancements in AuNP technology, especially their combination with bioreceptors like antibodies, nucleic acids, and aptamers, highlight their essential role in pushing biosensing technologies forward. As we work on developing aptameric nanobiosensors for small molecule biomarkers, our work aims to contribute to the progress of this field by focusing on understanding conjugate stability, which is crucial for technological advancements. The specific objectives of this thesis are detailed in the following chapter, emphasizing these critical elements to further improve the capabilities and uses of AuNP-based lateral flow assays.

1.5. References

1. Bhalla N, Jolly P, Formisano N, Estrela P. Introduction to biosensors. *Essays Biochem*. 2016;60(1):1–8.
2. Quesada-González D, Merkoçi A. Nanoparticle-based lateral flow biosensors. *Biosens Bioelectron*. 2015;73:47–63.
3. Nishat S, Awan FR, Bajwa SZ. Nanoparticle-based point of care immunoassays for *in vitro* biomedical diagnostics. *Analytical Sciences*. 2019;35(2):123–31.
4. Morales MA, Halpern JM. Guide to Selecting a Biorecognition Element for Biosensors. *Bioconjug Chem*. 2018;29(10):3231–9.
5. Martinkova P, Kostelnik A, Valek T, Pohanka M. Main streams in the construction of biosensors and their applications. *Int J Electrochem Sci*. 2017;12(8):7386–403.
6. Sharma S, Zapatero-Rodríguez J, Estrela P, O'Kennedy R. Point-of-Care diagnostics in low resource settings: Present status and future role of microfluidics. *Biosensors (Basel)*. 2015;5(3):577–601.
7. Kosack CS, Page AL, Klatser PR. A guide to aid the selection of diagnostic tests. *Bull World Health Organ*. 2017;95(9):639–45.
8. Land KJ, Boeras DI, Chen XS, Ramsay AR, Peeling RW. REASSURED diagnostics to inform disease control strategies, strengthen health systems and improve patient outcomes. *Nat Microbiol*. 2019;4(1):46–54.
9. Wu G, Zaman MH. Low-cost tools for diagnosing and monitoring HIV infection in low-resource settings. *Bull World Health Organ*. 2015;90(12):914–20.
10. Yoshizawa JM, Schafer CA, Schafer JJ, Farrell JJ, Paster BJ, Wong DTW. Salivary biomarkers: Toward future clinical and diagnostic utilities. *Clin Microbiol Rev*. 2013;26(4):781–91.
11. Qiu J, Keyser B, Lin ZT, Wu T. Autoantibodies as potential biomarkers in breast cancer. *Biosensors (Basel)*. 2018;8(3).
12. Lee GC, Jeon ES, Kim WS, Le DT, Yoo JH, Chong CK. Evaluation of a rapid diagnostic test, NanoSign® Influenza A/B Antigen, for detection of the 2009 pandemic influenza A/H1N1 viruses. Vol. 7, Virology Journal. 2010.
13. Yang Y, Peng F, Wang R, Guan K, Jiang T, Xu G, *et al.* The deadly coronaviruses: The 2003 SARS pandemic and the 2020 novel coronavirus epidemic in China. *J Autoimmun*. 2020;109(March):102434.
14. Rosati G, Idili A, Parolo C, Fuentes-Chust C, Calucho E, Hu L, *et al.* Nanodiagnostics to Face SARS-CoV-2 and Future Pandemics: From an Idea to the Market and Beyond. *ACS Nano*. 2021 ;15(11):17137–49.

15. Sakai-Tagawa Y, Ozawa M, Tamura D, Le MTQ, Nidom CA, Sugaya N, *et al.* Sensitivity of influenza rapid diagnostic tests to H5N1 and 2009 pandemic H1N1 viruses. *J Clin Microbiol*. 2010;48(8):2872–7.
16. Li Q, Guan X, Wu P, Wang X, Zhou L, Tong Y, *et al.* Early Transmission Dynamics in Wuhan, China, of Novel Coronavirus-Infected Pneumonia. *New England Journal of Medicine*. 2020;382(13):1199–207.
17. WHO | Severe Acute Respiratory Syndrome (SARS) - multi-country outbreak - Update 30. *WHO*. 2015.
18. ROCHE. ACCU-CHECK. 2024.
19. Rodbard D. Quality of Glycemic Control: Assessment Using Relationships between Metrics for Safety and Efficacy. *Diabetes Technol Ther*. 2021;23(10):692–704.
20. Dungan K, Verma N. Monitoring Technologies – Continuous Glucose Monitoring, Mobile Technology, Biomarkers of Glycemic Control. *Endotext*. 2000;
21. Klonoff DC, Wang J, Rodbard D, Kohn MA, Li C, Liepmann D, *et al.* A Glycemia Risk Index (GRI) of Hypoglycemia and Hyperglycemia for Continuous Glucose Monitoring Validated by Clinician Ratings. *J Diabetes Sci Technol*. 2023;17(5):1226–42.
22. Latifi N, Kriegel G, Herskovits ZA. Point-of-Care Urine Pregnancy Tests. *Journal of American Medical Association*. 2019;E1–2.
23. Cole LA. The hCG assay or pregnancy test. *Clin Chem Lab Med*. 2012 [2024 Jul 6];50(4):617–30.
24. Clearblue. Pregnancy tests. 2024.
25. Deeks JJ, Dinnes J, Takwoingi Y, Davenport C, Leeflang MMG, Spijker R, *et al.* Diagnosis of SARS-CoV-2 infection and COVID-19: accuracy of signs and symptoms; molecular, antigen, and antibody tests; and routine laboratory markers. Vol. 2020, Cochrane Database of Systematic Reviews. 2020.
26. Yin C. Genotyping coronavirus SARS-CoV-2: methods and implications. *Genomics*. 2020;112(5):3588–96.
27. Berlinger J, McKeehan B. Coronavirus pandemic: Updates from around the world. CNN. 2020.
28. Cui J, Li F, Shi ZL. Origin and evolution of pathogenic coronaviruses. *Nat Rev Microbiol*. 2019;17(3):181–92.
29. Morley J, Cowls J, Taddeo M, Floridi L. Ethical guidelines for COVID-19. *Nature*. 2020;582:29–31.
30. Sheridan C. Coronavirus and the race to distribute reliable diagnostics. Vol. 38, Nature biotechnology. NLM (Medline); 2020. p. 382–4.

31. Holshue ML, DeBolt C, Lindquist S, Lofy KH, Wiesman J, Bruce H, *et al.* First Case of 2019 Novel Coronavirus in the United States. *N Engl J Med*. 2020;382(10):929–36.
32. FDA. At-Home COVID-19 Antigen Tests-Take Steps to Reduce Your Risk of False Negative Results: FDA Safety Communication | FDA. U.S. Food and Drug Administration. 2022.
33. Artron | Zika Test Kit.
34. WHO Emergency Use Assessment and Listing for Ebola Virus Disease IVDs PUBLIC REPORT Product: ReEBOV™ Antigen Rapid Test Kit.
35. WHO Emergency Use Assessment and Listing for Ebola Virus Disease IVDs PUBLIC REPORT Product: OraQuick® Ebola Rapid Antigen Test Kit (Cadaveric Oral fluid and Whole Blood).
36. Fenzl C, Hirsch T, Baeumner AJ. Nanomaterials as versatile tools for signal amplification in (bio)analytical applications. *TrAC - Trends in Analytical Chemistry*. 2016;79:306–16.
37. Jain PK, Huang X, El-Sayed IH, El-Sayed MA. Review of some interesting surface plasmon resonance-enhanced properties of noble metal nanoparticles and their applications to biosystems. *Plasmonics*. 2007;2(3):107–18.
38. Liang W, Lin H, Chen J, Chen C. Utilization of nanoparticles in microfluidic systems for optical detection. Vol. 22, Microsystem Technologies. Springer Verlag; 2016. p. 2363–70.
39. Sadowska-Bartosz I, Bartosz G. Redox nanoparticles: synthesis, properties, and perspectives of use for treatment of neurodegenerative diseases. *J Nanobiotechnology*. 2018;16(1):1–16.
40. Braun T, Schubert A, Zsindely S. Nanoscience, and nanotechnology on the balance. *Scientometrics*. 1997;38(2):321–5.
41. Song W, Anselmo AC, Huang L. Nanotechnology intervention of the microbiome for cancer therapy. *Nat Nanotechnol*. 2019;14(12):1093–103.
42. Tang B, Zhang N, Chen Z, Xu K, Zhuo L, An L, *et al.* Probing hydroxyl radicals and their imaging in living cells by use of FAM-DNA-Au nanoparticles. *Chemistry - A European Journal*. 2008;14(2):522–8.
43. Gao JL, Liu YH, Zheng B, Liu JX, Fang WK, Liu D, *et al.* Light-Activated and Self-Driven Autonomous DNA Nanomachine Enabling Fluorescence Imaging of MicroRNA in Living Cells with Exceptional Precision and Efficiency. *ACS Appl Mater Interfaces*. 2021;13(27):31485–94.
44. Wen Q, Liang X, Pan H, Li J, Zhang Y, Zhu W, *et al.* Rapid and sensitive electrochemical detection of microRNAs by gold nanoparticle-catalyzed silver enhancement. *Analyst*. 2020;1–5.
45. Russo L, Puntes V, Merkoçi A. Tunable electrochemistry of gold-silver alloy nanoshells. *Nano Res*. 2018;11(12):6336–45.

46. Mekuye B, Abera B. Nanomaterials: An overview of synthesis, classification, characterization, and applications. *Nano Select*. 2023;4(8):486–501.
47. Saleh TA. Nanomaterials: Classification, properties, and environmental toxicities. *Environ Technol Innov*. 2020;20:101067.
48. Marcelo GA, Lodeiro C, Capelo JL, Lorenzo J, Oliveira E. Magnetic, fluorescent and hybrid nanoparticles: From synthesis to application in biosystems. *Materials Science and Engineering: C*. 2020;106:110104.
49. Russo L, Merkoçi F, Patarroyo J, Piella J, Merkoçi A, Bastús NG, *et al.* Time- and Size-Resolved Plasmonic Evolution with nm Resolution of Galvanic Replacement Reaction in AuAg Nanoshells Synthesis. *Chemistry of Materials*. 2018;30(15):5098–107.
50. Quesada-González D, Merkoçi A. Nanomaterial-based devices for point-of-care diagnostic applications. *Chem Soc Rev*. 2018;47(13):4697–709.
51. Merkoçi A, Ambrosi A, de la Escosura-Muñiz A, Pérez-López B, Guix M, Maltez M, *et al.* Nanomaterials for Electroanalysis. In: Encyclopedia of Analytical Chemistry. 2010.
52. Kara P, de la Escosura-Muñiz A, Maltez-da Costa M, Guix M, Ozsoz M, Merkoçi A. Aptamers based electrochemical biosensor for protein detection using carbon nanotubes platforms. *Biosens Bioelectron*. 2010 ;26(4):1715–8.
53. Yu L, Li P, Ding X, Zhang Q. Graphene oxide and carboxylated graphene oxide: Viable two-dimensional nanolabels for lateral flow immunoassays. *Talanta*. 2017;165:167–75.
54. Omanović-Mikličanin E, Badnjević A, Kazlagić A, Hajlovac M. Nanocomposites: a brief review. *Health Technol (Berl)*. 2020 ;10(1):51–9.
55. Hadden M, Martinez-Martin D, Yong KT, Ramaswamy Y, Singh G. Recent Advancements in the Fabrication of Functional Nanoporous Materials and Their Biomedical Applications. *Materials*. 2022;15(6):2111.
56. Mayorga-Martinez CC, Cadevall M, Guix M, Ros J, Merkoçi A. Bismuth nanoparticles for phenolic compounds biosensing application. *Biosens Bioelectron*. 2013;40(1):57–62.
57. Mathieu P, Coppel Y, Respaud M, Nguyen QT, Boutry S, Laurent S, *et al.* Silica Coated Iron/Iron Oxide Nanoparticles as a Nano-Platform for T2 Weighted Magnetic Resonance Imaging. *Molecules 2019, Vol 24, Page 4629*. 2019;24(24):4629.
58. Soldado A, Barrio LC, Díaz-Gonzalez M, de la Escosura-Muñiz A, Costa-Fernandez JM. Advances in quantum dots as diagnostic tools. *Adv Clin Chem*. 2022;107:1–40.
59. Díaz-González M, de la Escosura-Muñiz A, Fernandez-Argüelles MT, Alonso FJG, Costa-Fernandez JM. Quantum Dot bioconjugates for diagnostic applications. 2020;133–76.
60. Xu L Di, Zhang Q, Ding SN, Xu JJ, Chen HY. Ultrasensitive Detection of Severe Fever with Thrombocytopenia Syndrome Virus Based on Immunofluorescent Carbon Dots/SiO2 Nanosphere-Based Lateral Flow Assay. *ACS Omega*. 2019;4(25):21431–8.

61. Li X, Lu D, Sheng Z, Chen K, Guo X, Jin M, *et al.* A fast and sensitive immunoassay of avian influenza virus based on label-free quantum dot probe and lateral flow test strip. *Talanta*. 2012;100:1–6.
62. Erdem Ö, Saylan Y, Cihangir N, Denizli A. Molecularly imprinted nanoparticles based plasmonic sensors for real-time Enterococcus faecalis detection. *Biosens Bioelectron*. 2019;126:608–14.
63. Marcelo GA, Montpeyo D, Novio F, Ruiz-Molina D, Lorenzo J, Oliveira E. Luminescent silicon-based nanocarrier for drug delivery in colorectal cancer cells. *Dyes and Pigments*. 2020;181:108393.
64. Solórzano R, Suárez-García S, Novio F, Lorenzo J, Alibés R, Busqué F, *et al.* Nanoscale coordination polymers for medicine and sensors. *Adv Inorg Chem*. 2020 ;76:3–31.
65. Liu JM, Wang XX, Jiao L, Cui ML, Lin LP, Zhang LH, *et al.* Ultra-sensitive non-aggregation colorimetric sensor for detection of iron based on the signal amplification effect of Fe3+ catalyzing H 2O2 oxidize gold nanorods. *Talanta*. 2013;116:199–204.
66. Elghanian R, Storhoff JJ, Mucic RC, Letsinger RL, Mirkin CA. Selective colorimetric detection of polynucleotides based on the distance-dependent optical properties of gold nanoparticles. *Science (1979)*. 1997;277(5329):1078–81.
67. Iglesias-Mayor A, Amor-Gutiérrez O, Costa-García A, de la Escosura-Muñiz A. Nanoparticles as Emerging Labels in Electrochemical Immunosensors. *Sensors 2019, Vol 19, Page 5137*. 2019;19(23):5137.
68. Merkoçi A, Anik U, Çevik S, Çubukçu M, Guix M. Bismuth film combined with screen-printed electrode as biosensing platform for phenol detection. *Electroanalysis*. 2010;22(13):1429–36.
69. Ambrosi A, Guix M, Merkoçi A. Magnetic and electrokinetic manipulations on a microchip device for bead-based immunosensing applications. *Electrophoresis*. 2011;32(8):861–9.
70. Englebienne P, Hoonacker A Van, Verhas M. Surface plasmon resonance: principles, methods, and applications in biomedical sciences. *Spectroscopy*. 2012;17(2–3):255–73.
71. Wang J, Munir A, Li Z, Zhou HS. Aptamer-Au NPs conjugates-enhanced SPR sensing for the ultrasensitive sandwich immunoassay. *Biosens Bioelectron*. 2009;25(1):124–9.
72. Fathi F, Rashidi MR, Omidi Y. Ultra-sensitive detection by metal nanoparticles-mediated enhanced SPR biosensors. Vol. 192, Talanta. Elsevier B.V.; 2019. p. 118–27.
73. Parolo C, Merkoçi A. Paper-based nanobiosensors for diagnostics. *Chem Soc Rev*. 2013;42(2):450–7.
74. Bergua Canudo JF. Nanobiosensors for contaminants detection in water. 2020.
75. Seok Kim Y, Ahmad Raston NH, Bock Gu M. Aptamer-based nanobiosensors. *Biosens Bioelectron*. 2016;76:2–19.

76. Ma X, Li X, Luo G, Jiao J. DNA-functionalized gold nanoparticles: Modification, characterization, and biomedical applications. *Front Chem*. 2022;10.
77. Lantero E, Directors E, Martínez De La J, Yulán F, García H. Functionalization of Gold Nanoparticles for Cell Transfection. 2015.
78. Guo Y, Wu J, Li J, Ju H. A plasmonic colorimetric strategy for biosensing through enzyme guided growth of silver nanoparticles on gold nanostars. *Biosens Bioelectron*. 2016;78:267–73.
79. Eryilmaz M, Acar Soykut E, Çetin D, Boyaci IH, Suludere Z, Tamer U. SERS-based rapid assay for sensitive detection of Group A: Streptococcus by evaluation of the swab sampling technique. *Analyst*. 2019;144(11):3573–80.
80. Wang C, Xiao R, Wang S, Yang X, Bai Z, Li X, *et al*. Magnetic quantum dot based lateral flow assay biosensor for multiplex and sensitive detection of protein toxins in food samples. *Biosens Bioelectron*. 2019;146:111754.
81. Rosati G, Gherardi G, Grigoletto D, Marcolin G, Cancellara P, Mammucari C, *et al.* Lactate Dehydrogenase and Glutamate Pyruvate Transaminase biosensing strategies for lactate detection on screen-printed sensors. Catalysis efficiency and interference analysis in complex matrices: from cell cultures to sport medicine. *Sens Biosensing Res*. 2018;21:54–64.
82. Walcarius A, Minteer SD, Wang J, Lin Y, Merkoçi A. Nanomaterials for bio-functionalized electrodes: Recent trends. *J Mater Chem B*. 2013;1(38):4878–908.
83. Khater M, Escosura-Muñiz AD La, Altet L, Merkoçi A. In Situ Plant Virus Nucleic Acid Isothermal Amplification Detection on Gold Nanoparticle-Modified Electrodes. *Anal Chem*. 2019;91(7):4790–6.
84. Arduini F, Micheli L, Moscone D, Palleschi G, Piermarini S, Ricci F, *et al.* Electrochemical biosensors based on nanomodified screen-printed electrodes: Recent applications in clinical analysis. *TrAC - Trends in Analytical Chemistry*. 2016;79:114–26.
85. Zhao L, Rosati G, Piper A, de Carvalho Castro e Silva C, Hu L, Yang Q, *et al.* Laser Reduced Graphene Oxide Electrode for Pathogenic Escherichia coli Detection. *ACS Appl Mater Interfaces*. 2023;15:9033.
86. Kwon HS, Han KC, Hwang KS, Lee JH, Kim TS, Yoon DS, *et al.* Development of a peptide inhibitor-based cantilever sensor assay for cyclic adenosine monophosphate-dependent protein kinase. *Anal Chim Acta*. 2007;585(2):344–9.
87. Cali K, Tuccori E, Persaud KC. Gravimetric biosensors. *Methods Enzymol*. 2020;642:435–68.
88. Pohanka M. Overview of piezoelectric biosensors, immunosensors and DNA sensors and their applications. *Materials*. 2018;11(3).

89. Tang D, Sauceda JC, Lin Z, Ott S, Basova E, Goryacheva I, *et al.* Magnetic nanogold microspheres-based lateral-flow immunodipstick for rapid detection of aflatoxin B2 in food. *Biosens Bioelectron*. 2009;25(2):514–8.
90. Conjugated magnetic beads applications | Cytiva.
91. Zheng Y, Shang N, Haddad PS, Sawan M. A Microsystem for Magnetic Immunoassay Based on Planar Microcoil Array. *IEEE Trans Biomed Circuits Syst*. 2016 ;10(2):477–86.
92. Nair MP, Teo AJT, Li KHH. Acoustic biosensors and microfluidic devices in the decennium: Principles and applications. *Micromachines (Basel)*. 2022;13(1).
93. Zida SI, Lin Y Der, Khung YL. Current Trends on Surface Acoustic Wave Biosensors. *Adv Mater Technol*. 2021;6(6):2001018.
94. Fogel R, Limson J, Seshia AA. Acoustic biosensors. *Essays Biochem*. 2016;60(1):101.
95. Boulware DR, Rolfes MA, Rajasingham R, von Hohenberg M, Qin Z, Taseera K, *et al.* Multisite validation of cryptococcal antigen lateral flow assay and quantification by laser thermal contrast. *Emerg Infect Dis*. 2014;20(1):45–53.
96. Lammers F, Scheper T. Thermal Biosensors in Biotechnology. *Adv Biochem Eng Biotechnol*. 1999;64:35–67.
97. Zheng YH, Hua TC, Xu F. A thermal biosensor based on enzyme reaction. *Conf Proc IEEE Eng Med Biol Soc*. 2005;2005:1909–12.
98. INTERNATIONAL PROGRAMME ON CHEMICAL SAFETY.
99. Paliwal S, Hwang BH, Tsai KY, Mitragotri S. Diagnostic opportunities based on skin biomarkers. Vol. 50, European Journal of Pharmaceutical Sciences. 2013. p. 546–56.
100. Morgan AR, Touchard S, Leckey C, O'Hagan C, Nevado-Holgado AJ, Barkhof F, *et al.* Inflammatory biomarkers in Alzheimer's disease plasma. *Alzheimer's & Dementia*. 2019;44:1–12.
101. Phillips KA, Van Bebber S, Issa AM. Diagnostics and biomarker development: Priming the pipeline. *Nat Rev Drug Discov*. 2006;5(6):463–9.
102. Parolo C, Sena-Torralba A, Bergua JF, Calucho E, Fuentes-Chust C, Hu L, *et al.* Tutorial: design and fabrication of nanoparticle-based lateral-flow immunoassays. *Nat Protoc*. 2020;15(12):3788–816.
103. Seo G, Lee G, Kim MJ, Baek SH, Choi M, Ku KB, *et al.* Rapid Detection of COVID-19 Causative Virus (SARS-CoV-2) in Human Nasopharyngeal Swab Specimens Using Field-Effect Transistor-Based Biosensor. *ACS Nano*. 2020;acsnano.0c02823.
104. WHO Emergency Quality Assessment Mechanism for EVD IVDs PUBLIC REPORT Product: RealStar® Filovirus Screen RT-PCR Kit 1.0.

105. Fuentes-Chust C, Parolo C, Rosati G, Rivas L, Perez-Toralla K, Simon S, *et al.* The Microbiome Meets Nanotechnology: Opportunities and Challenges in Developing New Diagnostic Devices. *Advanced Materials*. 2021;2006104:1–18.
106. Rajpoot M, Sharma AK, Sharma A, Kumar G. Seminars in Cancer Biology Understanding the microbiome: Emerging biomarkers for exploiting the microbiota for personalized medicine against cancer. *Semin Cancer Biol*. 2018;52:1–8.
107. Gohel V, Jones JA, Wehler CJ. Salivary biomarkers and cardiovascular disease: A systematic review. *Clin Chem Lab Med*. 2018;56(9):1432–42.
108. Molinuevo JL, Ayton S, Batrla R, Bednar MM, Bittner T, Cummings J. Current state of Alzheimer's fluid biomarkers . Vol. 136, Acta Neuropathologica. Springer Berlin Heidelberg; 2018. 821–853 p.
109. Yan X, Yang M, Liu J, Gao R, Hu J, Li J, *et al.* Discovery and validation of potential bacterial biomarkers for lung cancer. *Am J Cancer Res*. 2015;5(10):3111–22.
110. Socha E, Koba M, Kośliński P. Amino acid profiling as a method of discovering biomarkers for diagnosis of neurodegenerative diseases. *Amino Acids.* 2019;(0123456789).
111. McDonald D, Hyde E, Debelius JW, Morton JT, Gonzalez A, Ackermann G, *et al.* American Gut: an Open Platform for Citizen Science Microbiome Research. 2018;3(3):1–28.
112. Bashiardes S, Godneva A, Elinav E, Segal E. Towards utilization of the human genome and microbiome for personalized nutrition. *Curr Opin Biotechnol*. 2018;51:57–63.
113. Zmora N, Zeevi D, Korem T, Segal E, Elinav E. Taking it Personally: Personalized Utilization of the Human Microbiome in Health and Disease. *Cell Host Microbe*. 2016;19(1):12–20.
114. Mach KE, Wong PK, Liao JC. Biosensor diagnosis of urinary tract infections: A path to better treatment? *Trends Pharmacol Sci*. 2011;32(6):330–6.
115. Castelli FA, Rosati G, Moguet C, Fuentes C, Marrugo-Ramírez J, Lefebvre T, *et al.* Metabolomics for personalized medicine: the input of analytical chemistry from biomarker discovery to point-of-care tests. *Anal Bioanal Chem*. 2022;414(2):759–89.
116. Težak Ž, Kondratovich, Marina V Mansfield E. US FDA and Personalized Medicine: *In vitro* Diagnostic Regulatory Perspective. *Per Med*. 2010;7(5):517–30.
117. Dai Z, Coker OO, Nakatsu G, Wu WKK, Zhao L, Chen Z, *et al.* Multi-cohort analysis of colorectal cancer metagenome identified altered bacteria across populations and universal bacterial markers. *Microbiome*. 2018;6(1):70.
118. Quince C, Walker AW, Simpson JT, Loman NJ, Segata N. Shotgun metagenomics, from sampling to analysis. *Nat Biotechnol*. 2017;35(9):833–44.
119. Thomas AM, Manghi P, Asnicar F, Pasolli E, Armanini F, Zolfo M, *et al.* Metagenomic analysis of colorectal cancer datasets identifies cross-cohort microbial diagnostic signatures and a link with choline degradation. *Nat Med*. 2019;25(4):667–78.

120. Biteen JS, Blainey PC, Cardon ZG, Chun M, Church GM, Dorrestein PC, *et al.* Tools for the microbiome: Nano and beyond. *ACS Nano*. 2016;10(1):6–37.
121. Callewaert C, Quinn RA, Debelius J, Thompson LR, Kosciolek T, Aksenov A, *et al.* Best practices for analysing microbiomes. *Nat Rev Microbiol*. 2018;16(7):410–22.
122. Raes J. Microbiome-based companion diagnostics: No longer science fiction? *Gut*. 2016;65(6):896–7.
123. Holmes E, Li J V., Athanasiou T, Ashrafian H, Nicholson JK. Understanding the role of gut microbiome-host metabolic signal disruption in health and disease. *Trends Microbiol*. 2011;19(7):349–59.
124. Hall EK, Bernhardt ES, Bier RL, Bradford MA, Boot CM, Cotner JB, *et al.* Understanding how microbiomes influence the systems they inhabit. *Nat Microbiol*. 2018;3(9):977–82.
125. Donohue TJ, Pollard KS, Green JL, Knight R, Cho MK, Northen TR, *et al.* Toward a Predictive Understanding of Earth's Microbiomes to Address 21st Century Challenges. *mBio*. 2016;7(3):1–16.
126. Cohan D. After the Integrative Human Microbiome Project, what's next for the microbiome community? *Nature*. 2019;569(599):169–73.
127. Baquero F, Nombela C. The microbiome as a human organ. *Clinical Microbiology and Infection*. 2012;18(SUPPL. 4):2–4.
128. Biochemistry C, Wa M, Hospital FS, Pathirana WPNGW, Chubb SAP, Gillett MJ, *et al.* Faecal Calprotectin. *Clin Biochem Rev*. 2018;39(3):77–90.
129. Wondfo SARS-CoV-2 Antibody Test (Lateral Flow Method) - wondfo.
130. Correia-neves M, Fröberg G, Korshun L, Viegas S, Vaz P, Ramanlal N, *et al.* Biomarkers for tuberculosis : the case for lipoarabinomannan. *ERJ Open Res*. 2019;5:1–13.
131. Shah M, Hanrahan C, Wang ZY, Dendukuri N, Lawn SD, Denkinger CM, *et al.* Lateral flow urine lipoarabinomannan assay for detecting active tuberculosis in HIV-positive adults. *Cochrane Database of Systematic Reviews*. 2016;2016(5):CD011420.
132. Takahashi MK, Tan X, Dy AJ, Braff D, Akana RT, Furuta Y, *et al.* A low-cost paper-based synthetic biology platform for analyzing gut microbiota and host biomarkers. *Nat Commun*. 2018;9(3347):1–12.
133. Leng J, Proudman C, Darby A, Blow F, Townsend N, Miller A, *et al.* Exploration of the Fecal Microbiota and Biomarker Discovery in Equine Grass Sickness. *J Proteome Res*. 2018;17(3):1120–8.
134. Annaházi A, Ábrahám S, Farkas K, Rosztóczy A, Inczefi O, Földesi I, *et al.* A pilot study on faecal MMP-9: A new noninvasive diagnostic marker of colorectal cancer. *Br J Cancer*. 2016;114(7):787–92.

135. Farrokhi V, Nemati R, Nichols FC, Yao X, Anstadt E, Fujiwara M, *et al.* Bacterial lipodipeptide, Lipid 654, is a microbiome- associated biomarker for multiple sclerosis. *Clinical and Translational Imunology*. 2013;2(11):1–7.
136. Yu J, Feng Q, Wong SH, Zhang D, Yi Liang Q, Qin Y, *et al.* Metagenomic analysis of faecal microbiome as a tool towards targeted non-invasive biomarkers for colorectal cancer. *Gut*. 2017;66(1):70–8.
137. Clària J, Moreau R, Fenaille F, Amorós A, Junot C, Gronbaek H, *et al.* Orchestration of Tryptophan-Kynurenine Pathway, Acute Decompensation, and Acute-on-Chronic Liver Failure in Cirrhosis. *Hepatology*. 2019;69(4):1686–701.
138. Oh TG, Kim SM, Caussy C, Fu T, Guo J, Bassirian S, *et al.* A Universal Gut-Microbiome-Derived Signature Predicts Cirrhosis. *Cell Metab*. 2020;(June).
139. Kuntz TM, Gilbert JA. Introducing the Microbiome into Precision Medicine. *Trends Pharmacol Sci*. 2016;38:81–91.
140. Petrosino JF. The microbiome in precision medicine: The way forward. *Genome Med*. 2018;10(1):10–3.
141. Dietert RR, Silbergeld EK. Biomarkers for the 21st Century: Listening to the Microbiome. 2015;144(2):208–16.
142. Wang J, Jia H. Metagenome-wide association studies: fine-mining the microbiome. *Nat Rev Microbiol*. 2016;14:508.
143. Marques L, Costa B, Pereira M, Silva A, Santos J, Saldanha L, *et al.* Advancing Precision Medicine: A Review of Innovative In Silico Approaches for Drug Development, Clinical Pharmacology and Personalized Healthcare. *Pharmaceutics 2024, Vol 16, Page 332*. 2024;16(3):332.
144. Beck H, Härter M, Haß B, Schmeck C, Baerfacker L. Small molecules and their impact in drug discovery: A perspective on the occasion of the 125th anniversary of the Bayer Chemical Research Laboratory. *Drug Discov Today*. 2022;27(6):1560–74.
145. Libertucci J, Young VB. The role of the microbiota in infectious diseases. *Nat Microbiol*. 2019;4(1):35–45.
146. Qiu S, Cai Y, Yao H, Lin C, Xie Y, Tang S, *et al.* Small molecule metabolites: discovery of biomarkers and therapeutic targets. *Signal Transduction and Targeted Therapy 2023 8:1*. 2023;8(1):1–37.
147. Martin CR, Osadchiy V, Kalani A, Mayer EA. The Brain-Gut-Microbiome Axis. *Cmgh*. 2018;6(2):133–48.
148. Coureuil M, Lécuyer H, Bourdoulous S, Nassif X. A journey into the brain: Insight into how bacterial pathogens cross blood-brain barriers. *Nat Rev Microbiol*. 2017;15(3):149–59.

149. Moreno MDL, Cebolla Á, Munõz-Suano A, Carrillo-Carrion C, Comino I, Pizarro Á, *et al.* Detection of gluten immunogenic peptides in the urine of patients with coeliac disease reveals transgressions in the gluten-free diet and incomplete mucosal healing. *Gut*. 2017;66(2):250–7.
150. Louis P, Hold GL, Flint HJ. The gut microbiota, bacterial metabolites and colorectal cancer. *Nat Rev Microbiol*. 2014;12(10):661–72.
151. Contorno S, Darienzo RE, Tannenbaum R. Evaluation of aromatic amino acids as potential biomarkers in breast cancer by Raman spectroscopy analysis. *Sci Rep*. 2021;11(1):1–9.
152. Wirbel J, Pyl PT, Kartal E, Zych K, Kashani A, Milanese A, *et al.* Meta-analysis of fecal metagenomes reveals global microbial signatures that are specific for colorectal cancer. *Nat Med*. 2019;25(4):679–89.
153. Brunkwall L, Orho-Melander M. The gut microbiome as a target for prevention and treatment of hyperglycaemia in type 2 diabetes: from current human evidence to future possibilities. *Diabetologia*. 2017;60(6):943–51.
154. Heintz-Buschart A, May P, Laczny CC, Lebrun LA, Bellora C, Krishna A, *et al.* Integrated multi-omics of the human gut microbiome in a case study of familial type 1 diabetes. *Nat Microbiol*. 2016;2(1):1–12.
155. Duranton F, Cohen G, De Smet R, Rodriguez M, Jankowski J, Vanholder R, *et al.* Normal and pathologic concentrations of uremic toxins. *Journal of the American Society of Nephrology*. 2012;23(7):1258–70.
156. Tsilimigras MCB, Fodor A, Jobin C. Carcinogenesis and therapeutics: The microbiota perspective. *Nat Microbiol*. 2017;2:1–10.
157. Misra BB, Langefeld C, Olivier M, Cox LA. Integrated omics: tools, advances and future approaches. *J Mol Endocrinol*. 2018;(2016):R21–45.
158. National T. Environmental Chemicals, the Human Microbiome, and Health Risk: A Research Strategy. Environmental Chemicals, the Human Microbiome, and Health Risk: A Research Strategy. 2018. 1–109 p.
159. Ahmed A, Rushworth J V., Hirst NA, Millner PA. Biosensors for whole-cell bacterial detection. *Clin Microbiol Rev*. 2014;27(3):631–46.
160. Rosati G, Cunego A, Fracchetti F, Del Casale A, Scaramuzza M, De Toni A, *et al.* Inkjet printed interdigitated biosensor for easy and rapid detection of bacteriophage contamination: A preliminary study for milk processing control applications. *Chemosensors*. 2019;7(8):1–13.
161. Chałupniak A, Merkoçi A. Toward integrated detection and graphene-based removal of contaminants in a lab-on-a-chip platform. *Nano Res*. 2017;10(7):2296–310.

162. Hudson M, Stuchinskaya T, Ramma S, Patel J, Sievers C, Goetz S, *et al.* Drug screening using the sweat of a fingerprint: Lateral flow detection of' " 9 -tetrahydrocannabinol, cocaine, opiates and amphetamine. *J Anal Toxicol*. 2019;43(2):88–95.
163. Chauvin A, Boisvert FM. Clinical Proteomics in Colorectal Cancer, a Promising Tool for Improving Personalised Medicine. *Proteomes*. 2018;6(4):49.
164. Blau N, Van Spronsen FJ, Levy HL. Phenylketonuria. *The Lancet*. 2010;376(9750):1417–27.
165. Arroyo V, Moreau R, Kamath PS, Jalan R, Ginès P, Nevens F, *et al.* Acute-on-chronic liver failure in cirrhosis. *Nature Reviews Disease Primers 2016 2:1*. 2016;2(1):1–18.
166. Liu G, Wang X, Fan X, Luo X. Metabolomics profiles in acute-on-chronic liver failure: Unveiling pathogenesis and predicting progression. *Front Pharmacol*. 2022;13:1–10.
167. Steventon GB, Mitchell SC. Phenylalanine hydroxylase: A biomarker of disease susceptibility in Parkinson's disease and Amyotrophic lateral sclerosis. *Med Hypotheses*. 2018;118:29–33.
168. Zhong B, Qin X, Xu H, Liu L, Li L, Li Z, *et al.* Interindividual- and blood-correlated sweat phenylalanine multimodal analytical biochips for tracking exercise metabolism. *Nat Commun*. 2024;15(1):1–14.
169. Oliva C, Arias A, Ruiz M, Pujol A, Garrabou G, Canto-Santos J, *et al.* Fibroblast phenylalanine concentration as a surrogate biomarker of cellular number. *J Chromatogr B Analyt Technol Biomed Life Sci*. 2023;1226:123787.
170. Akram M, Daniyal M, Ali A, Zainab R, Muhammad Ali Shah S, Munir N, *et al.* Role of Phenylalanine and Its Metabolites in Health and Neurological Disorders. In: Synucleins - Biochemistry and Role in Diseases. IntechOpen; 2020.
171. Clària J, Moreau R, Fenaille F, Amorós A, Junot C, Gronbaek H, *et al.* Orchestration of Tryptophan-Kynurenine Pathway, Acute Decompensation, and Acute-on-Chronic Liver Failure in Cirrhosis. *Hepatology*. 2019;69(4):1686–701.
172. Tessari P, Vettore M, Millioni R, Puricelli L, Orlando R. Effect of liver cirrhosis on phenylalanine and tyrosine metabolism. Vol. 13, Current Opinion in Clinical Nutrition and Metabolic Care. Curr Opin Clin Nutr Metab Care; 2010. p. 81–6.
173. Moreau R, Gao B, Papp M, Bañares R, Kamath PS. Acute-on-chronic liver failure: A distinct clinical syndrome. *J Hepatol*. 2021;75:S27–35.
174. Arroyo V. Acute-on-Chronic Liver Failure: Definition, Diagnosis, and Clinical Characteristics. 2016; 7;456-467
175. Trebicka J, Amoros A, Pitarch C, Titos E, Alcaraz-Quiles J, Schierwagen R, *et al.* Addressing profiles of systemic inflammation across the different clinical phenotypes of acutely decompensated cirrhosis. *Front Immunol*. 2019;10.
176. Xiong QF, Xiong T, Huang P, Zhong YD, Wang HL, Yang YF. Early predictors of acute hepatitis B progression to liver failure. *PLoS One*. 2018;13(7).

177. Chen EQ, Zeng F, Zhou LY, Tang H. Early warning and clinical outcome prediction of acute-onchronic hepatitis B liver failure. *World J Gastroenterol.* 2015;21(42):11964–73.
178. Hernaez R, Solà E, Moreau R, Ginès P. Acute-on-chronic liver failure: an update.
179. Kumar A, Saraswat VA. Hepatitis E and Acute-on-Chronic Liver Failure. *J Clin Exp Hepatol*. 2013;3(3):225–30.
180. Qin N, Yang F, Li A, Prifti E, Chen Y, Shao L, *et al.* Alterations of the human gut microbiome in liver cirrhosis. *Nature*. 2014;513(7516):59–64.
181. Woodhouse CA, Patel VC, Singanayagam A, Shawcross DL. Review article: the gut microbiome as a therapeutic target in the pathogenesis and treatment of chronic liver disease. *Aliment Pharmacol Ther*. 2018;47(2):192–202.
182. Microb-Predict - MICROB-PREDICT.
183. Miné, Manuèle; Chen J min, Desguerre I, Marchant D, Abitbol M, Ricquier D, Lonlay P De, *et al.* The PAH Gene, Phenylketonuria, and a Paradigm Shift. *Hum Mutation*. 2007;28(9):831–45.
184. Hasan Mohajeri M, La Fata G, Steinert RE, Weber P. Relationship between the gut microbiome and brain function. *Nutr Rev*. 2018;76(7):481–96.
185. How do health care providers diagnose phenylketonuria (PKU)? | NICHD - Eunice Kennedy Shriver National Institute of Child Health and Human Development.
186. Centerwall SA, Centerwall WR. The discovery of phenylketonuria: The story of a young couple, two retarded children, and a scientist. *Pediatrics*. 2000;105(1 I):89–103.
187. GUTHRIE R, SUSI A. A Simple Phenylalanine Method for Detecting Phenylketonuria in Large Populations of Newborn Infants. *Pediatrics*. 1963;32:338–43.
188. Brosco JP, Paul DB. The political history of pku: Reflections on 50 years of newborn screening. *Pediatrics*. 2013;132(6):987–9.
189. Groselj U, Tansek MZ, Battelino T. Fifty years of phenylketonuria newborn screening - A great success for many, but what about the rest? *Mol Genet Metab*. 2014;113(1):8–10.
190. Coene KLM, Timmer C, Goorden SMI, ten Hoedt AE, Kluijtmans LAJ, Janssen MCH, *et al*. Monitoring phenylalanine concentrations in the follow-up of phenylketonuria patients: An inventory of pre-analytical and analytical variation. *JIMD Rep*. 2021;58(1):70–9.
191. van Spronsen FJ, van Wegberg AM, Ahring K, Bélanger-Quintana A, Blau N, Bosch AM, *et al.* Key European guidelines for the diagnosis and management of patients with phenylketonuria. *Lancet Diabetes Endocrinol*. 2017;5(9):743–56.
192. Hillert A, Anikster Y, Belanger-Quintana A, Burlina A, Burton BK, Carducci C, *et al*. The Genetic Landscape and Epidemiology of Phenylketonuria. *Am J Hum Genet*. 2020;107(2):234–50.

193. MacLeod EL, Ney DM. Nutritional management of phenylketonuria. *Annales Nestle*. 2010;68(2):58–69.
194. Gregory CO, Yu C, Singh RH. Blood phenylalanine monitoring for dietary compliance among patients with phenylketonuria: Comparison of methods. *Genetics in Medicine*. 2007;9(11):761–5.
195. Chakravarty R, Goel S, Cai W. Nanobody: The "magic bullet" for molecular imaging? *Theranostics*. 2014;4(4):386–98.
196. Zhou W, Jimmy Huang PJ, Ding J, Liu J. Aptamer-based biosensors for biomedical diagnostics. *Analyst*. 2014;139(11):2627–40.
197. Vashist SK, Luong JHT. Chapter 17 - Immunoassays: Future Prospects and Possibilities. Handbook of Immunoassay Technologies. 2018;455–66.
198. Li Z, Yi Y, Luo X, Xiong N, Liu Y, Li S, *et al.* Development and clinical application of a rapid IgM-IgG combined antibody test for SARS-CoV-2 infection diagnosis. *J Med Virol*. 2020;92(9):1518–24.
199. Ou X, Liu Y, Lei X, Li P, Mi D, Ren L, *et al.* Characterization of spike glycoprotein of SARS-CoV-2 on virus entry and its immune cross-reactivity with SARS-CoV. *Nat Commun*. 2020;11(1620):1–12.
200. Sande MG, Rodrigues JL, Ferreira D, Silva CJ, Rodrigues LR. Novel biorecognition elements against pathogens in the design of state-of-the-art diagnostics. *Biosensors (Basel)*. 2021;11(11).
201. Buglak AA, Samokhvalov A V., Zherdev A V., Dzantiev BB. Methods and applications of in silico aptamer design and modeling. *Int J Mol Sci*. 2020;21(22):1–25.
202. Sanford AA, Manuel BA, Romero-Reyes MA, Heemstra JM. Combating small molecule environmental contaminants: detection and sequestration using functional nucleic acids. *Chem Sci*. 2022;13(26):7670–84.
203. Chieng A, Wan Z, Wang S. Recent Advances in Real-Time Label-Free Detection of Small Molecules. *Biosensors (Basel)*. 2024;14(2).
204. Liang YF, Yang JY, Shen YD, Xu ZL, Wang H. A breakthrough of immunoassay format for hapten: recent insights into noncompetitive immunoassays to detect small molecules. *Crit Rev Food Sci Nutr*. 2024;14:1–11.
205. Bai Y, Wang Y, Li Q, Dou L, Liu M, Shao S, *et al.* Binding affinity-guided design of a highly sensitive noncompetitive immunoassay for small molecule detection. *Food Chem*. 2021;351:129270.
206. Ruscito A, DeRosa MC. Small-Molecule Binding Aptamers: Selection Strategies, Characterization, and Applications. *Front Chem*. 2016;4:14.

207. Prante M, Segal E, Scheper T, Bahnemann J, Walter J. Aptasensors for Point-of-Care Detection of Small Molecules. *Biosensors (Basel)*. 2020;10(9).
208. Sun H, Zhu X, Lu PY, Rosato RR, Tan W, Zu Y. Oligonucleotide aptamers: New tools for targeted cancer therapy. *Mol Ther Nucleic Acids*. 2014;3(April):e182.
209. Ganji A, Islami M, Ejtehadifar M, Zarei-Mehrvarz E, Darvish M. Nanobody and aptamer as targeting moiety against bacterial toxins. *Reviews in Medical Microbiology*. 2019;30(3):183–90.
210. Bauer M, Strom M, Hammond DS, Shigdar S. Anything you can do, i can do better: Can aptamers replace antibodies in clinical diagnostic applications? *Molecules*. 2019;24(23):1–13.
211. Marimuthu C, Tang TH, Tominaga J, Tan SC, Gopinath SCB. Single-stranded DNA (ssDNA) production in DNA aptamer generation. *Analyst*. 2012;137(6):1307–15.
212. Tuerk C, Gold L. Systematic Evolution of Ligands by Exponential Enrichment: RNA Ligands to Bacteriophage T4 DNA Polymerase. *Science (1979)*. 1990;249(4968):505–10.
213. Sun H, Zhu X, Lu PY, Rosato RR, Tan W, Zu Y. Oligonucleotide Aptamers: New Tools for Targeted Cancer Therapy. 2014;
214. Srinivasan S, Ranganathan V, McConnell EM, Murari BM, DeRosa MC. Aptamer-based colorimetric and lateral flow assay approaches for the detection of toxic metal ions, thallium(i) and lead(ii). *RSC Adv*. 2023;13(29):20040–9.
215. Thiviyanathan V, G. Gorenstein D. Aptamers and the Next Generation of Diagnostic Reagents. *Proteomics Clin Appl*. 2012;6(0):563–73.
216. Keefe AD, Cload ST. SELEX with modified nucleotides. *Curr Opin Chem Biol*. 2008;12(4):448–56.
217. Liu J, Lu Y. Preparation of aptamer-linked gold nanoparticle purple aggregates for colorimetric sensing of analytes. *Nat Protoc*. 2006;1(1):246–52.
218. Ohno Y, Maehashi K, Matsumoto K. Label-free biosensors based on aptamer-modified graphene field-effect transistors. *J Am Chem Soc*. 2010;132(51):18012–3.
219. Schüling T, Eilers A, Scheper T, Walter J. Aptamer-based lateral flow assays. *AIMS Bioeng*. 2018;5(2):78–102.
220. Sun J, Guo A, Zhang Z, Guo L, Xie J. A conjugated aptamer-gold nanoparticle fluorescent probe for highly sensitive detection of rHuEPO-α. *Sensors*. 2011;11(11):10490–501.
221. Seferos DS, Prigodich AE, Giljohann DA, Patel PC, Mirkin CA. Polyvalent DNA-Nanoparticle Conjugates Stabilize Nucleic Acids. *Spherical Nucleic Acids: Volume 1*. 2021;1:425–35.
222. Komarova N, Kuznetsov A. Inside the black box: What makes Selex better? *Molecules*. 2019;24(19):3598.

223. Vorobyeva MA, Davydova AS, Vorobjev PE, Pyshnyi D V., Venyaminova AG. Key aspects of nucleic acid library design for *in vitro* selection. *Int J Mol Sci*. 2018;19(2).
224. Stoltenburg R, Nikolaus N, Strehlitz B. Capture-SELEX: Selection of DNA aptamers for aminoglycoside antibiotics. *J Anal Methods Chem*. 2012;1(1).
225. Tolle F, Wilke J, Wengel J, Mayer G. By-product formation in repetitive PCR amplification of DNA libraries during SELEX. *PLoS One*. 2014;9(12):1–12.
226. Ellington AD, Szostak JW. *In vitro* selection of RNA molecules that bind specific ligands. *Nature*. 1990;346(6287):818–22.
227. Legiewicz M, Lozupone C, Knight R, Yarus M. Size, constant sequences, and optimal selection. *Rna*. 2005;11(11):1701–9.
228. Hu J, Easley CJ. A simple and rapid approach for measurement of dissociation constants of DNA aptamers against proteins and small molecules via automated microchip electrophoresis. *Analyst*. 2011;136(17):3461–8.
229. Schindler P, Robinson RA, Bates RG. Solubility of tris(hydroxymethyl)aminomethane in water-methanol solvent mixtures and medium effects in the dissociation of the protonated base. *J Res Natl Bur Stand A Phys Chem*. 1968;72A(2):141.
230. Qi S, Duan N, Khan IM, Dong X, Zhang Y, Wu S, *et al.* Strategies to manipulate the performance of aptamers in SELEX, post-SELEX and microenvironment. *Biotechnol Adv*. 2022;55.
231. Kohlberger M, Gadermaier G. SELEX: Critical factors and optimization strategies for successful aptamer selection. *Biotechnol Appl Biochem*. 2022;69(5):1771.
232. Hamula CLA, Peng H, Wang Z, Newbigging AM, Tyrrell GJ, Li XF, *et al.* The Effects of SELEX Conditions on the Resultant Aptamer Pools in the Selection of Aptamers Binding to Bacterial Cells. *J Mol Evol*. 2015;81(5–6):194–209.
233. Vorobyeva MA, Davydova AS, Vorobjev PE, Pyshnyi D V., Venyaminova AG. Key Aspects of Nucleic Acid Library Design for *in Vitro* Selection. *International Journal of Molecular Sciences 2018, Vol 19, Page 470*. 2018;19(2):470.
234. Frackman BS, Kobs G, Simpson D, Storts D, Corporation P. Betaine and DMSO: Enhancing Agents for PCR. *Promega Notes*. 1998;65(65):9–12.
235. PCR - Variations to the System | ABM Inc.
236. Yeoh TS, Anna A, Tang TH, Citartan M. Development of an optimization pipeline of asymmetric PCR towards the generation of DNA aptamers: a guide for beginners. *World J Microbiol Biotechnol*. 2022;38(2).
237. Rotherham LS, Maserumule C, Dheda K, Theron J, Khati M. Selection and Application of ssDNA Aptamers to Detect Active TB from Sputum Samples. *PLoS One*. 2012 ;7(10).

238. Gowland R, Gowers DM. A Lambda-Exonuclease SELEX Method for Generating Aptamers to Bacterial Targets. *Methods Mol Biol*. 2023;2633:145–61.
239. Liu Q, Zhang W, Chen S, Zhuang Z, Zhang Y, Jiang L, *et al.* SELEX tool: A novel and convenient gel-based diffusion method for monitoring of aptamer-target binding. *J Biol Eng*. 2020;14(1):1–13.
240. Darmostuk M, Rimpelova S, Gbelcova H, Ruml T. Current approaches in SELEX: An update to aptamer selection technology. *Biotechnol Adv*. 2014;33(6):1141–61.
241. Tolle F, Mayer G. Preparation of SELEX samples for next-generation sequencing. *Methods in Molecular Biology*. 2016;1380:77–84.
242. Fredlake CP, Barron AE. Advantages and limitations of next- generation sequencing technologies : A comparison of electrophoresis and non-electrophoresis methods. 2008;4618–26.
243. Guo L, Song Y, Yuan Y, Chen J, Liang H, Guo F, *et al.* Identification of nucleic acid aptamers against lactate dehydrogenase via SELEX and high-throughput sequencing. *Anal Bioanal Chem*. 2021;413(17):4427–39.
244. Tenaglia E, Guiducci C. Selection of structure-switching DNA aptamers binding soluble small molecules and SPR validation of enrichment. In: Methods in Molecular Biology. Humana Press Inc.; 2018. p. 183–97.
245. Hamidi SV, Perreault J. Simple in-vitro single stranded linear and circular DNA preparation and validation via SELEX using phosphor-derived modifications. 2023;1–25.
246. Stewart KD, Tan W, Park JY. Aptamer selection for detecting molecular target using CELL-SELEX (systematic evolution of ligands by exponential enrichment) technology. *Methods in Molecular Biology*. 2019;2054:223–41.
247. Zhao Y, Li AZ, Liu J. Capture-SELEX for Chloramphenicol Binding Aptamers for Labeled and Label-Free Fluorescence Sensing. *Environment & Health*. 2023;1(2):102–9.
248. Liu J, Stormo GD. Combining SELEX with quantitative assays to rapidly obtain accurate models of protein–DNA interactions. *Nucleic Acids Res*. 2005;33(17):e141.
249. Guan J, He K, Gunasekaran S. Selection of ssDNA aptamer using GO-SELEX and development of DNA nanostructure-based electrochemical aptasensor for penicillin. *Biosens Bioelectron X*. 2022;12:100220.
250. Stoltenburg R, Nikolaus N, Strehlitz B. Capture-SELEX: Selection of DNA aptamers for aminoglycoside antibiotics. *J Anal Methods Chem*. 2012;1(1).
251. Stoltenburg R, Reinemann C, Strehlitz B. FluMag-SELEX as an advantageous method for DNA aptamer selection. *Anal Bioanal Chem*. 2005;383(1):83–91.
252. Boussebayle A, Groher F, Suess B. RNA-based Capture-SELEX for the selection of small molecule-binding aptamers. *Methods*. 2019;161:10–5.

253. Mendonsa SD, Bowser MT. *In Vitro* Evolution of Functional DNA Using Capillary Electrophoresis. *J Am Chem Soc*. 2004;126(1):20–1.
254. Volpi N. Separation of flavonoids and phenolic acids from propolis by capillary zone electrophoresis. *Electrophoresis*. 2004;25(12):1872–8.
255. Yang J, Lu X, Chen M, Tang C, Wei Z, Liu Y, *et al.* Non-immobilized GO-SELEX screening of aptamers against cyclosporine A and its application in a AuNPs colorimetric aptasensor. *Analytical Methods*. 2024;16(2):227–36.
256. Miller PS, Evans JP. SELEX screen for zona pellucida-binding DNA aptamers. *Biol Reprod*. 2018;99(5):903–4.
257. Challa S, Tzipori S, Sheoran A. Selective Evolution of Ligands by Exponential Enrichment to Identify RNA Aptamers against Shiga Toxins. *J Nucleic Acids*. 2014;2014.
258. Jauset-Rubio M, Botero ML, Skouridou V, Aktas GB, Svobodova M, Bashammakh AS, *et al.* One-Pot SELEX: Identification of Specific Aptamers against Diverse Steroid Targets in One Selection. *ACS Omega*. 2019;4(23):20188–96.
259. Cube Biotech. (n.d.). PureCube Maleimide Activated MagBeads.
260. Scoville DJ, Uhm TKB, Shallcross JA, Whelan RJ. Selection of DNA Aptamers for Ovarian Cancer Biomarker CA125 Using One-Pot SELEX and High-Throughput Sequencing. *J Nucleic Acids*. 2017;2017.
261. Zhu Y, Hart GW. Dual-specificity RNA aptamers enable manipulation of target-specific O-GlcNAcylation and unveil functions of O-GlcNAc on β-catenin. *Cell*. 2023;186(2):428-445.e27.
262. Park J, Ban C. Development of a one-shot dual aptamer-based fluorescence nanosensor for rapid, sensitive, and label-free detection of periostin. *Scientific Reports 2023 13:1*. 2023;13(1):1–14.
263. Zamora Gálvez A. Nanobiosensors for diagnostics applications. 2017.
264. Roda A, Michelini E, Zangheri M, Di Fusco M, Calabria D, Simoni P. Smartphone-based biosensors: A critical review and perspectives. *TrAC Trends in Analytical Chemistry*. 2016;79:317–25.
265. Quesada-González D, Merkoçi A. Mobile phone-based biosensing: An emerging "diagnostic and communication" technology. *Biosens Bioelectron*. 2017;92:549–62.
266. Hristov DR, Rodriguez-Quijada C, Gomez-Marquez J, Hamad-Schifferli K. Designing paper-based immunoassays for biomedical applications. *Sensors (Switzerland)*. 2019;19(3).
267. Van Amerongen A, Veen J, Arends HA, Koets M. Lateral flow immunoassays. *Handbook of Immunoassay Technologies: Approaches, Performances, and Applications*. 2018;157–82.
268. Koczula KM, Gallotta A. Lateral flow assays. *Essays Biochem*. 2016;60(1):111–20.
269. NanoComposix. Lateral Flow Assay Development Guide. *nanoComposix*. 2016:1–37.

270. Parolo C, de la Escosura-Muñiz A, Merkoçi A. Enhanced lateral flow immunoassay using gold nanoparticles loaded with enzymes. *Biosens Bioelectron*. 2013;40(1):412–6.
271. De La Escosura-Muñiz A, Parolo C, Merkoi A. Immunosensing using nanoparticles. Vol. 13, Materials Today. Elsevier; 2010. p. 24–34.
272. Taton TA. Preparation of Gold Nanoparticle–DNA Conjugates. *Curr Protoc Nucleic Acid Chem*. 2002;9(1):1–12.
273. López-Marzo AM, Pons J, Blake DA, Merkoçi A. High sensitive gold-nanoparticle based lateral flow Immunodevice for Cd2+ detection in drinking waters. *Biosens Bioelectron*. 2013;47:190–8.
274. Quesada-González D, Baiocco A, Martos AA, de la Escosura-Muñiz A, Palleschi G, Merkoçi A. Iridium oxide (IV) nanoparticle-based electrocatalytic detection of PBDE. *Biosens Bioelectron*. 2019;127:150–4.
275. Yen CW, De Puig H, Tam JO, Gómez-Márquez J, Bosch I, Hamad-Schifferli K, *et al.* Multicolored silver nanoparticles for multiplexed disease diagnostics: Distinguishing dengue, yellow fever, and Ebola viruses. *Lab Chip*. 2015;15(7):1638–41.
276. Ko YJ, Maeng JH, Ahn Y, Hwang SY, Cho NG, Lee SH. Real-time immunoassay with a PDMS-glass hybrid microfilter electro-immunosensing chip using nanogold particles and silver enhancement. *Sens Actuators B Chem*. 2008;132(1):327–33.
277. Anfossi L, Di Nardo F, Cavalera S, Giovannoli C, Spano G, Speranskaya ES, *et al.* A lateral flow immunoassay for straightforward determination of fumonisin mycotoxins based on the quenching of the fluorescence of CdSe/ZnS quantum dots by gold and silver nanoparticles. *Microchimica Acta*. 2018 ;185(94):1–10.
278. Renzi E, Piper A, Nastri F, Merkoçi A, Lombardi A. An Artificial Miniaturized Peroxidase for Signal Amplification in Lateral Flow Immunoassays. *Small*. 2023;19(51):2207949.
279. Salminen T, Juntunen E, Talha SM, Pettersson K. High-sensitivity lateral flow immunoassay with a fluorescent lanthanide nanoparticle label. *J Immunol Methods*. 2019;465:39–44.
280. Song S, Liu N, Zhao Z, Njumbe Ediage E, Wu S, Sun C, *et al.* Multiplex lateral flow immunoassay for mycotoxin determination. *Anal Chem*. 2014;86(10):4995–5001.
281. Foubert A, Beloglazova N V., Gordienko A, Tessier MD, Drijvers E, Hens Z, *et al.* Development of a Rainbow Lateral Flow Immunoassay for the Simultaneous Detection of Four Mycotoxins. *J Agric Food Chem*. 2017;65(33):7121–30.
282. Ji T, Xu X, Wang X, Zhou Q, Ding W, Chen B, *et al.* Point of care upconversion nanoparticles-based lateral flow assay quantifying myoglobin in clinical human blood samples. *Sens Actuators B Chem*. 2019;282:309–16.

283. Kihyeun K, Eun-Jung J, Ki Joong L, Jiyoon P, Gun Young J, Shin YB, *et al.* Gold nanocap-supported upconversion nanoparticles for fabrication of a solid-phase aptasensor to detect ochratoxin A. *Biosens Bioelectron*. 2020;150:111885.
284. Calucho E, Álvarez-Diduk R, Piper A, Rossetti M, Nevanen TK, Merkoçi A. Reduced graphene oxide electrodes meet lateral flow assays: A promising path to advanced point-of-care diagnostics. *Biosens Bioelectron*. 2024;258:116315.
285. Hassan AHA, Bergua JF, Morales-Narváez E, Mekoçi A. Validity of a single antibody-based lateral flow immunoassay depending on graphene oxide for highly sensitive determination of E. coli O157:H7 in minced beef and river water. *Food Chem*. 2019;297:124965.
286. Álvarez-DIduk R, Orozco J, Merkoçi A. Paper strip-embedded graphene quantum dots: a screening device with a smartphone readout. *Scientific Reports 2017 7:1*. 2017;7(1):1–9.
287. Wang W, Yang X, Rong Z, Tu Z, Zhang X, Gu B, *et al.* Introduction of graphene oxide-supported multilayer-quantum dots nanofilm into multiplex lateral flow immunoassay: A rapid and ultrasensitive point-of-care testing technique for multiple respiratory viruses. *Nano Res*. 2023;16(2):3063.
288. Dalirirad S, Han D, Steckl AJ. Aptamer-Based Lateral Flow Biosensor for Rapid Detection of Salivary Cortisol. *ACS Omega*. 2020;5(51):32890–8.
289. Kaiser L, Weisser J, Kohl M, Deigner HP. Small molecule detection with aptamer based lateral flow assays: Applying aptamer-C-reactive protein cross-recognition for ampicillin detection. *Sci Rep*. 2018;8(1):6–15.
290. Shen K, Hu X, Sun L, Han C, Yang J. Development of a Lateral Flow Strip with a Positive Readout for the On-Site Detection of Aflatoxin B1. *Molecules*. 2022;27(15).
291. Vijitvarasan P, Cheunkar S, Oaew S. A point-of-use lateral flow aptasensor for naked-eye detection of aflatoxin B1. *Food Control*. 2022;134:108767.
292. Wu Z, Shen H, Hu J, Fu Q, Yao C, Yu S, *et al.* Aptamer-based fluorescence-quenching lateral flow strip for rapid detection of mercury (II) ion in water samples. *Anal Bioanal Chem*. 2017;409(22):5209–16.
293. Jing L, Xie CY, Li QQ, Yao HF, Yang MQ, Li H, *et al.* A Sandwich-type Lateral Flow Strip Using a Split, Single Aptamer for Point-of-Care Detection of Cocaine. *J Anal Test*. 2022;6(2):120–8.
294. Mermiga E, Pagkali V, Kokkinos C, Economou A. An Aptamer-Based Lateral Flow Biosensor for Low-Cost, Rapid and Instrument-Free Detection of Ochratoxin A in Food Samples. *Molecules*. 2023;28(24).
295. Özalp VC, Çam D, Hernandez FJ, Hernandez LI, Schäfer T, Öktem HA. Small molecule detection by lateral flow strips via aptamer-gated silica nanoprobes. *Analyst*. 2016;141(8):2595–9.

296. Dalirirad S, Steckl AJ. Lateral flow assay using aptamer-based sensing for on-site detection of dopamine in urine. *Anal Biochem*. 2020;596:113637.
297. Li Y, Xu J, Wang L, Huang Y, Guo J, Cao X, *et al.* Aptamer-based fluorescent detection of bisphenol A using nonconjugated gold nanoparticles and CdTe quantum dots. *Sens Actuators B Chem*. 2016;222:815–22.
298. Jauset-Rubio M, El-Shahawi MS, Bashammakh AS, Alyoubi AO, O′Sullivan CK. Advances in aptamers-based lateral flow assays. *TrAC Trends in Analytical Chemistry*. 2017;97:385–98.
299. Wang T, Chen L, Chikkanna A, Chen S, Brusius I, Sbuh N, *et al.* Development of nucleic acid aptamer-based lateral flow assays: A robust platform for cost-effective point-of-care diagnosis. *Theranostics*. 2021;11(11):5174.
300. Turkevich J, Cooper P, Hillier J. A study of the nucleation and growth processes in the synthesis of colloidal gold. *Discuss Faraday Soc*. 1951;11:55–75.
301. Rivas L, de la Escosura-Muñiz A, Pons J, Merkoçi A. Lateral Flow Biosensors Based on Gold Nanoparticles. Vol. 66, Comprehensive Analytical Chemistry. 2014. 569–605 p.
302. Li M, Lin YC, Wu CC, Liu HS. Enhancing the efficiency of a PCR using gold nanoparticles. *Nucleic Acids Res*. 2005;33(21):e184.
303. Hasenoehrl C, Alexander CM, Azzarelli NN, Dabrowiak JC. Enhanced detection of gold nanoparticles in agarose gel electrophoresis. *Electrophoresis*. 2012;33(8):1251–4.
304. Bailes J, Mayoss S, Teale P, Soloviev M. Gold nanoparticle antibody conjugates for use in competitive lateral flow assays. *Methods in Molecular Biology*. 2012;906:45–55.
305. Page Faulk W, Malcolm Taylor G. Communication to the editors. An immunocolloid method for the electron microscope. *Immunochemistry*. 1971;8(11):1081–3.
306. Leuvering JHW, Goverde BC, Thal PJHM, Schuurs AHWM. A homogeneous sol particle immunoassay for human chorionic gonadotrophin using monoclonal antibodies. *J Immunol Methods*. 1983;60(1–2):9–23.
307. Mirkin CA, Letsinger RL, Mucic RC, Storhoff JJ. A DNA-Based Method for Rationally Assembling Nanoparticles into Macroscopic Materials. Vol. 1, Spherical Nucleic Acids: Volume 1. 2021. p. 3–11.
308. Sarah J. Hurst Abigail K. R. Lytton-Jean and CAM. Maximizing DNA Loading on a Range of Gold Nanoparticle Sizes. *Mol Cell Biochem*. 2012;23(1):1–7.
309. Park SY, Lytton-Jean AKR, Lee B, Weigand S, Schatz GC, Mirkin CA. DNA-programmable nanoparticle crystallization. *Nature 2008 451:7178*. 2008;451(7178):553–6.
310. Storhoff JJ, Elghanian R, Mucic RC, Mirkin CA, Letsinger RL. One-pot colorimetric differentiation of polynucleotides with single base imperfections using gold nanoparticle probes. *J Am Chem Soc*. 1998;120(9):1959–64.

311. Mirkin CA, Rathmann GB. The polyvalent gold nanoparticle conjugate-materials synthesis, biodiagnostics, and intracellular gene regulation. *MRS Bull*. 2010;35(7):532–9.
312. Liu B, Liu J. Methods for preparing DNA-functionalized gold nanoparticles, a key reagent of bioanalytical chemistry. *Analytical Methods*. 2017;9(18):2633–43.
313. Zhao W, Lin L, Hsing IM. Rapid synthesis of DNA-functionalized gold nanoparticles in salt solution using mononucleotide-mediated conjugation. *Bioconjug Chem*. 2009;20(6):1218–22.
314. Li M, Yang H, Li S, Zhao K, Li J, Jiang D, *et al.* Ultrasensitive and quantitative detection of a new β-agonist phenylethanolamine a by a novel immunochromatographic assay based on surface-enhanced Raman scattering (SERS). *J Agric Food Chem*. 2014;62(45):10896–902.
315. Lim DK, Jeon KS, Kim HM, Nam JM, Suh YD. Nanogap-engineerable Raman-active nanodumbbells for single-molecule detection. *Nat Mater*. 2010;9(1):60–7.
316. Fu W, Jiang L, van Geest EP, Lima LMC, Schneider GF. Sensing at the Surface of Graphene Field-Effect Transistors. *Adv Mater*. 2017;29(6):1603610.
317. So HM, Park DW, Jeon EK, Kim YH, Kim BS, Lee CK, *et al.* Detection and titer estimation of Escherichia coli using aptamer-functionalized single-walled carbon-nanotube field-effect transistors. *Small*. 2008;4(2):197–201.
318. Aveyard J, Mehrabi M, Cossins A, Braven H, Wilson R. One step visual detection of PCR products with gold nanoparticles and a nucleic acid lateral flow (NALF) device. *Chemical Communications*. 2007;(41):4251–3.
319. Ding Q, Qiu W, Sun C, Ren H, Liu G, Jiangsu B, *et al.* Comparison of DNA - Gold Nanoparticle Conjugation Methods : Application in Lateral Flow Nucleic Acid Biosensors. *Molecules*. 2023;28(11):4480.
320. Chen A, Yang S. Replacing antibodies with aptamers in lateral flow immunoassay. *Biosens Bioelectron*. 2015;71:230–42.
321. Kolm C, Martzy R, Führer M, Mach RL, Krska R, Baumgartner S, *et al.* Detection of a microbial source tracking marker by isothermal helicase-dependent amplification and a nucleic acid lateral-flow strip test. *Sci Rep*. 2019;9(1):1–9.
322. Yan C, Cui J, Huang L, Du B, Chen L, Xue G, *et al.* Rapid and visual detection of 2019 novel coronavirus (SARS-CoV-2) by a reverse transcription loop-mediated isothermal amplification assay. *Clinical Microbiology and Infection*. 2020;26:7.

CHAPTER 2. OBJECTIVES

CHAPTER 2. OBJECTIVES

The main objective of this thesis is to advance the field of aptamer-based diagnostic technologies, with a particular focus on developing PoC devices for small molecule biomarker sensing. The research is organized into three experimental chapters, each addressing specific aspects of aptamer performance, conjugation methods, and SELEX processes for small molecule biomarker detection.

More in detail, the objectives of this Thesis can be summarized as following:

- In chapter 3 the feasibility and efficacy of utilizing aptamer-based LFA for the detection of phenylalanine (Phe), an essential marker for monitoring PKU and ACLF patients is presented. In this work:
    - The binding affinity, specificity, and sensitivity of Phe aptamers in both liquid and LFA formats is investigated.
    - Various assay formats, including displacement and competitive assays, are compared to identify the most suitable approach for Phe detection.
    - The impact of nucleic acid sequence immobilization directionality on assay performance is determined by creating and testing aptamers with chemical modifications on different ends.
    - Research optimization strategies for LFA, including the exploration of blocking agents and alternative nucleic acid sequences, to improve assay sensitivity and specificity were explored.

- Chapter 4 evaluates and compares different methods for conjugating DNA to AuNPs in order to assess the stability, functionality, and performance of DNA-AuNP in LFA.
    - Analyze methods such as salt-aging, pH-assisted, and butanol-assisted protocols to understand the impact of various parameters on the characteristics of these nucleic acid functionalized nanoparticles.
    - Investigate how different storage conditions, including various buffers, affect the long-term stability and functionality of DNA-AuNP conjugates.
    - Determine the best combinations of conjugation methods and storage conditions to ensure the reliability and consistency of the DNA-AuNP in practical applications.

- In chapter 5, develop SELEX processes for identifying aptamers targeting small molecule biomarkers associated with ACLF.
    - Simultaneously, develop two SELEX approaches: a conventional SELEX process and a novel variation called Joint One-Pot SELEX.
    - Utilize NGS analysis, supported by customized MATLAB code, to overcome limitations related to the number of SELEX rounds and low enrichment levels. This will enable comprehensive sequence comparison and expedite the selection process.

CHAPTER 3. Development and Performance Evaluation of Aptamer-Based Lateral Flow Assays for Phenylalanine Detection

3.1. Aptamer Lateral Flow Assay proof-of-concept for Phe monitoring

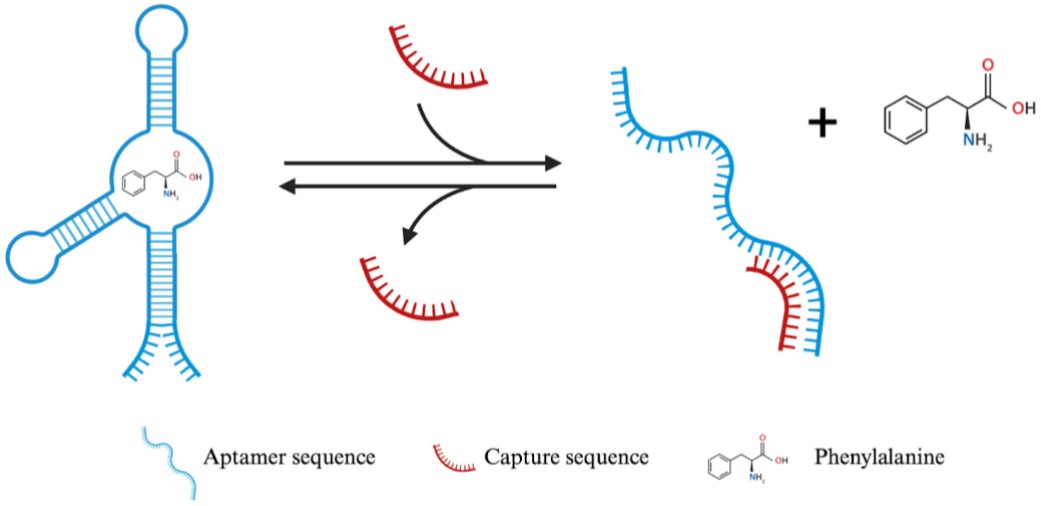
3.1.1. Overview of Aptamer Research for Phe Detection

As previously stated, Phenylalanine (Phe) is an essential amino acid that serves as a valuable small molecule biomarker for identifying various conditions such as Phenylketonuria (PKU), Acute-on-Chronic Liver Failure (ACLF), Parkinson's disease, or amyotrophic lateral sclerosis.[1–5] In recent years, considerable efforts have been directed towards developing the capability to detect Phe at the PoC.[5–8] Aptamers designed to target Phe have garnered attention due to their distinct advantages in detecting small molecules. Various approaches, including colorimetric and electrochemical methods, have been explored.

In 2013, researchers successfully immobilized an RNA aptamer targeting Phe on gold surface electrodes for the first time, enabling the detection of conformational changes using cyclic voltammetry.[9] Additionally, Xiang *et al*. utilized the conformational change of a DNA aptamer to release a DNA sequence that triggers a catalytic hairpin assembly (CHA) and a Mg^{2+}-dependent DNAzyme amplification cascade, resulting in a colorimetric change due to 3,3′,5,5′-Tetramethylbenzidine (TMB) oxidation.[10] Furthermore, standard DNA aptamers against Phe have been employed in fluorescence assays and other sensing strategies such as nanopore functionalization with aptamers for enhanced proteomics.[11,12] However, these methods are not fully compatible with PoC platforms and often necessitate benchtop equipment or additional portable devices.[13] As a result, there is a need for the development of a completely user-friendly PoC platform that does not require additional equipment, enabling at-home monitoring.[14]

In 2014, Yang and colleagues devised a Systematic Evolution of Ligands by Exponential Enrichment (SELEX) methodology to selectively isolate aptamers against various small molecules, including Phe.[15] To accomplish this, Phe was used as a hapten and coupled with an inorganic receptor, pentamethylcyclopentadienyl-rhodium (III) (Cp*Rh(III)), which amplified the number of epitopes and size of the complex, and implemented a counter-selection step against the inorganic receptor to elute aptamer competitors. Besides, they were able to test these aptamers in spiked human sera, which proved them valuable for real sample testing. Later in 2019, Idili *et al.* developed an electrochemical aptamer-based sensor using a truncated version of the same aptamer against the Phe- Cp*Rh(III) receptor complex.[6,16] The aptamer was modified with a thiol group at its 5' end for anchoring and a methylene blue at its 3' end for signal generation. When the aptamer binds to the Phe-Cp*Rh(III) receptor complex, it causes a change in distance between the methylene blue and the gold surface of the electrode, resulting in a signal change. This work reported the ability of this aptamer to bind and change conformation when anchored by thiol groups to an electrode. Besides, a later publication

from Yang and colleagues published aptamer sequences able to detect free Phe as a result of an excess of Phe used in the selection process, thereby creating by-product aptamers for free Phe.[17] In this work, each aptamer is paired with a complementary, shorter sequence (Capture sequence, Scheme 1) that is displaced by the target.



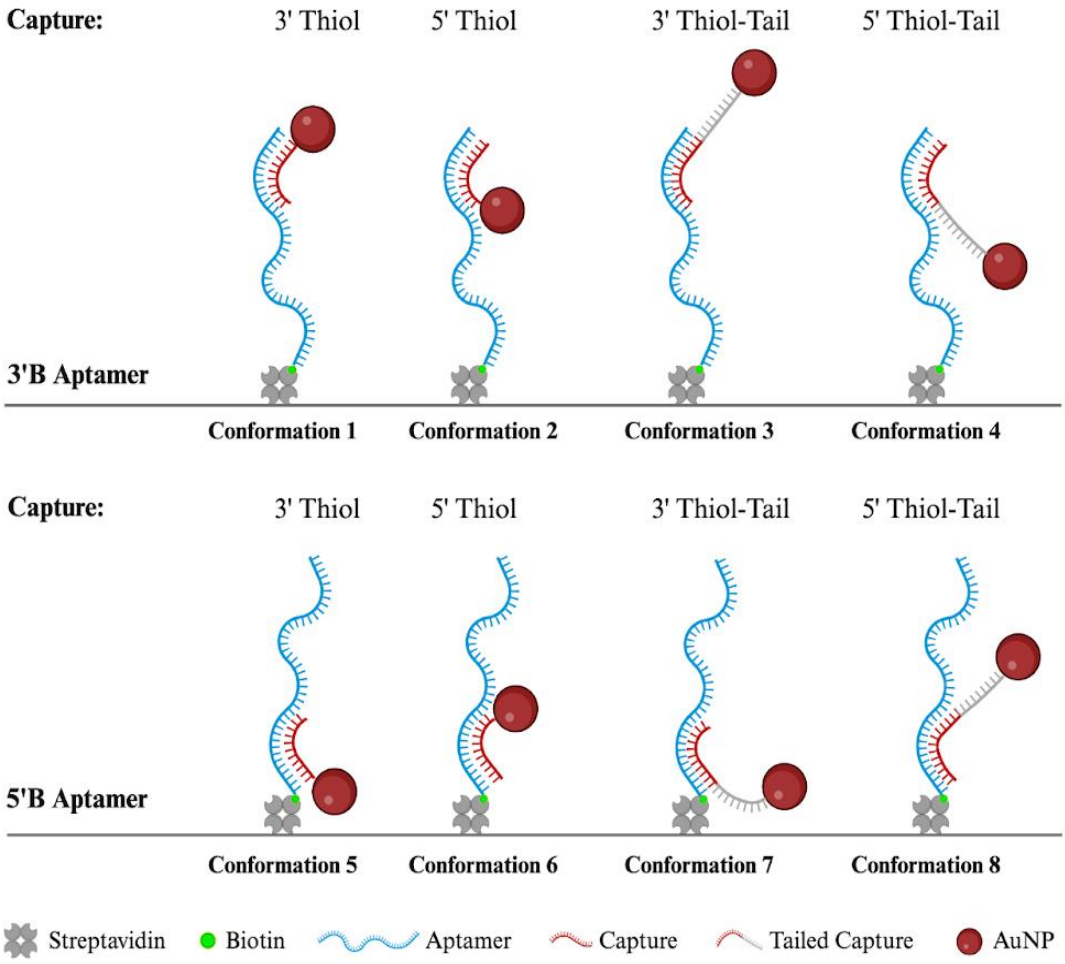
Scheme 1: Schematic representation of the equilibrium of the nucleic acid system and the Phe target. Aptamer-Target binding is thermodynamically favorable over nucleic acid hybridization, displacing the Capture sequence (red). Created with Biorender. Created with Biorender.

3.1.1.1. Hypothesis

Thus, there is the potential to integrate this system into a Lateral Flow Assay (LFA) utilizing the aptamer target binding as one sensing event, but also by incorporating labels onto the complementary short sequence that can be detected once they have been displaced. Reducing the complexity of the system theoretically increases the chances of success when translating it into a paper format, so it was determined from the start to use a 'Cp*Rh(III)'-free sensing mechanism. The publication of this aptamer served as a catalyst for the development of a PoC LFA monitoring tool that could be useful for Phe detection for PKU and ACLFA patients.

3.1.1.2. Probe design

Various chemical modifications were considered for the Aptamer. To anchor the molecule to the LFA paper platform, biotin was selected due to its fast-binding kinetics with streptavidin (Str).[18,19] Str has a high affinity for nitrocellulose, allowing for precise and solid printing of the complex and preventing biomolecules from being washed off during flow.[20] Thiol groups were also considered for nucleic acid conjugation with 20 nm Gold Nanoparticles (AuNPs) (Scheme 2).

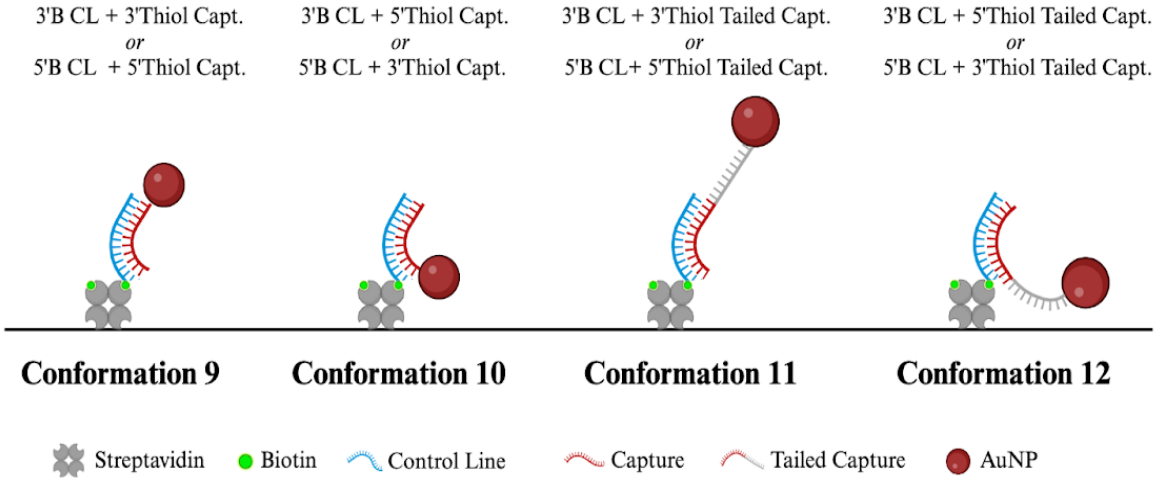


Scheme 2: Schematic representation of the combination of the four Capture and the two Aptamer sequence versions when the Aptamer sequence is immobilized onto nitrocellulose through Str-Biotin interactions (grey horizontal line: nitrocellulose). Created with Biorender.

The directionality of the sequences and the possible steric hindrances might affect the optical signal generation. As depicted in Scheme 4, chemical modifications added on one end (5') or the other (3') of a sequence can change the immobilization directionality of the conjugated sequences, either if they are attached to nitrocellulose through Str (Aptamer) or conjugated to AuNPs (Capture). The large size of AuNPs or Str, compared to the size of nucleic acids, can add steric hindrances by covering or impeding a hybridization event, thus affecting the sensitivity of the final assay.[21,22] For the purpose of determining the most effective hybridization and signal generation in LFA, Aptamer with biotin on either 5' or 3' (3'B or 5'B Aptamer) were procured (Scheme 2). Additionally, Capture sequences with thiol groups on 5' or 3' (3'Thiol or 5'Thiol Capture) and poly-Thymine (polyT) fragments were added (3' or 5' Thiol-Tail Capture) for separation and to avoid steric hindrances, were also ordered (Scheme 2). Considering the possible combinations of Aptamer and Captures

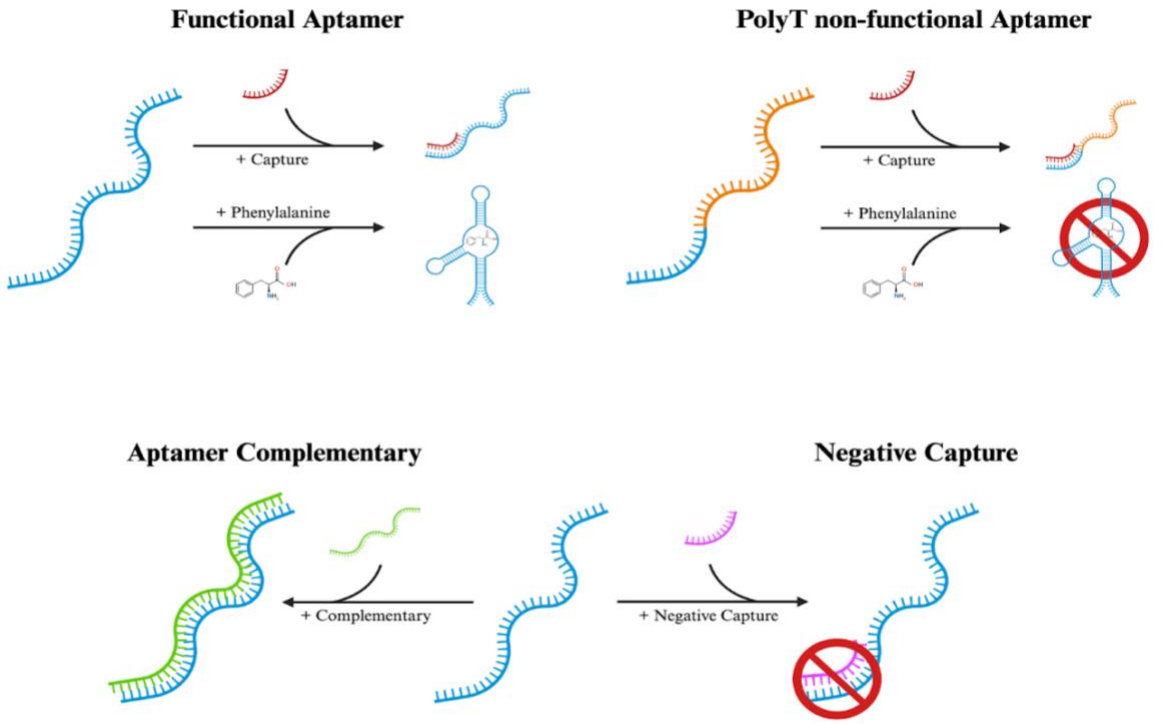
sequences (Scheme 2, Conformations 1-8), there are eight total Conformations available for a first line or Test Line (TL), to which we will refer for simplicity.

Similarly, complementary sequences to the Capture sequence were procured for the establishment of a second line or a Control Line (CL), with thiol groups on one end (3'B CL) or the other (5'B CL) to evaluate more possible steric hindrances once printed onto nitrocellulose (Scheme 3). There are combinations that are schematically and practically identical, for this reason they are grouped under the same Conformation names (Conformations 9-12).



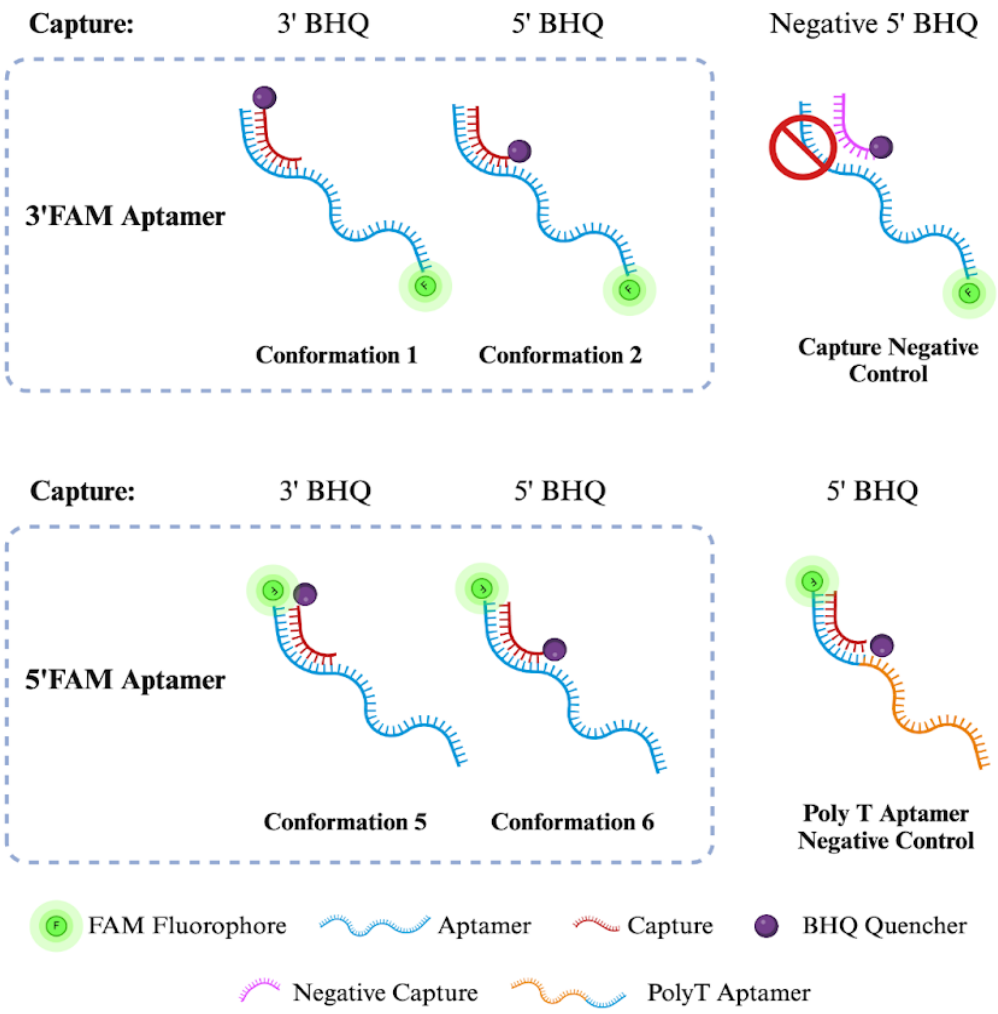
Scheme 3: Schematic representation of the combination of the four Capture and the two Control sequence versions (3'B and 5'B CL) when the Control sequence is immobilized onto nitrocellulose through Str-Biotin interactions. Note that certain combinations were grouped together because they appear to be schematically identical. Created with Biorender.

Negative aptamers containing a polyT in the binding region (polyT Aptamer), rendering them unable to bind to the phenylalanine target while still carrying the complementary region to the Capture sequence were ordered for tracing purposes (Scheme 4). Additionally, a sequence completely complementary to the aptamer (Aptamer Complementary, AC) was procured as a target competitor, to prevent the Phe binding and hybridization of the Capture sequence. Specificity control was established through negative Capture sequences non-complementary to the Aptamer nor CL sequences (Negative Capture).



Scheme 4: Schematic representation of the functionality of the Aptamer (top left), the polyT aptamer (top right), the Aptamer complementary (Bottom left) and the Negative Capture (bottom right) sequences.

6-Carboxyfluorescein (6'FAM) fluorophore and Black Hole Quencher (BHQ-1) were chosen for the Aptamer and Capture sequences, respectively, for use in binding assays (Scheme 5).

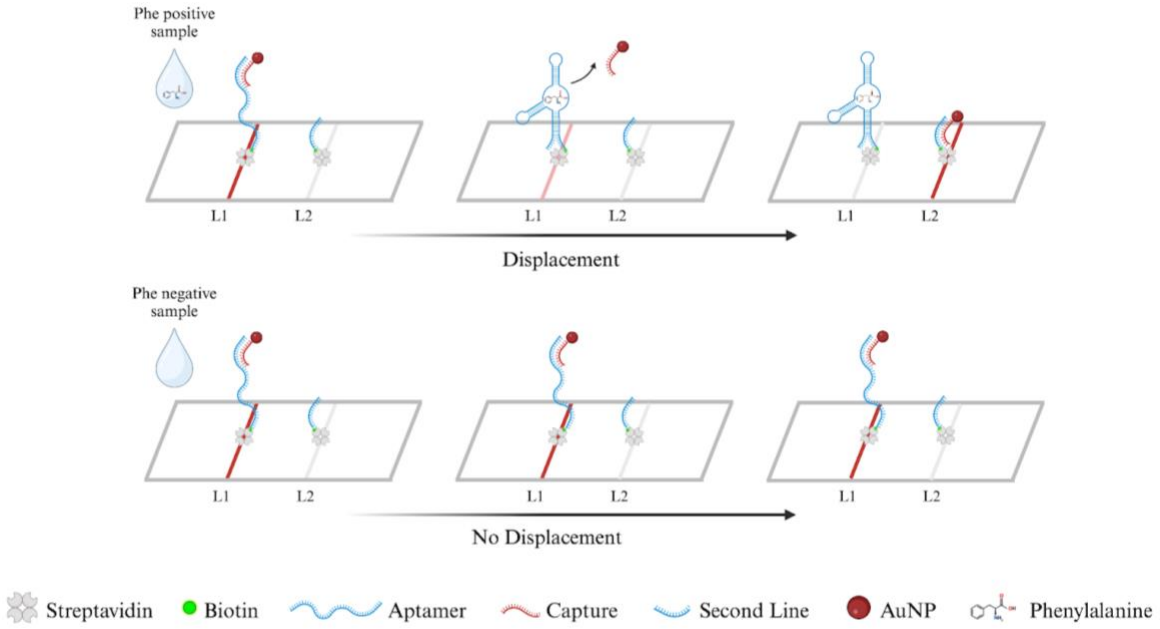


Scheme 5: 6'FAM and BHQ-1 probes and their interactions. Note that Negative Capture and polyT Aptamer can be combined with other Aptamers and Captures, respectively. Note that the Conformation names match their corresponding Conformations of Scheme 4. Created with Biorender.

Given these three nucleic acid elements (the Aptamer, Capture sequence and Control sequence) and the various chemical modifications available, different sensing strategies could be investigated to develop a LFA biosensor.

3.1.1.2.1. Method 1: The Displacement Assay

The first sensor design to be investigated is the displacement assay.[23,24] The thiolated Capture, previously conjugated to 20 nm AuNPs, is incubated with the biotinylated aptamer and Str to create a complex. This complex is printed in a first line (Line 1, L1), which will be red-colored from the initial moment of the assay (Scheme 6). A biotinylated control sequence is also incubated with Str prior to being printed in a second line (Line 2, L2), which will be invisible to the naked eye.



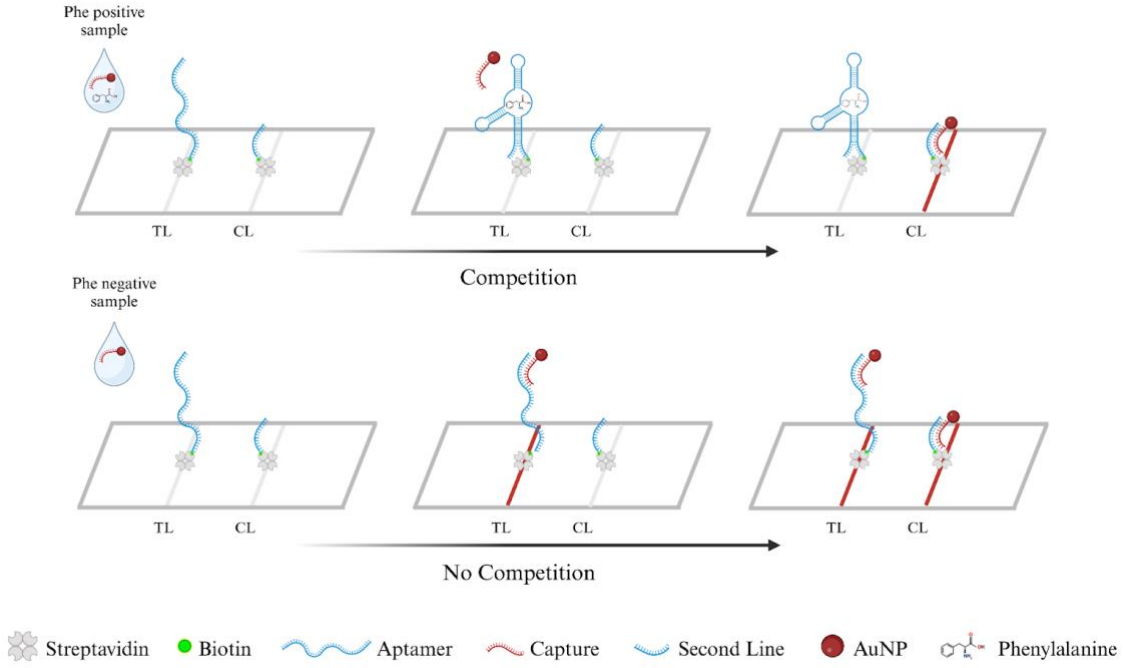
Scheme 6: Displacement assay for positive Phe samples (top) and negative Phe samples (bottom). Conformations 1 and 9 were chosen for the representations of L1 and L2, respectively. Created with Biorender.

When a fluid sample containing the Phe complex (Target) is added to the strip, it starts to flow by capillarity, and soon, the target molecule encounters L1 (Scheme 6, top). Upon making contact, attached aptamers have an affinity for the target that causes a conformational change of the aptamer, releasing the Capture sequence and binding to the target. As the liquid sample continues to flow through the nitrocellulose, the Capture sequences are dragged to the second line, Line 2, where they hybridize by complementarity to the Control sequence. Consequently, the first line progressively and proportionally turns fainter as the AuNPs are displaced, while the second line appears progressively red upon the accumulation of the released sequences. Conversely, if a sample that does not contain the target complex is added to the assay, the aptamers do not change conformation and do not release the Capture sequence, therefore not producing any change in either of the lines (Scheme 6, bottom). Due to the nature of this assay, both printed lines on the nitrocellulose are called L1 and L2, respectively, as they do not fit in the definition of TL and CL.

3.1.1.2.2. Method 2: The competitive assay

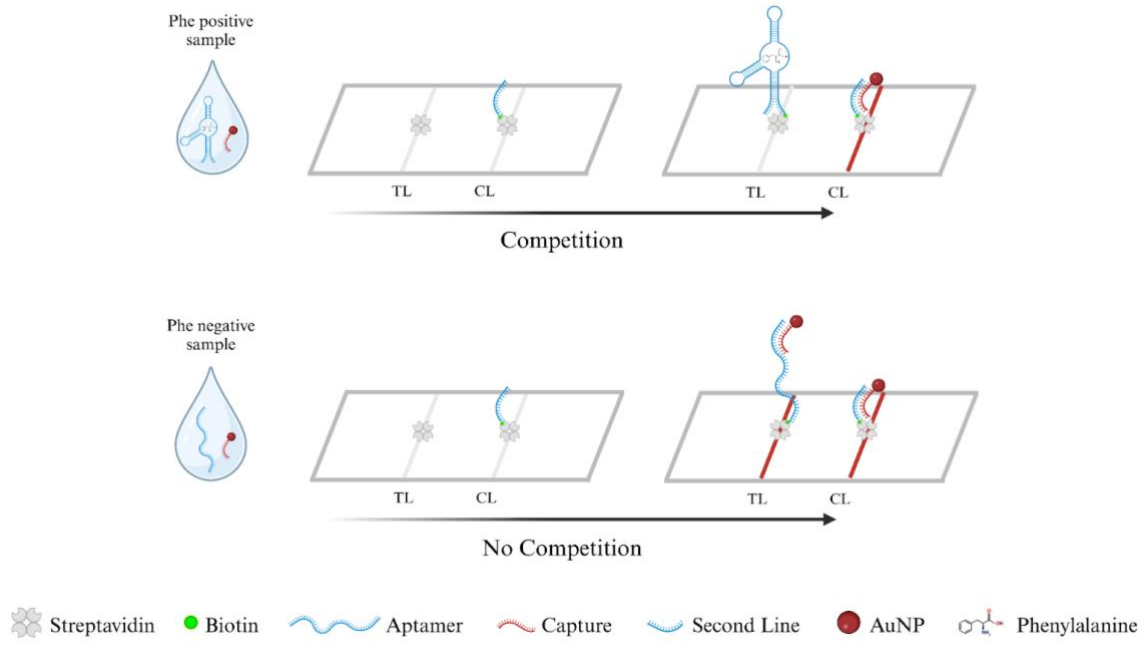
On the other hand, it can be exploited as a competitive assay, in which the sample and the Capture travel together from the sample pad (or conjugate pad) to the, in this case, TL and compete for the binding with the aptamer (Scheme 7, top).[25] As the aptamer changes its conformation to bind target molecules, the Capture can't access its complementary sequence in the end region of the aptamer

and, therefore, continues flowing until reaching the CL, where it is captured by hybridization, along with the excess of the Capture. However, when there is no target available in the sample, the Capture conjugate can hybridize with the aptamer, with the appearance of the TL (Scheme 7, bottom).



Scheme 7: Printed Aptamer Competitive assay for positive Phe samples (top) and negative Phe samples (bottom). Conformations 1 and 9 were chosen for the representations of TL and CL, respectively. Created with Biorender.

An alternative to this strategy consists of printing only the anchoring molecule, in this case, Str, as a TL, and the complex of Aptamer, Capture, and target are incubated before the loading of the strip (Scheme 8). [26,27]



Scheme 8: Printed Streptavidin Competitive assay for positive Phe samples (top) and negative Phe samples (bottom). Conformations 1 and 9 were chosen for the representations of TL and CL, respectively. Created with Biorender.

This alternative can be advantageous when longer incubation times of aptamer and sample are required (due to very high dissociation constant, K_D, for instance), if a very specific environment is required for binding to occur, or to extend the storage lifespan of the device.[28] Although it implies an extra step prior to the application onto the LFA strip, other successful commercial LFA devices have demonstrated the feasibility of this format, as happened with the nasal swab lysis step for antigen SARS-CoV-19 LFA devices.[29,30]

In this Chapter, both Displacement and Competitive strategies will be put to the test for the development of a nucleic acid LFA test for PKU monitorization. Iterative LFA and conjugation optimization will be performed to improve binding and flow capabilities.

3.2. Objectives

The main objective of this chapter is to investigate the feasibility and effectiveness of using aptamer-based LFA for the detection of Phe. The ultimate goal is to develop a PoC device for monitoring PKU and ACLF patients. To achieve this objective, specific aims have been described below:

Firstly, the performance of the aptamer will be evaluated. This involves assessing the performance of the Phenylalanine aptamer in solution and LFA format. The aptamer's binding affinity, specificity, and sensitivity towards Phe will be addressed.

Secondly, different assay formats, including one displacement assay and two competitive assays, will be investigated and compared to determine the most suitable approach for Phe detection in the LFA format.

Thirdly, the impact of nucleic acid sequence immobilization directionality on the performance of aptamer-based LFA will be explored. This objective involves designing and testing aptamers with varying chemical modifications to identify combinations that offer optimal sensitivity and signal generation in the LFA format.

Lastly, strategies for optimizing the performance of LFA for Phe detection will be investigated. This includes exploring blocking agents to minimize non-specific binding and evaluating alternative nucleic acid sequences to enhance assay sensitivity and specificity.

By addressing these objectives, this chapter aims to advance our understanding of aptamer-based LFA for Phe detection and contribute to the development of a novel PoC diagnostic tool for Phe detection.

3.3. Materials and Methods

3.3.1. Materials

DNA sequences were purchased from LGC Biorearch Technologies. Tetrachloroauric(III) acid ($HAuCl_4$), sodium citrate, Tween-20, polyethylene glycol (PEG) 2050, 6000 and 20000, Bovine serum albumin (BSA) sodium chloride (NaCl), phosphate buffer saline (PBS) tablets, tris(hydroxymethyl)aminomethane salts (Tris), phosphate salts, magnesium chloride ($MgCl_2$), Tris-(2-Carboxyethyl)phosphine hydrochloride (TCEP), n-butanol, anti-biotin antibody, and L-Phe, were purchased from Merck (Spain). Transparent and black 96-well plates and TriTrack DNA Loading Dye were purchased from FisherScientific (Hampton, NH, USA). SpectraMax iD3 (San José, CA, USA) UV-Vis spectrophotometer was used for absorbance measurements. Dynamic Light Scattering (DLS) and Z-potential measurements were performed using DTS1070 cuvettes in a Zetasizer Nano ZS from Malvern Panalytical. Electrophoretic and transillumination system Gelato, and GelGreen-TBE (Tris-Borate-EDTA) Agarose Tabs were purchased from miniPCR (Cambridge, MA, USA). LFA strips were scanned using a Canon LiDe 400 (Canon, Japan) and analyzed using ImageJ software. LFA strips were made of nitrocellulose (CN 150 from Sartorius), cellulose (GE Healthcare), and laminated card (Millipore). Ultrasonic digital bath (Ovan, Spain) was used for sonication of the AuNPs. All DNA sequences used in this work are listed in Annex 1.

3.3.2. AuNPs synthesis and conjugation

We synthesized 20 nm AuNPs using the Turkevich method, which involves reducing gold ions to nanoparticles using sodium citrate as the reducing agent. AuNPs were conjugated using the following salt-aging (SA) protocol. 100 μM Thiolated DNA sequences were treated with 10 mM TCEP for one hour in the dark with moderate shaking before addition to the AuNP solution. The solution was then incubated overnight (16h), and a 0.125 volume of 1M NaCl and a 0.125 volume of 0.1M sodium phosphate buffer pH 7 are slowly dropcast for salt aging. The solution is then incubated for 24 hours under the same conditions before being centrifuged at 10.000 rpm for 30 minutes. The supernatant was removed, and the pellet resuspended in the desired solution to the desired final concentration.

This SA protocol was modified in order to reduce aggregation in the glass vials and during the resuspension of the conjugates in the desired buffers, as well as for the optimization of the performance of these conjugates in a LFA. These modifications included pH adjustment, addition of surfactants, sonication step, and the addition of blocking agents of different natures and sizes. The resulting protocol was called “LF-optimized protocol”. This protocol is described and evaluated in Chapter 4.

3.3.3. Lateral Flow preparation

In this work, different versions of LFA were utilized to conduct different experiments. LFA half-sticks, which are formed by detection and absorbent pads only, were used in earlier stages for screening of diverse parameters (hybridization of different conformations, running buffer testing, printing conditions, etc.). In later stages of this work, complete or almost complete (without conjugate pad) versions were used for flow and biorecognition evaluation and optimization. In the same way, dropcasting or printing of the lines using an Isoflow dispenser (Imagene Technology, USA) or Biospotter (BioFluidiX GmbH, Germany) was used as appropriate. 3 mm wide half-stick formats required 20 μL of sample, whereas 3 mm complete strips required 60 μL for complete soaking and proper flow.

To prevent the tubing of the IsoFlow dispenser from being permanently contaminated, the Biospotter was utilized for printing AuNP conjugates due to the use of disposable plastic tubing. Due to the presence of a colored line before the start of the assay, printed strips were scanned before and after 15 minutes running. CL and TL of the competitive assays, which do not contain AuNPs, were printed using the IsoFlow dispenser and were scanned only 15 minutes after the assay.

3.3.4. Conjugate and sequence characterization.

To confirm the size and homogeneity of the synthesized AuNPs, they were characterized using both UV-Vis spectroscopy and DLS techniques. DNA-AuNP conjugates were characterized using the same techniques. The nucleic acid concentration for the conjugation process was optimized according to the length of the sequence used for optimal coverage and protection of the AuNPs against high salt concentrations. This was achieved by performing a Gold Aggregation Test (GAT) for both of the main length sequences (14 and 28 pb) used in this Chapter. GAT results were adjusted empirically using 100 mM Tris-$MgCl_2$ buffer for conjugate resuspension and evaluate aggregation, instead of 1M NaCl to reduce the amount of DNA and packing density, thus, reducing the cost. An electrophoretic mobility shift assay (EMSA) was used to characterize the correct size and hybridization of all sequences used in this work. A 6% agarose gel was prepared using GelGreen-TBE Agarose Tabs in milli-Q (MQ) or deionized water. 5μL of 5 μM DNA samples were mixed with 1 μL of loading dye. Gels were run for 30 min using 120V. Results were visualized using blue light in a dark chamber (miniPCR, USA) with access for smartphone photography.

3.3.5. Binding studies

Aptamers modified with 6'FAM and capture sequences modified with BHQ-1 were utilized to assess the binding of the aptamer to its target molecule under four different buffer systems. The buffers screened were PBS, PBS-$MgCl_2$, Tris-$MgCl_2$, and water. To ensure the accuracy and reliability of the experiment, the complementary sequence to the aptamer was used as a positive control. It was observed that complementary sequences completely remove the quencher and produce a constant signal from >100 nM in any buffer system. This was expected due to the limited amount of aptamer and capture sequences present at a concentration of 50 nM. As a result of these findings, Complementary concentrations higher than 1 μM were not tested. Phenylalanine concentrations up to 200 μM were used to achieve signal saturation and facilitate the calculation of the K_D.

3.4. Results

Before developing the different LFA formats, it was deemed prudent to characterize all the different components (AuNPs, DNA conjugates, aptamers, etc.) and check that they were all functional. Sections 3.4.1. to 3.4.3 of this chapter detail the characterization of all these components.

3.4.1. Conjugate characterization and Control Line optimization.

The UV-Vis spectrum of bare AuNPs give a maximum absorbance peak at 520 nm, as reported in the literature, while conjugated AuNPs showed a shift of the peak to 525 nm, thus confirming the conjugation (Figure 1). DLS data showed a hydrodynamic diameter increase from 23.37 +/- 0.629 nm to 47.22 +/- 0.86 nm after conjugating the Capture sequence. PdI was increased from 0.266 to 0.417 (Table 1). Z-potential and conductivity changes further confirmed the conjugation had been successful.

Table 1: DLS and Z-potential results of conjugated and non-conjugated AuNPs.

Sample	Z-Average (d.nm)	PdI	Z potential (mV)	Conductivity (mS/cm)
Non-conjugated AuNPs	23.37 +/- 0.629	0.266 +/- 0.047	-44.7 +/- 2.88	0.487 +/- 0.01
Conjugated AuNPS	47.22 +/- 0.86	0.417 +/- 0.017	-9.56 +/- 0.206	0.717 +/- 0.0223

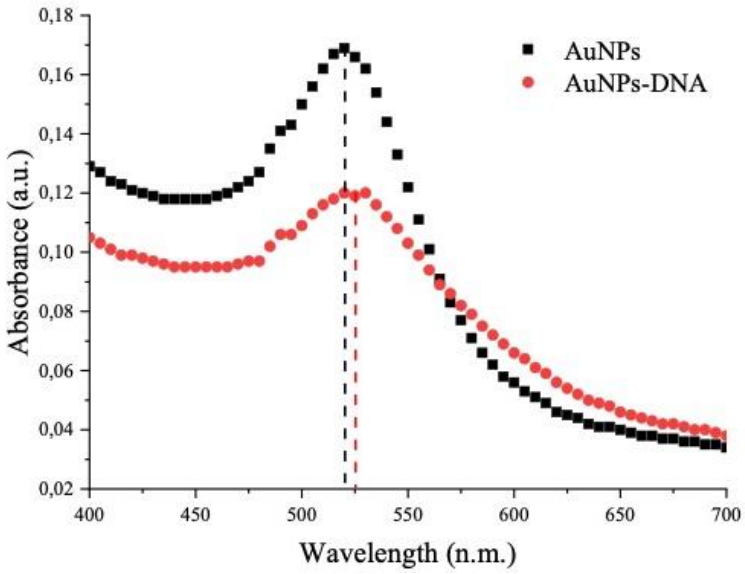


Figure 1: UV-Vis Spectra of conjugated (red) and non-conjugated (black) 20 nm AuNPs. Dotted lines indicate maximum Absorbance wavelength for each.

Based on the GATs results, it was found that the ideal final concentration of DNA for AuNP conjugation is approximately 3.2 μM for the short Capture and 0.8 μM for the tailed Capture (as shown in Figure 2A). However, when using the LFA running buffer instead of 1M NaCl for GAT testing (Figure 2B), a lower concentration of short Capture sequence was enough to provide coverage and protection, requiring less DNA (a final concentration of 1.6 μM vs. 3.2 μM), and thus reducing the cost of the conjugations. These GATs conjugates were then tested on a half-stick LFA to assess their hybridization potential with the control sequence printed on nitrocellulose (Figure 2C). The tested Conformations for these lines are Conformations 9 and 11 for the Capture and Tailed Capture, respectively.

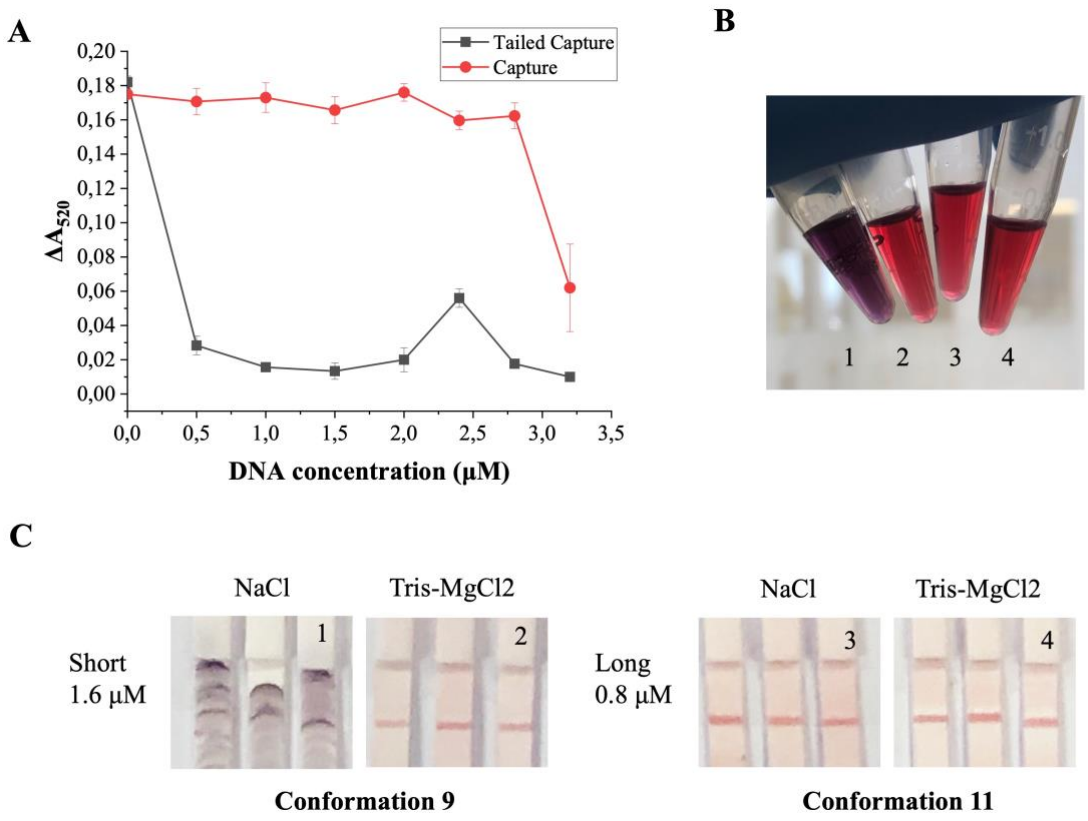


Figure 2: a) GAT for Capture and Tailed Capture sequences, aggregated with 1M NaCl. b) In-tube GAT using 1M NaCl (tubes 1 and 3) and 100 mM Tris-$MgCl_2$ (tube 2 and 4) buffer of the Capture (1 and 2) and Tailed Capture sequence (3 and 4). c) Resulting LFA half-strip CL of the conjugates shown in B.

To establish suitable working conditions for subsequent experiments and screening, an initial assessment was conducted on the molar ratios and concentration of the control line and conjugate, respectively. These conditions underwent continuous review and modification to improve signal generation during the course of this work. It is possible to alter the molar ratio between the streptavidin and biotinylated DNA for the establishment of a CL in the paper format (Figure 3A). In these experiments we tested 1:2 and 1:4 stoichiometric ratios of the two species manually dispensed

onto half-strips. Likewise, after conjugation we can re-suspend the DNA-AuNP conjugates in different volumes of buffer and test different concentrations of conjugate for optimal signal generation. Concentration of conjugates of 4x, 7x and 14x in respect to synthesis concentration were tested and dropcasted onto the half-strips. A Negative Capture sequence, non-complementary to the Control Line sequence, was conjugated to AuNPs and tested for selectivity. For simplicity, only Conformation 9 was screened.

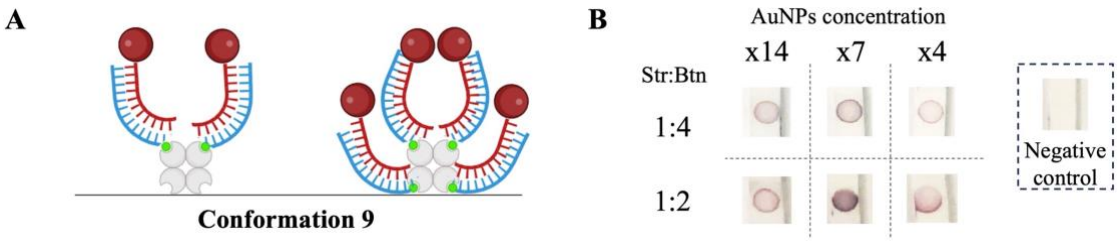


Figure 3. a) Schematic representation of 1:4 and 1:2 molar ratios of Str and biotinylated DNA printed onto nitrocellulose. Conformation 9 was chosen for schematic representation. b) Signal saturation evaluation between different molar ratios of the CL and different resuspensions concentrations of the conjugate.

It was found that a 1:2 molar ratio of Str to biotinylated DNA and a 7X re-suspension of the conjugate performed the best (Figure 3B). Tests showed clear selectivity against a Negative Capture sequence.

Next, the directionality of both capture and control sequences was screened in search of possible steric hindrances onto a nitrocellulose platform due to the difference in size between the nucleic acid sequences (14 nucleotides, nt) and their anchoring elements, either AuNPs or Str, respectively (Scheme 5, Conformations 9 and 10). It is of interest to evaluate if the distancing of AuNP and Str (both Conformations 9) has a positive effect in signal generation over the proximity of the same (both Conformations 10). Tailed Capture sequences theoretically should suffer from less steric hindrances, for this reason they were evaluated in further experiments, while determination of the biotinylated Control Line sequence was prioritized. 3'Thiol and 5'Thiol Capture conjugates were dropcasted onto half-strips with 3'B or 5'B printed Control sequences, representing both Conformations 9 and 10.

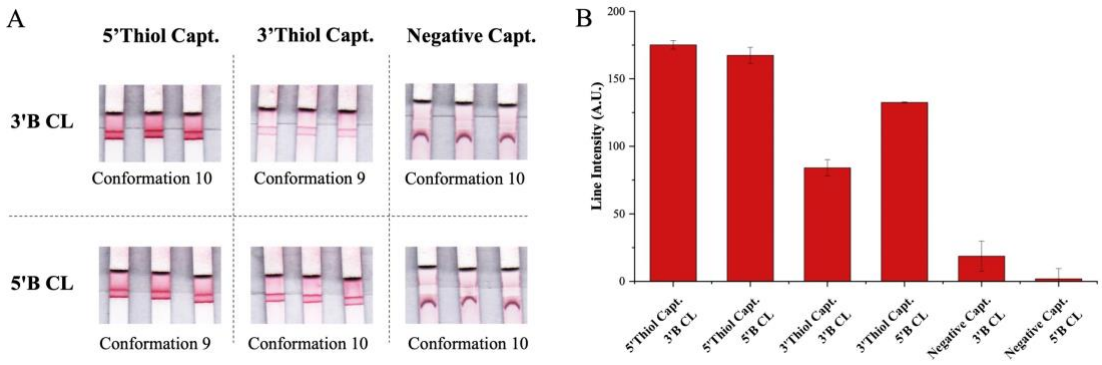


Figure 4: a) Lateral Flow half-strips for CL intensity determination. b) Signal Intensity (arbitrary units) extracted with ImageJ from triplicates.

As shown in Figure 4, the 5'Thiol Capture sequence produced greater intensities than the 3'Thiol Capture sequence, regardless of the control sequence employed. However, it was found that Conformations 10 yielded more intensity than Conformations 9. The role of steric hindrances due to the separation between the AuNPs and Str remains unclear and was further investigated. Negative Capture sequences did not hybridize with the CL sequence, demonstrating its specificity, but also displayed a repulsion effect that inhibited the conjugates' flow, as shown in Figure 4A.

5'B Control sequences were used in the following experiments and tested against the four Capture sequences repeatedly during the different screening processes conducted in this work to continue elucidating possible steric hindrances. This choice helps to reduce redundant Conformations of Control and Capture sequences, as depicted in Scheme 3. From the unspecific signal generated in the non-complementary Capture sequences, 5'B Control sequences yielded better results.

3.4.2. Nucleic Acid Characterization

To ensure the accuracy of our work, we verified the appropriate length and hybridization of nucleic acid sequences through the use of EMSA. This method employs an electric field to separate DNA molecules based on their charge and size within an agarose gel. By assessing the retardation effect of hybridized DNA molecules in comparison to non-hybridized ones, we can validate that the sequences are binding to each other as desired.

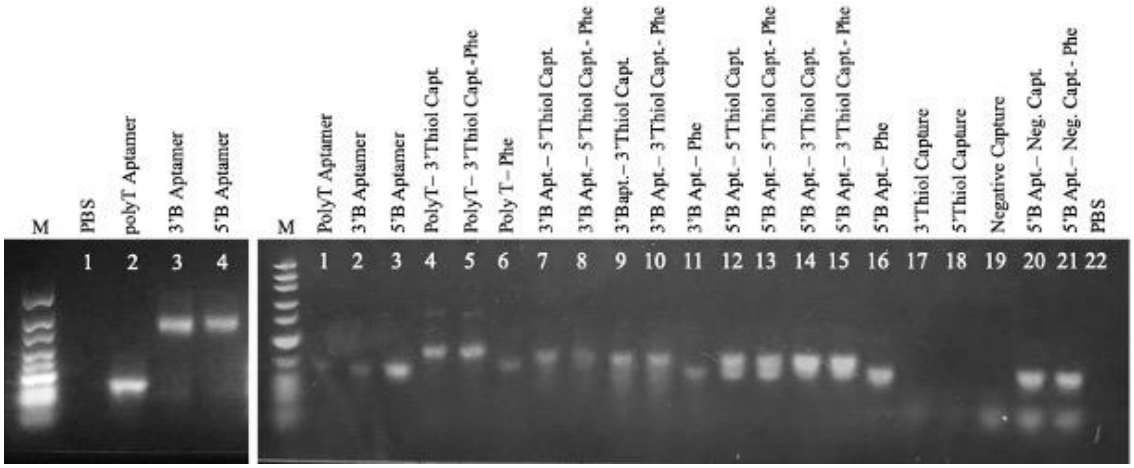


Figure 5: EMSA assays on 6% Agarose gels. Str and Biotinylated DNA correct hybridization (left, lanes 2-4). Aptamer and Capture combinations, and Phe additions (right, lanes 1-21). M: DNA marker ruler.

The results of the EMSA assay depicted in Figure 5 confirm the successful conjugation of the biotinylated aptamers and Str (Figure 5, left, lanes 2, 3, and 4). Similarly, the EMSA reveals the correct hybridization of polyT, 3'B, and 5'B Aptamers (lanes 1, 2, and 3, respectively) with the Capture sequences (lanes 4, 7, 9, 12, and 14), and no hybridization with a non-related sequence (lanes 20 and 21). It is noteworthy that the presence of Phe (lanes 5, 6, 8, 10, 11, 13, 15, 16, and 21) did not affect the migration for any of the three aptamers, indicating no changes in secondary structure or recognition of the target molecule. However, the absence of recognition can't be confirmed, considering that the presence of GelGreen (containing intercalating fluorescent molecules for revelation) and glycerol to increase the density of the samples can greatly alter the electrostatic environment of the aptamer, thus impeding recognition. Besides, DNA is usually in linear form while flowing through agarose. Therefore, fluorescent binding studies were required to check if the aptamer was functioning correctly.

3.4.3. Binding studies

Fluorescence assays were performed in solution to determine the binding affinity to Phe and to evaluate the proximity effect of fluorophore and quencher variations presented in Scheme 5. Tailed Capture sequences and Control Line sequences were not included in these assays for simplicity.

First, the fluorophore-quencher system was assessed in PBS to determine the quenching effect of complementary and non-complementary BHQ-1 sequences on three different aptamers, as well as the proximity between fluorophore and quencher (Scheme 5, Conformations 1, 2, 5 and 6). 5' and 3'

6'FAM modified Aptamers, and a 6'FAM polyT Aptamer were incubated with 5' and 3' BHQ-1 Capture sequences and a 5' BHQ-1 non-complementary Capture sequence.

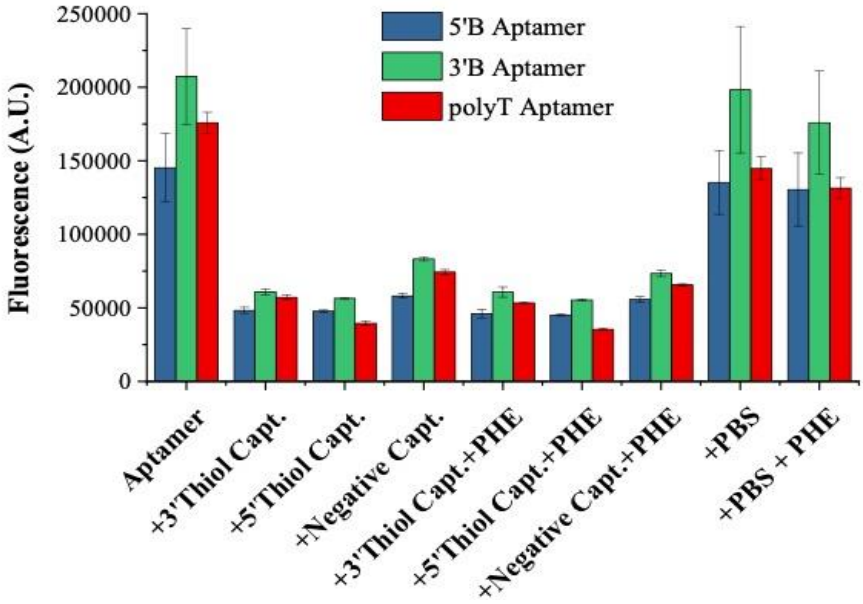


Figure 6: Proximity quenching assay of the 3 6'FAM-Aptamers and 3 BHQ-1-Capture sequences. Groups 1 to 9 (left to right).

In Figure 6, the initial fluorescence of the three aptamers is measured (group 1, Aptamers alone), as well as the resulting fluorescence when incubated with the same molar ratio of the three different Capture sequences (groups 2, 3, and 4). It was observed that the distance difference between the aptamers and both Capture sequences did not have a significant impact on the quenching effect. The proximity of a non-complementary quencher (group 4) had a quenching effect similar to that of complementary sequences. Groups 5, 6, and 7 do not present a fluorescence recovery attributable to Aptamer secondary structure nor displacement of the Capture due to Phe's presence. Instead, only the sample with just Phe incubated with aptamers (group 9) showed a small quenching effect, presumably due to the aromatic ring of the amino acid. PBS masking of the fluorescence (group 8) was found to be minimal. However, the response of the aptamer to the addition of Phe was not as expected. As a next step, therefore, we decided to screen different buffers, to determine if this was the cause of the aptamer not binding to the Phe, even if it did not cause fluorescence issues.

As a means to simplify the assay, only 6'FAM aptamer and 3'BHQ-1 capture sequences were chosen for buffer screening (Scheme 7, Conformation 5). For this assay, displacement of the capture sequences was evaluated with increasing concentrations of Phenylalanine and the Aptamer Complementary (AC) sequence as a positive control.

The binding buffer (BB) reported in the original SELEX work (20 mM HEPES, 1M NaCl, 10 mM $MgCl_2$, 5 mM KCl, pH 7.5) did not display the expected aptamer binding in solution, hence, other buffers, 100mM Tris-$MgCl_2$ pH 7 buffer, 10mM PBS- $MgCl_2$ pH 7.4 buffer, 10 mM PBS pH 7.4 buffer and MQ water were tested. The results of these tests are given in Figure 7 and Table 2.

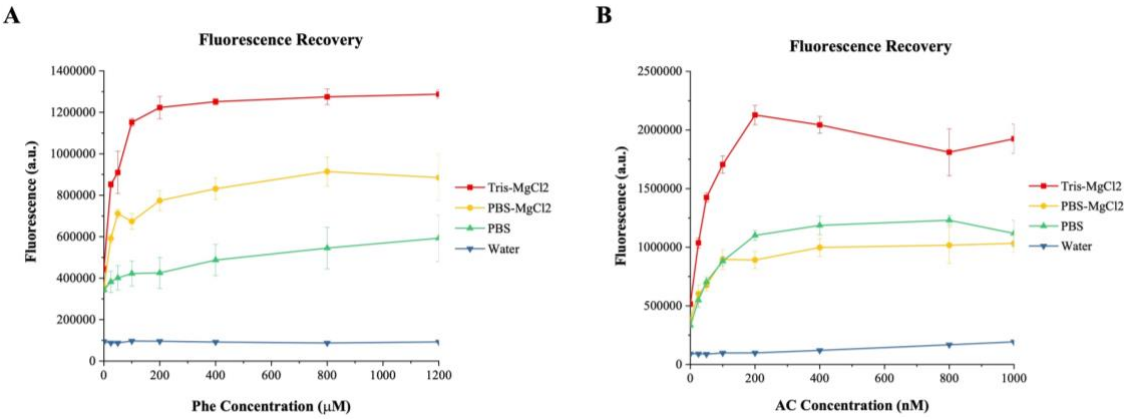


Figure 7: Buffer screening quenching assays. a) Increasing Phe concentrations. b) Increasing Aptamer Complementary sequence (AC) concentrations. The presented conformation in all conditions is Conformation 5.

It was found that 100 mM Tris-$MgCl_2$ pH 7 buffer achieved the most significant binding for both targets, also showing lower calculated K_D obtained by fitting to the Hill equation (Table 2). As a result of this, all experiments from this point on were conducted in this buffer.

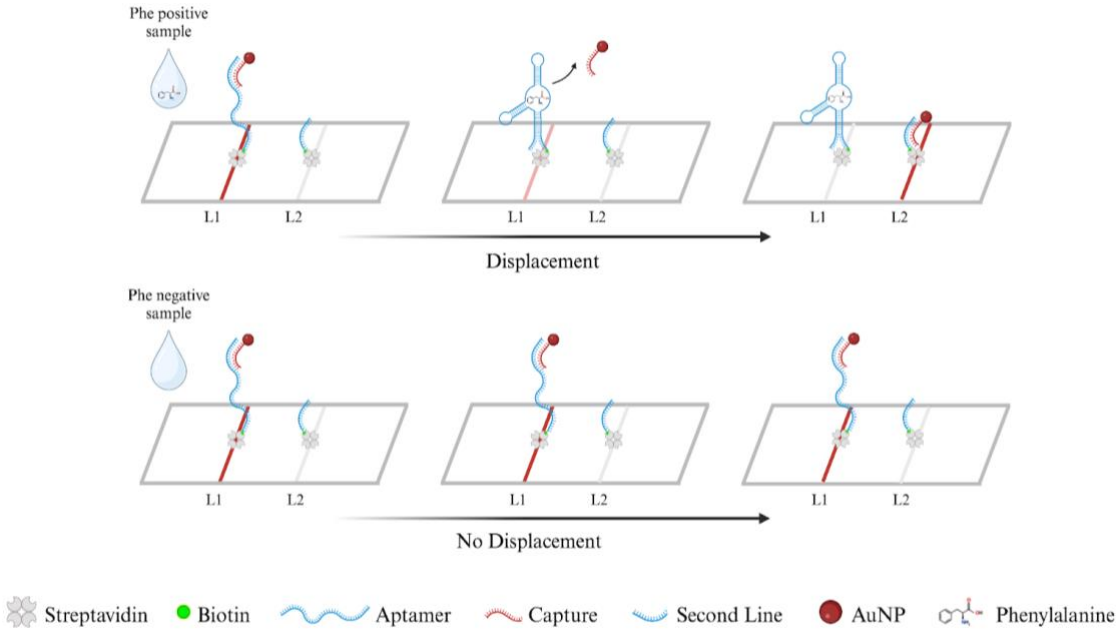
Table 2: Aptamer K_D Calculations of the different buffers and targets used.

Buffer	Tris-$MgCl_2$		PBS-$MgCl_2$		PBS		Water	
Target	AC	Phe	AC	Phe	AC	Phe	AC	Phe
KD	43,32 nM	26,43 μM	73,57 nM	34,13 μM	74,56 nM	335,7 μM	2 μM	366,24 μM

3.4.4. Phenylalanine Detection strategies

After characterizing all the components of our system and determining the conditions under which each component functioned best, we moved on to evaluate the aptamer's performance on a nitrocellulose platform in the different sensor designs.

3.4.4.1. Displacement assays



Scheme 6: Displacement assay for positive Phe samples (top) and negative Phe samples (bottom). Conformations 1 and 9 were chosen for the representations of L1 and L2, respectively. Created with Biorender.

In order to ensure the accuracy and effectiveness of displacement assays, it is crucial to assess the successful printing of the intricate molecular complex, composed of DNA-AuNP conjugates, biotinylated aptamer, and Str, onto the nitrocellulose. This initial assessment is necessary to confirm that the displacement of the DNA-AuNP conjugates occurs solely as a result of aptamer-target binding in a proportional manner. Further optimization would then be required to improve the sensor performance.

Different Phe concentrations were tested to evaluate the aptamer's ability to specifically bind phenylalanine and release the Capture conjugates in paper platform (Conformations 3 and 4). A polyT sequence was used as a control in place of each aptamer.

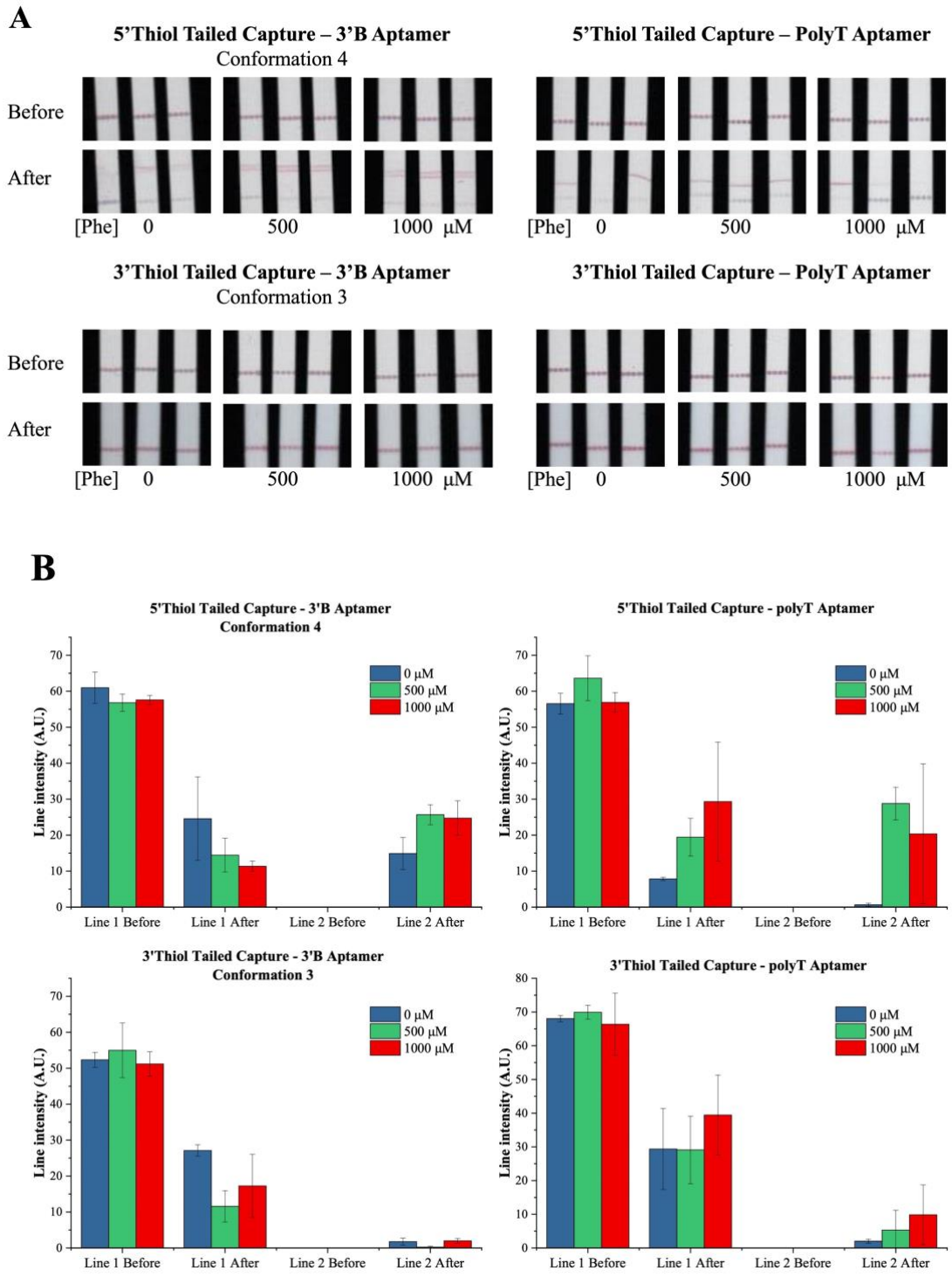


Figure 8: Displacement specificity test. A) LFA Half Strips. B) Image J measurements before (Lines 1 and 2, Before) and after (Lines 1 and 2, After) testing increasing Phe concentrations. Standard deviation error bars were obtained from triplicates.

Based on the results presented in Figure 8A and B, it appears that there is a correlation between the detachment of the capture sequence and an increase in target concentration (L1 After) for the

combination of the 5'Thiol Tailed Capture sequence with the functional aptamer (Conformation 4). While there is certainly room for improvement and optimization, this tendency is not seen in the case of 3'Thiol Tailed Capture (Conformation 4) and non-functional aptamers. However, a faint signal from capture sequences displaced from polyT aptamers in the control line indicated either a lack of specificity in the displacement or an excess of the conjugate that was washed out of L1. Although polyT aptamers experienced a signal decrease of approximately 50%, the intensity of hybridization in the second line did not correspond to that percentage. We could attribute this to the change in red tonality between dried lines (L1 Before) and after wetting with the sample (L1 After). This change in tonality was not perceived as a loss of intensity to the naked eye but can impact ImageJ measurements.

L2, on the other hand, displays varying intensities based on the direction of the capture strand used, indicating that 5'B Control sequence with 3'Thiol Tail Captures (Conformation 12) face steric hindrances that 5'Thiol Tail Capture does not (Conformation 11). This observation was not correlated with the findings shown in Figure 4, where more distanced Conformations (Conformation 9) yielded lower signal, suggesting that the addition of tails could have overcomed this issue. In addition, L1 of the functional aptamers demonstrated some aggregation in the displaced lines (Fig 8A, top, L1 After). Thus, further optimization is required in the conjugation process or LFA conditions.

3.4.4.1.1. Specificity tests

Tests were conducted to evaluate the specificity of the displacement tests in order to ensure the accuracy and reliability of the results. These tests aimed at determining whether there was any non-specific detachment of conjugates from the aptamer or an excess of the conjugate present in printed L1. At the same time, these assays were used to track possible aggregation of conjugates observed in previous experiments. Conformations 3 and 4 were put to test (Figure 9C and A, respectively), as well as the polyT Aptamer (Figures 9B, D and F) and the non-complementary Capture (Figure 9E and F).

As depicted in Figure 9, non-complementary Capture sequences were entirely displaced from the aptamers, flowing past Line 2 with no accumulation (Figure 9E and F). This confirms the specificity between the Aptamer, polyT Aptamer, Capture and Control Line sequences. Complementary Capture sequences, on the other hand, demonstrated specificity in the control line, as well as with both functional and non-functional aptamers (Figure 9A to C). Capture sequence were not displaced from non-functional aptamers (Figure 9B and D), indicating correct hybridization of the sequences prior to printing and a better control of possible excess of the conjugate (Figure 9B). However, unspecific

displacement was observed when Phe-free samples were applied to functional aptamers, obtaining very similar displacements with or without Phe (Figure 9A and C), which will be monitored in the following experiments.

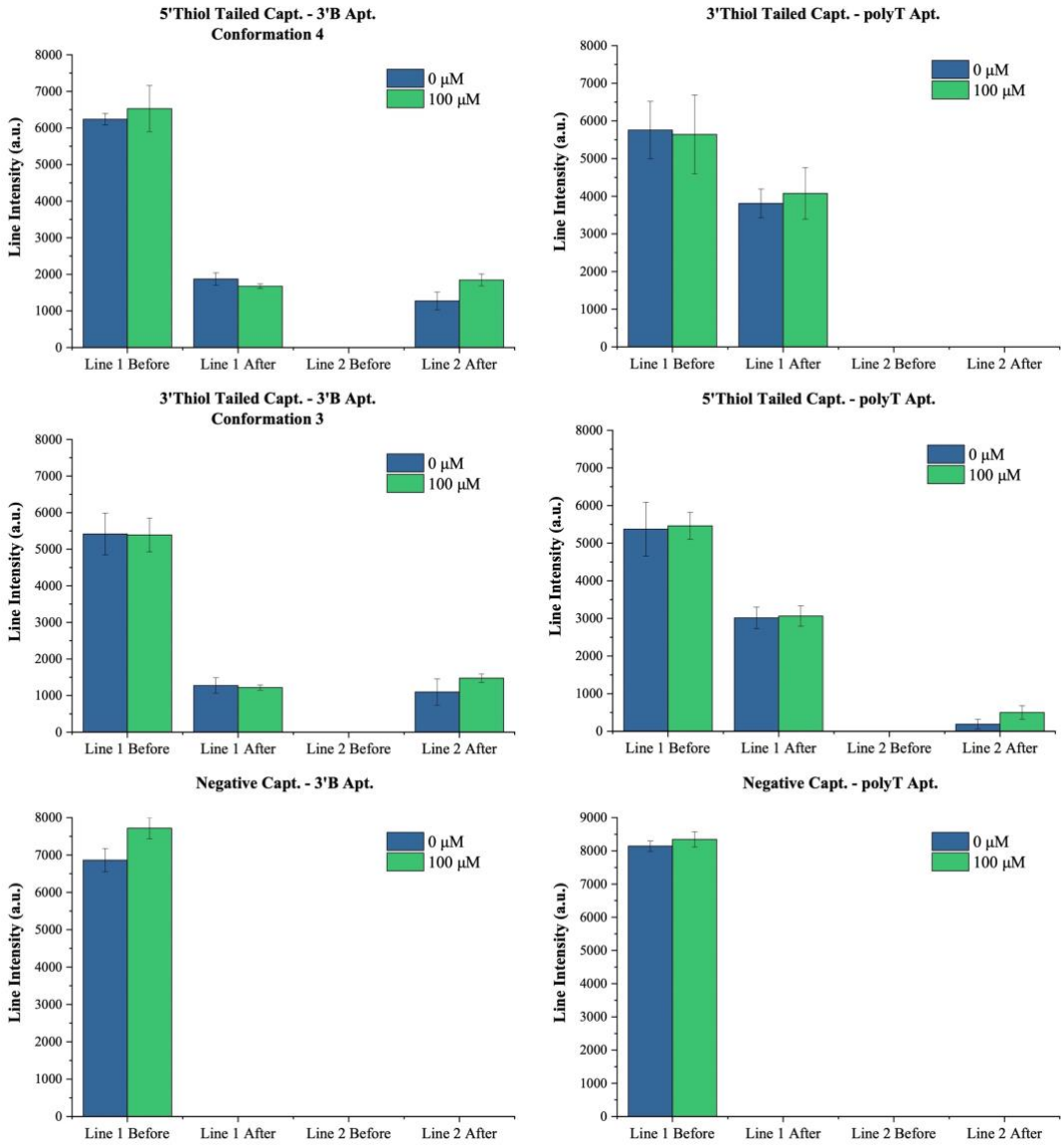


Figure 9: Specificity displacement test of Conformations 4 (A) and 3 (C), as well as polyT Aptamer (B, D,F) and Negative Capture (E and F) controls. Triplicated strips were scanned before (Lines 1 and 2, Before) and after running the samples (Lines 1 and 2, After) with (green) or without Phe (blue) and analyzed using ImageJ.

To ensure that the capture conjugates are effectively hybridized to the aptamer, rather than merely deposited onto the nitrocellulose, we conducted further specificity tests. These tests involved evaluating the unspecific adsorption of the conjugated Captures to the nitrocellulose. We performed displacement tests on functional (Figure 10, top) and non-functional aptamers (Figure 10, middle),

as well as without aptamer, by directly printing the conjugated Capture onto the nitrocellulose (Figure 10, bottom).

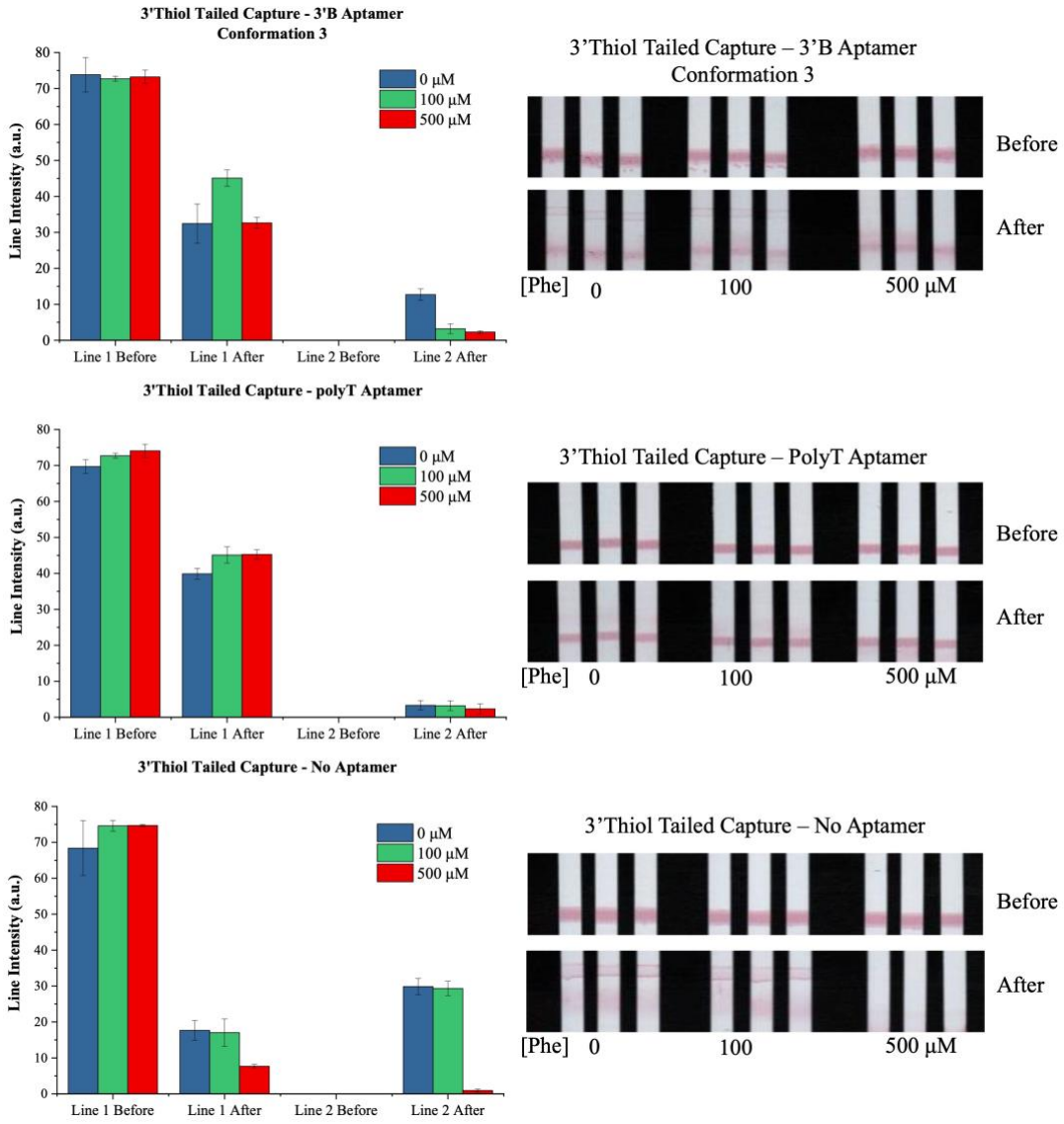


Figure 10: Specificity displacement test using Functional Aptamer (top), non-functional polyT Aptamer (middle) and without Aptamer (bottom). Triplicated strips (right) were scanned before (Line 1 and 2 Before) and after (Line 1 and 2 After) running increasing concentrations of Phe using ImageJ (left). Conformations 3 and 12 were used for Lines 1 and 2, respectively.

The flow effectively displaced almost all of the directly printed Capture sequences, while some of them were retained in the L1 area (Figure 10, bottom). This highlights the importance of optimizing the flow to prevent any residual unspecifically adsorbed conjugate from remaining on the nitrocellulose. However, the Aptamers and Capture sequences printed together (Figure 10 top and middle) performed similarly to the previous assay. The non-functional aptamer (Figure 10, middle)

displaced very few conjugates that were invisible to the naked eye in the L2, whereas functional aptamers showed more displacement, although non related to the Phe concentration.

3.4.4.1.2. Screening tests

Screening assays were conducted to find the optimal Aptamer-Capture sequence combination (or Conformation) for superior binding, displacement, and effective LFA performance. Both directions of the functional aptamer were tested against the two capture sequences and their two tailed versions (Conformations 1 to 8), while the non-functional aptamer served as a no-displacement control.

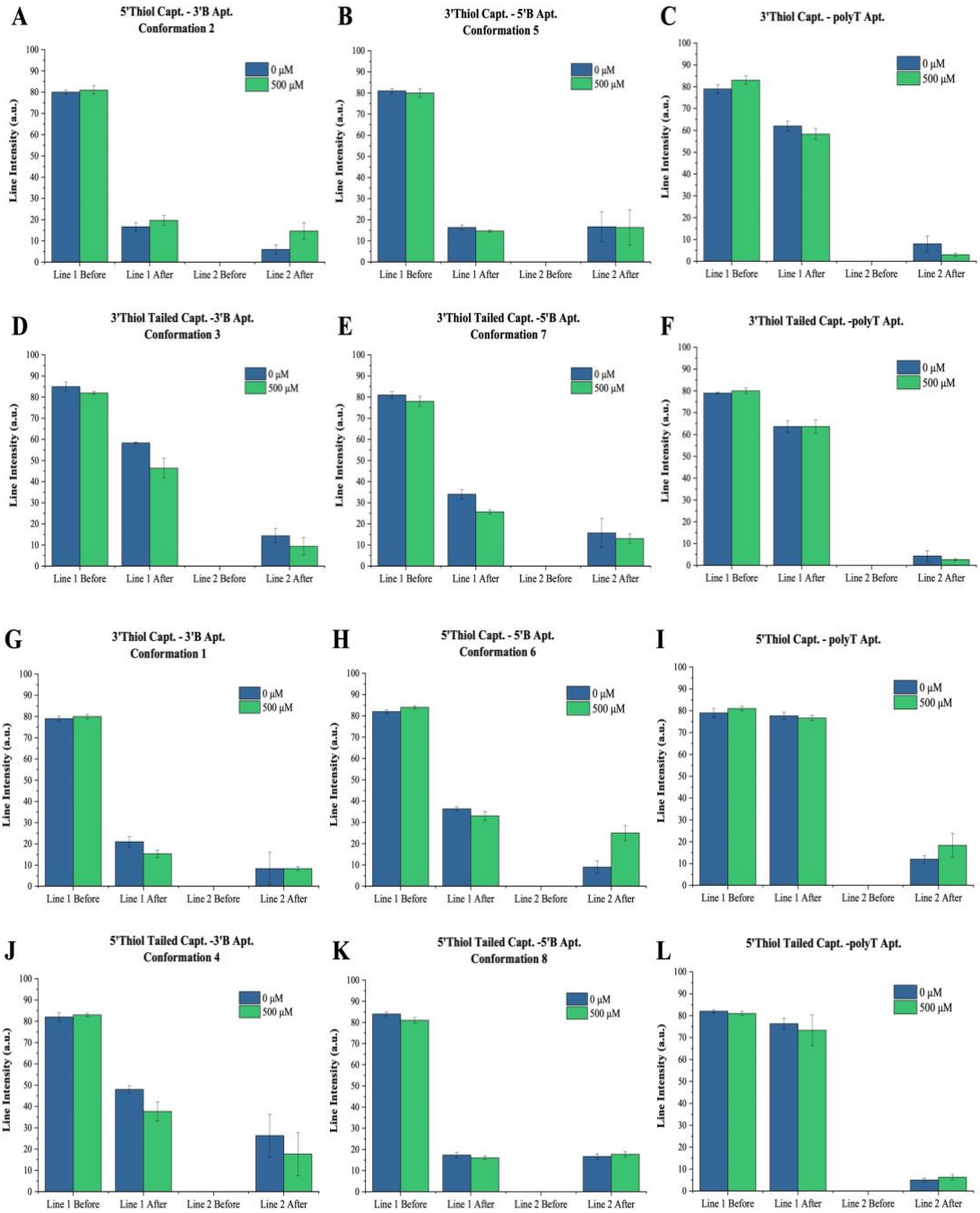


Figure 11: Screening tests of all Conformations (1-8) available for L1. PolyT Aptamers were used as controls (C, F, I and L) that did not displace for each Capture sequence.

Based on the data presented in Figure 11, the polyT aptamers were effective in identifying unspecific displacement, as established in previous assays. The L2 values for these aptamers (values <10 A.U in this case) were barely noticeable to the naked eye, whereas most L2 values for the functional aptamers were visible. Upon comparing the directionality of the functional aptamers, it was observed that the 3'B aptamer maintained a higher intensity in L1 than the 5'B aptamer after displacement for each of the Capture cases (A vs. B, D vs. E, G vs. H and J vs. K), which can be desirable for further optimization and modulation of the lines' intensity. However, we observed that only the combination of the 5'B aptamer and 5'Thiol capture sequence (Conformation 6) responded positively to the presence of Phe, and the intensities of the L2 were more correlated to the Phe concentration than in the rest of the cases.

The reason why the blank samples released more capture sequence from the functional aptamers than the poly T remains uncertain. Our theory is that the binding buffer induces a conformational change into a secondary structure, independent of the target's presence, which partially displaces the capture sequence. However, the polyT "aptamer's" vastly different sequence does not undergo such conformational change and, therefore, does not displace the capture sequences.

Efforts to replicate previous results for further optimization were unsuccessful. After several rounds of adjustments and optimization, there were significant variations in the results. However, through further screenings and iterative adjustments, positive results were obtained (Figure 12) for the same orientation of Aptamer and Capture sequence, although using the tailed version of the Capture (Conformation 8 instead of 6). Despite attempts to reproduce these results using both the current (5'B aptamer and 5'Thiol tailored capture sequence, Conformation 8) and previous working combinations (5'B aptamer and 5'Thiol capture sequence, Conformation 6), success was not achieved.

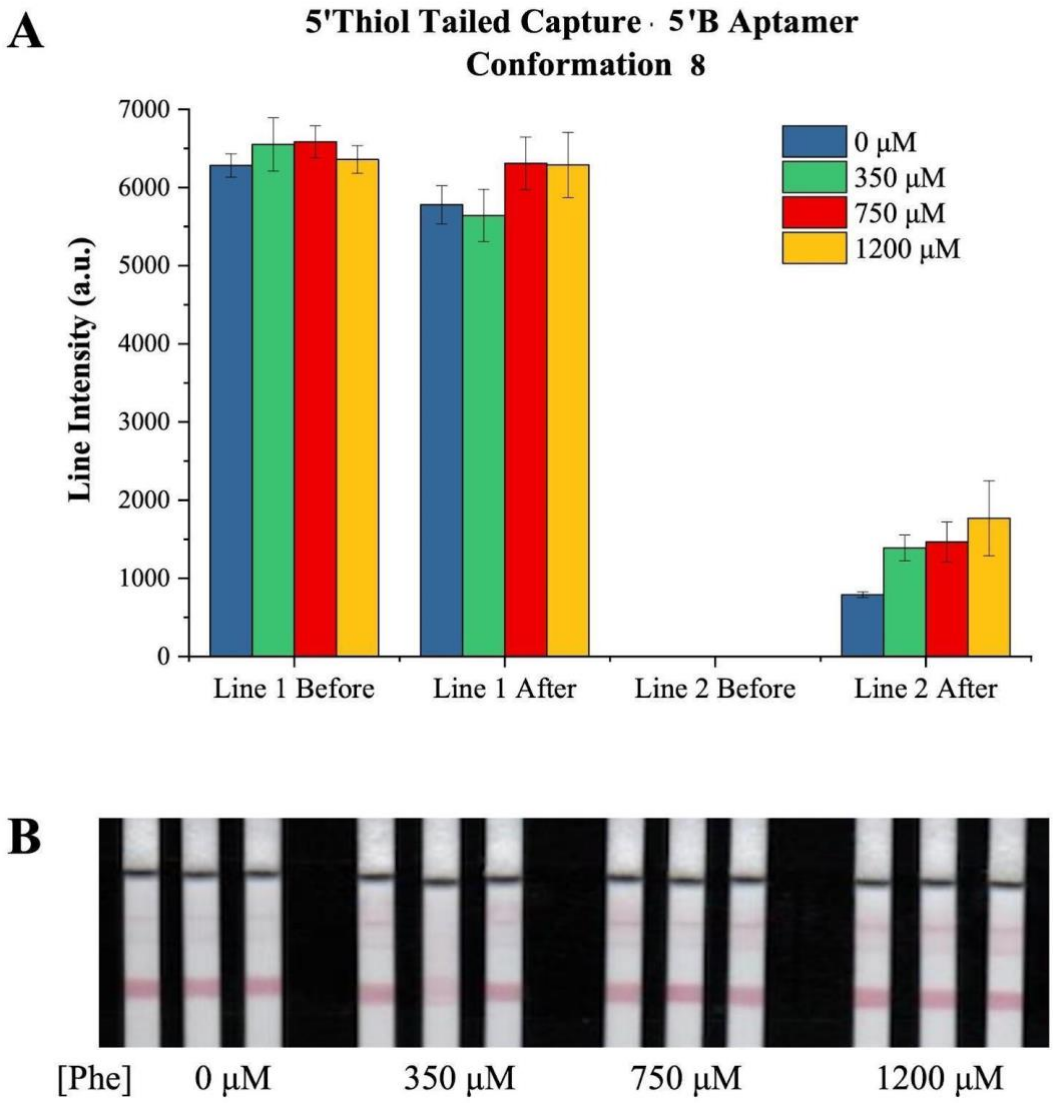


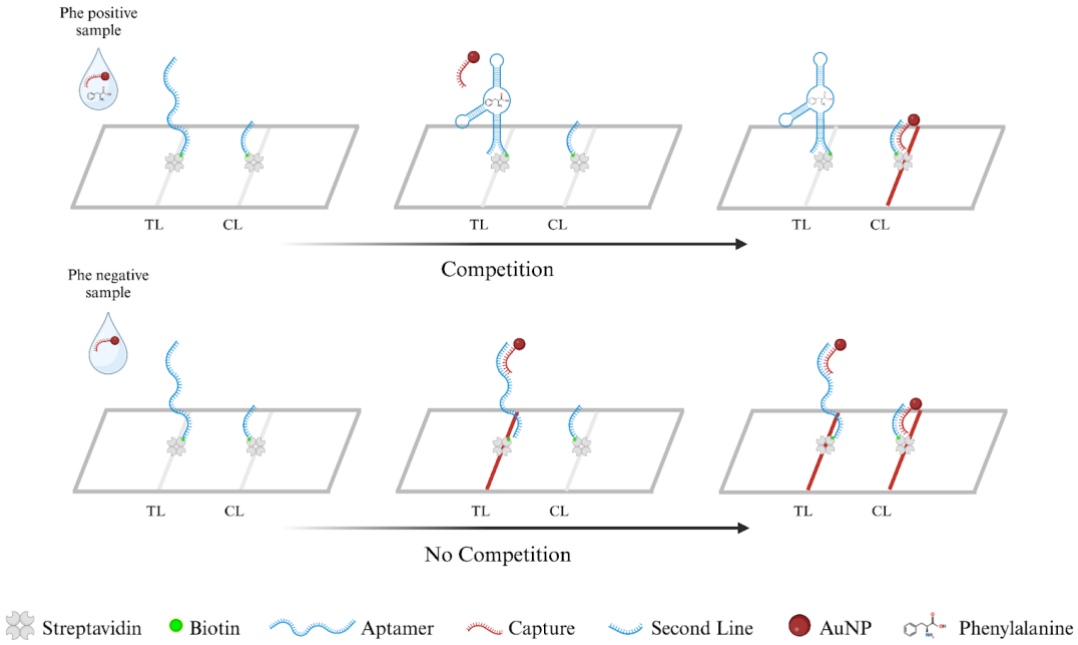
Figure 12: Best attempt of Displacement assay, using Conformation 8. A) ImageJ measurements. B) Strips triplicates 20 minutes after running the samples with increasing concentrations of Phe.

The displacement assays conducted in this chapter exhibited a concerning level of irreproducibility, which unfortunately posed a significant challenge to the optimization process. This issue warrants further investigation to identify the underlying causes and develop strategies to enhance the reproducibility of the assays. Besides, the inability to achieve reproducibility with the Biospotter for printing solutions containing AuNPs hindered the optimization of the initial signal and, as a result, the optimization of the detachment of conjugates and their accumulation in L2. Thanks to the possibility of printing in an IsoFlow dispenser, competitive assays might overcome these limitations.

3.4.4.2. Competitive assays

3.4.4.2.1. Printed aptamer

In this version of competitive assays, Str and biotinylated Aptamer are printed and dried onto the nitrocellulose in the TL (Scheme 7).



Scheme 7: Printed Aptamer Competitive assay for positive Phe samples (top) and negative Phe samples (bottom). Conformations 1 and 9 were chosen for the representations of TL and CL, respectively. Created with Biorender.

The conjugated Capture has to flow through all the strip, i.e., both lines. Up until now hybridization between the Aptamer and the Capture sequence has only been tested in solution, it was not certain that they would bind to each other in the nitrocellulose matrix.

To evaluate if Aptamer-Capture sequence binding is possible in the LFA, strips were printed with both functional Aptamers (with biotin on either terminus) and with polyT Aptamer separately, and a Capture and Negative Capture controls run through the strips (Figure 13). Phe target concentrations were applied to evaluate competition between target and conjugated Capture. As depicted in Scheme 7, we would hypothesize that if the aptamers bind to the Phe target, it would create a change in the secondary structure that would not allow the Capture sequence to hybridize, and therefore imepede the apparition of TL, and viceversa. Printed polyT aptamers, however, are not reactive to Phe and should allow TL apparition in every case. Negative Capture sequences should flow through the entire strip and not generate any of the Lines, independently of the Aptamer and CL sequences used.

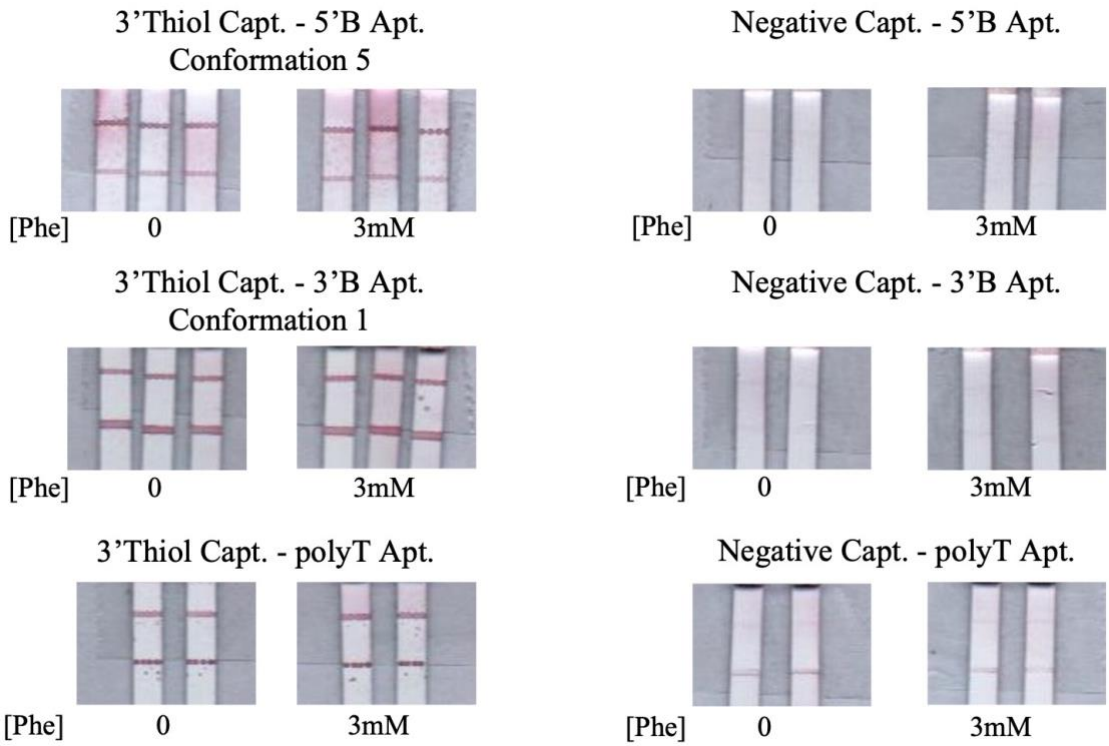


Figure 13: Specificity assay in competitive format. Complementary or Positive (left) and non-complementary or Negative Capture sequences (right) were tested against functional (5'B and 3'B) and non-functional (polyT) aptamers.

From the results presented in Figure 13, we were able rule out any non-specific accumulation of conjugate in both the TL and CL, since the Negative Capture sequences did not hybridize in either of them. However, some nonspecific signal appeared between non-functional polyT Aptamer and Negative Capture sequences, which we attribute to the high adenine content of the Negative Capture (Annex 1).

Additionally, we observed that the directionality of the printed aptamer played a significant role in the conjugate's ability to hybridize with the complementary region. Notably, the 3'B aptamer, featuring the complementary region to the capture at the opposite end of the anchoring point (Conformation 1), appeared to facilitate the conjugate's hybridization. However, competition between the conjugate and the Phe to bind to the aptamer was not observed. Neither functional aptamer presented any signal variation even in high target concentrations, as non-functional aptamers did. This means that in these experiments the Phe is not capable of binding to the aptamer or has a much lower binding affinity than the capture sequence, so the effect of its binding is not visible in this format. In order to remedy this, we began by trying to evaluate the binding affinity between the aptamer and the capture sequence.

To simplify these experiments, we decided to focus on just one of the two functional aptamers, we chose the 3'B aptamer since it had performed best in the initial screening (Figure 13). We then tested it against the 4 different Capture sequences, enabling us to compare Conformations 1 to 4.

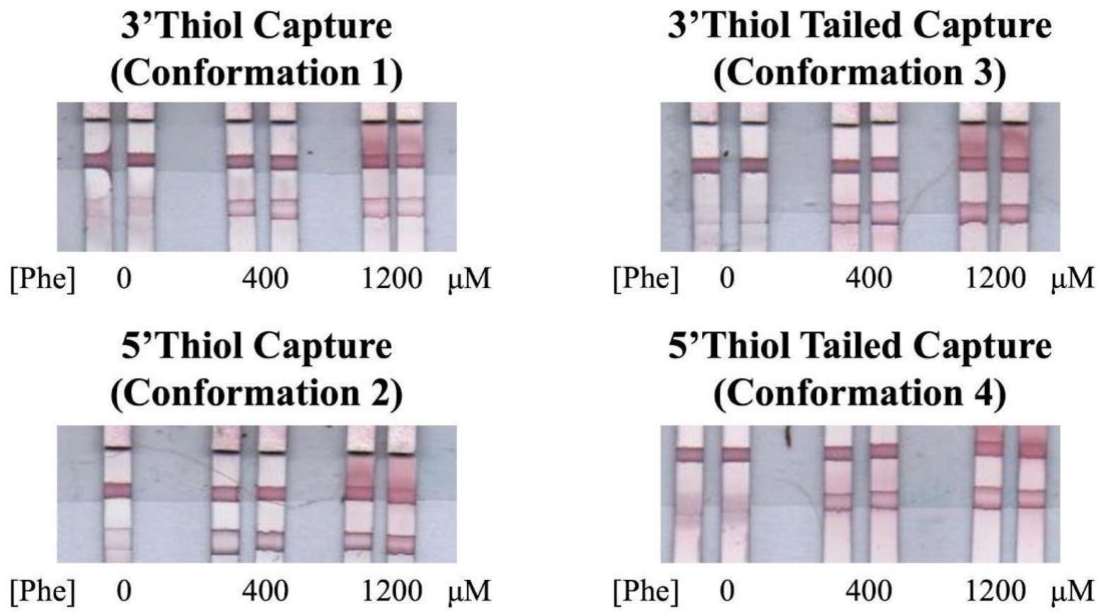
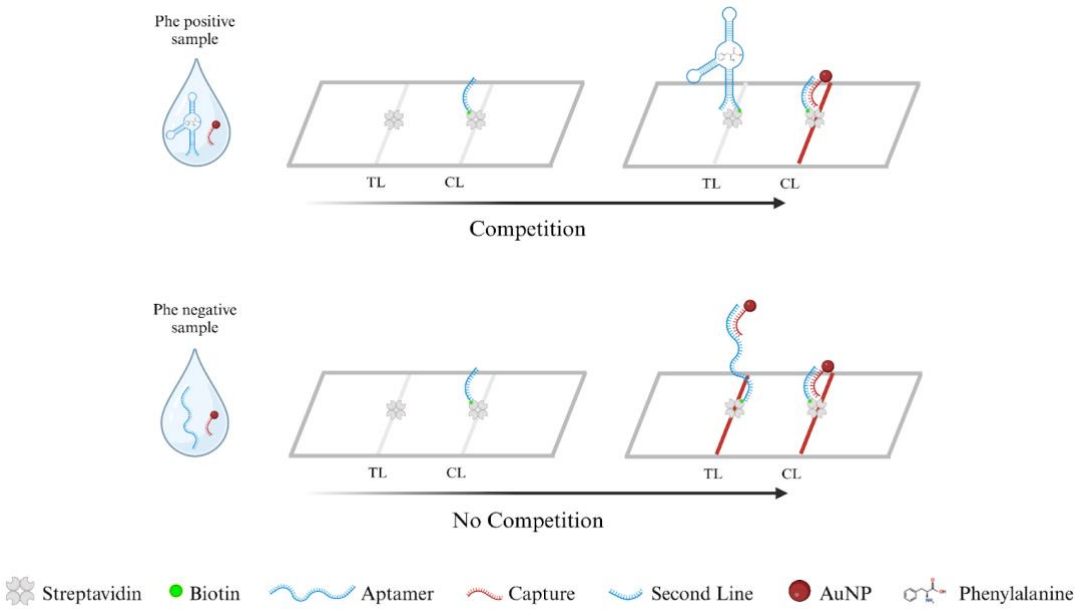


Figure 14: Capture sequence screening in competition with increasing concentration of Phe using 3'B Aptamer, resulting in Conformations 1 to 4.

Based on the data presented in Figure 14, increasing concentrations of Phe did not appear to compete with the different Capture sequences. Conformation 1 strips seemed to generate less intense TL in high concentrations of Phe in comparison to the other Conformations, suggesting a lower affinity for the conjugated Capture. However, every conformation seemed to have a higher affinity for the Capture sequence than for the target. Besides, we have discovered an anomalous result in which the absence of the target corresponds to the absence of the TL, and vice versa. Despite numerous attempts to modify this outcome for both functional aptamers, we have repeatedly observed this contradictory behavior. Our current theory suggests that the presence of Phe may trigger a conformational shift in the printed aptamer, thereby enabling access to both the target and the Capture sequence. Conversely, the lack of Phe may fail to restore the aptamer's state after being printed and dried onto nitrocellulose. What is clear from these experiments is that the aptamer does not seem to be binding to the Phe in nitrocellulose like it did in solution (see the fluorescence data in section 3.4.3.). We therefore devised a new competition assay in which the binding could be done in solution prior to running in the LFA, this involved printing streptavidin onto the nitrocellulose.

3.4.4.2.2. Printed Streptavidin



Scheme 8: Printed Streptavidin Competitive assay for positive Phe samples (top) and negative Phe samples (bottom). Conformations 1 and 9 were chosen for the representations of TL and Control Line CL, respectively. Created with Biorender.

This approach to the competitive format differs in that biorecognition and competition events occur in solution prior to loading the sample onto the LFA strip, eliminating any inhibitory effect the nitrocellulose might be playing on the hybridization/Phe binding. The strip then generates a signal that corresponds, ideally, to the events that occurred in solution. This method has the potential to enable successful biorecognition events due to the stringent requirements of the aptamer, which can be better controlled in solution. However, it is important to note that this approach requires flowing the Aptamer, capture DNA and target molecules through the entire LFA strip, which could result in varying flow rates, selective filtration of some of the elements, or a loss of sensitivity.

An initial screening of Capture sequences (Figure 15) was carried out, targeting the 3'B aptamer (Conformations 1 to 4) at varying concentrations of Phe.

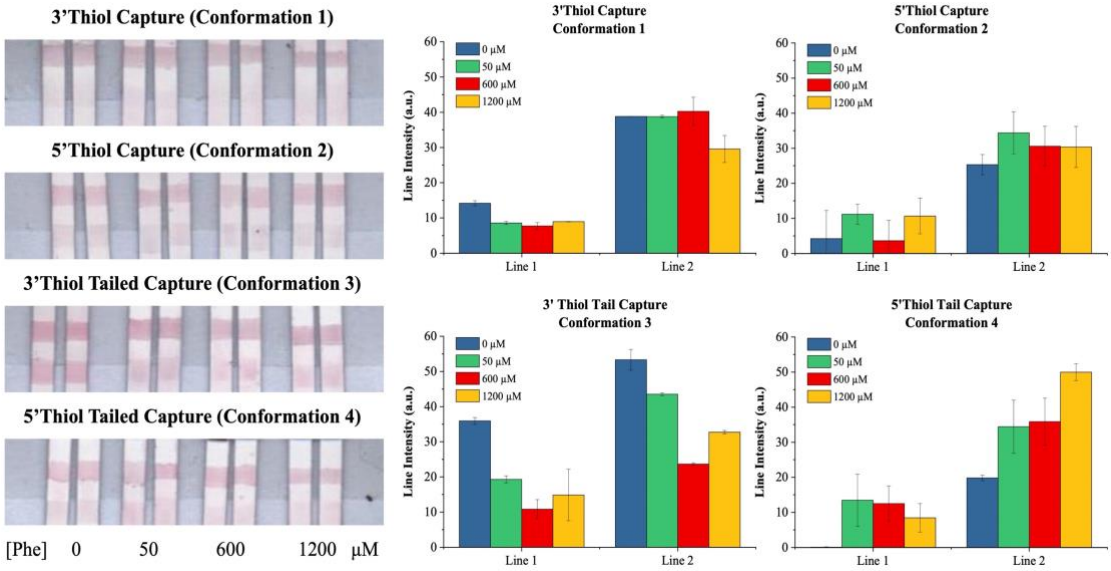


Figure 15: Capture sequence screening in competition assay with increasing concentrations of Phe using 3'B Aptamer (Conformations 1 to 4).

The shorter capture sequence failed to produce a signal in the TL (Conformations 1 and 2). Neither of the 5'Thiol capture sequences (Conformations 2 and 4) exhibited discernible differences in signal intensity relative to Phe concentration. As depicted in Figure 15, the pairing of the 3'Thiol tailed Capture sequence with the 3'B aptamer (Conformation 3) initially displayed a favorable response to Phe concentrations. Unfortunately, efforts to replicate this result were met with repeated failure.

At this point it seemed prudent to determine if the competitive sensing strategy would work with this aptamer or not. To do so experiments were designed using the AC as an alternative target. This would logically outcompete the shorter conjugate DNA strands. These tests were conducted using 3'Thiol capture sequences of the two different lengths and the 3'B functional aptamer (Conformations 1 and 3). Strips flowing only the conjugate with no Aptamer, target nor AC allowed us to investigate if the presence of Str alone results in nonspecific binding of the conjugate, which would lead to signal generation.

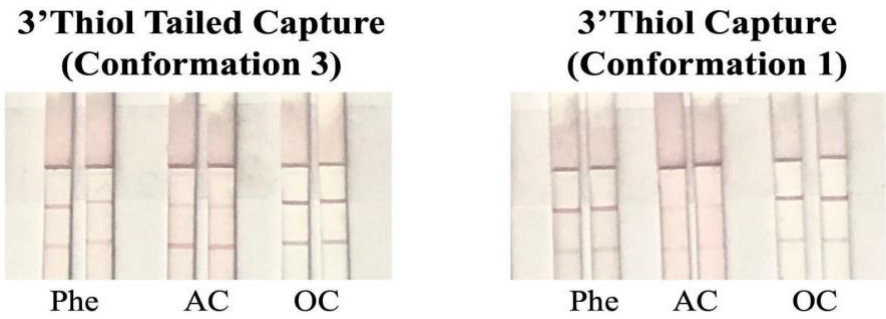


Figure 16: Competition test of Phe target or Aptamer Complementary (AC). Only Capture (OC) conjugates were used as specificity control, without the presence of aptamer.

As illustrated in Figure 16, both conjugated Capture sequences' versions display nonspecific TL generation, even in the absence of any aptamer (OC). It is believed that the functional groups of Str may interact with the conjugates, causing them to be retained in the TL. Although this lack of specificity caused by proteic elements (antibodies, proteins, or peptides) is a well-known concern within the LFA community, they can be easily remedied through the use of blocking agents or the addition of surfactants.[31]

In the case of samples containing the AuNP-DNA incubated with both the aptamer and an excess of Phe target (Figure 16, Phe), it was observed that Phe did not completely hinder the hybridization to the aptamer, regardless of the Conformation used. However, in the case of Conformation 1 we can observe a decay in the intensity that suggests possible binding of Phe.

When examining incubations with AC (rather than Phe), two distinct events occurred that did depend on the length of the Capture sequence used. Specifically, AC was able to almost completely prevent the hybridization of the 3'Thiol Capture (Conformation 1) to both the Aptamer and the CL sequence. However, the longer version of the capture sequence (Conformation 3) was able to either displace the AC, significantly compete with the AC and the aptamer, or nonspecifically accumulate in the streptavidin loaded TL. It is suspected that the presence of the AC might provide structural stability to the aptamer, allowing access to the longer version of Capture sequence (Conformation 3) over the shorter version (Conformation 1). The underlying cause for this behavior remains unknown and additional investigations were performed to evaluate the limiting factor or other relevant factors in the system (Figure 20).

The previously outlined optimizations to the displacement and competitive assay approaches did not yield functioning tests, although they did establish that come of the sensing strategies could potentially work. Displacement assays (Figure 12) and competitive assays with printed streptavidin (Figure 15, Conformation 3) did show the potential of responding to Phenylalanine, whereas competitive assays with printed Aptamer did show contradictory results. Displacement assays relied on more irreproducible printing methods, often leading to loss material and time, and entailed more complicated logistics.

Consequently, we initiated a comprehensive exploration of alternative optimizations aimed at enhancing the platform´s performance in printed Str competitive assays, since the simplicity of printing equal TL and CL for all conditions and the simplicity of single lecture of the results, versus the double lecture required by displacement assays (before and after).

3.4.5. Strategies for Enhancing Lateral Flow Assay Performance

The strategies for enhancing the response primarily focused on modulating the signal in response to Phe. This involved modifying the aptamer's environment in the LFA conditions to ensure optimal structural stability and binding to the Phe target. Additionally, efforts were made to minimize potential unspecific interactions that could obscure the response to Phe, and gain insight into the structural stability of the aptamer in the LFA nitrocellulose platform. These strategies involved the introduction of blocking agents and surfactants, the substitution of key components within the assay, and further adjustments. Each of these optimizations will be discussed in turn in this section.

3.4.5.1. Lateral Flow optimization strategies for signal modulation

We conducted several optimization strategies to improve the binding conditions and sensitivity in printed Str competitive strips. Firstly, we treated the sample pad to reduce affinity interactions between the capture and the aptamer and increase aptamer-Phe interactions, as well as reducing non-specific binding on the TL. To start with, we tested the efficacy of BSA for this application, which is a typical blocking agent in LFA. However, upon realizing that BSA contains Phe in its structure, which could lead to cross-reactivity of the Aptamer, we discarded it for further tests. Instead, we tested PEG 2050 and switched to PBS or Tris-$MgCl_2$ as solvents for the sample pad blocking (Figure 17). After careful consideration, we concluded that the Tris-$MgCl_2$ buffer was best suited for the continuation of the experiments, as it also served as the BB and slightly improved the flow of the strips.

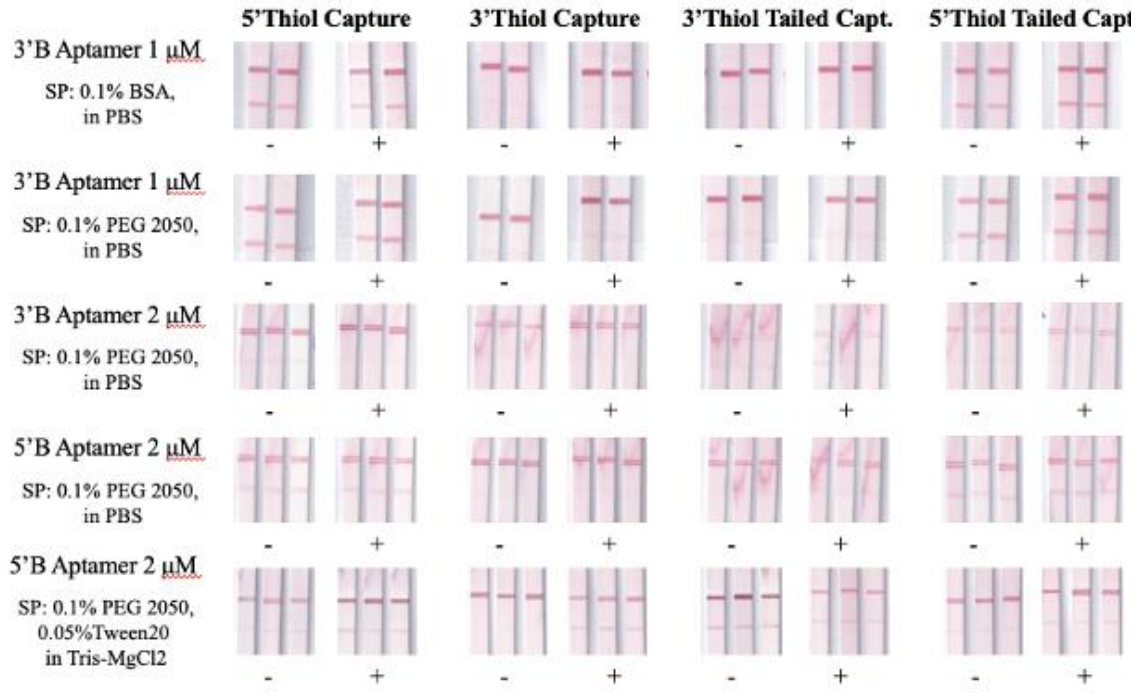


Figure 17: Sample pad blocking strategies in different combinations of Aptamer and Capture sequences, tested with samples without (-) or with (+) Phenylalanine.

Next, we tried blocking the nitrocellulose with PEG of three sizes, 2050, 6000 and 20000. However, it did not allow proper functioning of the LFA strips. We also experimented with the addition of blocking agents to the Running buffer (Figure 18). In this case, we tested the same three sizes of PEG in the running buffer, so that the blocking agents were present during the binding events, and not after, as happens with the sample pad blocking. We also tested Tris-$MgCl_2$ buffer to match the sample pad blocking buffer and the same buffer diluted to half in order to compensate the ionic strength added by the reconstitution of the crystalized buffer of the sample pad, but none of these modifications to the running buffer resulted in an improvement.

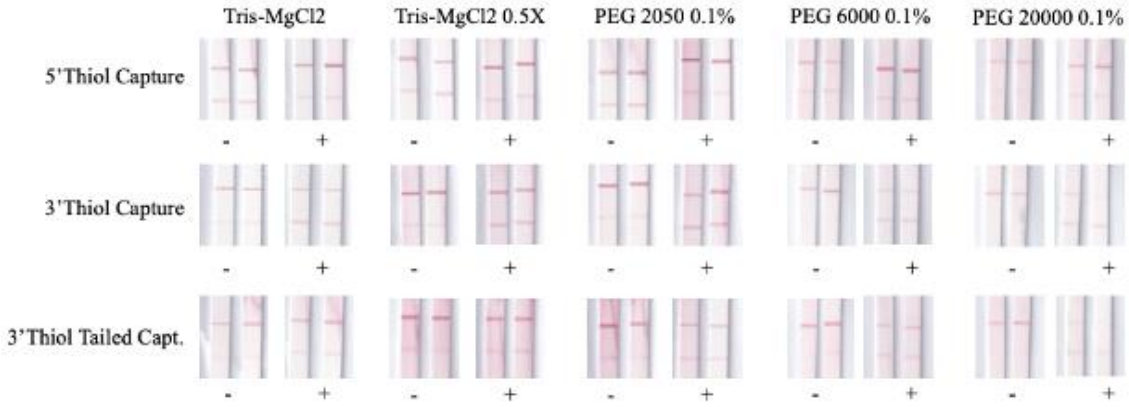


Figure 18: Running buffer blocking strategies.

Lastly, we added betaine to the running buffer to evaluate if this isostabilizing agent (a reagent that helps to stabilize proteins and nucleic acids, especially under conditions that might otherwise lead to their denaturation or aggregation) could improve the capture-aptamer interactions in Phe-free samples. However, this addition also did not yield any improvement and the opposite behavior was observed as in previous assays (Figure 19).

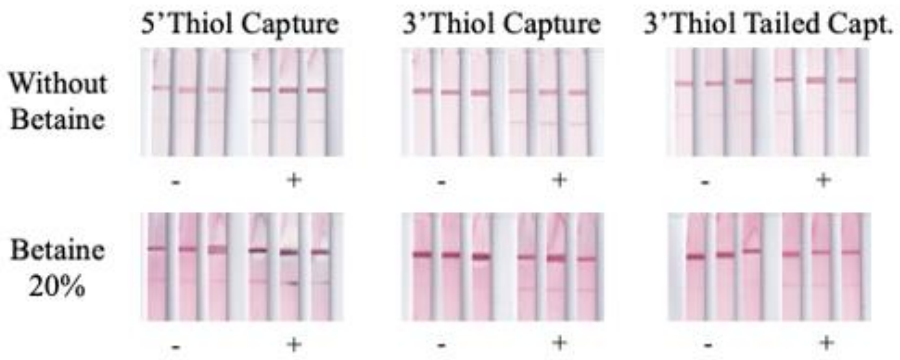
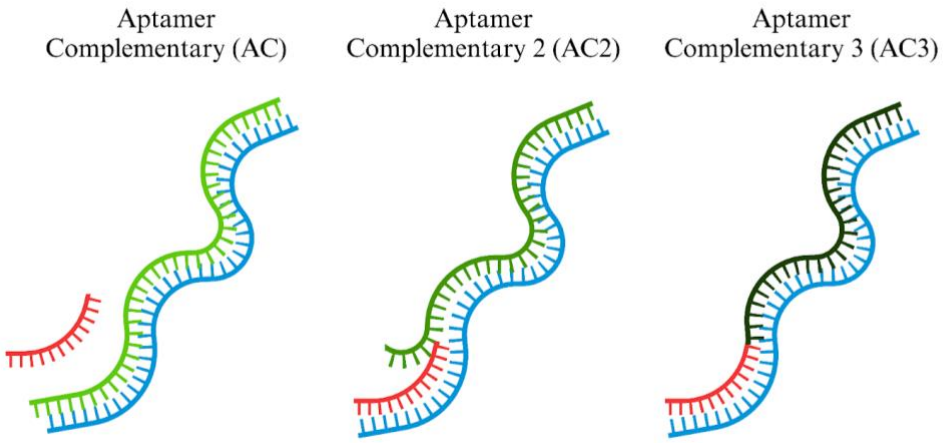


Figure 19: Betaine addition in Running buffer as isostabilizing agent.

To gain a better understanding of the nucleic acid system and the state of the aptamer during the assay, we tested the aptamer against varying sizes of its AC in competition with the Phe molecule (Scheme 9).



Scheme 9: Schematic representation of the different lengths of AC used. AC is 51 nt, AC2 is 46 nt, and AC3 is 41 nt long. A Capture sequence (red) is represented in competition with the respective ACs. Created with Biorender.

The aim of this evaluation is to test the previously mentioned structural stability that the complementary sequences could be providing to the aptamer, in terms of signal generation (Figure 20).

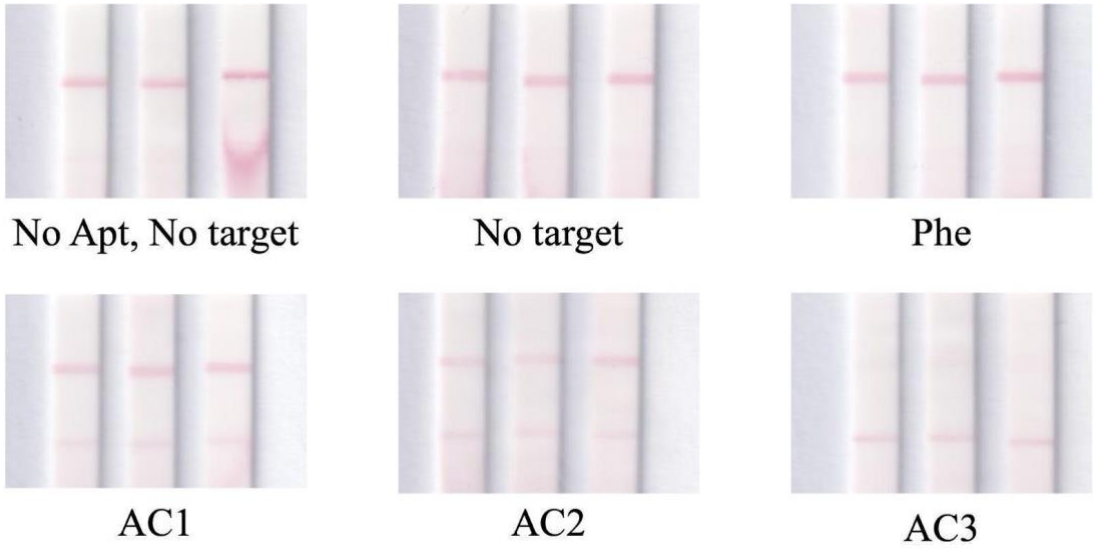
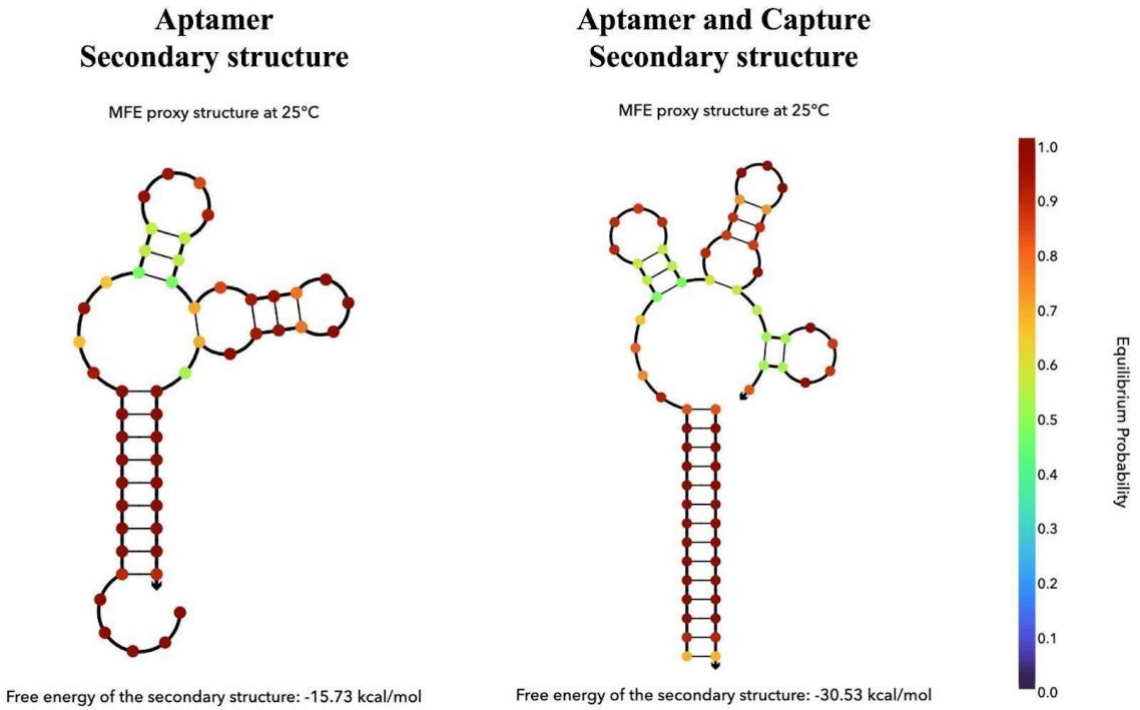


Figure 20: Testing of different sizes of Complementary sequences and Phe target.

As observed in Figure 20, the three sizes of complementary sequence (AC, AC2 and AC3) could bind simultaneously to the aptamer with the AuNP-DNA. In this assay, the aptamer failed to

hybridize to the Capture sequence in blank samples (Figure 20, No target), and Phe samples (Figure 20, Phe), whereas the opposite scenario occurred when any of the three complementary sequences were present. This suggests that, although the complementarity and specificity between aptamer and Capture have been repeatedly proven, the position of the complementary region plays a role in the structural conformation of the aptamer and the exposure of the biotin groups. If that is the case, though, Aptamer and Capture sequences could be hybridizing in the strips without any target present, but the site of the hybridization may not suppose a conformational change that allows biotin exposure and, therefore, TL apparition. Alternatively, we could theorize that the single stranded region of the aptamer after Aptamer-Capture binding (Scheme 10, right) could potentially interact with the nitrocellulose and be retained before the TL, whereas the coverage of these nucleotide bases by the different AC lengths could block potential interactions between the nucleotide bases and the nitrocellulose.

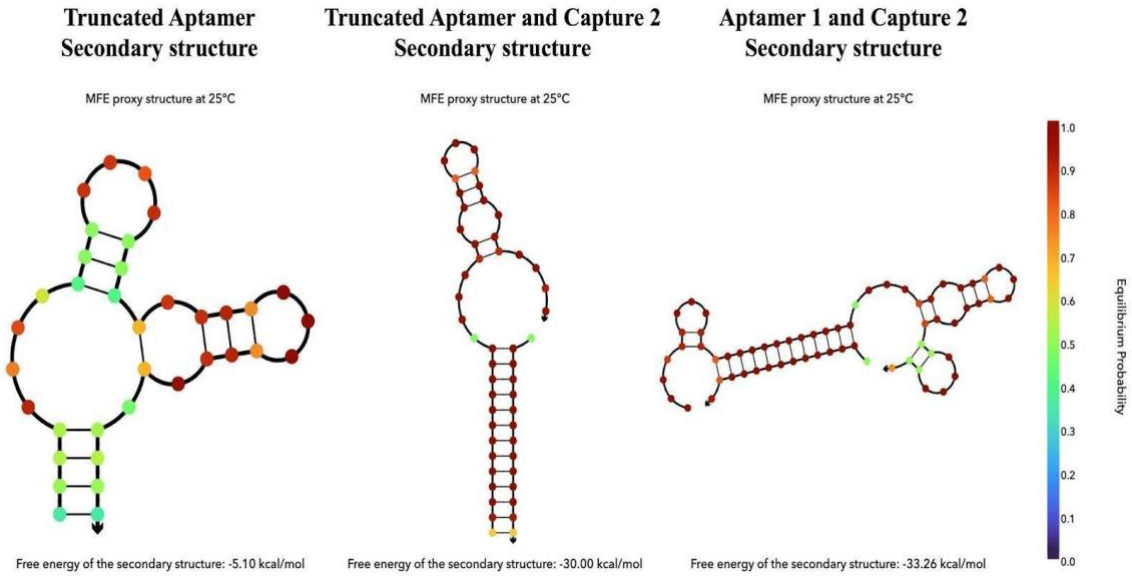


Scheme 10: In Silico representation of the secondary structure of a) Aptamer sequence, and b) Aptamer and Capture sequences. Obtained with NUPACK.

3.4.5.2. Substituting Nucleic Acid System Elements: Evaluating Alternatives

In our quest to develop a PoC LFA for Phe detection, we took a final opportunity to apply all of our accumulated knowledge and expertise. After an *in-silico* comparison of the secondary structures of the sequences reported by Yang *et al.*, we sought to identify a nucleic acid system that would generate signals with fewer steric hindrances and, ideally, exhibit a stronger affinity for the Phe molecule in

a paper platform. In the previously introduced work by Yang *et al.*, they utilized a truncated thiolated version of the aptamer for tuning aptamer-field-effect transistor (FET) responses (Scheme 11). The original aptamer was employed for competitive fluorescence assays, while its truncated thiolated version was utilized while immobilized to a In_2O_3 surface for the sensitive detection of free Phe, suggesting compatibility with its anchorage to a biosensing platform. Besides, the shorter length of this aptamer could imply a more stable secondary structure and lower interactions between the aptamer and nitrocellulose.



Scheme 11: In Silico representation of the secondary structure of a) Truncated Aptamer sequence, b) Truncated Aptamer and Capture 2 sequences, and C) Aptamer 1 and Capture 2 sequences. Obtained with NUPACK.

This involved testing a new set of nucleic acid sequences featuring the truncated version of the aptamer and its corresponding Capture (Capture 2) and CL (CL2) sequences (Figure 21). Besides, a thiolated version of the original Aptamer and the Truncated aptamer were procured to evaluate an inverse competitive system. Similarly, biotinylated versions of the AC and Truncated AC were procured as the anchor to the streptavidin TL for these inverse systems. Additionally, complementary sequences to the two aptamers were utilized as target as in the previous system. All these combinations underwent competitive assay testing in the printed Str format to simplify the tests (Figure 21).

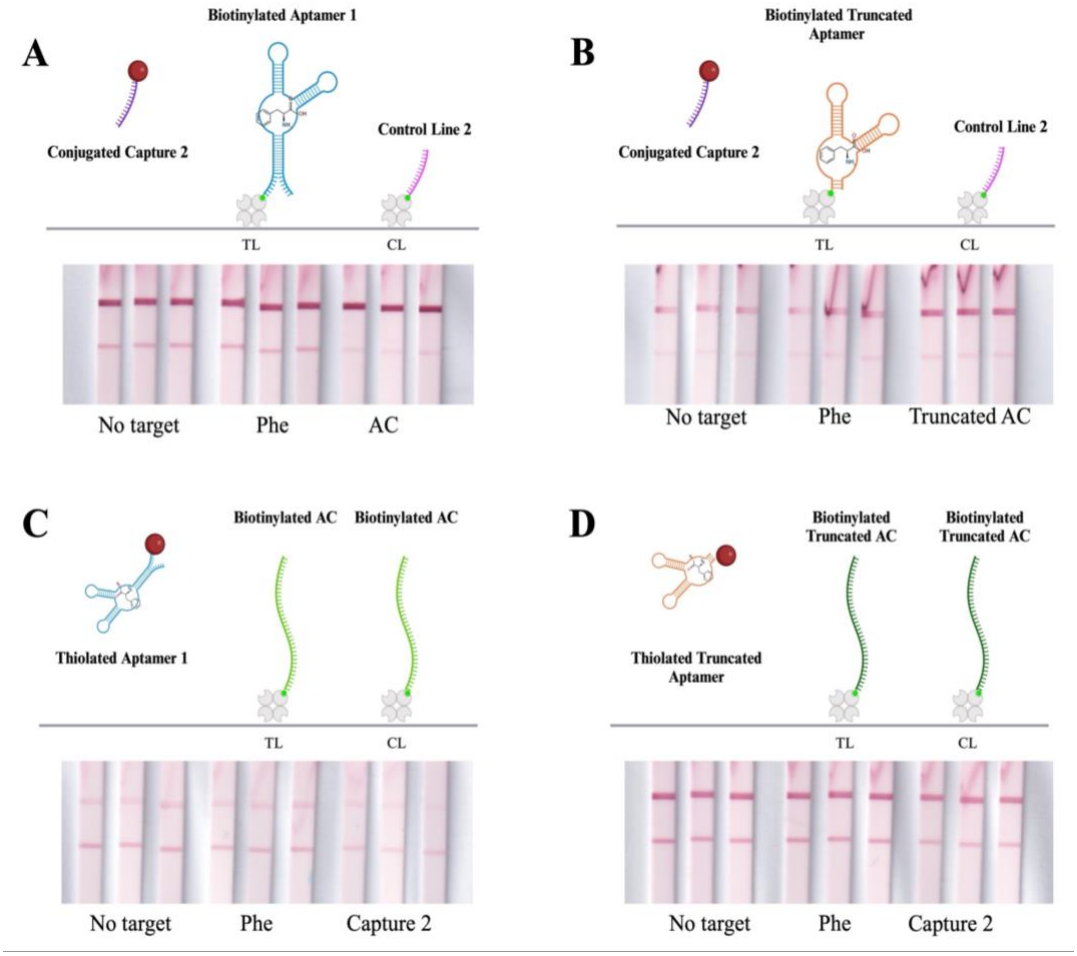


Figure 21: Schematic representation and LFA strips for the following combinations: A) Conjugation of Capture 2 sequence combined with biotinylated Aptamer and B) combined with biotinylated truncated aptamer. C) Conjugation of thiolated Aptamer combined with biotinylated AC. D) Conjugated Truncated Aptamer combined with biotinylated Truncated AC. All four combinations were tested without target, with Phe, and with a complementary sequence.

None of the combinations shown in Figure 21 responded to the presence of Phe target as we would expect. The combination of the original Aptamer with Capture 2 sequence (Figure 21A) did not improve the steric hindrances presented during the previous competitive assays. Similarly, the implementation of the Truncated Aptamer and its Capture 2 and CL 2 sequences (Figure 21B) did not perform as expected in the paper platform, with no changes in TL intensity regardless of the presence of target(s), as well as a poor CL generation. Lastly, conjugation of the Aptamer (Figure 21C) or the Truncated Aptamer (Figure 21 D) did not suppose an improvement in the recognition environment, observing poor to no response to the presence of target(s).

In the final experiment depicted in this study, Str was replaced with an anti-biotin antibody for the printing of the TL. Given the difference in size between the two and the proficiency of antibodies in LFA applications, the efficacy of using antibodies was examined to enhance signal detection in blank samples and to assess any potential impact on the sequence arrangement when bound to an alternative

anchor molecule. The anti-biotin printing method was tested for all four of the aptamers utilized in this research.

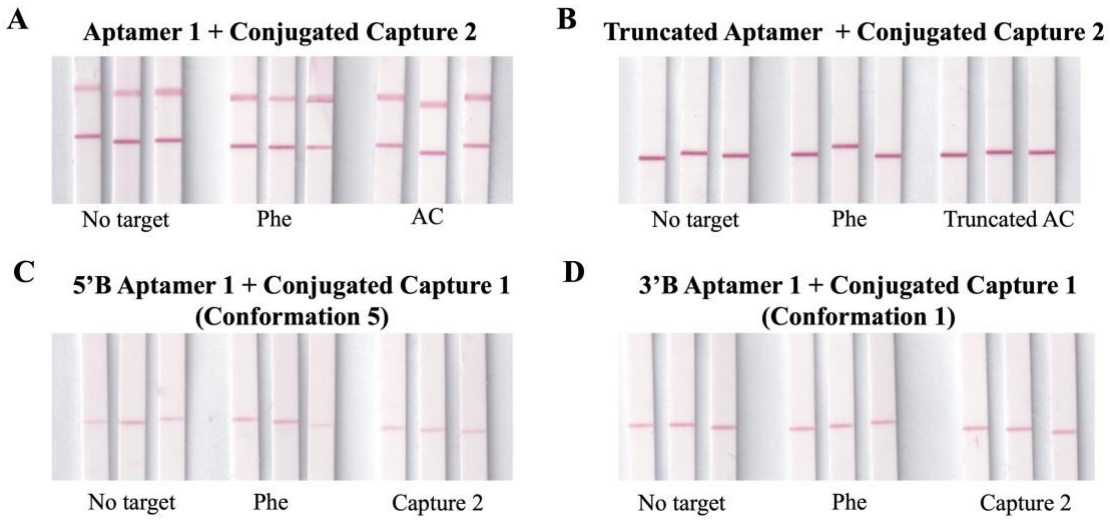


Figure 22: Anti-biotin antibody printed as the Test Line tested against a) Biotinylated Aptamer 1 and Conjugated Capture 2. b) Biotinylated Truncated Aptamer and Conjugated Capture 2. C) Conformation 5, and D) Conformation 1. All four combinations were tested without target, with Phe, and with a complementary sequence.

The printing of Anti-Biotin antibodies (as shown in Figure 22) did not result in any significant changes to the environment of any of the aptamers. The "anchoring" differences did not improve the aptamers' ability to bind to Phenylalanine or create a more electrostatically favorable environment for binding.

3.5. Discussion

Characterization experiments confirmed the size and hybridization of the sequences utilized in this study. The concentration of Capture sequence for DNA-AuNP conjugations was determined using GATs (Figure 3), and confirmation of the conjugations was achieved through UV-Vis (Figure 1), DLS (Table 3), and Lateral Flow techniques (Figure 4). Target recognition of the Aptamer, as well as the determination of BB, was conducted through fluorescence-quencher binding studies in solution (Figure 7).

Early screening of displacement assays was unsuccessful due to the printed conjugate not being released, which was attributed to aggregation of the AuNPs (Figure 8). To remedy this, the conjugation protocol was modified, and the aggregation measured qualitatively by assessing the aggregation in the walls of the glass vials and in the pellets obtained after centrifugation. Modifications to reduce aggregation included substituting NaCl with PBST, which includes Tween20 surfactant. Two sonication steps of 10 seconds were included during the SA process as well. Centrifugation was reduced from 14.000 rpm for 20 minutes to 10.000 rpm for 30 minutes to avoid aggregation in the pellet. Pellets were reconstituted in Tris-$MgCl_2$ using low-retention tubes. The first signs of the displacement sensors functioning were observed after all these modifications were introduced (Figure 10). Unfortunately, this method resulted in high levels of irreproducibility due to the printing restrictions, ultimately causing undesirable effects such as spotted lines, the coffee ring effect, and line diffusion. While displacement was achieved in response to increasing Phe concentrations (see Figure 12), this result could not be replicated.

Both iterations of the competitive assays utilized a more consistent printing system. While the adjustment in printing method did lead to improved reproducibility, it did not result in enhanced aptamer performance. This was particularly evident in competitive assays with printed Aptamer, which exhibited contradictory behavior; the absence of Phe led to the absence of TL, and vice versa (see Figure 14). One hypothesis is that the immediate environment created by the nitrocellulose directly influences the interactions between the aptamer and other molecules, hindering recognition and altering the aptamer's secondary structure, ultimately impeding proper signal generation.

On the other hand, competitive assays with printed Str involved that recognition of the target occurs in solution, which should greatly improve Aptamer-target binding. The Aptamer-Phe binding was confirmed during fluorescent-quencher binding assays in solution, resulting in a calculated Kd of 26,43 μM (Table 4). However, in LFA, this Aptamer-Target complex is required to flow through the nitrocellulose until the TL, which we believe modifies the secondary structure of the aptamer. Despite this, we observed that this format could potentially respond to Phe by the events presented in Figure 15C.

In analyzing the directionality and potential obstacles of the sequences used in this work, we assessed eight different conformations for Line 1 (or TL) generation (Scheme 2) and another eight conformations for Line 2 (or CL) generation (Scheme 3). In Displacement assays, we found that directionality played a significant role, with Conformation 8 being the only one to elicit a minimal response to increasing concentrations of Phe (Figure 12). However, the results of displacement were not consistent. Other conformations appeared to be more suitable for Competitive assays. In the Printed aptamer method, Conformation 1 seemed to offer better accessibility for Capture hybridization due to the intensity of the lines, but we repeatedly observed an unexpected response when Phe was absent. For the printed Str competitive method, Conformation 3 appeared to be the only one to exhibit a positive response to Phe, albeit with low reproducibility levels (Figure 15C). In this case, we recognized the potential in Conformation 3 and sought to optimize the working conditions of the aptamer in order to achieve a more sensitive response to Phe.

As a result, we developed a series of strategies to enhance the immediate environment of the aptamer in order to preserve its optimal secondary structure for Phe binding and signal generation. Additionally, we assessed the structural integrity of the aptamer using various sizes of nucleic acid targets (or AC) (see Figure 20). The findings from this competitive assay indicated that AC sequences actually promoted TL generation instead of competing with the Capture sequence (see Figure 16). These results suggest that AC sequences contribute to the structural stability of the aptamers, leading to increased Capture-Aptamer binding, exposure of the biotin group, and ultimately, enhanced TL generation.

Strategies for optimizing LFAs focused on screening blocking agents at different concentrations to reduce unspecific signals, with the goal of identifying a response to the Phe target (see Figure 17) were performed. Additionally, efforts were made to replicate the ideal binding environment of the Aptamer, previously defined in the binding assays as the 100mM Tris-$MgCl_2$ buffer, in the LFA strips. Treating the sample pad with this buffer and PEG blocking agents improved the overall LF performance but did not result in an improvement in the aptamer's response to the Phe target. However, these conditions for LF optimization, as well as the modifications made to the DNA-AuNP conjugation protocol, were utilized, and further evaluated in Chapter 4. The results of that further work showed that aptamers and DNA that work in solution do not work in LFAs when phosphate and Mg^{2+} containing buffers are used, which may explain the difficulties and issues observed in this chapter.

Hence, an alternative immobilization method for the aptamer on AuNPs was assessed, along with the exploration of a different capture sequence. Additionally, a truncated version of the aptamer was tested for both immobilization methods (refer to Figure 21). Finally, an alternative nitrocellulose anchoring approach was investigated, involving the printing of anti-biotin antibodies instead of Str

(see Figure 22). Regrettably, none of these approaches yielded a response from the aptamer to the Phe target.

3.6. Conclusions

Aptamers are specialized molecules that rely heavily on their surrounding environment to achieve optimum conformational changes and binding. This is particularly important during the SELEX process, where the BB used can dictate the aptamer's optimal environment.[32] This importance was clearly reflected during the binding assays, where the buffer used directly affected the calculated dissociation constants, allowing us to find a working binding buffer for the aptamer used in this work.

However, when using aptamers in different sensing platforms, the new environment can alter the interactions between the aptamer and its target.[33] In a LFA format, aptamers can be dispensed onto nitrocellulose, flown through nitrocellulose, or conjugated with AuNPs. This can alter their immediate electrostatic environment and affect their binding affinity even if the BB is present. Steric hindrances associated to the LFA platform can also play a role in limiting sensitivity. Aptamer or nucleic acid immobilization, either on paper or AuNPs, can sometimes block the access of the target or complementary sequences to their binding pocket or complementary region, thus limiting sensitivity. Nucleic acids conjugated with AuNPs can suffer from steric hindrance in highly packed and dense conjugates, limiting access to complementary sequences or target molecules. In the case of Aptamer-AuNP conjugates, the highly negatively charged environment created by both the DNA and the AuNP, can greatly alter the aptamer conformation and target binding. Furthermore, the chemistry of the nitrocellulose matrix assumes significant importance, as it influences the accessibility and the immediate environment of the embedded nucleic acids, potentially impeding their interactions.[34]

The diverse range of conformations examined in this study, along with the tested displacement and competitive formats, had the potential to address these challenges. However, the aptamer's limited tolerance for the LFA platform indicated a lack of versatility for its implementation in this system. Additionally, despite optimization efforts, the performance and sensitivity of the aptamer could not be improved.

In summary, although there has been considerable advancement in comprehending aptamer-based LFA for Phe detection, there are still several obstacles to overcome. Additional research is necessary to tackle concerns regarding reproducibility, specificity, and sensitivity, with a particular emphasis on enhancing assay formats, refining conditions, and exploring innovative methods. By persistently addressing these challenges, our goal is to progress towards creating a dependable PoC diagnostic tool for PKU and ACLF management, ultimately enhancing patient outcomes and quality of life.

3.7. References

1. Blau N, Van Spronsen FJ, Levy HL. Phenylketonuria. *The Lancet*. 2010;376(9750):1417–27.
2. Tessari P, Vettore M, Millioni R, Puricelli L, Orlando R. Effect of liver cirrhosis on phenylalanine and tyrosine metabolism. Vol. 13, Current Opinion in Clinical Nutrition and Metabolic Care. Curr Opin Clin Nutr Metab Care; 2010. p. 81–6.
3. Oliva C, Arias A, Ruiz M, Pujol A, Garrabou G, Canto-Santos J, *et al.* Fibroblast phenylalanine concentration as a surrogate biomarker of cellular number. *J Chromatogr B Analyt Technol Biomed Life Sci*. 2023;1226:123787.
4. Steventon GB, Mitchell SC. Phenylalanine hydroxylase: A biomarker of disease susceptibility in Parkinson's disease and Amyotrophic lateral sclerosis. *Med Hypotheses*. 2018;118:29–33.
5. Zhong B, Qin X, Xu H, Liu L, Li L, Li Z, *et al.* Interindividual- and blood-correlated sweat phenylalanine multimodal analytical biochips for tracking exercise metabolism. *Nat Commun*. 2024;15(1):1–14.
6. Idili A, Parolo C, Ortega G, Plaxco KW. Calibration-Free Measurement of Phenylalanine Levels in the Blood Using an Electrochemical Aptamer-Based Sensor Suitable for Point-of-Care Applications. *ACS Sens*. 2019;4(12):3227–33.
7. Groselj U, Murko S, Zerjav Tansek M, Kovac J, Trampus Bakija A, Repic Lampret B, *et al.* Comparison of tandem mass spectrometry and amino acid analyzer for phenylalanine and tyrosine monitoring-Implications for clinical management of patients with hyperphenylalaninemia. *Clin Biochem*. 2015;48(1–2):14–8.
8. How do health care providers diagnose phenylketonuria (PKU)? | NICHD - Eunice Kennedy Shriver National Institute of Child Health and Human Development.
9. Farjami E, Campos R, Nielsen JS, Gothelf K V., Kjems J, Ferapontova EE. RNA aptamer-based electrochemical biosensor for selective and label-free analysis of dopamine. *Anal Chem*. 2013;85(1):121–8.
10. Xiang J, Zhang J, Li S, Yuan R, Xiang Y. Aptamer-based and sensitive label-free colorimetric sensing of phenylalanine via cascaded signal amplifications. *Anal Chim Acta*. 2022;1230:340393.
11. Omidinia E, Shadjou N, Hasanzadeh M. Aptamer-based biosensor for detection of phenylalanine at physiological pH. *Appl Biochem Biotechnol*. 2014;172(4):2070–80.
12. Schlotter T, Kloter T, Hengsteler J, Yang K, Zhan L, Ragavan S, *et al.* Aptamer-Functionalized Interface Nanopores Enable Amino Acid-Specific Peptide Detection. *ACS Nano*. 2024;18(8):6286–97.
13. Determination of Phenylalanine With High Affinity Aptamers: Accurate, Precise, Point-of-Care. | American Journal of Clinical Pathology | EBSCOhost.

14. Gregory CO, Yu C, Singh RH. Blood phenylalanine monitoring for dietary compliance among patients with phenylketonuria: Comparison of methods. *Genetics in Medicine*. 2007;9(11):761–5.
15. Yang KA, Barbu M, Halim M, Pallavi P, Kim B, Kolpashchikov D, *et al.* Recognition and Sensing of Low-Epitope Targets via Ternary Complexes with Oligonucleotides and Synthetic Receptors Kyung-Ae. *Nat Chem*. 2014;6(11):1003–8.
16. Idili A, Gerson J, Parolo C, Kippin T, Plaxco KW. An electrochemical aptamer-based sensor for the rapid and convenient measurement of l-tryptophan. *Anal Bioanal Chem*. 2019;411(19):4629–35.
17. Cheung KM, Yang KA, Nakatsuka N, Zhao C, Ye M, Jung ME, *et al.* Phenylalanine Monitoring via Aptamer-Field-Effect Transistor Sensors. *ACS Sens*. 2019;4(12):3308–17.
18. Ma X, Li X, Luo G, Jiao J. DNA-functionalized gold nanoparticles: Modification, characterization, and biomedical applications. *Front Chem*. 2022;10.
19. Parolo C, Merkoçi A. Paper-based nanobiosensors for diagnostics. *Chem Soc Rev*. 2013;42(2):450–7.
20. NanoComposix. Lateral Flow Assay Development Guide. *nanoComposix*. 2016;:1–37.
21. Ruscito A, DeRosa MC. Small-Molecule Binding Aptamers: Selection Strategies, Characterization, and Applications. *Front Chem*. 2016;4:14.
22. McKeague M, Derosa MC. Challenges and opportunities for small molecule aptamer development. *J Nucleic Acids*. 2012;2012.
23. Han B, Fang C, Sha L, Jalalah M, Al-Assiri MS, Harraz FA, *et al.* Cascade strand displacement reaction-assisted aptamer-based highly sensitive detection of ochratoxin A. *Food Chem*. 2021;338.
24. Alyamani BJ, Alsager OA, Zourob M. Label-free fluorescent aptasensor for small targets via displacement of groove bound curcumin molecules. *Sensors (Switzerland)*. 2019;19(19).
25. Schüling T, Eilers A, Scheper T, Walter J. Aptamer-based lateral flow assays. *AIMS Bioeng*. 2018;5(2):78–102.
26. Sun J, Guo A, Zhang Z, Guo L, Xie J. A conjugated aptamer-gold nanoparticle fluorescent probe for highly sensitive detection of rHuEPO-α. *Sensors*. 2011;11(11):10490–501.
27. Dalirirad S, Han D, Steckl AJ. Aptamer-Based Lateral Flow Biosensor for Rapid Detection of Salivary Cortisol. *ACS Omega*. 2020;5(51):32890–8.
28. Borsci S, Kuljis J, Barnett J, Pecchia L. Beyond the User Preferences: Aligning the Prototype Design to the Users' Expectations. *Hum Factors Ergon Manuf*. 2016;26(1):16–39.
29. WHO. Advice on the use of point-of-care immunodiagnostic tests for COVID-19. 2020.
30. WHO NRA in I jurisdictions. Update on COVID-19 *in vitro* diagnostics listed by National Regulatory Authorities in IMDRF jurisdictions. (March).
31. Parolo C, Sena-Torralba A, Bergua JF, Calucho E, Fuentes-Chust C, Hu L, *et al.* Tutorial: design and fabrication of nanoparticle-based lateral-flow immunoassays. *Nature Protocols 2020 15:12*. 2020;15(12):3788–816.

32. Kohlberger M, Gadermaier G. SELEX: Critical factors and optimization strategies for successful aptamer selection. *Biotechnol Appl Biochem*. 2022;69(5):1771.
33. Qi S, Duan N, Khan IM, Dong X, Zhang Y, Wu S, *et al.* Strategies to manipulate the performance of aptamers in SELEX, post-SELEX and microenvironment. *Biotechnol Adv*. 2022;55.
34. Chen A, Yang S. Replacing antibodies with aptamers in lateral flow immunoassay. *Biosens Bioelectron*. 2015;71:230–42.

3.8. ANNEX

Table S1. Sequence used in this work:

Name	Sequence (5'->3')	nt.
3'B Aptamer	CTCTCGGGACGACCGCGTTTCCCAAGAAAGCAAGTATTGGTTGGTCGTCCC-Biotin-3'	51
5'B Aptamer	5'-Biotin-CTCTCGGGACGACCGCGTTTCCCAAGAAAGCAAGTATTGGTTGGTCGTCCC	51
polyT Aptamer	5'-CTCTCGGGACGACCTTTTTTTTTTTTTTTTTTTTTTTTTTTTTTTTTTTTT-Biotin-3'	51
Aptamer Complementary	GGGACGACCAACCAATACTTGCTTTCTTGGGAAACGCGGTCGTCCCGAGAG	51
3'Thiol Capture	GGTCGTCCCGAGAG-ThiolC6-3'	14
5'Thiol Capture	5'-ThiolC6-GGTCGTCCCGAGAG	14
3'Thiol Tailed Capture	GGTCGTCCCGAGAGTTTTTTTTTTTTTT-ThiolC6-3'	28
5'Thiol Tailed Capture	5'-ThiolC6-TTTTTTTTTTTTTTGGTCGTCCCGAGAG	28
3'B Control Line	CTCTCGGGACGACC-Biotin-3'	14
5'B Control Line	5'-Biotin-CTCTCGGGACGACC	14
Negative Capture	5'-ThiolC6-GCAGTAACAAGAATAAAACGCCACTG	28
Apt. Complem. 2	GGGACGACCAACCAATACTTGCTTTCTTGGGAAACGCGGTCGTCCC	46
Apt. Complem. 3	GGGACGACCAACCAATACTTGCTTTCTTGGGAAACGCGGTC	41

3’FAM Aptamer	CTCTCGGGACGACCGCGTTTCCCAAGAAAGCAAGTATTGGTTGGTCGTCCC-6’FAM-3’	51
5’FAM Aptamer	5’-6’FAM-CTCTCGGGACGACCGCGTTTCCCAAGAAAGCAAGTATTGGTTGGTCGTCCC	51
5’BHQ Capture	5’-BHQ1-GGTCGTCCCGAGAG	14
3’BHQ Capture	GGTCGTCCCGAGAG-BHQ1-3’	14
BHQ Negative Capture	5’-BHQ1-GCAGTAACAAGAATAAAACGCCACTG	28
FAM polyT Aptamer	5’-6’FAM-CTCTCGGGACGACCTTTTTTTTTTTTTTTTTTTTTTTTTTTTTTTT-3’	51
5’Thiol Aptamer 1	5’-ThiolC6-CTCTCGGGACGACCGCGTTTCCCAAGAAAGCAAGTATTGGTTGGTCGTCCC	51
3’Thiol Aptamer 1	CTCTCGGGACGACCGCGTTTCCCAAGAAAGCAAGTATTGGTTGGTCGTCCC-ThiolC6-3’	51
5’Thiol Truncated Aptamer 2	5’-ThiolC6-GACCGCGTTTCCCAAGAAAGCAAGTATTGGTTGGTC-3’	36
5’B Truncated Aptamer 2	5’-Biotin-GACCGCGTTTCCCAAGAAAGCAAGTATTGGTTGGTC-3’	36
Truncated Complementary	GACCAACCAATACTTGCTTTCTTGGGAAACGCGGTC	36
Capture 2	5’-ThiolC6-TGGGAAACGCGGTC	14
Control Line 2	GACCGCGTTTCCCA -Biotin-3’	14

CHAPTER 4. Effects of Conjugation Methods and Storage Conditions on AuNP-DNA Conjugates for Long-Term Stability in Lateral Flow Sensors

4.1. Complexities in the Selection of Optimal AuNP-DNA Methods

Over **27 years** since the first introduction of the salt-aging (SA) method for Gold Nanoparticle (AuNPs) conjugation with DNA, a multitude of variations of this protocol have been published by various research groups.[1–3] These variations include differences in the duration of the aging process, inclusion or exclusion of sonication, pH adjustments, use of surfactants, varying numbers of centrifuge steps, and whether preservatives are used for storage.[4–6] Additionally, other **alternatives** to the SA method have been reported in the literature.[7,8] These alternatives include pH-assisted, butanol-mediated, freezing-assisted, or microwave-assisted methods.[9–14] These methods offer different advantages and disadvantages compared to the SA method, and researchers can choose the appropriate method based on their specific needs and goals for their research. **This abundance of protocols and variations understandably can create confusion for the inexperienced reader, making it challenging to identify how adequate every variation of these protocols is for a particular application.**[15–17] Moreover, the impact of different conjugation protocols on the storage, half-life, and stability of DNA-AuNP conjugates is essential for Lateral Flow Assay (LFA) manufacturers to ensure product performance, consistency, regulatory compliance, and cost-effectiveness.[18,19] By understanding and controlling these factors, manufacturers can improve the quality and reliability of LFA, thereby benefiting both the manufacturer and end-users.

Consequently, the composition of the **storage buffer** is also pivotal in determining the efficacy of these conjugates in different settings.[20] For instance, the composition of the binding buffer (BB) used in the Systematic Evolution of Ligands by Exponential Enrichment (SELEX) process is essential for aptamers to bind into the proper secondary structures and allow recognition.[21–23] Additionally, cations are important for shielding the negative charge of the DNA backbone, thereby eliminating potential electrostatic binding interactions of DNA to the target.[24] Divalent cations like Mg^{2+} play a significant role in Polymerase Chain Reactions (PCR) applications as DNA polymerase cofactors.[25] Moreover, different biorecognition elements, such as antibodies and aptamers, have different tolerances and optimal work ranges in different buffers, making it crucial to select the appropriate buffer for each application. In addition to the aforementioned scenarios, a wide variety of conjugation protocols are employed to prepare DNA-AuNPs, utilizing different buffer compositions and salt concentrations.[26–28] These variations can impact the functionality of the conjugate, and resuspension in different storage buffers might have different effects on different conjugation methods.

When choosing a conjugation protocol, the **final application** should be taken into consideration. Factors such as ionic concentration, pH, and the composition of salts used during the conjugation process can significantly impact the performance and stability of AuNPs-DNA conjugates for a specific application, whether LFA, Gold Aggregation Tests (GATs), or drug delivery.[17,29,30] In LFA,

in particular, the parameters mentioned above can significantly impact the flow, recognition, and specificity of the biorecognition elements utilized, making specific protocols unsuitable for this application. For instance, as previously described, nucleic acid hybridization is less sensitive to changes in the buffer than aptamers or antibodies binding to their targets; since the process is not as dependent on the secondary structure of the probe molecule.[31,32] Protocols that use organic solvents during the conjugation process may affect the solubility of biomolecules (either the aptamer, the target, or any other), which may affect harness biorecognition.[33]

Other determinant factors that come into play when considering a particular protocol are **time and cost**. While nucleic acid costs are generally low, modifications such as thiols or biotins can significantly increase their price.[34] Similarly, AuNPs are costly, even when synthesized rather than purchased commercially.[35] Additionally, the amount of initial materials needed for a particular amount of conjugate varies depending on the protocol and the final application, which can impact cost and resource availability. In terms of time, lengthy protocols usually imply higher costs. Besides, a larger number of steps in a protocol can impact its reproducibility and scalability.

Another factor is the **half-life** of a conjugate while stored in adequate conditions. As Phan *et al.* explain, stability in the field of nanotechnology involves maintaining specific properties of a nanostructure, such as aggregation, composition, crystallinity, shape, size, and surface chemistry, which can only exist for a limited period of time based on thermodynamic and energetic principles.[36,37]

4.1.1. Design of a AuNP-DNA Stability Study for Lateral Flow Applications

With these factors in mind and taking the point of view of an inexperienced user or in the interest of industry optimization, it is important to evaluate the impact of various conjugation methods and storage conditions on the stability and functionality of these conjugates on LFA within a practical timeframe. **Combining different conjugation methods of varying characteristics (duration, complexity, or principle) with different storage buffers of typical use in these practices can offer a broad practical guide on the variable expectancy of their functionality and stability.** Thus, in this work, "nanoparticle stability" is defined as the ability to maintain the size (or prevent aggregation), optical properties, and functionality of these DNA-nanoparticle conjugates on a LFA device. In terms of functionality, it will be considered that the conjugates are not functional anymore as the DNA sequences attached can no longer hybridize with their complementary sequences, either due to particle aggregation, detachment of the sequences, high packing density, or digestion by

nucleases. In other words, conjugates are no longer functional as they do not serve as an optical reporter.

4.1.1.1. Conjugation techniques

Five techniques were selected for comparison considering factors such as popularity, protocol duration, principle, number of steps, or ionic strength used. Table 1 depicts the main differences of the five conjugation processes.

Firstly, SA methods were considered, which are very widely used and facilitate covalent conjugation.[28] As previously explained, the principle of these conjugations relies on salt addition to reduce electrostatic repulsion between the negatively charged DNA and AuNPs. In addition, thiolated DNA is treated with tris(2-carboxyethyl)phosphine (TCEP) to reduce disulfide bonds and allow covalent gold-sulfur bonding.[38] Three SA methods with varying parameters such as pH, time, ionic strength, etc. were selected to offer a true representation of the many available protocols. Besides, SA methods are also known for relying on lengthy and multistep protocols, depending on the duration intervals between salt addition, which was also considered.

The three conjugation protocols chosen are the following:

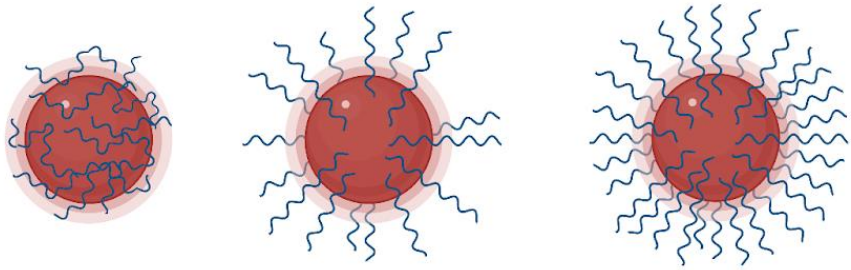
The first reported SA conjugation was by Mirkin *et al.* and Alvisatos *et al*. simultaneously. This first protocol uses 1M NaCl and 0.1 M sodium phosphate pH 7 dropcasting, and its total duration is three days.[2,28]

SA pH-assisted (SA-pH). In 2006, Juewen Liu included two pH-adjusting events (at 5.2 and 8.2) to promote conjugation thanks to the partial protonation of the nucleobases at low pH. An initial pH adjustment to 5.2 increases the amount of nucleotides adsorbed to the AuNPs, reducing the duration of the subsequent SA process. The duration of this protocol is two days instead.[6]

A personalized protocol developed in the course of this thesis was included as “LF-Optimized” conjugation (SA-LF). This protocol includes surfactant addition and sonication events, both previously reported in the literature and combined to prevent the observed aggregation in the conjugation process empirically and to improve subsequent flow properties in LFA strips. The duration of this protocol is also two days, although it involves more steps than the other two SA protocols.

Secondly, an Adsorption method, which has proven popular not just for oligonucleotides but also for aptamer conjugations, was included. Although the mechanism is still unclear, different models suggest that it relies on electrostatic repulsive interactions between DNA nucleobases and the citrate

anions from the gold surface, which are displaced, allowing for the interaction of the nucleobases with the gold surface, and increasing the stability of AuNPs in contrast to bare AuNPs.[11,39] Despite the reversibility of this electrostatic interaction, this non-covalent conjugation has been harnessed as an optical mechanism by exploiting the desorption of the nucleotides against hybridization or other binding events. Adsorption protocols are usually shorter and generally need fewer steps. It is also usual to find adsorption protocols that include blocking steps with molecules such as polyethylene glycol (PEG) or Bovine Serum Albumin (BSA), which were discarded for this assay in order to exclude extra variables. The chosen protocol was first described in 2004 by Rothberg and Lewis.[39] The total duration of this protocol is around 1 hour, which can be extended to almost 2 hours in case of the addition of blocking agents.



Scheme 1: Schematic illustration of AuNPs with adsorbed oligonucleotides (left), covalently conjugated oligonucleotides (middle) and densely packed conjugated oligonucleotides (right). Created with Biorender.

The above conjugation methods cover the most commonly used methodologies in the literature, however, there have been the development of recent "Rapid" conjugations such as microwave assisted or freezing assisted methods, as listed above. It is not possible to test all the different possible conjugation methods, therefore one of these rapid methods, butanol dehydration, was chosen for its investigation.[13] This method enables conjugation by instant dehydration in butanol (INDEBT) of both DNA and AuNPs in the presence of TCEP. This dehydration creates an extremely concentrated, size-reduced, and charge-suppressed environment that alleviates electrostatic hindrances between DNA and AuNPs within seconds. These densely packed DNA-AuNP conjugates are later rehydrated and recovered from the aqueous phase. This covalent conjugation happens instantly, and the duration of this protocol goes under 30 minutes, including the preparation of the materials.

Table 1. Characteristics of the conjugation protocols of choice.

Conjugation	Principle	Duration	Buffer	pH	Ionic strength	Sonication	Ref.
SA	Salt aging	3 days	100 mM PB pH 7 and 1 M NaCl	7	0.14 mol/L	No	4
SA-pH	Salt aging	2 days	500 mM Sodium Acetate pH 5.2, 500 mM Tris-Acetate pH 8	5.2 and 8.2	0.09 mol/L	No	8
SA-LF	Salt aging	2 days	PBST, 1M NaCl	7.4	0.12 mol/L	Yes	-
Adsorption	Adsorption	1 hour	None	No	None	No	13
INDEBT	Instant dehydration by butanol	30 minutes	TBE 0.5X	8.3	0.024 mol/L	Yes	11

4.1.1.2. Storage buffer

In this work, the storage of DNA-AuNPs was assessed using four different buffers.

Firstly, 100 mM Tris-$MgCl_2$ pH 7.4 was chosen because tris(hydroxymethyl)aminomethane (Tris) is frequently used as a buffering agent in SELEX processes, and $MgCl_2$ is known to play a crucial role in the secondary structure conformation of DNA aptamers, in polymerase cofactors of PCR applications, and in avoiding mismatching in DNA hybridization.[21,24] Tris is also present during the SA pH-assisted conjugation, which will be evaluated in this work. This choice in buffers allows us to systematically investigate the influence of the $MgCl_2$ and Tris on AuNP/conjugate stability. $MgCl_2$ is commonly used in DNA sensing systems as it is crucial to the Nucleic acid structure and function, as well as being an important cofactor for Taq polymerase in PCR.

Secondly, 10 mM PBS-$MgCl_2$ pH 7.4 was selected as it is another popular combination used in many biochemical experiments, including as a binding buffer in SELEX. This allows a differential study of the effect of Phosphate buffer saline (PBS) versus Tris when also in the presence of $MgCl_2$.[40]

Thirdly, PBS was chosen as it is a common buffer utilized in various stages of LFA preparation, such as sample dilution, biorecognition element dilution, blocking buffers, and conjugate pad

preparation.[41–43] It also enables the study of components of the previous buffers to be evaluated separately, particularly the impact of $MgCl_2$.

Lastly, deionized water (MQ water, water from this point) was included to evaluate storage in the absence of ionic forces, and to act as a control. It is also a useful storage medium if the conjugates are intended to be split into different buffers later on by the end user.

4.1.1.3. Characterization techniques

To monitor the stability and functionality of different DNA-AuNP conjugates over three weeks, several techniques were chosen. The first technique is LFA, which evaluates the capability of the conjugates to flow through the LFA strips and hybridize to their complementary sequence printed on the line.[15,44] As described in Chapter 2, intensive work has been dedicated to adequate the physicochemical characteristics of the DNA-AuNP conjugates to optimize the recognition of the phenylalanine target by its aptamer counterpart in an LFA. Although aptamer recognition of the target was not reproducibly achieved in this format, optimization of the physicochemical characteristic of the conjugates, as well as the conditions of the strip preparation (sample pad, printing concentrations, conjugate concentration, etc.), were seized to achieve a correct hybridization with their complementary sequences in a LFA strip and ensure a homogeneous flow and speed. This particular LFA strip optimization will be put to the test against all twenty conjugates to evaluate the effects of the different conjugations and storage buffers on their functionality over three weeks.

Utilizing ImageJ for analysis can be an extremely valuable tool in semi-quantifying LFA line intensity.[41,45] This can be particularly helpful in distinguishing between very similar intensities, aiding in the creation of calibration curves, optimization of signal, and determining sample concentrations. However, it is important to note that this is generally most effective when comparing signal intensity under similar conditions (whether optimal or not). Factors such as differences in background noise or flow imperfections have the potential to skew semiquantitative values away from optical qualitative perception. For example, two lines with what appear to be identical intensities to the naked eye may actually have varying semiquantitative values due to signal-to-noise calculations. Similar issues have been raised in non-competitive traditional LFA in cases when the saturation of the test line provokes a depletion of the AuNPs available for the control line, therefore deviating the control-to-test line ratios when analyzing data extracted from software like Image J.[46–48]

The functionality of the conjugates and their evolution in time is directly dependent on the conditions established in many factors: ionic strength and/or pH of the conjugate, of the sample pad, the presence or absence of blocking agents or surfactants, the pore size of the nitrocellulose of choice,

etc. Because a particular set of "optimized strip conditions" is going to be compared against 20 different conjugates, minor flow issues or background noises will be usual. However, these are considered minor defects, as they are easily removable by minor optimizations of certain conditions. That being said, the evolution of the flow properties and functionality through the weeks will be analyzed, independently of the initial performance or minor defects. Furthermore, and for the reasons stated above, semiquantitative and qualitative analyses will both be performed. It is also important to note that testing is limited to the functionality of DNA probes. The stability of proteins and enzymes is out with the scope of this investigation. This is a crucial consideration since antibodies are commonly used for AuNP conjugation.[49] The stability of the conjugation method alone is being determined rather than the biorecognition element. This decision was made specifically because the stability of proteins in different buffers can vary greatly depending on their nature, whereas DNA is recognized for its functionality and greater stability. It is assumed that no DNA degradation occurs in any of the conditions tested over the three weeks during which these experiments were conducted.

The second technique is Electrophoretic Mobility Shift Assay (EMSA), which applies an electric field to particles in a polymeric matrix, which separates them as they migrate depending on their charge and size.[50] Because AuNPs and DNA are both negatively charged, DNA-AuNP conjugates migrate toward the positive electrode. It has been observed that the quantity of DNA present has a larger effect on the size than changes in charge during the electrophoresis gel process.[51] These studies suggest that an increase in the number of DNA strands results in retardation due to the upsurge in both size and density. However, the inclusion of additional DNA does not lead to a rise in negative charge that could potentially accelerate the mobility of the particle. However, the heterogeneity of DNA amount in a conjugate sample can have a noticeable impact on the charge heterogeneity, which can result in more diffuse bands compared to homogeneous conjugate samples. Events such as aggregation or DNA loss over time can also be translated in retardation and acceleration, respectively.

The third technique is UV-Vis spectroscopy, which measures the Surface Plasmon Resonance (SPR) of the AuNPs.[52,53] SPR is the collective oscillation of electrons on the surface of metal excited by photons, which results in a peak in the absorption spectrum of a sample. The position and width of the SPR absorption peak depend on the size and agglomeration of the AuNPs. A shift to longer wavelengths and broadening of the SPR peak is observed as the size of AuNPs increases and as the distance between particles decreases due to aggregation. The intensity of the SPR peak is related to the concentration of AuNPs. Conjugation increases nanoparticle size and shifts the peak to higher wavelengths.[41] The different conjugation techniques used can cause more or less aggregation during the process, causing an increase in the absorbance in the 580 nm region. Thus, combining peak

wavelength, broadening, and intensity of the SPR peak allows the determination of the size and aggregation of AuNPs.

The fourth technique is Dynamic Light Scattering (DLS) and Z-potential. DLS is used to determine the size distribution of particles in a sample by measuring the fluctuations in the intensity of scattered light caused by the Brownian motion of particles. DLS can help determine the size distribution of the AuNPs and their conjugates with DNA molecules. It provides valuable information about the homogeneity of the sample and the effectiveness of the functionalization process. Zeta potential is a measure of the electrostatic potential at the surface of a nanoparticle. It provides information about the stability of the nanoparticles in solution. Nanoparticles with very high or low (>+30 or <-30 mV) zeta potentials are typically more stable because they repel each other due to electrostatic forces. In the case of DNA-AuNPs, measuring the zeta potential can help assess the stability of the DNA-AuNP conjugates in solution. Additionally, it can provide insights into the surface charge of the nanoparticles.[36,54,55]

4.2. Objectives

Firstly, this thesis chapter aims to evaluate and compare the impact of various AuNP-DNA conjugation methods on the stability, functionality, and performance of DNA-AuNP conjugates. The methods to be scrutinized include SA, pH-assisted, and butanol-assisted protocols to understand how different parameters such as duration, complexity, and buffer composition affect the characteristics of these conjugates.

Secondly, the study will investigate the influence of different storage conditions, including buffers like Tris-$MgCl_2$, PBS-$MgCl_2$, PBS, and deionized water, on the long-term stability and functionality of DNA-AuNP conjugates. The goal is to determine how these storage buffers impact the maintenance of size, optical properties, and hybridization capability over a practical period of time.

Additionally, a key objective is to assess and monitor the stability of DNA-AuNP conjugates specifically for LFA. By comparing various conjugation methods and storage buffers, the study aims to identify which combinations maintain optimal performance over time. This evaluation will provide practical guidance for users of LFA technology, ensuring the reliability and consistency of DNA-AuNP conjugates in practical applications.

Finally, the chapter will utilize multiple characterization techniques, including LFA, EMSA, UV-Vis spectroscopy, and DLS, to comprehensively analyze the behavior of DNA-AuNP conjugates. These techniques will provide insights into changes in size, aggregation, optical properties, and electrostatic potential under different experimental conditions, further supporting the objectives of optimizing AuNP-DNA conjugation methods and storage conditions for LFA applications.

4.3. Materials and Methods

4.3.1. Materials

DNA sequences were purchased from LGC Biosearch Technologies. HAuCl4, sodium citrate, Tween-20, polyethylene glycol 2050 (PEG2050), sodium chloride, PBS tablets, trizma salts (Tris), phosphate salts, magnesium chloride, Tris-(2-Carboxyethyl)phosphine hydrochloride (TCEP), n-butanol, Tris-Borate-EDTA (TBE) buffer 10X, glycerol and agarose were purchased from Merck. Transparent 96-well plates were purchased from FisherScientific (Hampton, NH, USA). SpectraMax iD3 (San José, CA, USA) UV-Vis spectrophotometer was used for absorbance measurements. DLS and Z-potential measurements were performed using DTS1070 cuvettes in a Zetasizer Nano ZS from Malvern Panalytical. Electrophoretic system shiroGEL Mini 10 was purchased from VWR International, LLC. LFAstrips were printed using IsoFlow dispenser (Imagene Technology, USA), scanned using a CanoScan LiDE400 (Canon, Spain), and analyzed using ImageJ software. LFA strips were made of nitrocellulose (CN 150 from Sartorius), cellulose (GE Healthcare), and laminated card (Millipore).

Sequences used in this work:

Conjugate sequence: 5'-GGTCGTCCCGAGAGTTTTTTTTTTTTTT-ThiolC6-3'
Printed sequence: 5'-CTCTCGGGACGACC-Biotin-3'

4.3.2. Methods

4.3.2.1. Conjugate preparation

AuNPs were synthesized using the Turkevich method and stored at 4ºC for its use on the same day. Synthesis concentration was determined with UV-Vis measurements to be 1.2 nM and established as 1X or for the following processes.

The starting amount of AuNPs and DNA for all five conjugation protocols was normalized and fixed to evaluate each protocol's conjugation effectiveness. All five conjugation protocols were followed using AuNPs synthesized on the same day and were scheduled to finish on the same day (Day 0) due to the difference in duration among the protocols.

SA protocol.

The following procedure is followed four times in parallel, one for each resuspension buffer.

21,2 µL of 100 µM DNA are mixed with 2 µL of 10 mM TCEP and incubated for one hour in dark shaking conditions (600 rpm). Then, 2650 µL of AuNPs are added to the solution and incubated overnight (16h). The following morning, (0.125 vol) 330 µL of 1M NaCl are added to the solution dropwise while shaking, followed by 330 µL of 0.1M Sodium Phosphate buffer pH 7 in the same fashion. The solution is incubated for 24 more hours in the same conditions. The solution is then centrifuged for 30 minutes at 10 000 rpm and 10ºC. The supernatant is removed, and the pellet is resuspended in the corresponding storage buffer to a final volume of 535 µL.

SA pH-assisted protocol.

The following procedure is followed four times in parallel, one for each resuspension buffer.

21,2 µL of 100 µM DNA are mixed with 2 µL of 10mM TCEP and 1 µL of 500 mM Acetate buffer pH 5.2 and incubated for one hour in dark shaking conditions (600 rpm). Then, 2650 µL of AuNPs are added and incubated overnight (16h). The following morning, 26.5 µL of 500 mM Tris-acetate buffer pH 8.2 are added dropwise while shaking, followed by 265 µL of 1M NaCl in the same fashion. The solution is incubated for 24 more hours in the same conditions. The solution is then centrifuged for 30 minutes at 10 000 rpm and 10ºC. The supernatant is removed, and the pellet is resuspended in the corresponding storage buffer to a final volume of 535 µL.

SA LF-optimized protocol.

The following procedure is followed four times in parallel, one for each resuspension buffer.

21,2 µL of 100 µM DNA are mixed with 2 µL of 10mM TCEP and incubated for one hour in dark shaking conditions (600 rpm). Then, 2650 µL of AuNPs are added to the solution and set for another hour in the same conditions. Then, 176.6 µL of 100 mM PBST (1M NaCl, 0.1% Tween-20) dropwise while shaking and incubated for an hour in the same conditions. The solution is sonicated for 10 seconds at moderate intensity (RT) and 88.3 µL of 1M NaCl are added dropwise while shaking. The solution is incubated for one hour under the same conditions. The solution is then sonicated again for 10 seconds, followed by the addition of another 88.3 µL of 1M NaCl. The solution is incubated overnight (16h) under shaking dark conditions. The solution is then centrifuged for 30 minutes at 10 000 rpm and 10ºC. The supernatant is removed, and the pellet is resuspended in the corresponding storage buffer to a final volume of 535 µL.

Adsorption protocol.

The following procedure is followed four times in parallel, one for each resuspension buffer.

Firstly, 21.2 µL of 100 µM thiolated DNA are added to 2650 µL of AuNPs. The mixture is then incubated for 30 minutes under shaking conditions of 250 rpm to facilitate DNA adsorption to the surface of the AuNPs. After incubation, the solution is centrifuged for 30 minutes at 10 000 rpm and

10ºC. The supernatant is removed, and the pellet is resuspended in the corresponding buffer to a final volume of 535 µL.

Instant dehydration by butanol (INDEBT) protocol.

12 mL of AuNPs are centrifuged for 30 minutes at 10 000 rpm and 10ºC and resuspended in MQ water to a final volume of 1200 µL. 10X AuNPs will be used in this protocol. From this point, the following procedure is followed four times in parallel, one for each resuspension buffer.

For each storage buffer group, 21.2 µL of 100 mM thiolated DNA are mixed with 3 µL of TCEP 100 mM and 265 µL of 10X AuNPs. The solution is mixed with 2700 µL of Butanol, followed by quick vortexing. Then, 300 µL of 0.5X TBE are added to the solution, followed by another quick vortex step. The solution is briefly centrifuged at 2.000 g for several seconds to reveal a concentrated pellet. The upper butanol layer is removed, and the pellet is resuspended in the corresponding storage buffer to a final volume of 535 µL.

All resulting solutions have a final concentration of 5X concerning the AuNPs synthesis concentration and are ready for further experiments. All twenty conjugates were tested on day 0 before being stored at 4ºC and in dark conditions.

4.3.2.2. Lateral Flow Tests

As reported in Chapter 3, the complementary DNA sequences of the system used have shown a clear specificity when tested over other non-complementary sequences, and LFA conditions of the strip and loading methods were optimized and showed a correct flow and hybridization of the complementary probes. Therefore, signal and flow changes were evaluated in respect to the performance in day 0.

Sample pad treatment consisted of soaking cellulose in a solution containing 0.1% PEG 2050 and 0.05% Tween20 dissolved in 100mM Tris-$MgCl_2$ pH 7.4 buffer, and let dry overnight at 37ºC. Control Lines were printed at a concentration of 40 µM DNA and 10 µM Streptavidin, previously incubated for 30 minutes. For optimal LFA performance, strips were printed one day before each testing event, left overnight for drying at 37ºC, and assembled on the testing day. In the same way, sample pad treatment was performed one day in advance for its drying before assembling.

Conjugates were diluted to 0.5X with their corresponding storage buffers, and 60 uL were added to each sample pad and let flow for 15 minutes. Bare AuNPs were diluted in MQ water and tested in the same fashion. Strips were scanned after 20 minutes of loading and analyzed using ImageJ software. Triplicates were made for every conjugate sample.

4.3.2.3. Electrophoretic Mobility Shift Assay

EMSA were performed using a 2% agarose gel. 5 uL of conjugate samples were mixed with 1uL of 30% glycerol to a final glycerol concentration of 5% and added to the wells. Running conditions were 30 minutes at 120 V, and results were photographed (iPhone 8, artificial light in the same position, 10 cm distance) and analyzed using ImageJ. It was observed that naked AuNPs suffered from aggregation after a few moments of the run when in contact with 0.5X TBE from the buffer tank (refer to Figure 1). Distance migration analysis was instead normalized by the measured length of the agarose gel (7 cm).

4.3.2.4. UV-Vis

UV-Vis measurements were performed in triplicates at a final concentration of 0.1X, using the corresponding storage buffer for each conjugate. Bare AuNPs were diluted in MQ water and measured in the same fashion. Every storage buffer was measured for base extraction. Absorbance values were obtained from 400 to 700 nm with a 5 nm interval.

4.3.2.5. DLS and Z-potential

DLS and Z-potential measurements were performed in a Malvern Zetasizer Nano ZS at 25 ºC at a final concentration of 0.5X and 0.125X, respectively. Triplicate measurements were made, and the attenuation factor and position were set to 11 and 2 mm, respectively.

4.4. Results

In this project, the stability of 5 different conjugation methods when stored in 4 different buffers is being compared using four different characterization techniques. As a result, a substantial amount of data is being analyzed and compared. For each characterization technique, the analysis will commence by comparing the differences between the conjugation methods on day 0, followed by comparisons of the buffers used, and finally evaluating the temporal stability trends across all groups.

4.4.1. Electrophoretic Mobility Shift Assay

4.4.1.1. Variation between conjugation methods

Upon reviewing the EMSA results on day 0 (Figure 1, top), it is apparent that the conjugation method utilized has a significant impact on the observed band features. Specifically, three distinct running fronts across the five conjugation methods, associated with adsorption, INDEBT, and SA principles were observed.

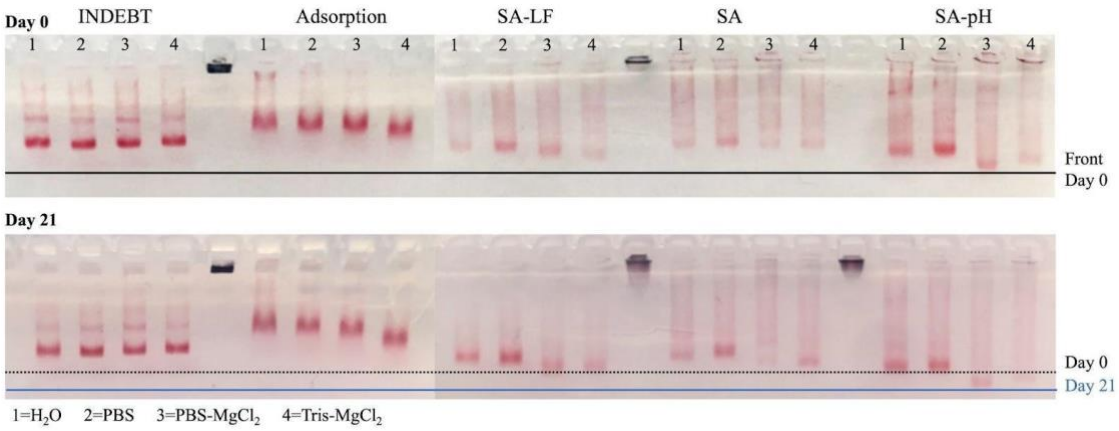


Figure 1: EMSA results of the 20 conjugates on day 0 (top) and day 21(Bottom). Black lines correspond to the maximum migration distance of the furthest conjugate on day 0 (solid line) and in reference to day 21 migrations (dotted line). The blue line corresponds to the maximum migration distance of the furthest conjugate on day 21. Black depositions in the wells correspond to aggregated AuNPs.

Adsorption conjugations show broad and diffuse running fronts (Figure 1) and a certain degree of smearing. This result suggests the stochastic packing of the nucleobases. As a result, there is a large spread of conjugation densities on the AuNPs in the sample and a wide range of charge states. Therefore, it can be observed that the least uniform AuNP coating within a single sample is achieved by the adsorption method.

Regarding the INDEBT conjugation, two distinct bands are observed in the EMSA from day 0 and across all the storage buffers. Since non-conjugated AuNPs were uniform and this phenomenon did not occur with any other conjugation method, it can be concluded that the INDEBT method results in two distinct and differently functionalized AuNPs with homogeneous mass-to-charge ratios. This is attributed to the method using a mix of butanol and water which are immiscible. Thus there are two distinct groups of AuNP arising from those functionalized in the aqueous bulk and those functionalized at the phase interface.

Last, SA conjugations show a single band with a solid but less intense running front, and a more homogeneous trail of conjugate, which can be attributed to a more heterogeneous population of conjugates with varying amounts of DNA and, thus, varying mass-to-charge ratios.

4.4.1.2. Variation between buffers

A gradual reduction in size can be observed between water, PBS, PBS-$MgCl_2$, and Tris-$MgCl_2$ buffer in two conjugation principles: adsorption and SA protocols (Figure 1). This phenomenon is attributed to the increasing ionic strength of each buffer and is noticeable since day 0, likely due to the moment of resuspension in the different buffers, which occurred on the same day. It can be theorized that the rising ionic strength of the resuspension buffer has an increasing impact, attributed to electrostatic shielding, which affects the conjugates' pellet resuspension and DNA packing density and secondary structures.

However, the opposite effect is observed within INDEBT conjugates, where conjugates seem to be less impacted by the resuspension buffer, which could be attributed to the higher packing density and protection of the AuNPs' surface. Besides, INDEBT conjugates resuspended in buffers with $MgCl_2$ seem to increase the size of the conjugates minimally. This may suggest that, thanks to the high density of DNA conferring protection to the AuNP, Mg^{2+} ions can contribute to the secondary structure of the nucleic acid, ordering DNA more radially and conferring them of a larger size. However, this $MgCl_2$ effect is not seen in the other conjugation methods, probably due to lower conjugation efficiencies, the loss of DNA during the resuspension process, or to the heterogeneity of the conjugates.

4.4.1.3. Stability over time.

A general increase in migration distance can be observed over time, as most conjugates progressively migrate further in the gel as weeks pass (Figures 1 and 2). This suggests a gradual loss of DNA, thereby reducing the size of the conjugates.

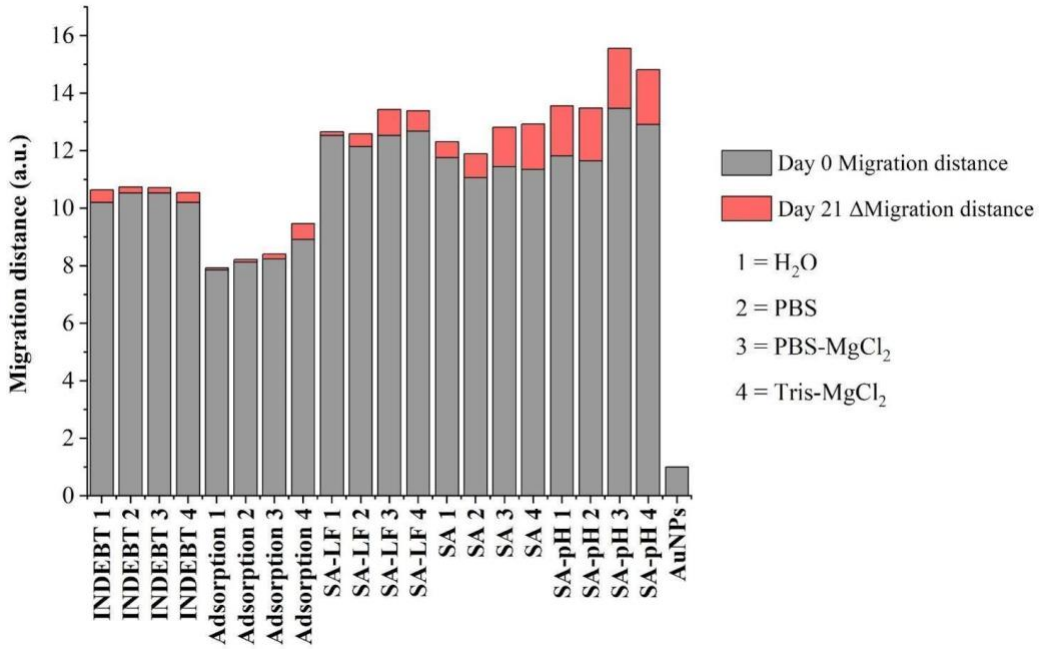


Figure 2: Migration distances of the conjugates on Day 0 (grey) and the increment of migration distance as of Day 21 (red).

The three SA techniques showed a similar initial pattern and tendency with time. The three showed the highest changes in migration distance over 21 days, suggesting DNA loss of some degree within time, especially for SA and SA-pH protocols (Figure 2). They also seem to be the most affected by the choice of buffer storage, showing increased migrations when stored in highly ionic buffers. Besides, SA and SA-pH, seem to suffer aggregation of some degree since bands of different sizes appear and disappear at different points in time (Figure 3). In the SA-LF conjugation, no bands of other sizes appeared for the three weeks and the difference in migration distance over 21 days was lower than for the other two SA techniques.

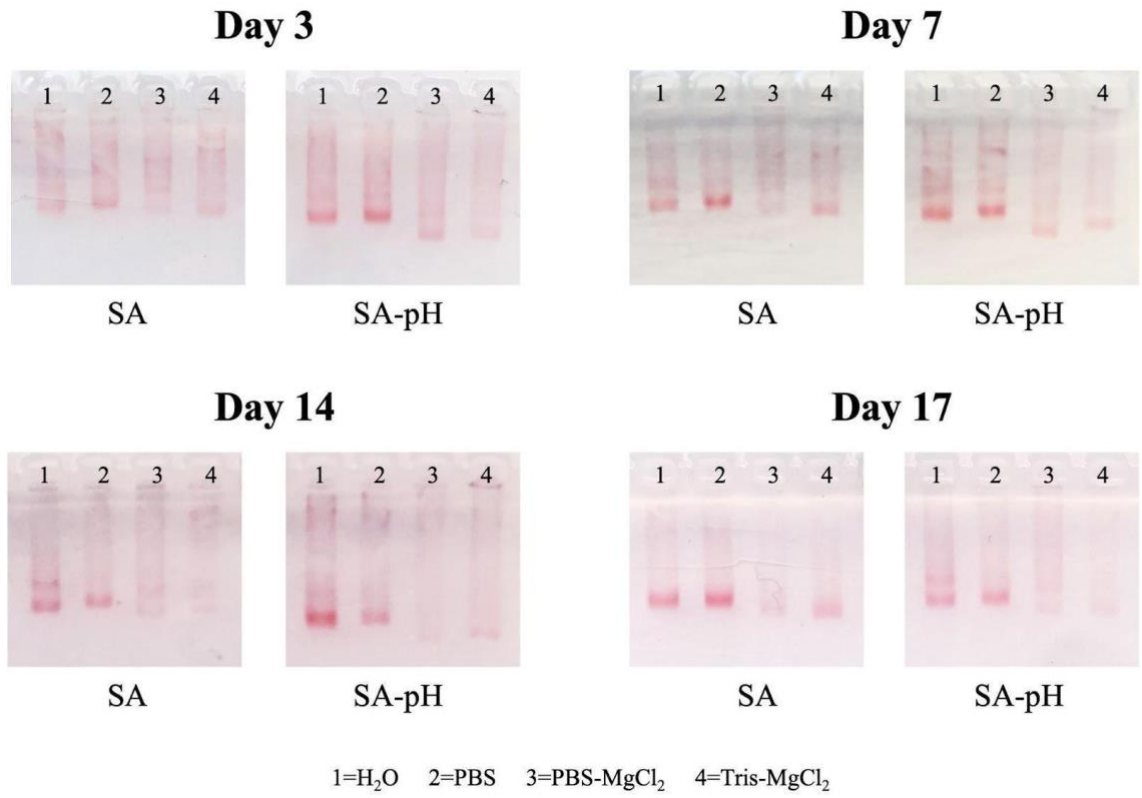


Figure 3: EMSA results of SA and SA-pH groups on days 3, 7, 14 and 17 with appearing and disappearing bands.

In the case of the INDEBT conjugation, no changes were observed during the three weeks, showing excellent stability in contrast to the other four techniques used. Lastly, Adsorption conjugates, although affected by the storage buffer of choice, showed good stability in terms of migration distance over the three weeks.

4.4.1.4. Electrophoretic Mobility Shift Assay General conclusions

The EMSA analysis can yield interesting conclusions. Regarding the conjugation method, INDEBT conjugation has shown great stability and tolerance to different storage buffers, which is an excellent feature for long-term assays, for instance. However, the presence of a second population of conjugates can be a disadvantage in certain applications where uniformity is necessary. Despite the diffuse running front of Adsorption conjugations, they suffered from little changes in migration, whereas the three SA conjugation methods (SA-pH conjugates specially) were affected the most by time and buffer composition. Finally, it can be observed that samples stored in water and PBS suffered from smaller changes in their migration distances within three weeks, suggesting that an increasing ionic force during storage could be detrimental for the conjugates in the long-term. It's worth noting that when non-conjugated AuNPs come into contact with the tank TBE buffer, they

tend to aggregate. This phenomenon could be used as a practical characterization method to determine whether AuNPs have been successfully conjugated.

4.4.2. UV-Vis

4.4.2.1. Variation between conjugation methods

Conjugation-wise, the three SA processes seem to present more aggregation than INDEBT and adsorption methods, safely due to the use of salts in the conjugation process shielding the citrates of the AuNPs. Maximum absorbance values are decreased in respect to non-conjugated AuNPs (Figure 4A, B, and C), probably due to the loss of colloidal nanoparticles and the increase of aggregates due to the salt additions, also flattening the spectra and decreasing the $A_{520/580}$ nm ratio (Figure 4F). It is to be noted, through the data depicted in Figure 4, that water resuspensions of the three SA processes yielded higher absorbances and $A_{520/580}$ nm ratios, suggesting that the final resuspension in highly ionic storage buffers exacerbates the stress from the conjugation process. On the other side, adsorption and INDEBT protocols (Figure 4D and E) seem to maintain closer values to non-conjugated AuNPs when resuspended in highly ionic buffers. This suggests that these protocols inflict lower impact on the AuNPs, while successfully achieving conjugation and, therefore, protecting them from an additional impact during the final resuspension step.

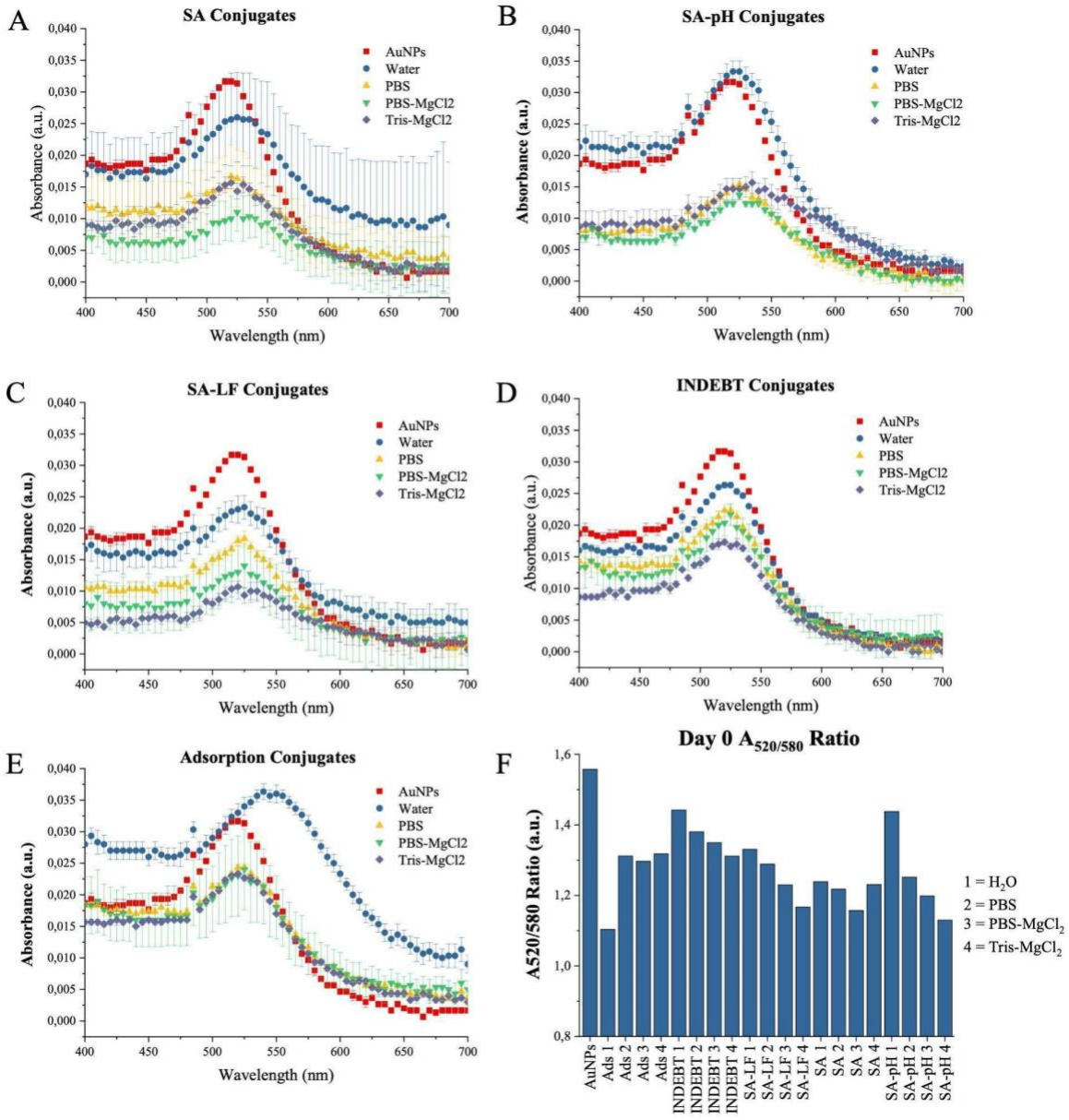


Figure 4: A-E) UV-Vis spectra of the 5 conjugation protocol groups on day 0. Non-conjugated AuNPs (AuNPs, red dotted lines) were plotted for reference of a typical AuNPs spectra. B) $A_{520/580}$ Ratio of all conjugates and non-conjugated AuNPs on day 0.

4.4.2.2. Variation between storage buffers

As previously explained, an additional impact attributed to the ionic force of the resuspension/storage buffer was detected. There is the noticeable exception of the water resuspension of the adsorption protocol, which peak was greatly shifted to 550 nm (Figure 4D and 5A). This is attributed to the low ionic strength of the buffer not shielding neighboring DNA molecules on the AuNP surface, increasing electrostatic stress within the layer, causing it to break apart and leading to bare Au and

therefore aggregation. Looking at the other three storage buffers (Figure 5), PBS is the one that achieves the most similar behavior to water resuspensions (Figure 5B), maintaining a low aggregation ratio, while avoiding the great shift of the water-adsorption conjugate.

PBS-MgCl2 and Tris-$MgCl_2$ buffers affect the conjugates differently (Figure 5C and 5D). They show the lowest absorbances and increased flattening of the spectra since day 0, with a special emphasis on the three SA conjugations. On the contrary, Adsorption and INDEBT protocols suffer from less aggregation in contact with these two buffers.

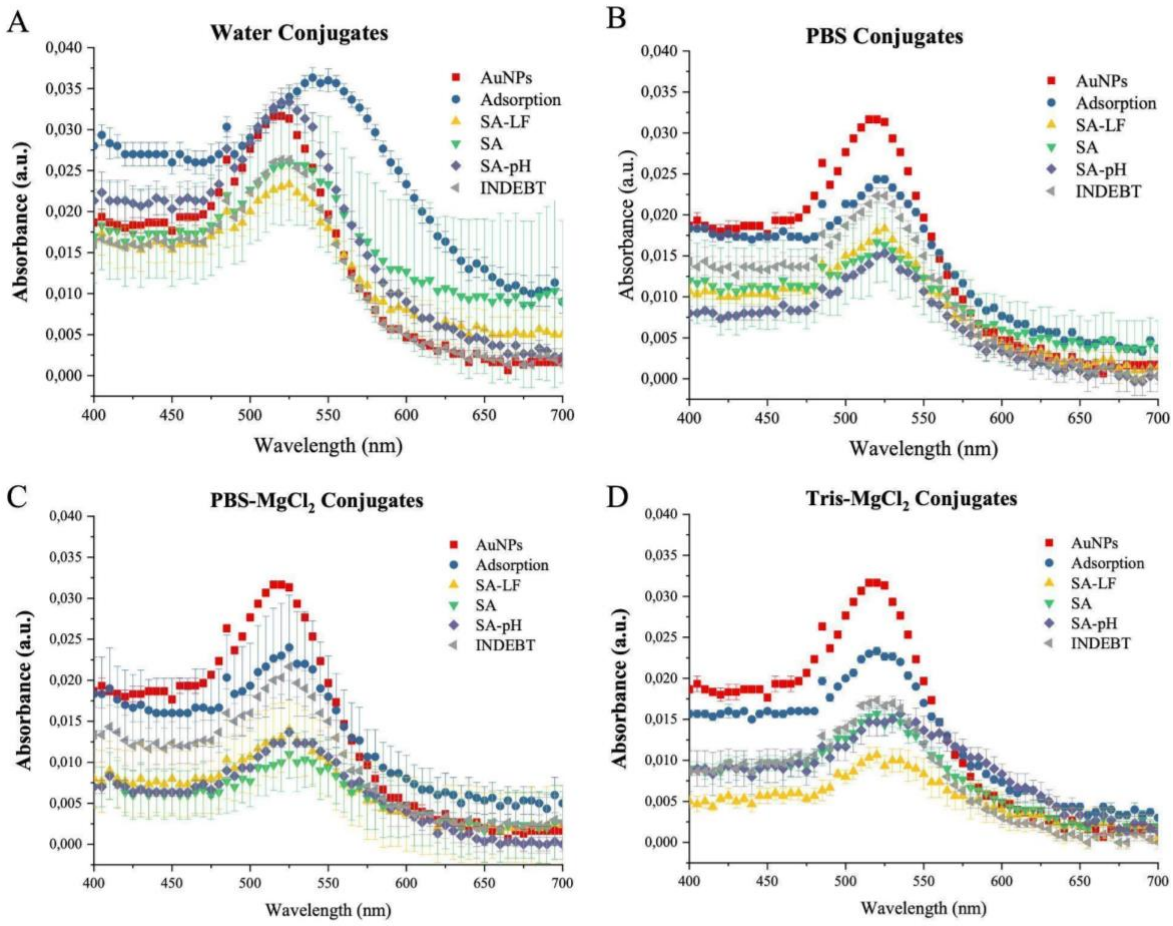


Figure 5: UV-Vis spectra of the 4 Storage Buffer groups on day 0. Non-conjugated AuNPs (AuNPs, red dotted lines) were plotted for reference of a typical AuNPs spectra.

4.4.2.3. Stability over time

The $A_{520/580}$ ratio evolution was studied as an aggregation indicator. However, it is to be noted the irregularity shown in the ratios of non-conjugated AuNPs on Days 3 and 14 (Figure 6D). Accidentally, AuNPs were minimally aggregated during the dilution process (in MQ water) of the sample preparation, which therefore altered the absorbance ratio of the non-conjugated AuNPs

shown, and is meant to be used as reference value for each figure. The absence of signs of aggregation in absorbance values from the same source of non-conjugated AuNPs on days 7, 10, 17, and 21 (Figure 6D) confirms that aggregation occurred during the dilution process accidentally.

Throughout the three-week assay period, three main groups can be distinguished among the chosen storage buffers. Water resuspensions (Figure 6A) showed more consistent stability or aggregation ratios compared to PBS and PBS-$MgCl_2$ buffers. With the aforementioned Adsorption-water conjugate exception, water resuspensions presented higher values of absorbance that were kept constant through the 21 days. Secondly, PBS and PBS-$MgCl_2$ conjugates (Figure 6B) seemed to present more ratio variability while maintaining their integrity over the 21 days. Differently and lastly, Tris-$MgCl_2$ conjugates (Figure 6C) succumbed to aggregation on day 21, which was clearly visible from the naked eye before dilution of the conjugates.

Conjugation-wise, SA protocols' conjugates ratios are generally found at the lower part of the graphs, confirming the aforementioned aggregation attributed to this principle (SA), while on the other side INDEBT and Adsorption conjugates' ratios are found over the SA ratios.

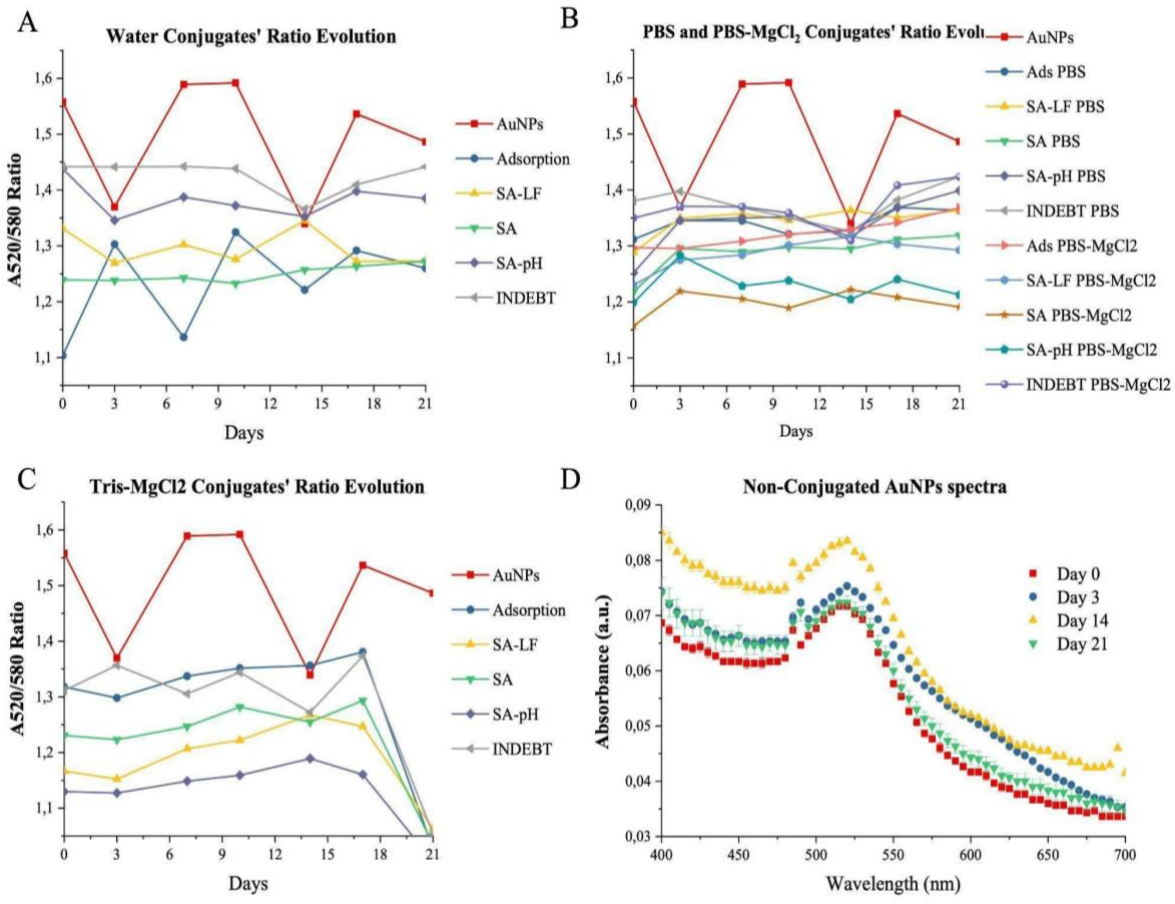


Figure 6: $A_{520/580}$ Ratio evolution for 21 days. A) Water conjugates Ratio evolution. B) PBS and PBS-$MgCl_2$ conjugates Ratio evolution. C) Tris-$MgCl_2$ Ratio evolution. Non-conjugated AuNPs (AuNPs, red dotted lines) were plotted for reference of a typical AuNPs ratio. D) UV-Vis spectra of non-conjugated AuNPs on days 0, 3, 14 and 21.

4.4.2.4. UV-Vis general conclusions

UV-Vis measurements have proven to be a useful tool for aggregation monitoring through the course of 21 days. Screening of the conjugates of day 0 using this technique allowed the determination and evaluation of two types of aggregation events or impacts attributed to the conjugation process. On the first place, aggregation occurred during the conjugation steps of the protocol. Stability and integrity of AuNPs was partially compromised during the three SA processes, whereas this impact was not witnessed for Adsorption and INDEBT protocols. On the second place, the additional aggregation occurred during the resuspension of the centrifuged pellet in different buffers, which was greatly impacted by the ionic strength of the same. Coinciding with EMSA results, INDEBT and Adsorption conjugates seemed to be less affected by the impact of the resuspension in highly ionic buffers and maintained the stability of the conjugates over time. This finding suggests that these methods successfully conjugate and protect the AuNPs with decreased AuNP or DNA loss and provide for further protection against reconcentration or eventual dilutions of the conjugate, which is an interesting factor to be considered when highly ionic buffers are precised in a particular application.

In regards of the evolution of the conjugates over 21 days, conjugates were, with varying degrees of irregularity, stable when resuspended in water or PBS, independently of the conjugation process used. However, $MgCl_2$-containing buffers, especially Tris-$MgCl_2$ buffer did not provide of a desired environment for long-term storage of DNA-AuNP conjugates, independently of the conjugation principle used. It is proposed that the presence of the divalent Mg^{2+} ions result in a change in the secondary structure of the DNA, through its coordination with the phosphate backbone of the DNA strands, which results in increased stress and instability of the films, which leads to rearrangement or loss of DNA and exposed Au, which causes aggregation.

It is to be noted that this aggregation was not reflected in the EMSA results of day 21, probably due to the direct dilution in glycerol. Conjugates' further dilution for UV-Vis sample preparation proved to be a useful small-scale GAT when using buffers with enough ionic strength as solvent.

4.4.3. Z-potential and Dynamic Light Scattering

During the three-week assay, measurements of Z-potential and DLS were conducted to monitor the stability of the conjugates. However, the two techniques showed differing levels of utility. Z-

potential measurements were only able to clearly distinguish AuNPs from the other groups on day 0 and Tris-aggregated conjugates of day 21, which was visible to the naked eye. Unfortunately, the rest of the data obtained from Z-potential were insufficient to differentiate other events occurring during the three weeks or attributed to the conjugation or buffer of choice. Conversely, DLS measurements did reflect some interesting events. The DLS results can be analyzed in various ways, but for this work the mean hydrodynamic diameter of the nanoparticles "z-average" and the polydispersity index (PdI) will be analyzed. The PdI is a measure of the distribution of sizes within the sample, the lower the value being more indicative of a monodispersed suspension.

PdI measurements did show similar tendencies to UV-Vis data. However, only the aggregation of only two out of the five Tris-$MgCl_2$conjugates of day 21 was clearly reflected with a sudden increase of the PdI value (Figure 8D).

4.4.3.1. Variation between conjugation methods

The previously observed effects of the conjugation principle did not appear to have an evident impact in the PdI of the conjugates. All the PdI are within the accepted range for nanoparticles of this size, 0.2-0.5 a.u. (Figure 8). However, INDEBT conjugates presented the lowest PdI values along the three weeks (Figure 8, green) independently of the resuspension buffer, generally ranging between 0.2 and 0.3 a.u., whereas the rest of the conjugations presented overall PdI values higher than 0.3. INDEBT's stability is also reflected in the Z-average (Figure 9, green) and mean Z-Average (Table 2) values, especially for water and PBS resuspensions. These two INDEBT resuspensions' variability amongst the 21 days are quite low, while showing the highest hydrodynamic size in comparison to Adsorption and SA resuspensions in the same buffers, indicating the previously theorized stable and radial organization of the DNA.

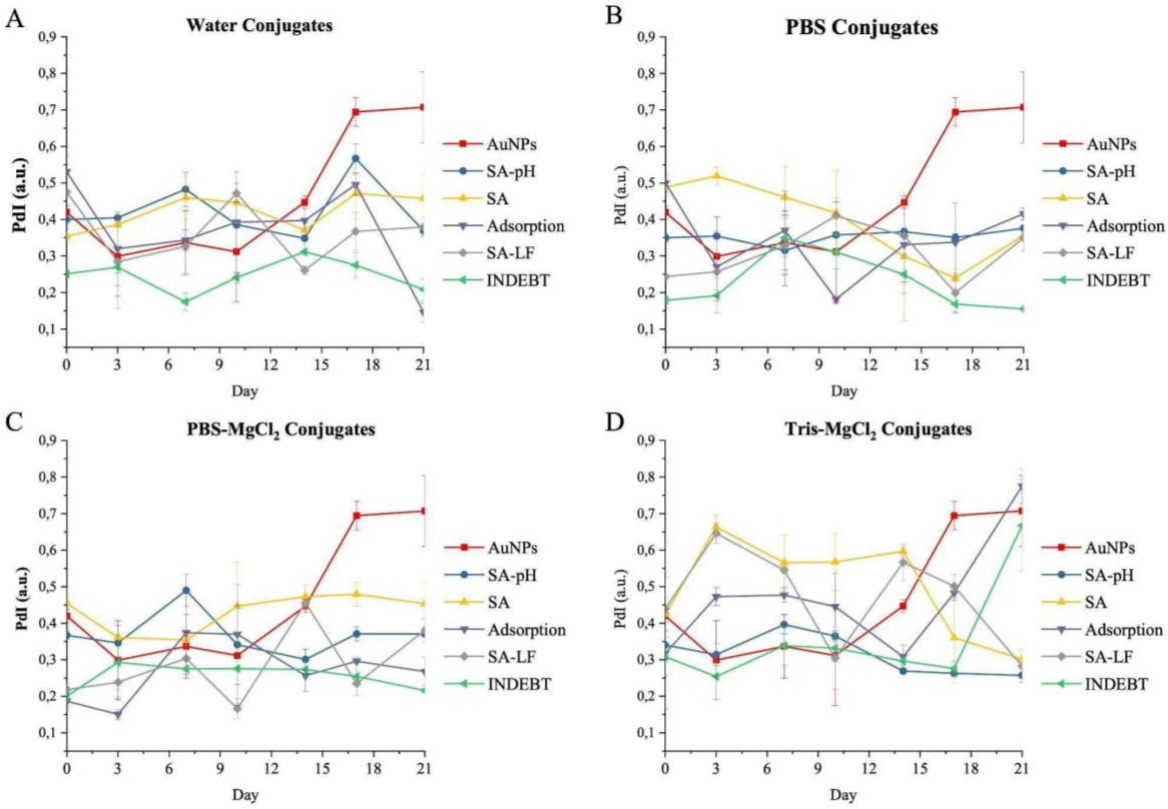


Figure 7: PdI values of every conjugate during the 21 days of assay.

An interesting finding was that SA-pH conjugates, especially water and PBS resuspensions, showed the lowest and more similar to AuNPs hydrodynamic range (Figure 9 and Table 2), which suggests a random or flattened DNA organization.

4.4.3.2. Variation between storage buffers

A dependence of the conjugates' hydrodynamic diameter on the buffer used was observed. As noted earlier, conjugates suspended in water and PBS exhibited a smaller Z-average (30-100 nm) compared to those in PBS-$MgCl_2$ and Tris-$MgCl_2$ buffers (Table 2 and Figure 8). This difference can be attributed to the presence of $MgCl_2$, which promotes radial orientation of the DNA phosphate backbone, thereby increasing the hydrodynamic diameter. However, sudden spikes in Z-average values from $MgCl_2$-containing conjugates indicate the presence of aggregation in the solution.

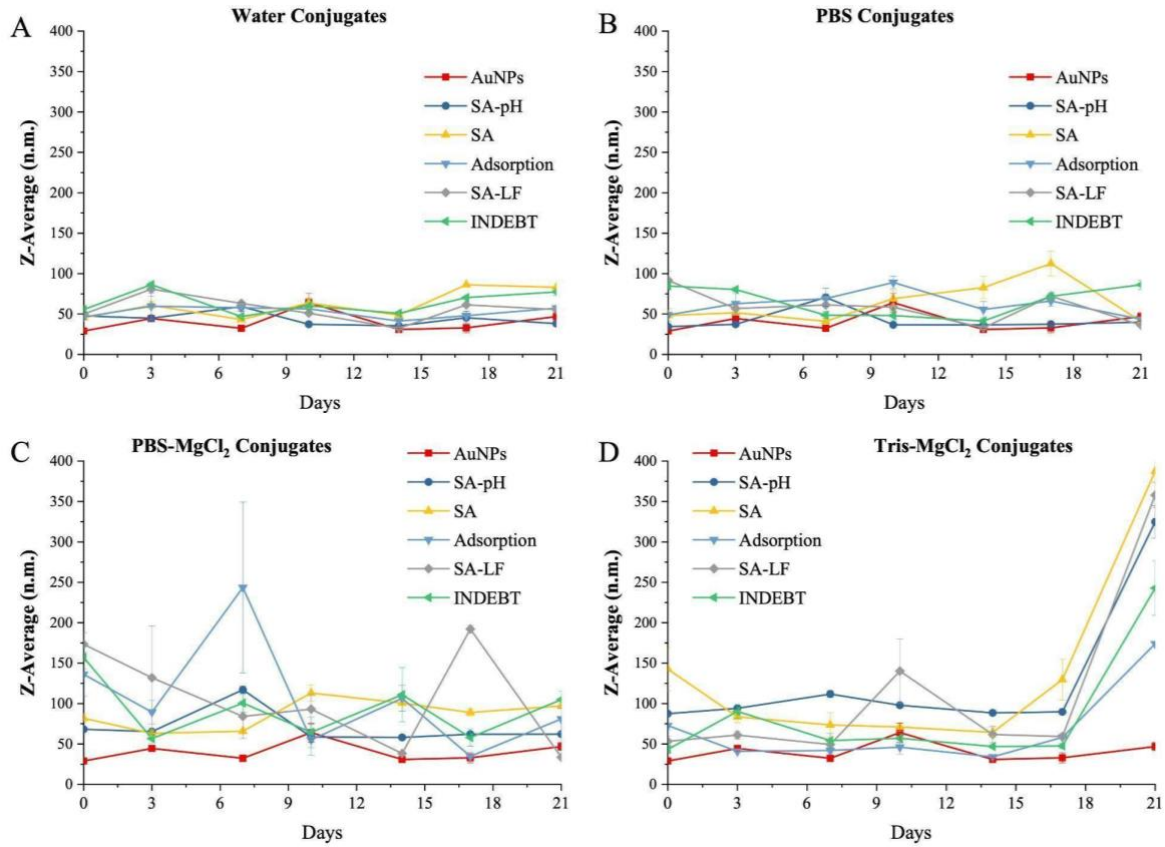


Figure 8: Z-Average (nm) of every conjugate during the 21 days.

4.4.3.3. Stability over time

The hydrodynamic diameter of all conjugates, in opposition to the PdI values, did confirm the aggregation of Tris-$MgCl_2$ conjugates on day 21 (Figure 8D). PBS-$MgCl_2$ and Tris-$MgCl_2$ conjugates showed the highest hydrodynamic range since day 0 (Figure 8 C and D) and kept this tendency until day 21 (Table 2). On the other side, conjugates resuspended in water and PBS yielded more constant Z-Averages over the 21 days. In regards of the conjugation method, INDEBT protocol seemed to provide more stable hydrodynamic diameters, except for irregularities related to PBS-$MgCl_2$ conjugates and the final aggregation of the Tris-$MgCl_2$ conjugates on day 21.

Table 2: Average of the 21 days of the conjugates and non-conjugated AuNPs' Z-Averages.

	SA	SA-pH	SA-LF	INDEBT	Adsorprtion
Water	61.59 +/- 16.19	43.99 +/- 7.52	56.35 +/- 13.72	63.9 +/- 13.45	52.39 +/- 6.5
PBS	63.71 +/- 24.45	41.81 +/- 11.84	58.51 +/- 18.71	65.87 +/- 17.85	62.11 +/- 13.9
PBS-MgCl2	87.24 +/- 16.96	70.23 +/- 19.4	106.63 +/- 57.46	93.2 +/- 33.75	106.64 +/- 63.7
Tris-MgCl2	136.03 +/- 106.44	127.78 +/- 80.8	111.82 +/- 104.58	83.175 +/- 66.81	66.85 +/- 44.36
AuNPs	40.05 +/- 11.72				

4.4.3.4. Z-potential and Dynamic Light Scattering General conclusions

Based on the DLS measurements, particularly the Z-Average results, an approximate assessment of the radial arrangement of DNA within the conjugates, as well as their stability, was obtained.

Firstly, DLS results suggest that conjugates resuspended in water or PBS, independently of the conjugation method used, were more stable throughout the 21 days. Bigger hydrodynamic diameters of PBS-$MgCl_2$ and Tris-$MgCl_2$ conjugates suggested that Mg^{2+} cations promote radial organization of the DNA strands. However, the stability of these samples was affected, showing irregularities on the Z-Average values during and at the end of the assay. These buffers causing issues is suggestive of the Mg^{2+} ions disrupting the AuNP-DNA conjugates, most probably by changing the secondary structure of the DNA through ionic interactions with the phosphate backbone. This is in agreement with the other techniques used in this study and suggests that DNA conjugates are susceptible to interference from divalent ions such as Mg^{2+}.

Conjugation-wise, INDEBT conjugation showed bigger and more constant hydrodynamic ranges along the 21 days. Unlike in UV-Vis measurements, Adsorption conjugation was not particularly differentiated from the three SA conjugation methods, apart from the irregularities attributed to the resuspension buffer. Lastly, from the three SA conjugation methods, SA-pH conjugates seem to stand out by their smaller size, which can be attributed to less radial conformation of the DNA, probably due to a lower packing density, which correlates with EMSA results.

Overall, the DLS technique, along with UV-Vis and EMSA assays, proves to be a valuable monitoring tool of stability over the 21 days. All three methods work together to confirm events and provide complementary information. For this particular number of conjugates, and their variability

between conjugation methods and storage buffers, Z-potential measurements were not able to be decisive for the characterization of such a big group of conjugates.

4.4.4. Lateral Flow

As previously mentioned, the three last characterization techniques aim to monitor the stability of the conjugates for 21 days. However, it remains to be seen if these stability data are correlated with their functionality, specifically in LFA and with a particular set of conditions. As previously explained, qualitative and semi-quantitavive evaluation of LFA strips has been performed due to the variations in the quality of the flow, which can impact the semi-quantitative values, but can be interpreted differently to the naked eye.

Looking at the results of the three weeks, at least five types of qualitative results can be differentiated: (1) Strong lines with clear background, which are considered the ideal outcome in LF; (2) Strong lines with dirty background, which indicates flow issues that are mostly optimizable for any particular application; (3) Faint lines either with a dirty or clean background, which indicates low DNA hybridization; (4) Flow staining, when nanoparticles aren't able to flow in a united front, causing aberrant results and total or partial absence of lines; and (5) Aggregation, when nanoparticles aren't able to flow through nitrocellulose. See Figure 9.

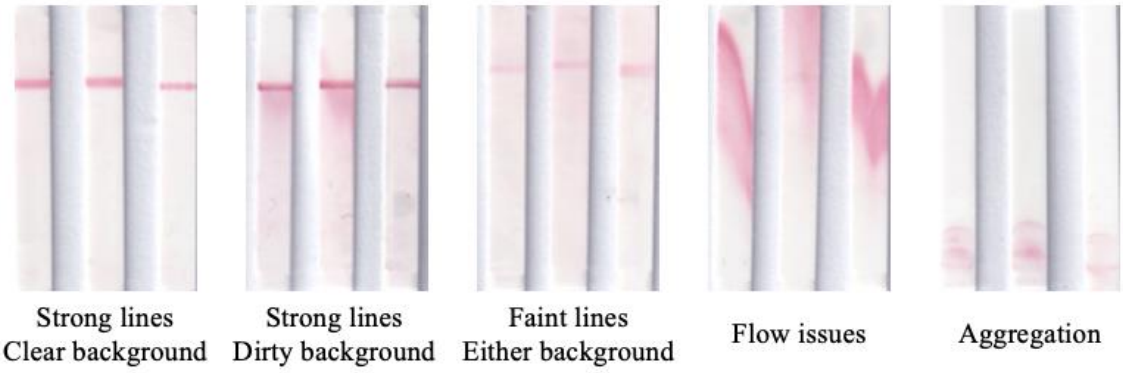


Figure 9: Types of qualitative results in LFA strips.

Semi-quantitatively speaking, there are fewer groups of signals to be differentiated. In the analysis conducted using ImageJ software, ranges of semi-quantitative signal intensities were assigned to three distinct qualitative outcomes. Signals falling within the range of 0 to approximately 15 were indicative of the absence of any detectable signal to the naked eye or attributed to aberrancies in flow. Intensities ranging from approximately 15 to 50 were interpreted as representing signal intensities ranging from faint to within the bounds of normalcy. Signals falling within the range of

approximately 50 to 100 were characterized by strong to saturated intensities, indicating strong positives.

On day 0, conjugates were applied to LFA strips on the same day as their resuspension in the storage buffer. These conjugates are considered fresh and ideally should perform to the best of their ability on day 0, with this ability potentially diminishing partially or completely within the three weeks. Non-functionalized AuNPs were run through LFA strips on each day as well. However, non-functionalized AuNPs are prone to aggregation in contact with highly ionic environments. When these AuNPs, originally resuspended in water, enter contact with the treated sample pad, the crystallized saline components of this treatment are dissolved, causing an immediate aggregation and, therefore, stopping the flow or creating flow aberrancies. This behavior of the negative control is maintained over the course of three weeks.

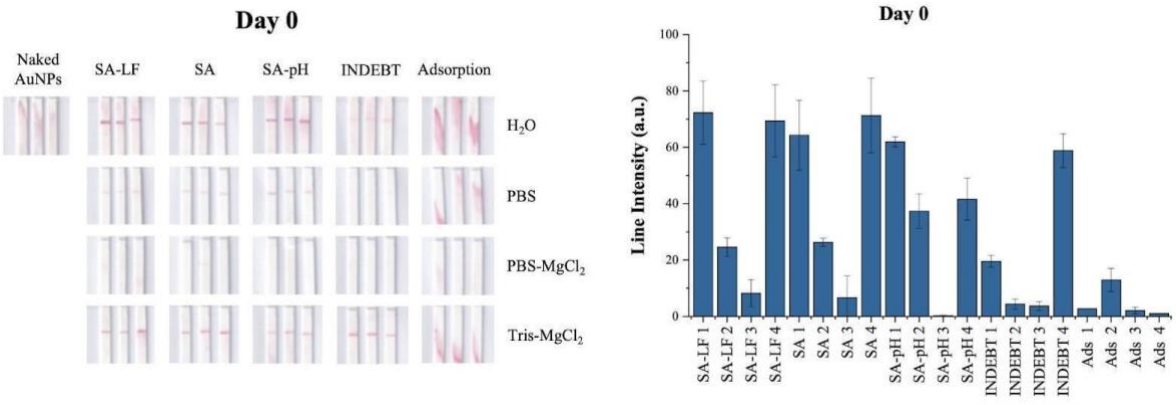


Figure 10: LFA results of day 0 and ImageJ measurements of the LFA strips.

4.4.4.1. Variations between conjugation methods

From all conjugation methods, a group quickly stands out by their inability to flow as a united front, presenting a pronounced trail or build-up of AuNPs along the LFA strip, Adsorption protocol (Figure 11). This trail of AuNPs does not present a purple coloration attributed to aggregation, which indicates that at least a minimum number of sequences are present on the surface of the AuNPs. However, the flow problems, along with the absence of line apparition, suggest that the disposition of these sequences could be non-directional and suffer from steric hindrance for their hybridization, therefore losing their functionality. Due to this, Adsorption conjugates will be excluded from further analysis/Figures.

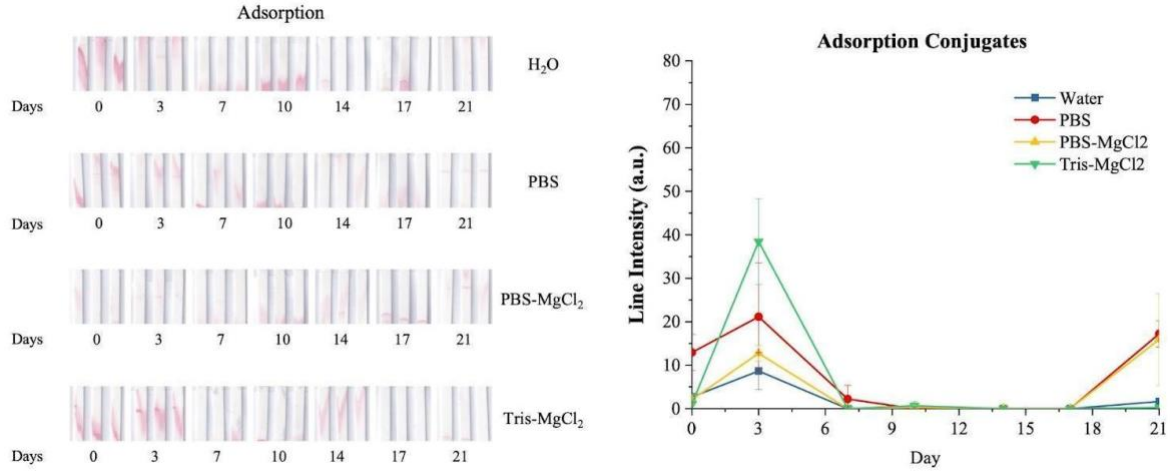


Figure 11: LFA strips of Adsorption conjugates over the 21 days. A) LFA strips. B) Semi-quantitative measurements on ImageJ software.

Based on the semi-quantitative findings of the Adsorption conjugates (as shown in Figure 11B), it appears that there may be some misleading semi-quantification related to the Tris-$MgCl_2$ resuspension on day 3. Although the graph shows an increase in intensity, such partial signals are not considered valid based on visual observation alone.

The four other conjugation methods show functionality with varying degrees of line intensity and/or background noise (Figure 10). These varying degrees are more dependent on the storage buffer used than the conjugation method used, especially amongst the three SA protocols. Therefore, these four groups will be evaluated in the following section.

4.4.4.2. Variations between storage buffers

On day 0, the four Tris-$MgCl_2$ resuspensions (excluding the fifth from Adsorption) show the best signal-to-noise ratio, with intense lines and a clear background (Figure 12A, bottom). This was expected since LFA strip optimization was undergone using this buffer, as previously described.

In the second place, a group of strips with strong lines but a poorer background is observed, specifically the three SA conjugations resuspended in water (Figure 12 A, top). These exhibit even stronger lines than Tris-$MgCl_2$ conjugates at Day 0. The background color of the nitrocellulose is considered easily improvable (i.e., by increasing surfactant in the sample pad). However, this background is not a desirable outcome in a LFA strip, and this noise is not totally reflected in the semi-quantitative values (Figure 12, Right), which can lead to confusion.

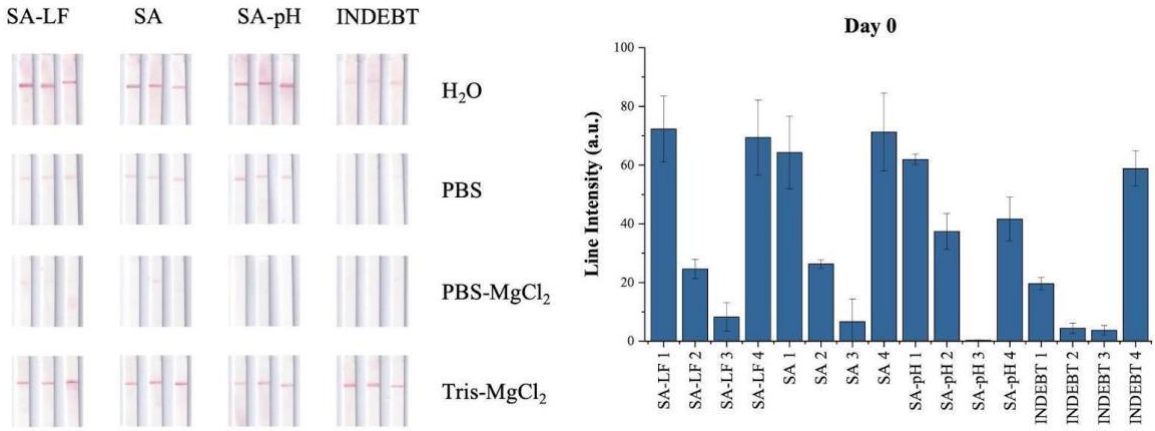


Figure 12: Observed qualitative results of the conjugates on LFA strips of day 0. A) LFA strips. B) Image J measurements.

In the third place, a group consisting of the three PBS resuspensions of SA conjugations and the water-INDEBT conjugation can be detected. This group was observed to have lower performance than the two previous groups, displaying faint lines since day 0, although with relatively clear background noise.

Finally, the last group was detected by its irreproducibility. All four remaining PBS-$MgCl_2$ conjugations with the addition of INDEBT-PBS conjugations showed either absence of signal or irreproducibility amongst its triplicates since day 0. The poorer performances of all the conjugates in the phosphate containing buffers may indicate that the presence of the phosphate ions may be hindering the LFA performance.

4.4.4.3. Stability over time

As for the behaviors or tendencies attributed to time and the method of conjugation used, there are some differences that can be analyzed. Except for the Adsorption protocol, all four other protocols showed varying degrees of functionality. Amongst the three SA protocols, a progressive decay of signal within time can be seen, with different paces each. However, the three protocols showed a signal for the water resuspensions on day 21.

The fastest one to decay in terms of signal was the SA-LF protocol (Figure 13), showing background noise as well as a decrease in line intensity from day 3. Except for the PBS-$MgCl_2$ resuspension, the other three suffered from a gradual loss of intensity. Water and, specially, PBS resuspensions, were still functional on day 21.

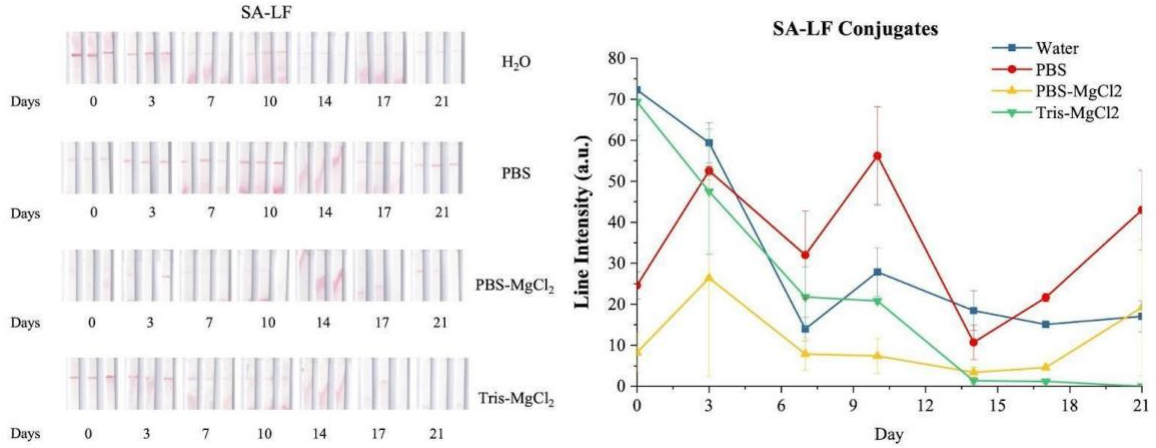


Figure 13: LFA results of the SA-LF conjugates of the 21 days of assay. Left, LFA strips. Right, Image J measurements.

SA-LF protocol was followed by the SA-pH on day 10. SA-PH protocol (Figure 14) achieved to maintain a stable signal until day 10 for the Water, PBS and Tris-$MgCl_2$ conjugates, whereas only Water and PBS conjugates remained functional on day 21 (Figure 14A). Semi-quantitatively speaking, however, due to the irreproducibility of PBS-$MgCl_2$ conjugates, on day 21 they appear at the same level of intensity as Water conjugates (Figure 14 B, day 21), which can be misleading.

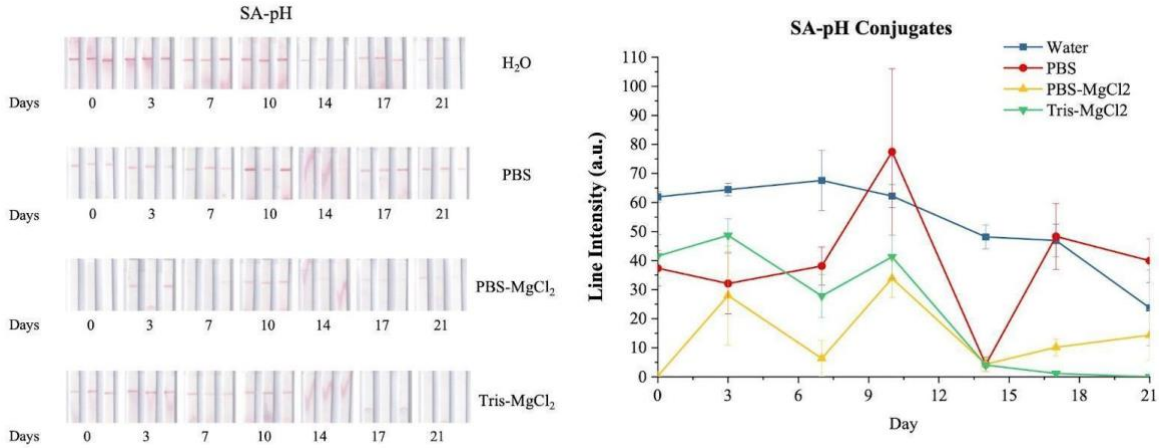


Figure 14: LFA results of SA.pH conjugates of the 21 days of assay. Left, LFA strips. Right, Image J measurements.

Last, SA protocol maintained stable line intensity also until day 14 but achieved cleaner background noises. The water resuspension achieved a more linear decrease in the signal, which is reflected in the semi-quantitative evaluation (Figure 15B).

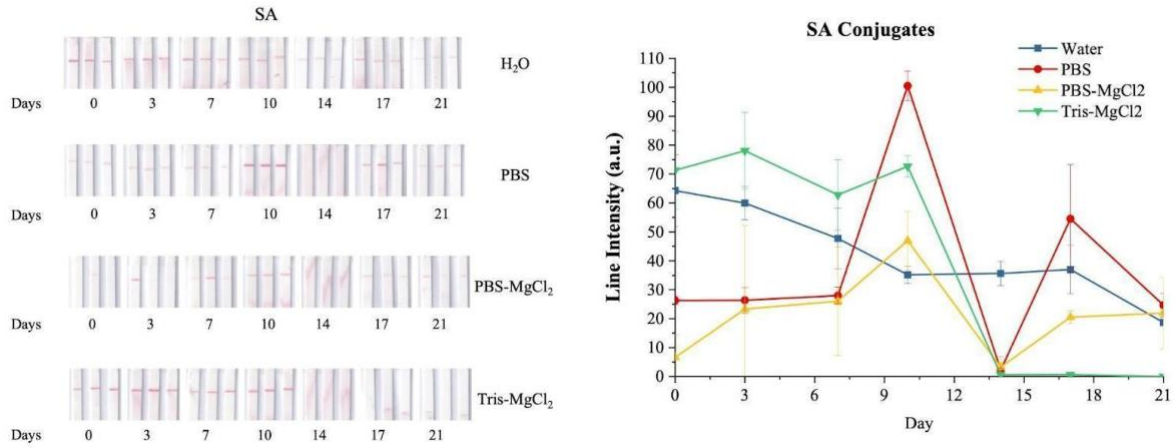


Figure 15: LFA results of SA conjugates of the 21 days of assay. Left, LFA strips. Right, Image J measurements.

The SA-PBS resuspension suffered a sudden increase of line intensity on day 10, before losing signal on day 14 and recovering signal on days 17 and 21. PBS-$MgCl_2$ and Tris-$MgCl_2$ conjugates follow the same tendency as in the other two SA protocols, suffering from irreproducibility and from eventual loss of signal, respectively.

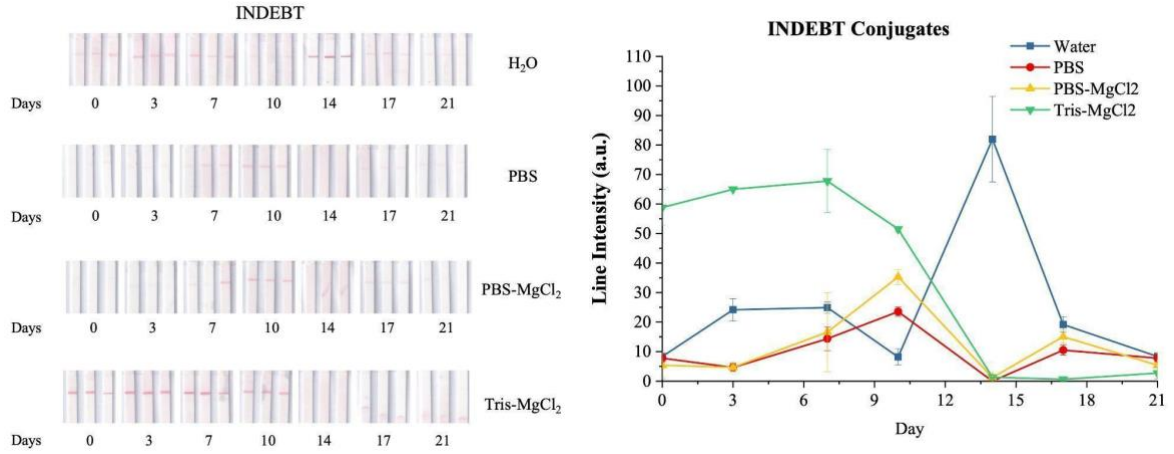


Figure 16: LFA results of INDEBT conjugates of the 21 days of assay. Left, LFA strips. Right, Image J measurements.

On the other side, the INDEBT conjugates have a less expected behavior. INDEBT conjugations, especially PBS and PBS-$MgCl_2$ resuspensions, did not show any signal until day 7. Except for Tris-$MgCl_2$ conjugate, they seem to improve their performance gradually until day 7 or 10 before gradually losing signal until day 21. The hydrodynamic diameter and electrophoretic mobility of these conjugates are stable over the three weeks investigated, and the samples did not aggregate. We hypothesize that this data is evidence of the presence of residual butanol on the nanoparticle conjugates. The partition coefficient of tris from water into alcohol solvents is known to be complex, varying with solvent composition, which we believe will change over the timescale measured herein

as the butanol evaporates. This causes large scale reordering of the water molecules at the conjugate solution interface over time, may explain the difference in performance over time in the Tris-$MgCl_2$ buffer and INDEBT conjugates. These data emphasize the importance of solvation in the functionality and performance of the conjugates.

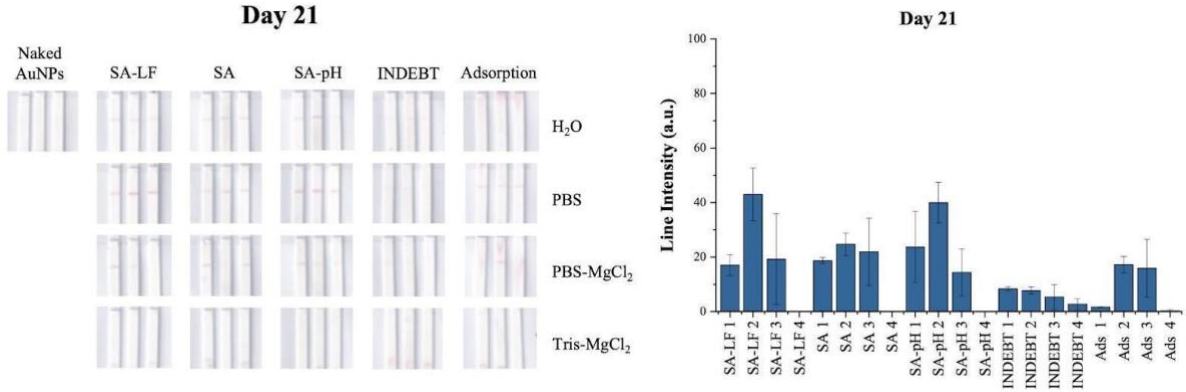


Figure 17: LFA results of every conjugate on day 21. A) LFA strips. B) Image J measurements. 1=Water, 2=PBS, 3=PBS-$MgCl_2$, 4=Tris-$MgCl_2$.

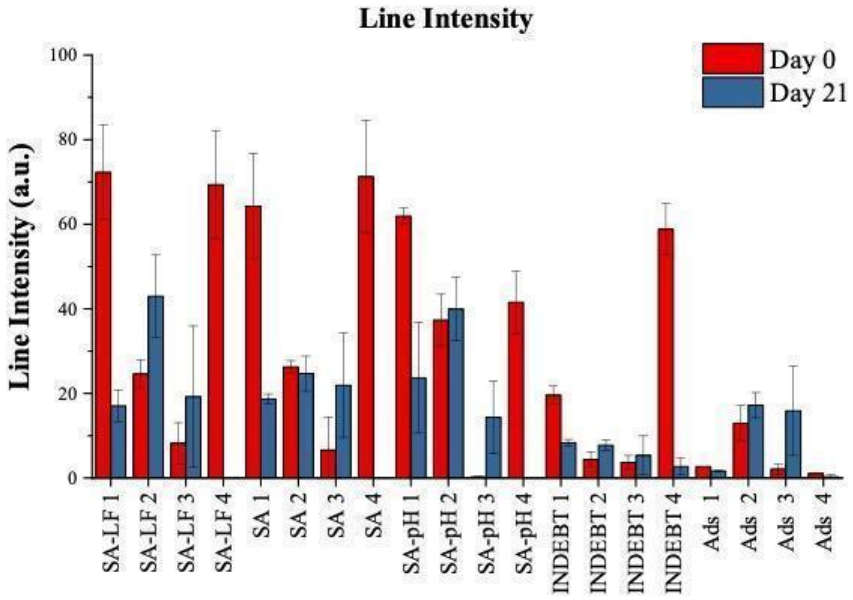


Figure 18: Line intensities of all conjugates on day 0 (red) and day 21 (blue). 1=Water, 2=PBS, 3=PBS-$MgCl_2$, 4=Tris-$MgCl_2$.

4.4.4.4. Lateral Flow general conclusions

After carefully reviewing qualitative and semi-quantitative results of the 21-day assay, a series of aspects related to the conjugation technique of choice arose. Adsorption conjugation technique proved unsuccessful for DNA-AuNP conjugates' proper flow and correct DNA hybridization in

nitrocellulose, probably due to the theorized adhesion of the nucleobases to the surface of the AuNP and the heterogeneity in charge observed in EMSA results.

Secondly, INDEBT protocol appeared to be functional with one main drawback; the presence of butanol debris in the conjugates can greatly affect the flow and behavior of the conjugates in a nitrocellulose platform. As mentioned above, it is suspected that this is the case due to the improvement of signal within the first week of assay, suggesting gradual evaporation of the solvent. However, this variable could be avoided with extra purification of the solvent and further studies on their functionality on LFA.

Last, the three SA techniques did reflect more stable and longer functionality, which is not surprising, due to the popularity of this method within DNA LFA users. Between the three SA conjugation methods tested, these could be classified considering the user's expectations and customary habits in the laboratory. As reported in the literature, it is recommended that AuNP conjugates be utilized shortly after the conjugation process or within a few days thereafter, given that their degradation is expected to occur at varying rates.[20] It is important to note that the method of conjugation employed and the buffer used for storage can directly affect the rate of degradation. Based on these recommendations and the data obtained, it is suggested that SA-LF conjugation techniques be employed for the use of the conjugates freshly. If the final user intends to use the conjugates over an extended period of time, SA-pH conjugation could be considered a reliable option, especially if a pH restriction is required for optimal assay performance. However, the original SA protocol yielded the most stable and clean signal for a longer period of time.

In regards of the resuspension and storage buffer of choice, two different effects were observed. On the first place, Water and Tris-$MgCl_2$ resuspensions yielded the best results in every conjugation method used. It can be attributed this to the compatibility with the sample pad treatment buffer composition, which also contains Tris-$MgCl_2$ buffer. PBS resuspensions suffer from a decrease in signal since day 0 in comparison with Water and Tris-$MgCl_2$ resuspensions and PBS-$MgCl_2$ resuspensions show irreproducibility since day 0, suggesting added incompatibility.

The second effect is related to the long-term stability of the conjugates. Storage in water appears to be the less detrimental option for the functionality of the conjugates, presumably due to the absence of salts maintaining the repulsion equilibrium of the conjugates and not inducing aggregation or unspecific hybridizations between them. Therefore, storage in water is recommended for long-term stability due to (1) compatibility with further LFA conditions, (2) its lower impact on the conjugates and (3) for the long-term functionality of the conjugates.

4.5. Discussion

The employment of EMSA assays, coupled with UV-Vis and DLS measurements, proved invaluable in assessing the effects of distinct conjugation techniques and resuspension buffers on various aspects such as size, packing density, structure of nucleic acids and aggregation state. This combination of techniques further facilitated the continuous monitoring of these characteristics over a span of 21 days. The wealth of information obtained from each technique was often interrelated, offering complementary insights that provided a comprehensive understanding of the conjugate's features. Although certain conjugate groups were deemed "stable" in terms of size, aggregation state, or packing density, this did not always correspond to their effectiveness in LFA. Firstly, Adsorption conjugates were consistently non-functional despite maintaining stable absorbance ratios, Z-Averages, and EMSA migration distances, indicating low levels of aggregation. All conjugates that were initially functional in LFAs showed declining performance over time. None more than INDEBT conjugates which showed two distinct EMSA populations and suffered irregular LFA functionality possibly due to butanol residues hindering flow and hybridization. Despite this, their stability suggests potential use in compatible applications.

In contrast, six conjugates, primarily the SA methods with water or PBS buffers, maintained functionality until day 21. SA techniques demonstrated compatibility with LFA, with SA and SA-pH methods showing similar functionality levels. LFA-optimized SA protocols initially performed well but deteriorated faster, suggesting limitations for long-term use.

The selection of resuspension buffers played a critical role in maintaining conjugate stability. Conjugates stored in Mg^{2+}-free, low-ionic strength buffers such as deionized water and PBS exhibited enhanced long-term stability and reduced aggregation. In contrast, buffers containing Mg^{2+} cations promoted aggregation and decreased functionality over time.

Conjugates resuspended in PBS-$MgCl_2$ were consistently non-functional in LFAs, showed increased migration in EMSA, more aggregation, and irregular absorbance and hydrodynamic profiles. There is a trend of phosphate containing buffers, PBS and PBS-$MgCl_2$, not being functional in LFA with any of the conjugates, implying that the phosphate, or some other component specific to these buffers, is somehow impairing DNA conjugate hybridization to the test line DNA. The exact methodology of this is not known as it does not fit with any of the other observations. All that can be said is that the explanation should comply with changes that do not show in DLS, Z-potential, UV-Vis or EMSA changes in the conjugates, and should apply to all the conjugation chemistries tested. All conjugates that were initially functional in LFAs showed declining performance over time, however, none more than those resuspended in Tris-$MgCl_2$. Conjugates resuspended in Tris-$MgCl^2$ initially performed well in LFA but degraded by day 14 with aggregation visible to the naked eye,

corroborated with changes in EMSA and UV-Vis metrics. Water resuspensions consistently supported LFA functionality, corroborated by EMSA, UV-Vis, and DLS measurements.

This study underscores the critical role of buffer compatibility and optimization conditions in LFA performance, providing insights into maintaining stability and functionality of DNA-AuNP conjugates across varied applications.

4.6. Conclusions

This thesis chapter has systematically evaluated the stability, functionality, and performance of DNA-AuNP conjugates across various conjugation methods and storage conditions, specifically focusing on their application in LFAs. Through the employment of multiple characterization techniques—LFA, EMSA, UV-Vis spectroscopy, and DLS—a comprehensive understanding of the behavior of these conjugates has been achieved.

Firstly, it has been confirmed that the choice of conjugation method significantly influences the nucleic acid density and functionality on the AuNP surface. This, in turn, affects the conjugates' protection against aggregation and their overall stability. For instance, the SA and SA-pH methods demonstrated higher compatibility and stability in LFAs, contrasting with the INDEBT method which, despite initially working in Tris-$MgCl_2$ buffer, failed over time due to residual butanol and tris interactions hindering hybridization processes. Future work will investigate if more stringent removal of butanol can overcome this issue.

Adsorption conjugates and those stored in phosphate containing buffers consistently failed in LFAs. Indicating that the phosphate ions may be inhibiting correct DNA-LFA function. This is an important consideration as phosphate containing buffers are routinely used in conventional antibody based LFAs, and in aptameric sensors, which may encounter problems when being transferred into a LFA format.

Conjugates stored in Mg^{2+}-free, low-ionic strength buffers, such as deionized water and PBS, exhibited enhanced long-term stability and reduced aggregation. Conversely, the inclusion of Mg^{2+} cations in the storage buffers was found to negatively impact the conjugates, promoting aggregation, and decreasing their functionality over time.

Practical recommendations derived from this study include the preferential use of SA-LF for immediate applications and the SA-pH method in phosphate and Mg^{2+}-free buffers for longer storage periods. Moreover, careful consideration of resuspension buffer composition and LFA treatment conditions is crucial to maintaining sensitivity and ensuring optimal performance.

The combined use of EMSA, UV-Vis spectroscopy, and DLS was essential for a detailed analysis of the conjugates. These techniques provided complementary data that, when analyzed together, offered a full picture of the conjugates' state, stability, and functionality. This multi-faceted approach was necessary to capture the nuanced changes occurring within the conjugate samples, which single techniques or exclusive reliance on LFA functionality could have missed.

In summary, this chapter has demonstrated that the careful selection of conjugation methods and storage buffers is vital for maintaining the stability and functionality of DNA-AuNP conjugates in

LFA. The insights gained from the extensive characterization and comparison of different protocols and conditions provide a robust framework for optimizing these conjugates for practical applications, ensuring their reliability and effectiveness in various assay environments.

4.7. References

1. Elghanian R, Storhoff JJ, Mucic RC, Letsinger RL, Mirkin CA. Selective colorimetric detection of polynucleotides based on the distance-dependent optical properties of gold nanoparticles. *Science (1979)*. 1997;277(5329):1078–81.
2. Park SY, Lytton-Jean AKR, Lee B, Weigand S, Schatz GC, Mirkin CA. DNA-programmable nanoparticle crystallization. *Nature 2008 451:7178*. 2008;451(7178):553–6.
3. Alivisatos AP, Johnsson KP, Peng X, Wilson TE, Loweth CJ, Bruchez MP, *et al.* Organization of "nanocrystal molecules" using DNA. *Nature 1996 382:6592*. 1996;382(6592):609–11.
4. Taton TA. Preparation of Gold Nanoparticle–DNA Conjugates. *Curr Protoc Nucleic Acid Chem*. 2002;9(1):1–12.
5. Zhao W, Lin L, Hsing IM. Rapid synthesis of DNA-functionalized gold nanoparticles in salt solution using mononucleotide-mediated conjugation. *Bioconjug Chem*. 2009;20(6):1218–22.
6. Liu J, Lu Y. Preparation of aptamer-linked gold nanoparticle purple aggregates for colorimetric sensing of analytes. *Nat Protoc*. 2006;1(1):246–52.
7. Cutler JI, Auyeung E, Mirkin CA. Spherical Nucleic Acids. *Spherical Nucleic Acids: Volume 1*. 2021;1:91–136.
8. Liu B, Liu J. Methods for preparing DNA-functionalized gold nanoparticles, a key reagent of bioanalytical chemistry. *Analytical Methods*. 2017;9(18):2633–43.
9. Huang Z, Liu J. Packing DNA on gold nanoparticles by dehydration. *Matter*. 2021;4(8):2585–6.
10. Liu B, Liu J. Freezing Directed Construction of Bio/Nano Interfaces: Reagentless Conjugation, Denser Spherical Nucleic Acids, and Better Nanoflares. *J Am Chem Soc*. 2017;139(28):9471–4.
11. Zhang X, Servos MR, Liu J. Surface science of DNA adsorption onto citrate-capped gold nanoparticles. *Langmuir*. 2012;28(8):3896–902.
12. Huang M, Xiong E, Wang Y, Hu M, Yue H, Tian T, *et al.* Fast microwave heating-based one-step synthesis of DNA and RNA modified gold nanoparticles. *Nature Communications 2022 13:1*. 2022;13(1):1–14.
13. Hao Y, Li Y, Song L, Deng Z. Flash Synthesis of Spherical Nucleic Acids with Record DNA Density. *J Am Chem Soc*. 2021;143(8):3065–9.
14. Xu Q, Lou X, Wang L, Ding X, Yu H, Xiao Y. Rapid, Surfactant-Free, and Quantitative Functionalization of Gold Nanoparticles with Thiolated DNA under Physiological pH and Its Application in Molecular Beacon-Based Biosensor. *ACS Appl Mater Interfaces*. 2016;8(40):27298–304.
15. Ding Q, Qiu W, Sun C, Ren H, Liu G. Comparison of DNA–Gold Nanoparticle Conjugation Methods: Application in Lateral Flow Nucleic Acid Biosensors. *Molecules*. 2023;28(11):4480.

16. Mekuye B, Abera B. Nanomaterials: An overview of synthesis, classification, characterization, and applications. *Nano Select*. 2023;4(8):486–501.
17. Ma X, Li X, Luo G, Jiao J. DNA-functionalized gold nanoparticles: Modification, characterization, and biomedical applications. *Front Chem*. 2022;10.
18. Wang T, Chen L, Chikkanna A, Chen S, Brusius I, Sbuh N, *et al.* Development of nucleic acid aptamer-based lateral flow assays: A robust platform for cost-effective point-of-care diagnosis. *Theranostics*. 2021;11(11):5174.
19. NanoComposix. Lateral Flow Assay Development Guide. *nanoComposix*. 2016;1–37.
20. Sangwan S, Seth R. Synthesis, Characterization and Stability of Gold Nanoparticles (AuNPs) in Different Buffer Systems. *J Clust Sci*. 2022;33(2):749–64.
21. Komarova N, Kuznetsov A. Inside the black box: What makes Selex better? *Molecules*. 2019;24(19):3598.
22. Qi S, Duan N, Khan IM, Dong X, Zhang Y, Wu S, *et al.* Strategies to manipulate the performance of aptamers in SELEX, post-SELEX and microenvironment. *Biotechnol Adv*. 2022;55.
23. Kohlberger M, Gadermaier G. SELEX: Critical factors and optimization strategies for successful aptamer selection. *Biotechnol Appl Biochem*. 2022;69(5):1771.
24. Schindler P, Robinson RA, Bates RG. Solubility of tris(hydroxymethyl)aminomethane in water-methanol solvent mixtures and medium effects in the dissociation of the protonated base. *J Res Natl Bur Stand A Phys Chem*. 1968;72A(2):141.
25. Li M, Lin YC, Wu CC, Liu HS. Enhancing the efficiency of a PCR using gold nanoparticles. *Nucleic Acids Res*. 2005;33(21):e184.
26. Liu B, Liu J. Methods for preparing DNA-functionalized gold nanoparticles, a key reagent of bioanalytical chemistry. *Analytical Methods*. 2017;9(18):2633–43.
27. Choi DY, Kim S, Oh JW, Nam JM. Conjugation strategies of DNA to gold nanoparticles. *Bull Korean Chem Soc*. 2022;43(12):1298–306.
28. Sarah J. Hurst Abigail K. R. Lytton-Jean and CAM. Maximizing DNA Loading on a Range of Gold Nanoparticle Sizes. *Mol Cell Biochem*. 2012;23(1):1–7.
29. Bhatt N, Huang PJJ, Dave N, Liu J. Dissociation and degradation of thiol-modified DNA on gold nanoparticles in aqueous and organic solvents. *Langmuir*. 2011;27(10):6132–7.
30. Rivas L, De La Escosura-Muñiz A, Serrano L, Altet L, Francino O, Sánchez A, *et al.* Triple lines gold nanoparticle-based lateral flow for enhanced and simultaneous Leishmania DNA detection and endogenous control Triple lines gold nanoparticle-based lateral flow for enhanced and simultaneous Leishmania DNA detection and endogenous control. *Nano Res,*. 2015;8;3704–3714.
31. Parolo C, de la Escosura-Muñiz A, Polo E, Grazú V, de la Fuente JM, Merkoçi A. Design, preparation, and evaluation of a fixed-orientation antibody/gold-nanoparticle conjugate as an immunosensing label. *ACS Appl Mater Interfaces*. 2013;5(21):10753–9.

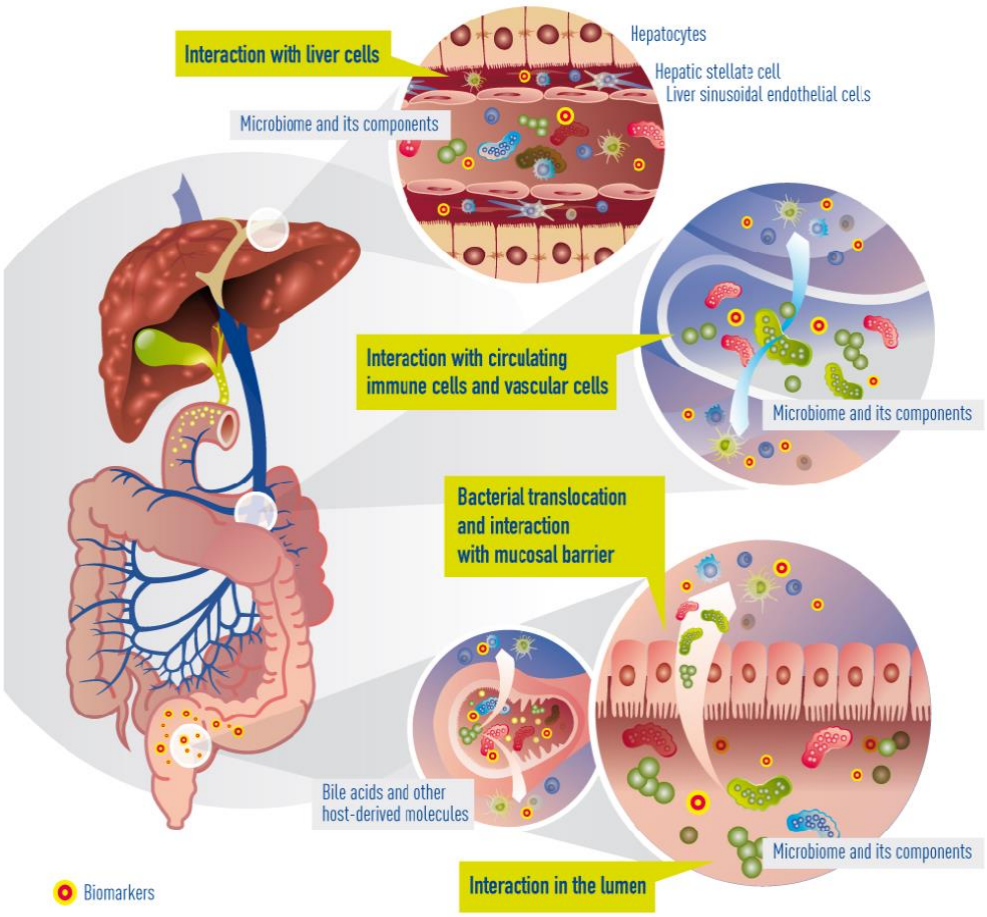
32. Chen A, Yang S. Replacing antibodies with aptamers in lateral flow immunoassay. *Biosens Bioelectron*. 2015;71:230–42.
33. Morales MA, Halpern JM. Guide to Selecting a Biorecognition Element for Biosensors. *Bioconjug Chem*. 2018;29(10):3231–9.
34. Keefe AD, Cload ST. SELEX with modified nucleotides. *Curr Opin Chem Biol*. 2008;12(4):448–56.
35. Turkevich J, Cooper P, Hillier J. A study of the nucleation and growth processes in the synthesis of colloidal gold. *Discuss Faraday Soc*. 1951;11:55–75.
36. Hoa T. Phan AJH. What does nanoparticle stabiity mean? *Physiol Behav*. 2017;176(1):100–106.
37. Seferos DS, Prigodich AE, Giljohann DA, Patel PC, Mirkin CA. Polyvalent DNA-Nanoparticle Conjugates Stabilize Nucleic Acids. *Spherical Nucleic Acids: Volume 1*. 2021;1:425–35.
38. Cárdenas M, Barauskas J, Schullén K, Brennan JL, Brust M, Nylander T. Thiol-specific and nonspecific interactions between DNA and gold nanoparticles. *Langmuir*. 2006;22(7):3294–9.
39. Li H, Rothberg LJ. Label-free colorimetric detection of specific sequences in genomic DNA amplified by the polymerase chain reaction. *J Am Chem Soc*. 2004;126(35):10958–61.
40. Pcr A, Assay A, Linked E, Assay A, Assay A bead A, Resonance SP. Binding assays and Truncation studies. :2–41.
41. Parolo C, Sena-Torralba A, Bergua JF, Calucho E, Fuentes-Chust C, Hu L, *et al.* Tutorial: design and fabrication of nanoparticle-based lateral-flow immunoassays. *Nature Protocols 2020 15:12*. 2020;15(12):3788–816.
42. Schüling T, Eilers A, Scheper T, Walter J. Aptamer-based lateral flow assays. *AIMS Bioeng*. 2018;5(2):78–102.
43. Rivas L, de la Escosura-Muñiz A, Pons J, Merkoçi A. Lateral Flow Biosensors Based on Gold Nanoparticles. Vol. 66, Comprehensive Analytical Chemistry. 2014. 569–605 p.
44. Fang WN, Fan CH, Liu HJ. Effect of pH on the stability of DNA origami. *Acta Polymerica Sinica*. 2017;(12):1993–2000.
45. Hassan AHA, Bergua JF, Morales-Narváez E, Mekoçi A. Validity of a single antibody-based lateral flow immunoassay depending on graphene oxide for highly sensitive determination of E. coli O157:H7 in minced beef and river water. *Food Chem*. 2019;297:124965.
46. Gao Y, Zhu Z, Xi X, Cao T, Wen W, Zhang X, *et al.* An aptamer-based hook-effect-recognizable three-line lateral flow biosensor for rapid detection of thrombin. *Biosens Bioelectron*. 2019;133(January):177–82.
47. Rey EG, O'Dell D, Mehta S, Erickson D. Mitigating the Hook Effect in Lateral Flow Sandwich Immunoassays Using Real-Time Reaction Kinetics. *Anal Chem*. 2017;89(9):5095–100.
48. Quesada-González D, Merkoçi A. Nanoparticle-based lateral flow biosensors. *Biosens Bioelectron*. 2015;73:47–63.

49. Nunes Pauli GE, De La Escosura-Muñiz A, Parolo C, Helmuth Bechtold I, Merkoçi A. Lab-in-a-syringe using gold nanoparticles for rapid immunosensing of protein biomarkers. *Lab Chip*. 2015;15(2):399–405.
50. Hasenoehrl C, Alexander CM, Azzarelli NN, Dabrowiak JC. Enhanced detection of gold nanoparticles in agarose gel electrophoresis. *Electrophoresis*. 2012;33(8):1251–4.
51. Liu Q, Zhang W, Chen S, Zhuang Z, Zhang Y, Jiang L, *et al.* SELEX tool: A novel and convenient gel-based diffusion method for monitoring of aptamer-target binding. *J Biol Eng*. 2020;14(1):1–13.
52. Stiles PL, Dieringer JA, Shah NC, Van Duyne RP. Surface-Enhanced Raman Spectroscopy. 2008;1(1):601–26.
53. Englebienne P, Hoonacker A Van, Verhas M. Surface plasmon resonance: principles, methods and applications in biomedical sciences. *Spectroscopy*. 2012;17(2–3):255–73.
54. Bhattacharjee S. DLS and zeta potential - What they are and what they are not? *Journal of Controlled Release*. 2016;235:337–51.
55. Kaszuba M, Corbett J, Watson FMN, Jones A. High-concentration zeta potential measurements using light-scattering techniques. *Philosophical Transactions of the Royal Society A: Mathematical, Physical and Engineering Sciences*. 2010;368(1927):4439–51.

CHAPTER 5. Tailored SELEX Protocols for the Identification of ACLF Biomarker Aptamers

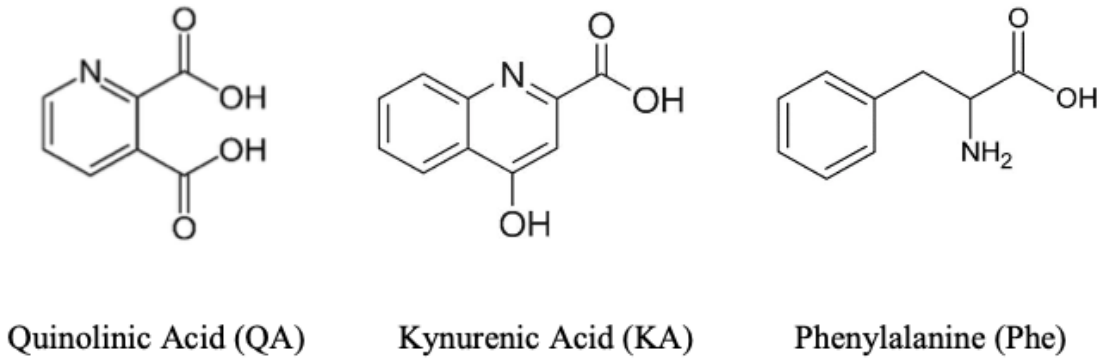
5.1. Acute-on-Chronic Liver Failure Biomarkers.

The MICROB-PREDICT consortium has identified a list of preliminary biomarkers associated with Acute-on-Chronic Liver Failure (ACLF) through extensive clinical studies in metabolomics (Scheme 1).[1–3] These studies have uncovered distinct metabolic profiles in patients with ACLF, highlighting key metabolic pathways involved in the progression of the disease.[4,5] Among the crucial findings, specific biomarkers have been identified, including phenylalanine (Phe) from the short-chain fatty acids pathway and quinolinic and kynurenic acids (QA and KA) from the kynurenine pathway (KP).[6,7] These metabolites serve as potential diagnostic and prognostic markers for ACLF and may also represent therapeutic targets. Therefore, it is of interest to develop biorecognition elements against these molecules that can be later implemented in Point-of-Care (PoC) tests for early ACLF diagnosis and monitoring.[8]



Scheme 1: Currently known and suggested gut-liver interactions in cirrhosis. Impaired epithelial barrier ("leaky gut") allows bacteria or bacterial products (metabolites) to translocate into the blood circulation and reach the liver. There, they interact with circulating and resident immune cells and liver cells. Concomitantly, bile acids and other molecules (e.g., antibacterial peptides) originating from the liver arbitrate between liver and gut microbiota. Available at: https://microb-predict.eu/for-scientists/summary/.

Phe (165.19 g/mol), QA (167.12 g/mol), and KA (189.17 g/mol) are small molecule metabolites endogenously present within the human body (Scheme 3).[9]



Scheme 3: Chemical structure of Phe, QA and KA small molecules.

Phe is classified as an essential amino acid, indispensable for protein synthesis and metabolic processes, as it must be obtained through dietary intake. QA and KA are intrinsic metabolites that function as key intermediates within the KP, a major route for the catabolism of the amino acid tryptophan (Trp). Due to their inherent non-immunogenic nature, Phe, QA, and KA do not elicit a robust immune response, making the generation of specific antibodies against these small molecules particularly challenging.[10] In light of this challenge, the Systematic Evolution of Ligands by Exponential Enrichment (SELEX) technique emerges as a promising avenue for overcoming these limitations. SELEX offers a viable and effective strategy for the generation of high-affinity nucleic acid aptamers capable of selectively binding to target molecules, irrespective of their size or immunogenicity.[11–13]

5.1.1. Systematic Evolution of Ligands by Exponential Enrichment for Small Molecule biomarkers.

There are several reported SELEX variations that are recommended for small molecule targets, some of which include the possibility of multiplexed selection. Graphene Oxide (GO)-SELEX is a viable option and has been applied to proteins and small molecules, Nguyen *et al*. developed a multiplexed GO-SELEX strategy that successfully screened for aptamers against three pesticides with affinities in the range of 10-100 nM.[14] However, GO-SELEX has some drawbacks in terms of efficiency and reproducibility, resulting in non-binding single stranded DNA (ssDNA) sequences being passed from round to round, and it optimally works against positively charged molecules.[15,16]

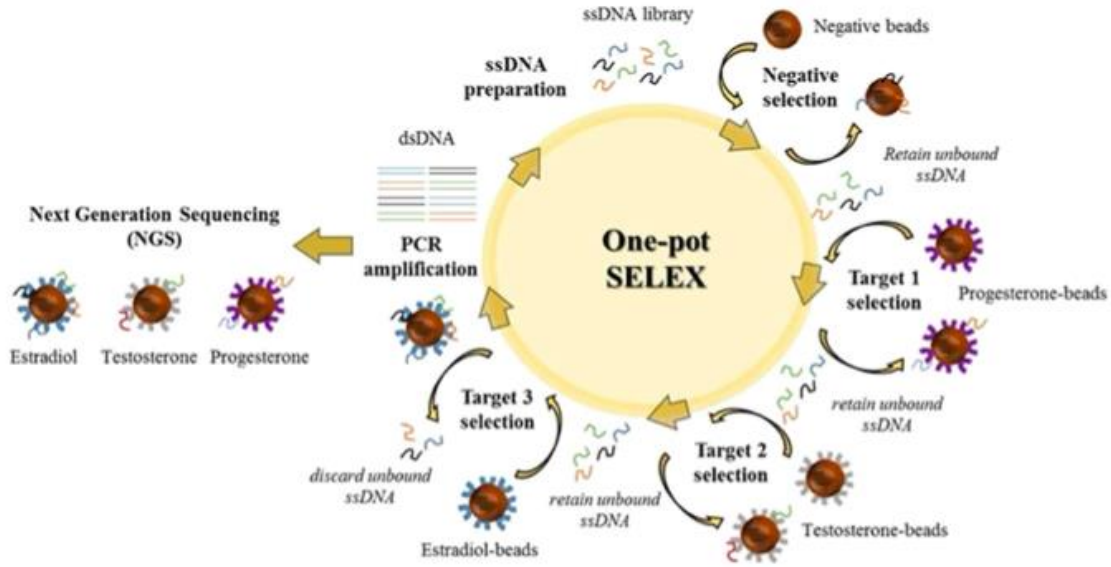
Capture-SELEX can be made suitable for small molecules by immobilizing the library and therefore avoiding the loss of epitopes due to the immobilization of the target.[17,18] Capture-SELEX has been

successfully developed for aptamers against many small molecules, such as pesticides, herbicides, antibiotics, hormones, or toxins.[11,19,20] Several Capture-SELEX strategies have been tested for multiple targets, showcasing the flexibility and utility of this approach in aptamer selection. For instance, Lauridsen *et al*. described a multiplexed Capture-SELEX that selected RNA aptamers against small molecules like rebaudioside A and carminic acid.[21] Another study applied a multiplexed Capture-SELEX scheme to identify RNA aptamers for quinine, caffeine, and guanine from RNA scaffolds contained in naturally occurring cellular riboswitches for its later use in a cellular environment.[22,23] These examples highlight the method's ability to meet the requirements of the selection process by avoiding ligand immobilization while efficiently targeting multiple molecules simultaneously. However, there are reported limitations regarding the undocking of the immobilized sequences, which can lead to the loss of highly specific aptamers during the process.[24]

Another strategy involves using a small molecule as a hapten, conjugating it to a molecule of a larger size, to create a larger structural molecule with more epitopes, which widens the SELEX strategy options, but often results in low affinity aptamers with low specificity.[25] This is the case of Yang *et al*, who developed Capture-SELEX to isolate aptamers against Phe amino acid conjugated to an nonspecific organometallic receptor, penta- methylcyclopentadienyl rhodium(III) (Cp*Rh(III)) complex, to create a high-epitope complex.[26]

Mag-SELEX employs magnetic beads as a partition strategy with high efficiency, but in the case of small molecule targets, immobilization of the target covers at least one epitope.[27,2829] However, there are many examples of Mag-SELEX techniques and variations that included immobilizing of small molecules to the beads that successfully isolated aptamers with low dissociation constants.[30] Mag-SELEX enables specific and directional immobilization of the targets, along with improved control of counter-selection steps. Besides, it allows negative selection, further increasing the specificity of the obtained pools.[31,32]

One-Pot SELEX has emerged as a particularly effective strategy for dealing with multiple targets simultaneously.[33,34] In this process, the library is sequentially exposed to target-conjugated magnetic beads for multiple rounds, those final sequences that bind to the three target molecules, are isolated and individually amplified (Scheme 6). These resultant sub-libraries are then examined to identify aptamer candidates with specificity to only one of the targets. This is achieved by identifying sequences that are highly represented in only one of the pools.[35,36] However, this entails preferential isolation of one of the targets over the others, which can lead to the loss of sensitive sequence pools for the “secondary” targets.



Scheme 6: Schematic representation of the One-Pot SELEX strategy, against three small molecule targets. Reprinted with permission from Jauset-Rubio M. et al., One-Pot SELEX: Identification of Specific Aptamers against Diverse Steroid Targets in One Selection. ***ACS Omega, 4,*** *20188−20196 (2019).*

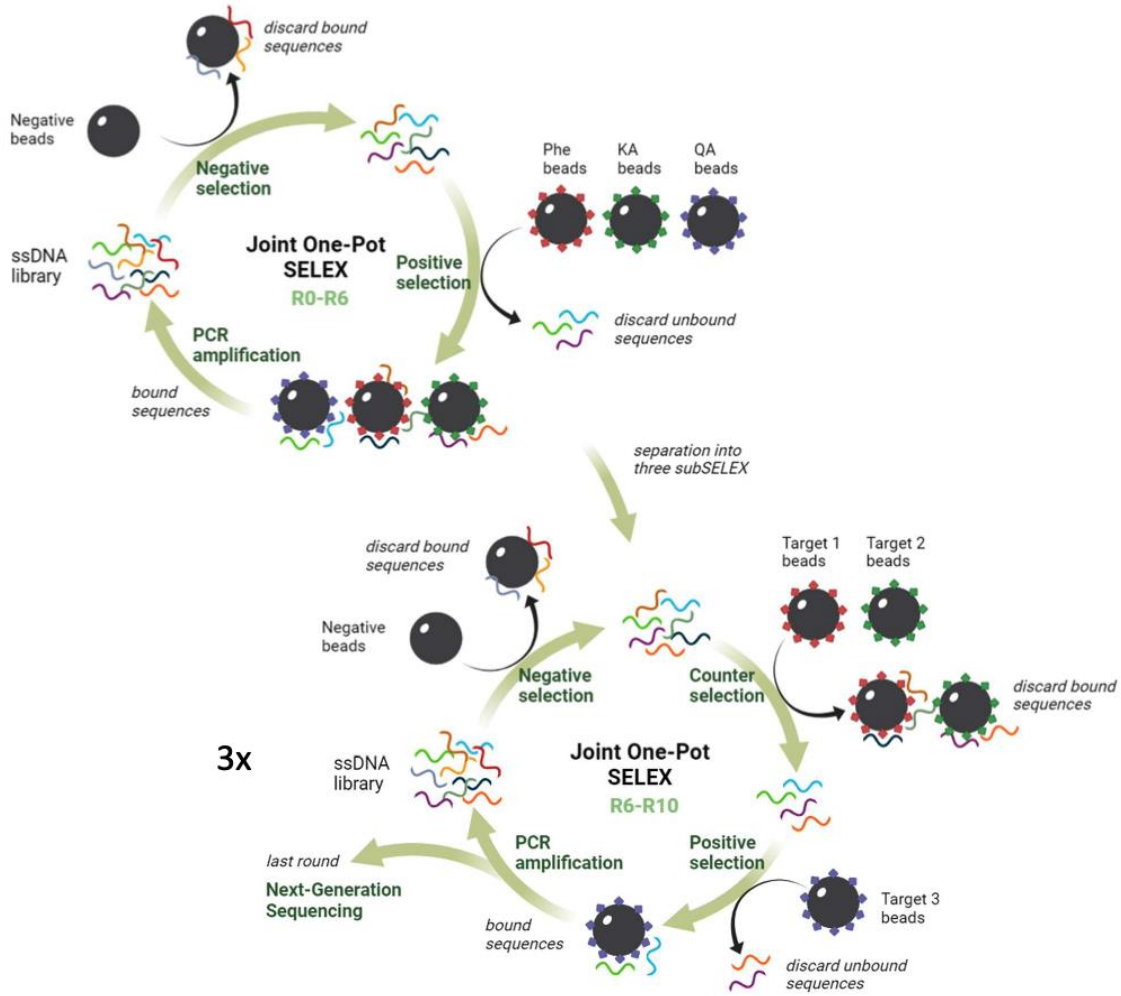
The field of SELEX provides diverse methodologies tailored for the selection of aptamers targeting small molecules. Moreover, advancements in multiplexed SELEX methodologies offer increasingly sophisticated strategies, allowing researchers to customize selection protocols according to their specific experimental needs and desired aptamer characteristics.[37,38] Therefore, we aim to tailor and develop a SELEX strategy to isolate multiple ACLF small molecule biomarkers equally.

5.1.2. Strategy for Multiplexed Aptamer Selection

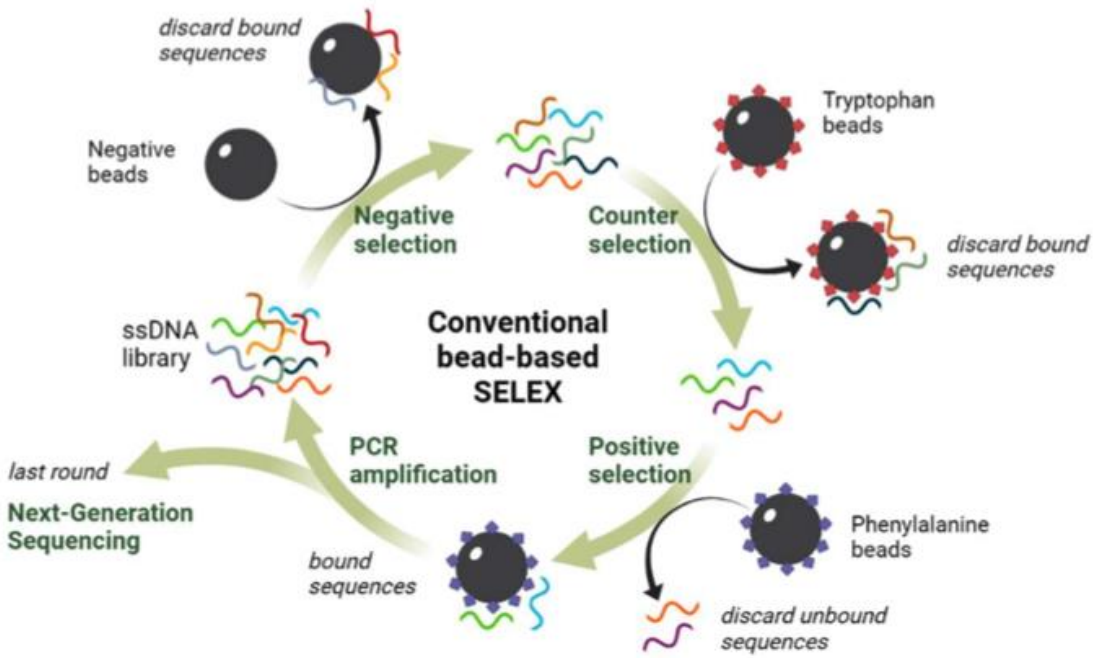
This work proposes a variation of the One-Pot SELEX technique, which includes the simultaneous incubation of the three targets (KA, QA, and Phe) instead of sequential counter-selection steps (Scheme 7). This is aimed at obtaining aptamers for all three targets equally without discarding potential binders. In the later stages of the SELEX process, the three targets are no longer incubated together. They undergo parallel SELEX processes, using the other two remaining target molecules simultaneously as counter-selection targets. This strategy was called “Joint-One-Pot SELEX” due to the inspiration from the One-Pot technique and due to the concurrent selection against three targets in the positive incubation in a single step, and the simultaneity of two targets in their counter-selection step.

In addition, a conventional SELEX will be conducted but only against one of the targets (Phe), with a later Trp counter-selection step as a proof-of-concept to study the effectiveness of simultaneous incubation versus individual selection (Scheme 8). This decision is also influenced by the existence of previously reported aptamers against Phe. The conventional SELEX approach has been chosen to

serve as a reference for comparing the effectiveness of the novel SELEX methodology and as a supplementary method to ensure the successful isolation of aptamers targeting Phe. This approach has been selected due to its well-documented success and reliability in existing literature.[37,39]

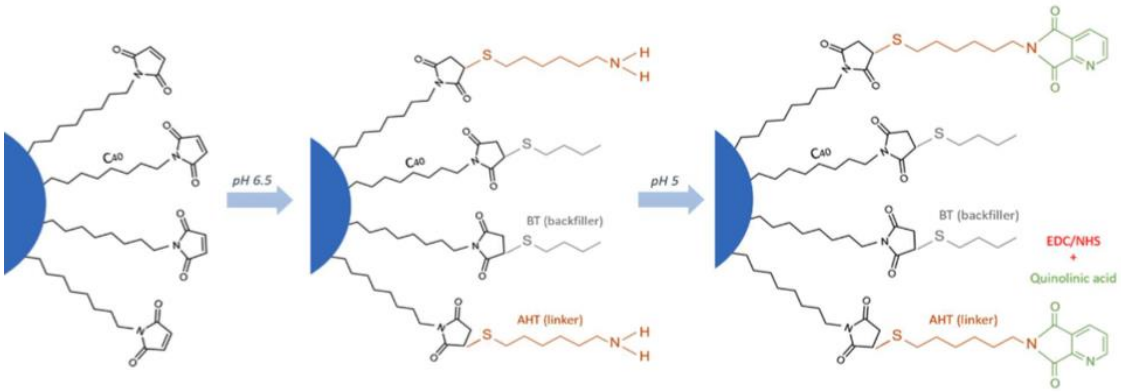


Scheme 7: Schematic representation of the Joint One-Pot SELEX strategy. During initial rounds (R0-R6, top), simultaneous positive selection of the three targets is performed. During later stages (R6-R10, bottom), the SELEX process is divided into three, introducing simultaneous counter selection with two targets, in each of the three branches (3x). Created with Biorender.



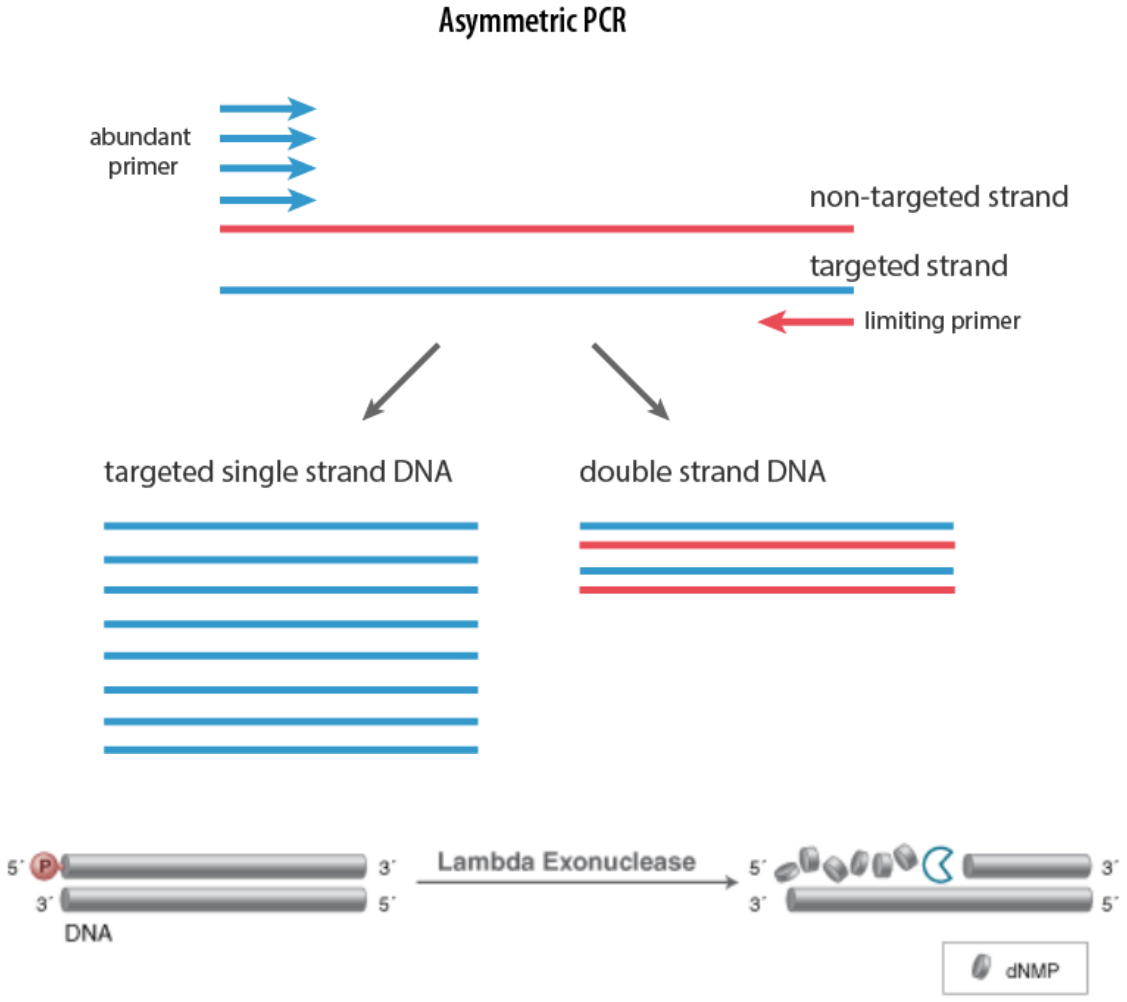
Scheme 8: Schematic representation of the conventional SELEX strategy against Phe, using Trp as a counter selection target. Created with Biorender.

Magnetic beads will be employed as a partitioning strategy by immobilizing the three targets, the Trp counter molecule of the conventional SELEX, and as negative selection. This technique is well-documented, offers high partitioning efficiency, is versatile in terms of immobilization strategies, and has been previously utilized with other small molecule targets. In this case, Maleimide Magnetic beads were chosen for conjugation through click chemistry with the carboxylic acid group of the three targets and counter (Scheme 9), and conjugations were verified using bead-based Enzyme-Linked Immuno Sorbent Assay (ELISA).[40]



Scheme 9: Schematic representation of the click chemistry conjugation process. QA acid was set as an example. The same process was followed for all targets. Created with Biorender.

For ssDNA regeneration, a comprehensive approach that includes Pilot Polymerase Chain Reaction (Pilot PCR), Asymmetric PCR (A-PCR) (Scheme 10, top), λ-exonuclease digestion (Scheme 10, bottom), and spin column purification will be employed. This method ensures the accurate amplification of target ssDNA through initial Pilot PCR using different numbers of cycles to determine optimal amplification, followed by the production of ssDNA via A-PCR using phosphorylated primers.[41–43] Subsequent λ-exonuclease digestion is used to efficiently remove complementary strands, and spin column purification is utilized to obtain a high-purity ssDNA product, optimizing the regeneration process for subsequent SELEX rounds.



Scheme 10: Schematic representation of A-PCR principle (top) and) λ-Exonuclease digestion principle, after addition of modified primers through PCR reaction using reverse primer with 5´ phosphorylation modification (red dot) (bottom). Available at: https://www.neb.com/en/products/m0262-lambda-exonuclease.

ssDNA quantification was conducted using a nanodrop spectrophotometer at the conclusion of each round to track the enrichment of the pools.[25,44] The SELEX rounds had to be halted at Round 10 (R10) following a human error during sample purification. Due to time constraints, NGS and analysis

took priority for gaining a deeper understanding of the process. Given more time, additional rounds would have been carried out before sending the samples for NGS, and binding assays using aptamer candidates from both SELEX processes would have been performed.

5.2. Objectives

In this chapter, the primary aim was to tailor and develop SELEX processes for identifying aptamers that target small molecule biomarkers associated with ACLF. To achieve this, two distinct SELEX methodologies were developed concurrently.

Firstly, a conventional SELEX process using maleimide magnetic beads conjugated to Phe as the target molecule was developed. Trp was used as a counter-selection target to enhance the specificity of the aptamers for Phe. Multiple rounds of SELEX were conducted to enrich the pool of aptamers specific to Phe.

Simultaneously, a novel SELEX variation, termed "Joint One-Pot SELEX" was investigated. This process involves the simultaneous incubation of three ACLF-related targets during the initial SELEX rounds. After several rounds, the process was divided into three parallel SELEX streams, each focused on one of the three targets. In each of these parallel SELEX processes, the remaining two targets served as counter-selection targets to improve the selection for specificity and reduce cross-reactivity.

To address the limitations of the number of SELEX rounds that could be performed due to time constraints, and the low enrichment levels obtained, NGS analysis was employed. Custom-developed MATLAB code facilitated an in-depth analysis of a larger number of sequences, allowing for comprehensive sequence comparison within rounds of the same SELEX process and between the parallel branches of the "Joint One-Pot SELEX". Validation of the efficacy of the MATLAB code in identifying potential aptamer candidates at earlier rounds than in other methods should form the basis of future work as it could potentially accelerate the aptamer selection process.

In summary, this thesis chapter aims to advance the field of aptamer development for multiple small molecule ACLF biomarkers, providing valuable insights and methodologies that could be applied to other multiplexed SELEX processes in the future.

5.3. Materials and Methods

5.3.1. Materials

The ssDNA library used in this work consists of 10^{30} randomized 94 nt-long sequences purchased from Ella Biotech (Germany). All sequences are composed of the same structure, containing a random central region of 50 nucleotides flanked by fixed primer binding regions: 5′-AGCTCCAGAAGATAAATTACAGG-nt(50)-CAACTAGGATACTATGACCCC-3′. The library has a molecular weight of 29885 g/mol and was brought to a concentration of 100 μM. PCR was performed using library-specific primers, with a 23 nt-long forward primer (5'-AGCTCCAGAAGATAAATTACAGG-3') and a 21 nt-long 5'-phosphorilated reverse primer (5'-phosphate-GGGGTCATAGTATCCTAGTTG-3'). Both oligonucleotides were synthesized and purchased from LGC Biosearch Technologies (Denmark).

PureCube Maleimide Activated MagBeads (25 μm) were purchased from Cube Biotech (Germany). QA, KA, Phe and Trp molecules, HRP-conjugated goat anti-rabbit pAb, 6-Amino-1-hexanethiol hydrochloride (AHT), 1-butanethiol (BT), Phosphate buffer saline (PBS) tablets, magnesium chloride ($MgCl_2$), Tween-20, polyethylene glycol 400 (PEG400), 3,3',5,5'-tetramethylbenzidine (TMB), sulfuric acid (H_2SO_4), agarose, ethanol, N-hydroxysuccinimide (NHS), 2-Morpholinoethanesulfonic acid hydrate (MES), Tris-Borate-EDTA (TBE) buffer 10X, and dry skim milk were purchased from Merck (Germany). 1X PlatinumTM II Taq Hot Start Polymerase, 10X λ exonuclease, 96-wells transparent microplates, GeneRuler Ultra Low Range DNA Ladder, SYBRTM Gold Nucleic Acid Gel Stain, TriTrack DNA Loading Dye, sulfo-NHS-acetate, and 1-ethyl-3-(3-dimethylaminopropyl) carbodiimide (EDC) were purchased from Thermo Fisher Scientific (US). GelGreen® Nucleic Acid Gel Stain was purchased from Biotium (US). Rabbit anti-quinolicic acid antibody and rabbit anti-KA antibody were purchased from Abcam (Netherlands). Rabbit anti-Phe antibody and rabbit anti-Trp acid antibody were purchased from Immusmol (France). Mini 10 Horizontal Electrophoresis kit and accessories were purchased from VWR (US), InGenius 3 Gel Doc System transilluminator from Syngene (UK), Oligo Clean & Concentrator kit was purchased from Zymo Research (US)

5.3.2. Methods

5.3.2.1. Target immobilization

Maleimide-coated Magnetic beads were selected for conjugation with the target molecules using click chemistry. Seven independent conjugations were conducted, including KA, QA, Trp, and two Phe conjugations, as well as two negative controls achieved by omitting the target conjugation step.

Each conjugation process involved placing 100 µL of beads in a microcentrifuge tube and washing them three times with 500 µL of 10 mM PBS (pH 6.5 – 7). Subsequently, 100 µL of 5.89 mM AHT in 10 mM PBS (pH 6.5 – 7) was added to the beads, followed by brief vortexing and a 2-hour incubation period. The supernatant was then removed, and AHT-modified beads were mixed with 100 µL of 100 mM BT in 10 mM PBS (pH 6.5 – 7) and incubated for another 2 hours. In the case of the target conjugation, the supernatant after AHT/BT conjugation was discarded, and the beads were incubated for 2 hours with 50 µL of 10 mM of its respective target in 0.1M MES buffer (pH 5.0), together with 50 µL of 644.14 mM EDC and 50 µL of 868.9 mM NHS in 0.1M MES buffer (pH 5.0). Finally, the beads were blocked by adding 100 µL of 10mM sulfo-NHS-acetate in PBS (pH 7.5) and incubating for 1 hour. All incubation steps were carried out using a tube rotator at room temperature and under dark conditions. The magnetic beads were washed three times with the buffer of each coupling step before and after the incubation to resuspend them and to remove remnants of uncoupled molecules, respectively. A magnetic stand was utilized to allow the magnetic beads to separate in order to remove the supernatant. The concentration and ratios of all reagents are listed in Table 1.

Table 1: Reagent ratios used for Maleimide magnetic beads conjugation with all target molecules.

Reagent:	**Target**	**Linker (AHT)**	**Backfiller (BT)**	**Sulfo-NHS-acetate**	**EDC : NHS**
Ratio:	1.7	1	380	1.85	40.64 : 54.8

5.3.2.2. Target verification

The method utilized for target conjugation was validated through bead-based ELISA. For the QA and KA-conjugated beads, 2 µL of beads were carefully transferred into microcentrifuge tubes and then washed three times with 200 µL of 10mM PBS with 0.1% Tween-20 (PBST) at pH 7.4. Following this, the beads were incubated with 200 µL of 2% dry skim milk (w/v) in PBST for 30 minutes. Subsequently, 50 µL of anti-target rabbit polyclonal antibody were added to the respective target-conjugated beads and incubated for 1 hour. The entire process was then repeated for Phe and Trp-conjugated beads, with PEG400 used instead of dry skimmed milk. All incubations were conducted at room temperature, on a tube rotator, and under dark conditions. After each incubation, the beads were meticulously washed 5 times with 200 µL of PBST to ensure the removal of any remaining residues. Negative beads underwent the same process as a means of serving as the negative control, and three replicates were performed for statistical significance. Subsequently, 50 µL of TMB were added to all tubes and incubated at room temperature for 5 – 10 minutes. The color development was allowed to generate as long as no significant color was observed in the negative control beads. The enzymatic reaction was stopped with 50 µL of 1 M H_2SO_4, resulting in a color shift to yellow.

The supernatant of each tube was then transferred to a 96-well microplate and the absorbance was measured using a plate reader (SpectraMax iD3, Molecular Devices, CA, USA) at 450 nm. The mean and standard deviation were obtained for each bead type from the three replicates.

5.3.2.3. Selection Conditions and Round Progress

Stringency conditions were carefully designed for both SELEX methodologies. Concentration of target, incubation times, and washing steps repetition and length were modified as the SELEX process evolves and as it is defined in Tables 2a and 2b. The binding buffer was defined as 10 mM PBS, 1.5 mM $MgCl_2$ at pH 6.4, and the temperature was kept constant at 23ºC during all the SELEX rounds.

Initial denaturation and renaturation of the 3 μM oligo library diluted in BB is performed at 95ºC and cooled down to room temperature (VeritiTM 96-Well Fast Thermal Cycler, Thermo FisherScientific, USA) so sequences are able to fold into their various 3D structures. An initial volume of 100uL of 3 μM library enters the first round of SELEX (in this case, R0), and the obtained volume at the end of the round is brought up to 100uL before entering the following round.

For both SELEX strategies, Round 0 (R0) is performed with only positive selection, using Phe as positive for conventional SELEX, and the three targets together as positive selection for the Joint-One-Pot SELEX. Negative selection using negative conjugated magnetic beads was implemented from Round 1 (R1) and onwards for both strategies. Negative selection is performed before the positive selection step. Therefore, it is the supernatant of the negative selection that is going to be sequentially incubated with the positive beads. Rounds 2 and 3 were performed similarly for both SELEX strategies, with the sole modification of increased washing steps, as depicted in Tables 2, in order to gradually increase the stringency conditions.

At Round 4 (R4), Trp counter selection is introduced for conventional SELEX, which is performed between the negative and positive selection steps. From rounds 5 to 9, conventional SELEX was performed similarly to R4, with gradual increases of stringency, as depicted in blue in Tables 2a and 2b.

Regarding Joint-one-pot SELEX, negative and positive selection of the three simultaneous targets is kept similar until Round 7 (R7), except for the same gradual increases in stringency conditions as in conventional SELEX. In R7, the three targets are no longer incubated simultaneously. First, negative selection is performed, and the supernatant is divided into the three different counter selection solutions containing a combination of two of the three targets each. After the counter incubation time, each supernatant is transferred to the positive selection solution, containing the remaining target. This results in three individual SELEX processes. This procedure is then repeated for rounds 8 and 9 (R8 and R9).

Tables 2a and 2b: Detailed selection conditions used for each round for both SELEX. In grey, highlighting the changes of stringency in respect to the previous round.

Joint One-Pot-SELEX		R0	R1	R2	R3	R4	R5	R6	R7	R8-10
Volume of Library (uL)		100	100	100	100	100	100	100	100	100
Volume of beads (uL)	Negative		3	3	3	3	6	6	6	6
	Counter								1	3
	Positive	3	3	3	3	3	3	3	1	3
Incubation time (h)	Negative		2	2	2	2	2	2	2	2
	Counter								2	3
	Positive	2	2	2	2	2	2	2	2	1
Buffer		BB	BB	BB	BB	BB	BB	BB	BB	BB
Washing steps (repetions with 100uL)		3	3	2	2	2	3	5	3	3
Vortex time (s)		3	3	3x3	9	9	9	9	9	9

Conventional SELEX		R0	R1	R2	R3	R4	R5	R6	R7	R8-10
Volume of Library (uL)		100	100	100	100	100	100	100	100	100
Volume of beads (uL)	Negative		3	3	3	3	6	6	6	6
	Counter					3	3	3	3	3
	Positive	3	3	3	3	3	3	3	3	3
Incubation time (h)	Negative		2	2	2	2	2	2	2	2
	Counter					2	2	2	2	3
	Positive	2	2	2	2	2	2	2	2	1
Buffer		BB	BB	BB	BB	BB	BB	BB	BB	BB
Washing steps (repetions with 100uL)		3	3	2	2	2	3	5	3	3
Vortex time (s)		3	3	3x3	9	9	9	9	9	9

5.3.2.4. Library amplification and conditioning

After the incubations of each round, the negative, counter, and positive selection beads with binding sequences are subjected to Pilot PCR directly, given that the high temperature of the PCR process separates the sequences from the beads by denaturation, therefore being able to undergo PCR.
90 µL of PCR master mix (0.4 µM forward primer, 0.4 µM reverse 5'-phosphorylated primer) are mixed with 10 µL of each bead suspension and divided into four PCR tubes, 25 µL each, for amplification with different PCR cycles (5−25). The thermocycler program was set to perform an initial denaturation for 5 min at 95ºC, followed by 5 to 25 repetitions of 30s at 95ºC, 30s at 55ºC, and 30s at 72ºC, as well as a final elongation step of 5 min at 72ºC. The quantity and quality of all bead suspensions after different cycles of PCR amplification were visualized by gel electrophoresis, loading 1 µL of the sample with 1 µL TriTrack DNA Loading Dye into 3% (w/v) non-denaturing agarose gels.

The amplified products obtained from the Pilot PCR were utilized as a template for an A-PCR after identifying the optimal number of PCR cycles from the Pilot PCR. For the A-PCR, 10 µL of the selected amplified product from the pilot PCR was combined with 90 µL of A-PCR master mix (0.39 µM forward primer). The amplification conditions were modified from the Pilot-PCR program by extending the annealing and extension times to 1 minute 30 seconds. Results of the A-PCR are visualized by electrophoresis gel following the same protocol. After A-PCR amplification, 10X λ exonuclease reaction buffer was added to each tube to achieve a final concentration of 1X. Subsequently, all tubes were incubated with 0.1U of λ (10 U/µL) at 37°C for 5 minutes, followed by heat deactivation at 80°C for 15 minutes. The resulting product was then assessed using gel electrophoresis, specifically in 4% (w/v) non-denaturing agarose gels.

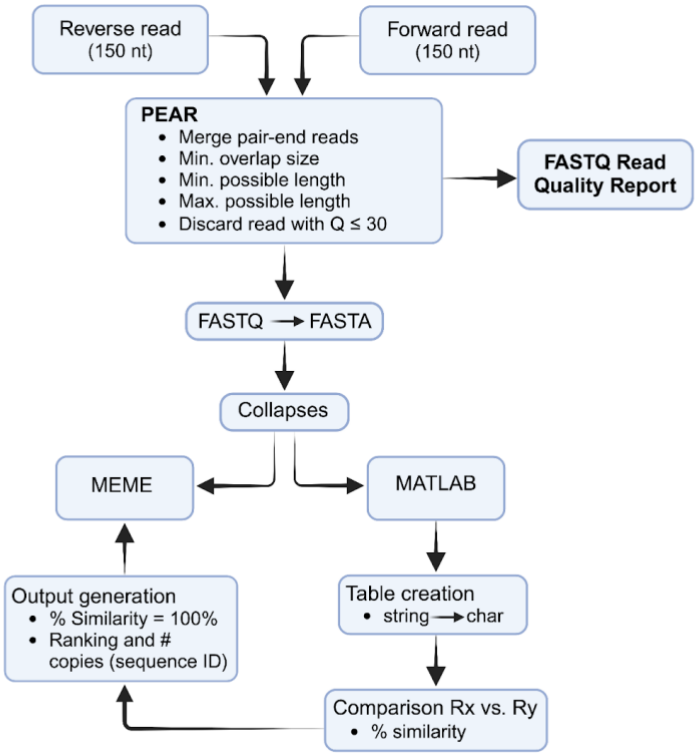
Following λ digestion, the generated ssDNA was purified using the Oligo Clean & Concentrator kit through spin column purification. To achieve this, 200 µL of Oligo Binding Buffer and 400 µL of ethanol (95-100%) were added to 100 µL of the sample, and the mixture was thoroughly mixed by pipetting. The solution was transferred to a Zymo-SpinTM IC Column, placed in a collection tube, and centrifuged to discard the flow-through. 750 µL of DNA Wash Buffer was added to the column and centrifuged twice to ensure complete removal of the buffer. To elute the purified ssDNA, the column was transferred into a sterile nuclease-free tube, and 15 µL of nuclease-free water were added to the column and then centrifuged at 14,000 rpm (17530 g) for 30 seconds. The eluted samples were collected, stored in PCR tubes at 4ºC, and validated by gel electrophoresis, in 4% (w/v) non-denaturing agarose gels.

The gels were run at 120V in 1X TBE buffer for 40 minutes and 50 minutes for the 3% and 4% gels, respectively. ssDNA quantification was carried out using a Nanodrop 2000c UV-vis

spectrophotometer, measuring the absorbance at 260 nm with the extinction coefficient set to 33 µg/mL for ssDNA, and 50 µg/mL for dsDNA.

5.3.2.5. Next Generation Sequencing

Aliquots from rounds R3, R4, R9 and counter R9 from the conventional SELEX and samples R3, R6 R7 (for the three targets) and R9 (for the three targets) were processed, quantified and sequenced by the Servei de Genòmica of the Universitat Autònoma de Barcelona (Spain, uab.cat/ca/servei-genomica). Sequencing was performed on the Illumina MiSeq platform using the MiSeq Reagent Micro Kit v2 (300 cycles) in paired-end mode, generating about 200.000 reads per sample. FASTQ files were obtained for both pair-end reads of each sample. Bioinformatic analysis was performed using Galaxy (usegalaxy.org) and MATLAB ®. The NGS data analysis workflow is the following:



Scheme 11: Schematic illustration of the NGS analysis workflow developed and followed during this study. Created with Biorender.

5.4. Results and Discussion

5.4.1. Target conjugation verification

Bead-based ELISA was performed for the four conjugated molecules, as well as for negative beads as a negative control. To minimize non-specific antibody interactions, two different blocking agents were utilized for QA and KA and for Phe and Trp. Due to the Phe and Trp targets being amino acids, the proteins contained in skimmed milk could create undesired competition. Therefore, 2% PEG400 was utilized, whereas 2% skimmed milk was used as a blocking agent for QA and KA targets, as it is broadly described in ELISA protocols.

Both KA and QA-conjugated beads demonstrated a mean optical density of 0.471±0.03 and 0.420±0.05, respectively, surpassing the values of the negatively conjugated beads, which were measured at 0.226±0.01 (Figure 1, left). Phe and Trp-conjugated beads exhibited higher optical signals compared to their negative controls as well, with mean values of 0.246±0.05 and 0.257±0.06, respectively (Figure 1, right). This confirmed the successful conjugation of all targets.

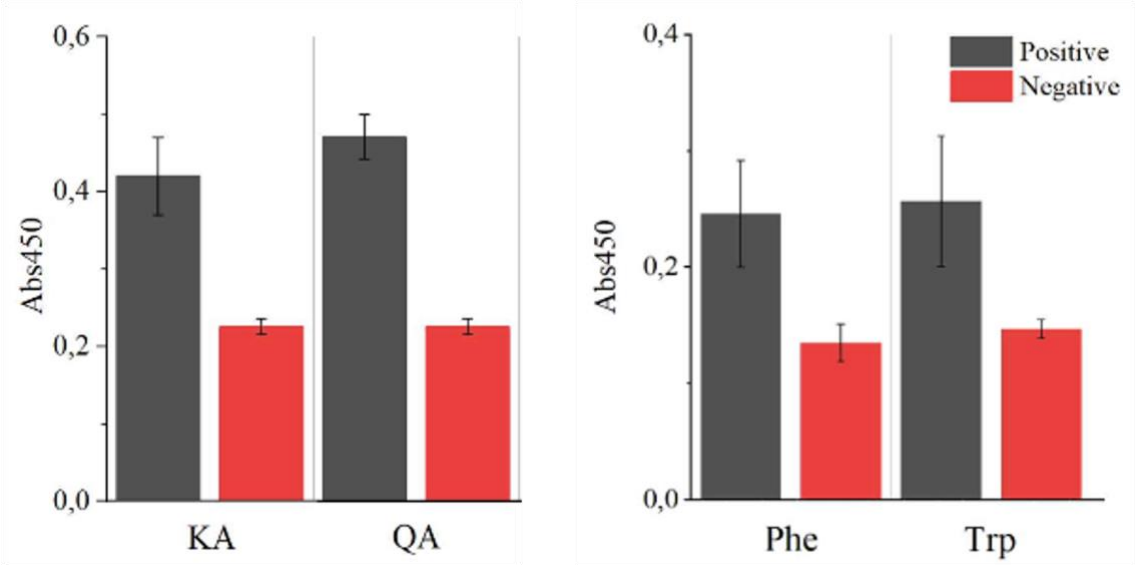


Figure 1: Average A_{450} results for positive (black) and negative (red) conjugated beads for the three target (KA, QA and Phe) and counter (Trp) molecules. Standard deviation was calculated from triplicates.

The observation that small molecules conjugated to magnetic beads through click chemistry, ostensibly obstruct the epitope used for conjugation, are still detectable by antibodies during bead-based ELISA for verification of conjugation suggests that the conjugated small molecules are sufficiently accessible to biorecognition elements. It is therefore reasonable to infer that oligonucleotides present in the SELEX library can also access any remaining epitopes of the small molecules during the SELEX process.

5.4.2. SELEX round progression

Only positive selection was implemented in the initial round (R0) to pre-enrich the sample. By not introducing negative selection in this round, a preliminary set of amplified binding sequences is sorted, irrespective of their interaction with the bead matrix or similar targets. This approach prevents the potential loss of sequences with low representation in the starting library. Amplifying these sequences enhances their probability of overcoming negative selection in the subsequent round.
The initial 10 cycles of Pilot PCR for R0 resulted in the highest dsDNA yield for the library. However, at 15 cycles, a longer byproduct started to appear which became more concentrated than the library after 20 rounds of PCR (see Figure 2).

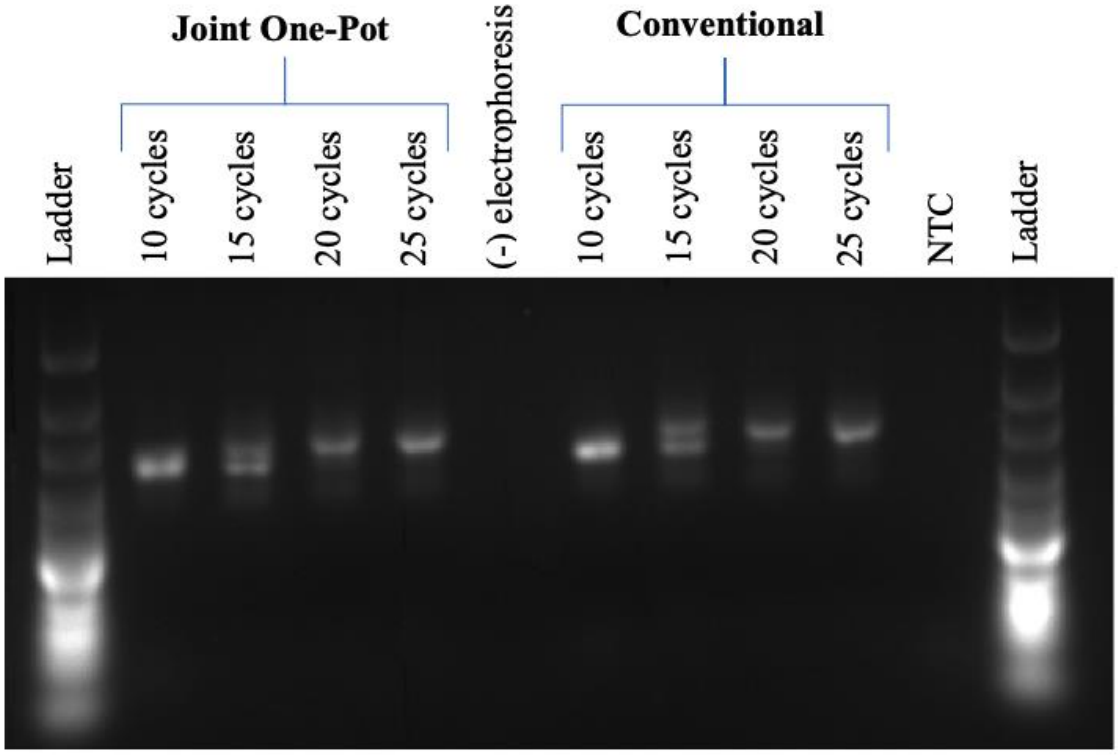


Figure 2: Agarose gel electrophoresis (3% agarose, 120V, 40min, 1X GelGreen pre-stained) of the products generated in the Pilot-PCR in R0, for both SELEX. Non-Template Control (NTC) and electrophoresis control (-) were performed for PCR amplification and electrophoresis, respectively.

This pattern was consistently observed for both SELEX methodologies. So as not to create PCR byproducts, the product generated from 10 cycles for both SELEX experiments was utilized for A-PCR. The appearance of a more migrated band in the agarose gel electrophoresis (Figure 3a), corresponding to ssDNA, confirms the successful generation of ssDNA.

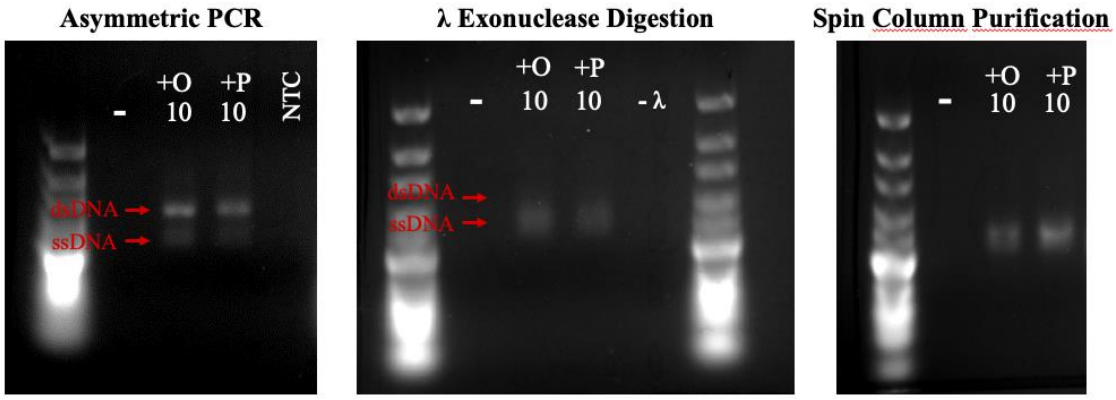


Figure 3: Agarose gel electrophoresis (3% agarose, 120V, 40min, 1X GelGreen pre-stained) of the products generated in A-PCR (left), λ Exonuclease digestion (center) and Spin Column Purification (right) in R0, for both the Joint One-Pot SELEX (+O) and the conventional SELEX (+P). Non-Template Control (NTC), and negative electrophoresis controls (-) were performed at every stage.

Subsequent λ-exonuclease digestion results in the disappearance of the dsDNA band, confirming the success of the digestion, and that the band was from dsDNA, while leaving the ssDNA band undigested (Figure 3, center). The resulting ssDNA library underwent purification using a spin column to prepare it for the next stage. This purification step effectively removed any remnants from previous processes, such as unincorporated nucleotides, enzymes, salts, and magnetic beads. Plus, the intensity of the ssDNA band is stronger, insinuating that it has been concentrated (Figure 3c). A-PCR, λ digestion, and spin column purification were performed between all rounds.

The experimental procedure in R1 involved the integration of a negative selection step before the positive selection. In order to assess the optimal number of cycles, 5, 10, 15, and 20 PCR cycles were tested due to the generation of byproducts in R0 as early as 15 rounds. Subsequently, the Pilot PCR on the positive beads revealed that the highest dsDNA yield for both SELEX experiments was achieved at 20 cycles, with no observed byproducts (see Figure X, left). As a result, the remainder of R1 was conducted using the product generated from 20 pilot PCR cycles. Additionally, the behavior of the negative beads was comparable to that of the positive beads, with the band intensity at 5 PCR cycles appearing to be somewhat greater than that of their positive counterparts (Figure 4), suggesting a similar or slightly higher concentration of sequences bound to the negative beads. The substantial reduction in dsDNA PCR amplification yield, coupled with the comparable band intensities in the negative beads, indicates that the negative selection likely eliminated approximately half of the sequences enriched in R0. Despite the significant decrease in yield, it is reasonable to infer that this comes with a more target-specific set of sequences.

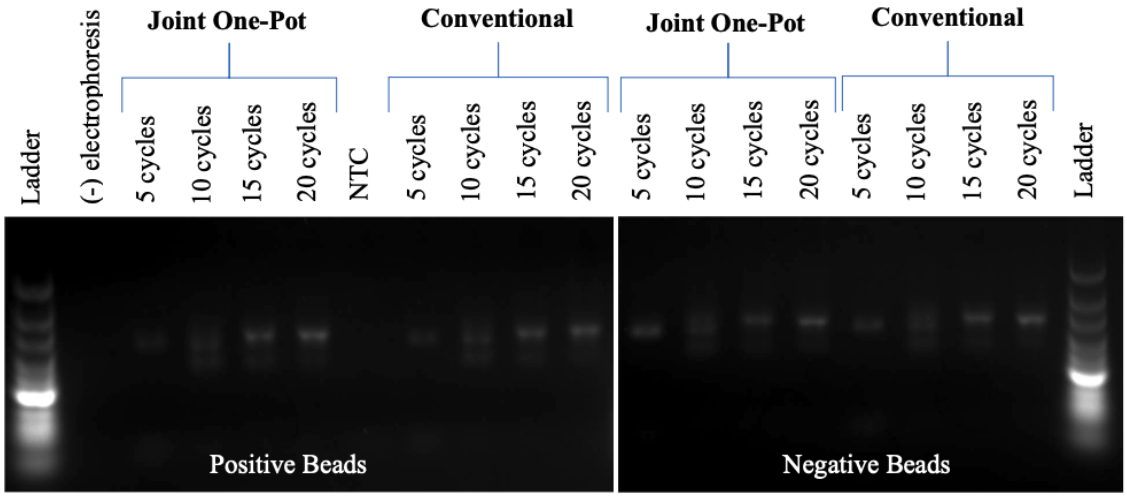


Figure 4: Agarose gel electrophoresis (3% agarose, 120V, 40min, 1X GelGreen pre-stained) of the products generated in the Pilot-PCR in R1, for both SELEX. On the left, the positive-bound sequences. On the right, the negative bound ones. Non-Template Control (NTC) and electrophoresis control (-) were performed for PCR amplification and electrophoresis, respectively.

In the subsequent rounds (R2 and R3), stringency was increased by implementing more rigorous washing steps after incubation with the positive beads. The goal was to dissociate sequences with lower affinities. Surprisingly, in R2, the highest ssDNA yield for both SELEX experiments was achieved with only 10 cycles of Pilot PCR (Figure 5, left), indicating that the library's concentration was increasing and requiring fewer PCR cycles for maximal amplification. After 5 PCR cycles, the bands were barely visible, likely due to less effective DNA staining in that particular gel. Regarding the study of negative beads in R2, the band intensities after 10 PCR cycles were slightly lower compared to those of the positive beads, and the appearance of longer byproducts was delayed until 20 cycles (Figure 5, right). This observation suggests that the ratio of nonspecific sequences was decreasing while the target-specific sequences were increasing.

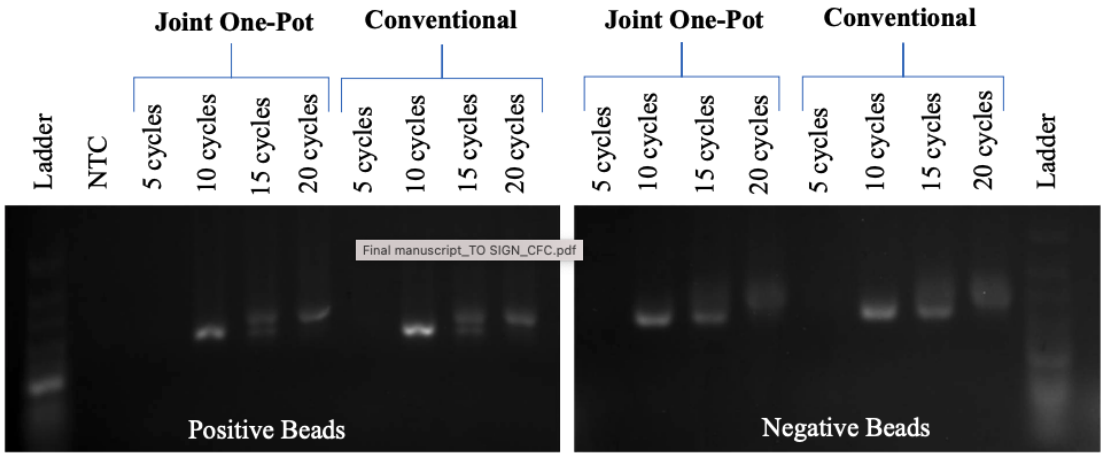


Figure 5: Agarose gel electrophoresis (3% agarose, 120V, 40min, 1X GelGreen pre-stained) of the products generated in the Pilot-PCR in round 2 (R2), for both SELEX. On the left, the positive-bound sequences. On the right, the negative bound ones. Non-Template Control (NTC) and electrophoresis control (-) were performed for PCR amplification and electrophoresis, respectively.

R2 and R3 were completed using the products from 10 and 15 cycles of PCR amplification, respectively. As expected, the transition to R3 necessitated 15 PCR cycles due to a significantly harsher washing procedure.

In R4, counter-selection was implemented in the conventional SELEX as the proportion of nonspecific sequences decreased. In the Joint One-Pot SELEX, R4 was conducted in the same manner as R3 to further enrich the library before isolating the targets individually. For the Pilot PCR of R4; 5, 10, 15, and 20 cycles were tested. Optimal dsDNA amplification was achieved after 10 cycles for both SELEX methods, whereas an increased presence of unwanted by-products was observed after 15 cycles (Figure 6, left). Additionally, a larger by-product estimated at 200 bp was found in 15 and 20 cycles' amplicons, which had not been observed in previous gels (Figure 6, red arrows). The formation of dimerized probes frequently occurs in SELEX, primarily due to the repeated amplification processes involved. dsDNA products obtained from 10 PCR cycles were used to terminate the rounds, in order to circumvent the formation of these larger byproducts.

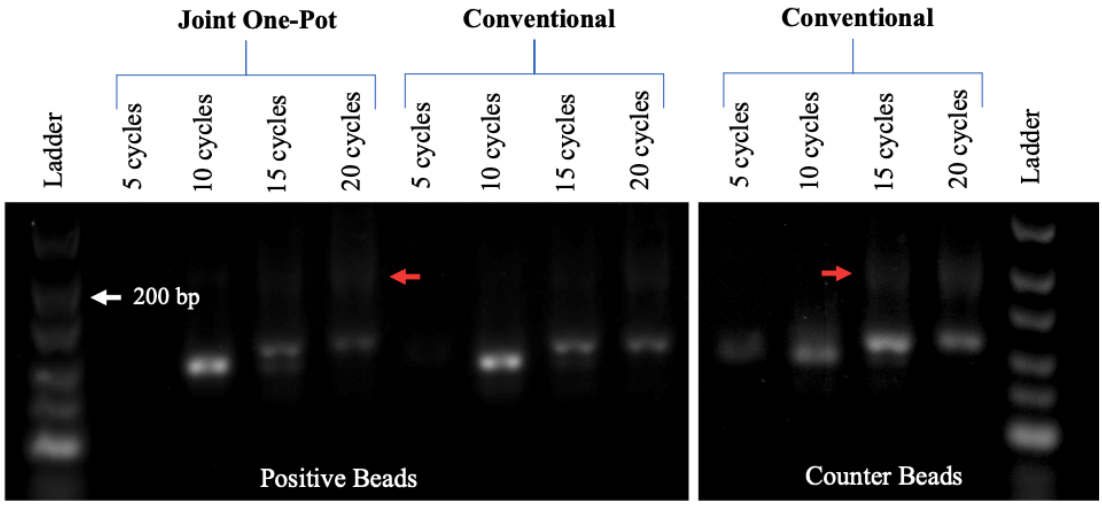


Figure 6: Agarose gel electrophoresis (3% agarose, 120V, 40min, 1X GelGreen pre-stained) of the products generated in the Pilot-PCR in R4. On the left, the positive-bound sequences for both SELEX. On the right, the counter-bound ones for the conventional SELEX. Red arrows indicate the 200 bp-estimated byproduct. Non-Template Control (NTC) and electrophoresis control (-) were performed for PCR amplification and electrophoresis, respectively.

In the analysis of the counter beads in the conventional SELEX, the pilot PCR product was detectable with as few as 5 cycles (Figure 6, right), suggesting a potentially higher concentration of nonspecific sequences bound to the counter beads, effectively discarding aptamers with affinity for both, Phe and Trp. Surprisingly, the pilot PCR of negative beads produced bands with higher intensity than the positive beads for the conventional SELEX (Figure 7, right). In contrast, for the Joint One-Pot SELEX, the negative beads exhibited similar band intensities to their positive counterparts (Figure 7, left).

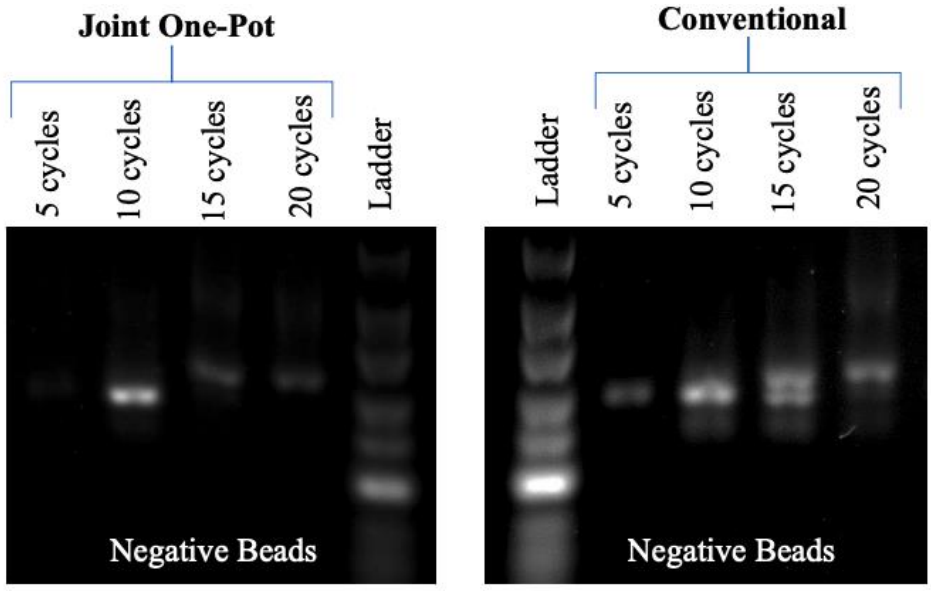


Figure 7: Agarose gel electrophoresis (3% agarose, 120V, 40min, 1X GelGreen pre-stained) of the products generated in the Pilot-PCR in R4, on the negative-bound sequences for both SELEX.

In response to a lack of reduction in non-specific sequences binding to the bead matrix, negative selections were intensified starting from round 5 (R5) by doubling the amount of beads used during incubation. In round 6 (R6), more rigorous washing of the positive beads was implemented, and subsequently the Joint One-Pot SELEX was divided into its three individual SELEX components after the negative selection of R7. The selection conditions remained consistent for Rounds 8, 9 and 10.

The results are presented in gels for each SELEX. These gels display the products from 10 PCR cycles of the Pilot PCR or each round, providing a visual overview of the progress in the final rounds. Additionally, each SELEX will be assessed in a single gel, featuring samples from rounds R5 to R10 showcasing all three types of selection (positive, negative, and counter beads). This approach helps minimize variability that may arise from comparing results across different gels.

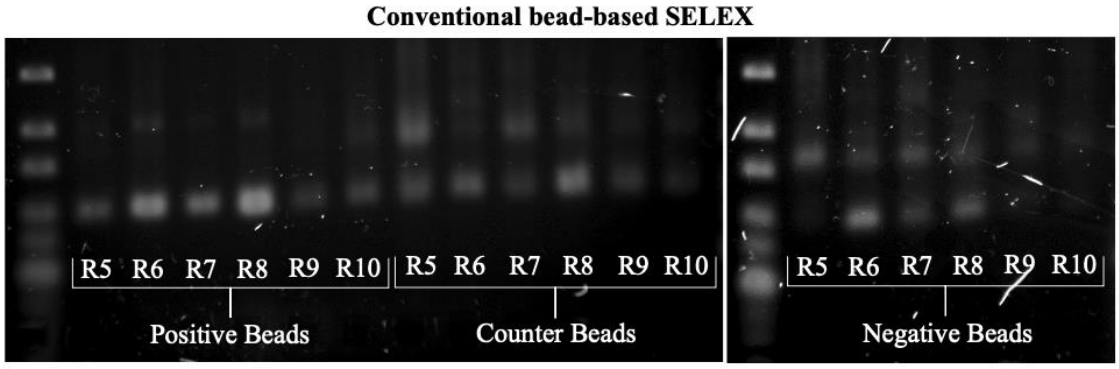


Figure 8: Agarose gel electrophoresis (3% agarose, 120V, 40min, 1X SYBRGold post-stained) of the products generated by 10 PCR cycles from rounds R5 to R10 on the Conventional SELEX.

In the conventional SELEX, the intensity of sequences bound to positive beads steadily increased from R5 to R8, before abruptly dropping in R9 and R10 (Figure 8, left). As for the sequences bound to counter beads, their intensity remained consistently low in comparison to the positive counterparts, with the exception of an unexpected high-intensity band in R8 (Figure 8). The intensity of sequences bound to negative beads decreased irregularly as the rounds progressed and nearly disappeared by R9 and R10 (Figure 8, right). Notably, the larger byproduct at approximately 170 bp was more visible on counter and negative beads, indicating effective removal of this byproduct from the positive pool through these two selections.

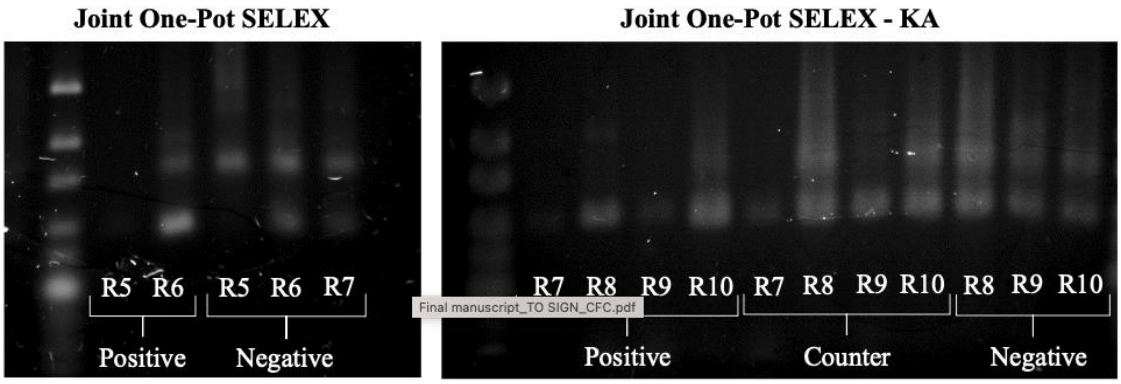


Figure 9: Agarose gel electrophoresis (3% agarose, 120V, 40min, 1X SYBRGold post-stained) of the products generated by 10 PCR cycles from rounds R5 to R10 on the Joint One-Pot SELEX. On the left, in the pre-enrichment phase (all three targets together). On the right, the Joint One-Pot once segregated, with KA as the target.

In the Joint One-Pot SELEX, there was a significant increase in the intensity of the positively-bound sequences in R6 (Figure 9, left). As a result, the SELEX was divided into three separate workflows, one for each of the targets. All three SELEX in R7 exhibited almost identical behavior to R6 considering that the pool was divided into three different pools and subjected to counter selection per separate target workflow (which decreases the intensity of the gel bands), with a strong increase in positively-bound sequences in R8 and R10, and a decrease in negatively-bound sequences from R9 and R10 (Figure 9 & 10). However, for the counter sequences, there was no visible decrease in intensity as the rounds advanced (Figures 20 and 21).

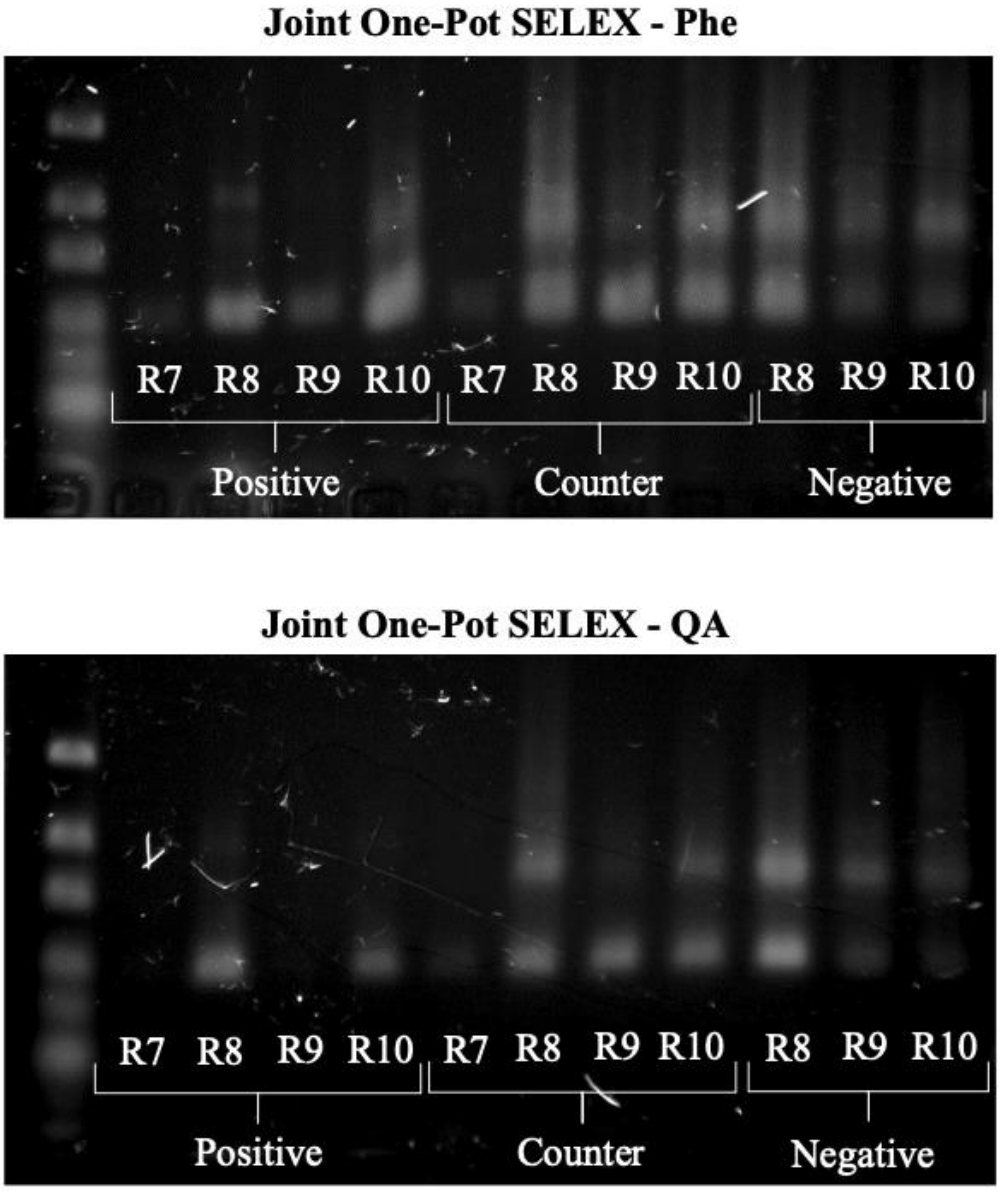


Figure 10: Agarose gel electrophoresis (3% agarose, 120V, 40min, 1X SYBRGold post- stained) of the products generated by 10 PCR cycles from rounds R7 to R10 on the Joint One-Pot for Phe target (top) and QA target (bottom).

The SELEX rounds' progress was meticulously monitored, with stringency conditions being gradually increased and customized based on the observed outcomes to effectively enrich the pools. Pilot PCR tests were conducted in all rounds to guarantee optimal amplification, prevent by-product formation, and avoid over-amplification. Additionally, DNA pools were purified, concentrated, and quantified to ensure the absence of impurities and to control the quantity and concentration of DNA entering the next round.

It has to be noted that, during the purification step of R10, samples were unfortunately lost due to human error, and therefore could not be used to continue with the SELEX process nor to be sent for NGS.

5.4.3. Enrichment monitoring

The quantification of ssDNA and the optimal number of cycles required for PCR amplification (Pilot PCR) were utilized to monitor the enrichment levels of DNA pools throughout the SELEX rounds. This monitoring process assists in determining when to conclude the rounds and submit the DNA pools for NGS, ensuring a reasonable certainty of obtaining aptamer candidates. Importantly, it should be noted that DNA quantification and the comparison of PCR cycles do not linearly increase and decrease, respectively. Changes in stringency, introduction of negative and counter steps, or the presence of byproducts, for example, can all influence DNA concentrations.

The results are summarized in Table 3 and Figure 11:

Table 3: ssDNA quantification with nanodrop spectrophotometer. Standard deviations were calculated from triplicates. Units: μM

	Conventional SELEX	**Joint One-Pot SELEX**		
	Phe	**KA**	**QA**	**Phe**
R1	0.91 ± 0.02		0.76 ± 0.03	
R2	1.06 ± 0.04		0.91 ± 0.03	
R3	1.89 ± 0.04		1.29 ± 0.10	
R4	1.00 ± 0.05		1.31 ± 0.09	
R5	0.75 ± 0.18		1.58 ± 0.08	
R6	1.51 ± 0.25		1.35 ± 0.33	
R7	0.9 ± 0.07	0.84 ± 0.05	0.81 ± 0.12	1.12 ± 0.02
R8	0.63 ± 0.10	0.84 ± 0.17	0.89 ± 0.11	0.65 ± 0.23
R9	1.67 ± 0.10	1.52 ± 0.16	1.26 ± 0.13	1.66 ± 0.15

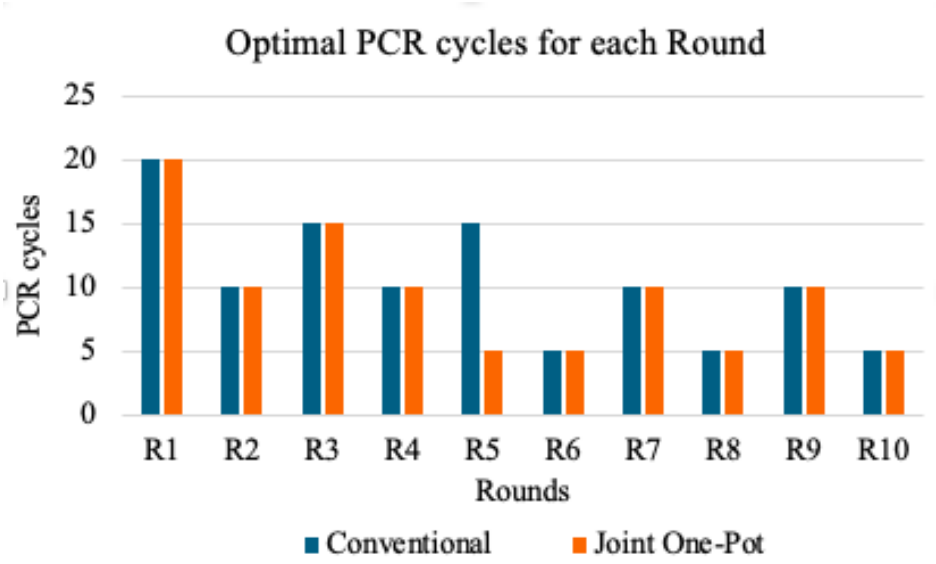


Figure 11: Optimal PCR cycles per each round, for conventional (blue) and Joint One-Pot SELEX (orange).

In the case of the conventional SELEX, despite increasing the stringency of the washing steps and performing a lower number of PCR cycles, there was a substantial increase in concentration from R1 to R3, almost reaching a 2μM concentration (Table 3). In R4, with the introduction of counter-selection, the concentration dropped due to the removal of a big portion of sequences, and it decreased further in R5 despite using a higher number of PCR cycles. This continued decrease in R5 could be attributed to the successful removal of the 200 bp by-products that had appeared in R4 and were observed in the negative and counter selection of R5 (Figure 8, R5). From R6 to R8, the higher stringency for positive selection (shorter incubation and harsher washing procedure) also resulted in low final concentrations; however, the number of PCR cycles needed had decreased to 10 or even 5. For R9, the concentration significantly increased despite only performing 5 PCR cycles.

In regard to the Joint One-Pot SELEX, the library concentration increased consistently during the pre-enrichment phase as the rounds progressed, requiring fewer PCR cycles for proper amplification. Following division of the three targets, the concentration decreased as expected, as the library from R6 was divided into three, thereby diluting it. Subsequently, the concentration increased again for all three SELEX, despite the removal of a significant portion of nonspecific sequences through counter selection, with only 5 PCR cycles performed.

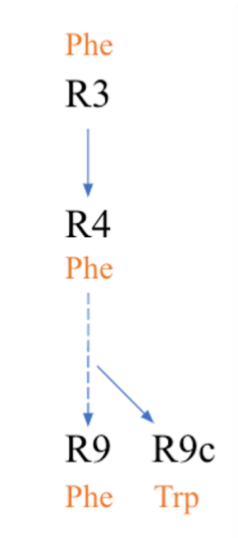
In summary, the increase in library concentration and the reduced need for PCR cycles in the amplification step across all SELEX indicates a growth of target-binding sequences. These findings, in conjunction with the decreasing ratio of negative binding sequences, suggest a tendence of enrichment of our pools towards potential aptamer sequences. As mentioned before, samples from R10 were lost during the purification process due to human error and could not be quantified nor stored. As a result of time constraints, R10 could not be repeated, and priority was given to NGS for further analysis of the progress and functionality of both SELEX processes. Ideally, with more time

and resources, and based on the observations made during the enrichment monitoring, it would have been advisable to conduct at least a couple more rounds to ensure the enrichment and overrepresentation of sequences, especially in the case of the Joint-One-Pot SELEX, which could have profited of more counter selection rounds due to the later introduction of this step.

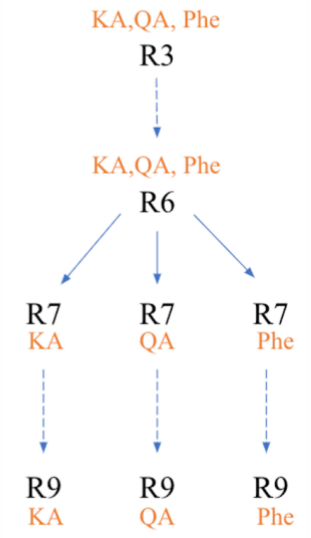
5.4.4. Next-generation sequencing

Due to the aforementioned events occurring in R10, the last round to be sent to NGS was R9 for both SELEX techniques. Due to the clear lack of definitive enrichment, more samples from previous rounds were sent to NGS in order to analyze and follow the effects of the selection process in the diversity and representation of the library. This includes rounds previous and after to counter selection introduction for both SELEX strategies investigated. Additionally, the last counter selection of the conventional SELEX was considered as well. Because the Joint One-Pot is divided into three different SELEX, samples from each of the three were sent to sequencing, as depicted in Table 4.

Table 4. Samples sent to NGS and schematic representation of the "SELEX relationship" between them.



Conventional SELEX	Joint One-Pot SELEX
R3	R3
R4 P	R6
R9 P	R7 K
R9 counter	R7 Q
	R7 P
	R9 K
	R9 Q
	R9 P



The quality of the raw data obtained was evaluated using the Galaxy FASTQC Quality Report and PEAR tools to provide comprehensive statistics. The PEAR tool was utilized to merge paired-end reads, eliminate low-quality reads, and narrow down the pool size to within +/-10 pb from the original library length of 97 nt. Subsequently, the data format of the pools was converted to FASTA and collapsed to form unique sequences. The overall statistics of the analysis carried out using the Galaxy server are presented in Tables 5a and 5b for the conventional and the Joint One-Pot SELEX, respectively.

Table 5a. General information of "Conventional" SELEX pools.

Conventional SELEX				
Round	**R3**	**R4**	**R9**	**R9-cT**
Total Sequences	735542	283675	246225	232242
Sequence length	47-151	35-151	44-151	36-151
Sequences 87-107 pb	720974	272252	235660	224274
Unique 87-107 pb sequences	629942	235248	206753	194910
%	87,37%	86,41%	87,73%	86,91%
Top 100 (count)	354	322	454	410
%	0,0491	0,1183	0,1927	0,1828
Top 10 count	43	40	64	62
%	0,0060	0,0147	0,0272	0,0276
Round Enrichment %	0,0007	0,0015	0,0034	0,0036

Table 5b. General information of Modified One-Pot SELEX pools.

Joint One-Pot SELEX								
Round	**R3**	**R6**	**R7-K**	**R7-Q**	**R7-P**	**R9-K**	**R9-Q**	**R9-P**
Total Sequences	184588	245042	270049	200748	207366	265230	226987	223106
Sequence length	55-151	46-151	45-151	36-151	44-151	36-151	46-151	44-151
Sequences 87-107 pb	179285	232281	251668	188494	200287	250506	207648	217161
Unique 87-107 pb sequences	158062	206316	219989	164652	176005	217054	181239	190795
%	88,16	88,82	87,41	87,35	87,88	86,65	87,28	87,86
Top 100 (count)	308	336	380	401	400	477	428	474
%	0,1718	0,1447	0,1510	0,2127	0,1997	0,1904	0,2061	0,2183
Top 10 count	38	49	51	52	55	71	65	85
%	0,0212	0,0211	0,0203	0,0276	0,0275	0,0283	0,0313	0,0391
Round Enrichment %	0,0022	0,0026	0,0028	0,0037	0,0035	0,0032	0,0039	0,0055

As indicated in Tables 5a and 5b, the calculated enrichment was low owing to the limited number of rounds conducted. A comprehensive bioinformatic analysis was conducted for completeness and in the hope that trends between the rounds might be observed. In all these analyses it should be remembered that there is no significant enrichment and the data should be treated with appropriate caution. Additional rounds of SELEX would be needed to accurately isolate aptamers targeting the intended molecules.

Furthermore, due to the low count of the collapsed sequences obtained, the identification and tracking of sequences during the selection process was deemed a complex task using the standard Galaxy workflow. Similarly, the minimal over-representation posed a challenge in identifying significant

sequence motifs using MEME (https://memesuite.org/meme/tools/meme). As a result of these limitations, the sequences were cross-checked and identified using MATLAB. A MATLAB code was developed to compare selected rounds, determine the similarity percentages of complete (97-nt) and trimmed (53-nt) sequences, where the primer sequences were removed, and track specific sequences across SELEX rounds.

In the Joint One-Pot SELEX experiment, three sequences were tracked from the KA and QA samples with 100% sequence similarity from R9 back to R6 (Table 6). However, the same was not achieved for Phe in either of the SELEX experiments. Due to the lack of SELEX rounds and overrepresentation, the tracked sequences were not characterized in binding assays, given that the probability that they display high sensitivity or selectivity towards their target is rather low.

Table 6. Tracking of sequences using MATLAB from the Joint One-Pot SELEX in all the pools sequenced. The first number denotes the ranking and the second one the number of copies (sequence ID), as per obtained in the collapsed files of unique sequences.

	R3	**R6**	**R7 K**	**R7 Q**	**R7 P**	**R9 K**	**R9 Q**	**R9 P**
Seq 1.	-	1-6	3-6	7-5	-	42-4	72-4	-
Seq 2.	-	244-3	5-6	-	58-4	61-4	-	-
Seq 3	-	124-3	13-5	36-4	-	1612-3	66-4	-

It needs to be noted, that about the 100 first collapsed sequences of the overrepresentation are usually analyzed for potential binders and tracking of sequences. In our SELEX processes, we encountered challenges with the Galaxy platform due to the low overrepresentation of sequences obtained, which impeded our ability to effectively analyze and compare SELEX rounds. Our computational resources were inadequate for running resource-intensive software like Aptasuite, which is tailored for comparative analysis of SELEX rounds. To address these challenges, we devised a MATLAB code that allowed us to examine parallel SELEX processes, such as the Joint-One-Pot SELEX after the ramification of targets, and to analyze rounds within the same SELEX experiment counting with 1000 instead the usual first 100 collapsed sequences to compensate the lack of overrepresentation.

This MATLAB workflow proved to be effective for our requirements and could be of significant interest for further exploration of other multiplexed SELEX processes. It has the potential to track aptamers from early rounds by enabling a more comprehensive analysis in cases where sufficient enrichment levels are attained, while requiring less computational power than other tools. However, this should be further confirmed through testing with validated data. Furthermore, this MATLAB code can be expanded to analyze complete sequenced pools (comprising millions of sequences) if

greater computational resources are available, thereby offering a versatile tool for future SELEX studies.

5.5. Conclusions and Future Perspectives

SELEX is a very complex procedure that counts with diverse methodologies that influence the overall outcome of the selection process. A combination of materials, procedures and protocols were carefully chosen and designed for the purposes of this project. An overview of the effectiveness of the chosen methodologies is provided.

Maleimide magnetic bead conjugation with the four presented small molecules through click chemistry has been proven to be a convenient partition strategy, and although it implies the coverage of an epitope of the molecule, it allowed accessibility of antibodies, as confirmed during bead-based ELISA, and the DNA sequences of the library. Besides, it allowed a good assessment of the stringency by controlling the mount of negative, counter and positive beads, and by allowing the modification of the strength and length of the partitioning event.

The combination of techniques chosen for DNA amplification and library conditioning, which included Pilot PCR, A-PCR, λ Exonuclease digestion, spin column purification and quantification, proved to be an effective option that also allows the study of the enrichment levels without the requirement of additional expensive equipment or lengthy protocols. Indeed, thanks to this combination with gel visualization, we were able to tailor the stringency of the SELEX processes in response to the events happening during each round.

In the context of individual SELEX processes, conventional SELEX demonstrated a logical response to all events occurring during the selection rounds, including the incorporation of negative and counter selection steps, as well as adjustments in stringency. Quantification of ssDNA indicated that conventional SELEX had achieved a significant enrichment level by round 9 (R9). Furthermore, by rounds 9 and 10, the occurrence of negative selection was minimal, and there was a decreasing trend in counter selection as well. While it would have been ideal to submit R10 for NGS, this was not feasible, and R9 had to be submitted instead. Moreover, carrying out an additional couple of rounds would not have been detrimental in achieving a higher level of enrichment, or even reaching saturation. However, the number of rounds completed, along with the addition of a couple of theoretical extra rounds, would still align with the typical results reported in the literature, where SELEX techniques utilizing Magnetic beads for target immobilization generally require 8 to 12 rounds before determining the cessation of rounds. Rounds R3, R4, and R9 were submitted to NGS to assess the enrichment and the impact of counter selection. Unfortunately, nine rounds of selection proved insufficient for the determination of Phe aptamer candidates, using both Galaxy and MATLAB resources.

The Joint One-Pot SELEX process implemented a similar strategy for increasing stringency, but with the distinction of including a longer pre-enrichment phase before dividing the three targets. This was done to ensure the isolation and amplification of different populations or families of sequences for

each of the three targets equally. From Rounds 1 to 6, the quantification of ssDNA steadily increased while the required PCR cycles decreased, despite the more stringent conditions, confirming some level of enrichment. The introduction of counter-selection resulted in a noticeable dilution of the pool, as observed in the gel visualization, the number of required PCR cycles, and the ssDNA quantification. Rounds 7-9 further enriched the three segregated SELEX with their respective counter selection, confirming that the pre-enrichment process successfully isolated and amplified DNA pools for the three targets. Additionally, the ssDNA quantification showed that the concentrations of the three targets were similar to that of the Phe target from the conventional SELEX, suggesting that the Joint One-Pot option could be a viable option for the isolation of aptamers against more targets in the same amount of time and rounds than a conventional SELEX requires to isolate aptamers for one single target. Given the delayed introduction of counter-selection or division of the positive selection, the Joint One-Pot SELEX would also have benefited from a few more rounds to further enrich the positive selection and isolate specific aptamer candidates.

To closely monitor the enrichment and the impact of the division of the DNA pools, samples from Rounds 3, 6, 7, and 9 were subjected to NGS. From the NGS analysis using both Galaxy and MATLAB, it was possible to do tracking of three sequences that were enriched and conserved since R6 and were later found in different pools of the SELEX ramification, confirming the selective isolation of sequences parallelly. Despite the low overrepresentation of sequences obtained due to the insufficient number of rounds, the implementation of MATLAB coding allowed a deeper analysis of the evolution of the selection process. Therefore, MATLAB coding has proven to be a very useful alternative in cases where computational power is limited and specific SELEX softwares are therefore out of reach, or when low overrepresentation of the pools limits the practicality of softwares like Galaxy. Future works would be focused on the validation of the developed analysis protocol in other SELEX processes, utilizing the raw data from successive rounds of selection, and attempt early tracking of sequences along the process.

In this project, our goal was to compare a Conventional SELEX protocol with a novel Joint One-Pot SELEX workflow for enriching and isolating aptamers for small molecules related to ACLF. However, due to time constraints, we were unable to complete enough SELEX rounds to adequately compare the two procedures.

Nevertheless, had counted with more time and resources, both SELEX processes would have been ceased at least two rounds later, carefully monitoring the enrichment of the different pools, to ensure a more manageable amount of overrepresentation of sequences. Had a number of aptamers candidates been identified, family and motif search and study would have been performed, to deeper understand the secondary structures and interactions involved in the recognition of this particular set of small molecules. Family and motif analysis could have been complemented with the data obtained from the binding assays study, which would have been necessary to confirm the correct isolation of

sensitive and selective aptamers against their corresponding target. Besides, specific binding assays can be tailored to determine whether if the isolated aptamers can be effectively used in a particular PoC nanobiosensing platform for ACLF monitoring, for example Lateral Flow assays, by testing the efficacy of the different aptamers while immobilized on different surfaces (nanoparticles, nitrocellulose, gold surface, etc.).

5.6. References

1. Microb-Predict - MICROB-PREDICT.
2. Clària J, Moreau R, Fenaille F, Amorós A, Junot C, Gronbaek H, *et al.* Orchestration of Tryptophan-Kynurenine Pathway, Acute Decompensation, and Acute-on-Chronic Liver Failure in Cirrhosis. *Hepatology*. 2019;69(4):1686–701.
3. Liu G, Wang X, Fan X, Luo X. Metabolomics profiles in acute-on-chronic liver failure: Unveiling pathogenesis and predicting progression. *Front Pharmacol*. 2022;13:1–10.
4. Xiong QF, Xiong T, Huang P, Zhong YD, Wang HL, Yang YF. Early predictors of acute hepatitis B progression to liver failure. *PLoS One*. 2018;13(7).
5. Arroyo V. Acute-on-Chronic Liver Failure: Definition, Diagnosis , and Clinical Characteristics. 2016;7;456-467.
6. Tessari P, Vettore M, Millioni R, Puricelli L, Orlando R. Effect of liver cirrhosis on phenylalanine and tyrosine metabolism. Vol. 13, Current Opinion in Clinical Nutrition and Metabolic Care. Curr Opin Clin Nutr Metab Care; 2010. p. 81–6.
7. Oh TG, Kim SM, Caussy C, Fu T, Guo J, Bassirian S, *et al.* A Universal Gut-Microbiome-Derived Signature Predicts Cirrhosis. *Cell Metab*. 2020;32(5):878-888.e6.
8. Hernaez R, Solà E, Moreau R, Ginès P. Acute-on-chronic liver failure: An update. *Gut*. 2017;66(3):541–53.
9. Akram M, Daniyal M, Ali A, Zainab R, Muhammad Ali Shah S, Munir N, *et al.* Role of Phenylalanine and Its Metabolites in Health and Neurological Disorders. In: Synucleins - Biochemistry and Role in Diseases. IntechOpen; 2020.
10. Bauer M, Strom M, Hammond DS, Shigdar S. Anything you can do, i can do better: Can aptamers replace antibodies in clinical diagnostic applications? *Molecules*. 2019;24(23):1–13.
11. Boussebayle A, Groher F, Suess B. RNA-based Capture-SELEX for the selection of small molecule-binding aptamers. *Methods*. 2019;161:10–5.
12. Ruscito A, DeRosa MC. Small-Molecule Binding Aptamers: Selection Strategies, Characterization, and Applications. *Front Chem*. 2016;4:14.
13. McKeague M, Derosa MC. Challenges and opportunities for small molecule aptamer development. *J Nucleic Acids*. 2012;2012.
14. Nguyen VT, Kwon YS, Kim JH, Gu MB. Multiple GO-SELEX for efficient screening of flexible aptamers. *Chemical Communications*. 2014;50(72):10513–6.
15. Guan J, He K, Gunasekaran S. Selection of ssDNA aptamer using GO-SELEX and development of DNA nanostructure-based electrochemical aptasensor for penicillin. *Biosens Bioelectron X*. 2022;12:100220.

16. Yang J, Lu X, Chen M, Tang C, Wei Z, Liu Y, *et al.* Non-immobilized GO-SELEX screening of aptamers against cyclosporine A and its application in a AuNPs colorimetric aptasensor. *Analytical Methods*. 2024;16(2):227–36.
17. Kohlberger M, Gadermaier G. SELEX: Critical factors and optimization strategies for successful aptamer selection. *Biotechnol Appl Biochem*. 2022;69(5):1771.
18. Stoltenburg R, Nikolaus N, Strehlitz B. Capture-SELEX: Selection of DNA aptamers for aminoglycoside antibiotics. *J Anal Methods Chem*. 2012;1(1).
19. Stoltenburg R, Nikolaus N, Strehlitz B. Capture-SELEX: Selection of DNA aptamers for aminoglycoside antibiotics. *J Anal Methods Chem*. 2012;1(1).
20. Zhao Y, Li AZ, Liu J. Capture-SELEX for Chloramphenicol Binding Aptamers for Labeled and Label-Free Fluorescence Sensing. *Environment & Health*. 2023;1(2):102–9.
21. Lauridsen LH, Doessing HB, Long KS, Nielsen AT. A Capture-SELEX Strategy for Multiplexed Selection of RNA Aptamers Against Small Molecules. *Methods Mol Biol*. 2018;1671:291–306.
22. Boussebayle A, Groher F, Suess B. RNA-based Capture-SELEX for the selection of small molecule-binding aptamers. *Methods*. 2019;161:10–5.
23. Boussebayle A, Torka D, Ollivaud S, Braun J, Bofill-Bosch C, Dombrowski M, *et al.* Next-level riboswitch development-implementation of Capture-SELEX facilitates identification of a new synthetic riboswitch. *Nucleic Acids Res*. 2019;47(9):4883–95.
24. Vorobyeva MA, Davydova AS, Vorobjev PE, Pyshnyi D V., Venyaminova AG. Key aspects of nucleic acid library design for *in vitro* selection. *Int J Mol Sci*. 2018;19(2).
25. Hamula CLA, Peng H, Wang Z, Newbigging AM, Tyrrell GJ, Li XF, *et al.* The Effects of SELEX Conditions on the Resultant Aptamer Pools in the Selection of Aptamers Binding to Bacterial Cells. *J Mol Evol*. 2015;81(5–6):194–209.
26. Yang KA, Barbu M, Halim M, Pallavi P, Kim B, Kolpashchikov DM, *et al.* Recognition and sensing of low-epitope targets via ternary complexes with oligonucleotides and synthetic receptors. *Nat Chem*. 2014;6(11):1003–8.
27. Conjugated magnetic beads applications | Cytiva.
28. Stoltenburg R, Reinemann C, Strehlitz B. FluMag-SELEX as an advantageous method for DNA aptamer selection. *Anal Bioanal Chem*. 2005;383(1):83–91.
29. Marcelo GA, Lodeiro C, Capelo JL, Lorenzo J, Oliveira E. Magnetic, fluorescent and hybrid nanoparticles: From synthesis to application in biosystems. *Materials Science and Engineering: C*. 2020;106:110104.
30. Manea I, Casian M, Hosu-Stancioiu O, de-los-Santos-Álvarez N, Lobo-Castañón MJ, Cristea C. A review on magnetic beads-based SELEX technologies: Applications from small to large target molecules. *Anal Chim Acta*. 2024;1297:342325.

31. Bruno JG. *In Vitro*Selection of DNA to Chloroaromatics Using Magnetic Microbead-Based Affinity Separation and Fluorescence Detection. *Biochem Biophys Res Commun*. 1997;234(1):117–20.
32. Düzel A, Bora B, Özgen GÖ, Evran S. Selection of DNA aptamers for the aptamer-assisted magnetic capture of the purified xylanase from Aspergillus niger. *Int J Biol Macromol*. 2024;257:128540.
33. Jauset-Rubio M, Botero ML, Skouridou V, Aktas GB, Svobodova M, Bashammakh AS, *et al.* One-Pot SELEX: Identification of Specific Aptamers against Diverse Steroid Targets in One Selection. *ACS Omega*. 2019;4(23):20188–96.
34. Scoville DJ, Uhm TKB, Shallcross JA, Whelan RJ. Selection of DNA Aptamers for Ovarian Cancer Biomarker CA125 Using One-Pot SELEX and High-Throughput Sequencing. *J Nucleic Acids*. 2017;2017.
35. Tolle F, Mayer G. Preparation of SELEX samples for next-generation sequencing. *Methods in Molecular Biology*. 2016;1380:77–84.
36. Cole KH, Lupták A. High-throughput methods in aptamer discovery and analysis. *Methods Enzymol*. 2019;621:329–46.
37. Lee SW, Kang J, Ren S, Laurell T, Kim S, Jeong OC. A cross-contamination-free SELEX platform for a multi-target selection strategy. *Biochip J*. 2013;7(1):38–45.
38. Abdelsayed MM, Ho BT, Vu MMK, Polanco J, Spitale RC, Lupták A. Multiplex Aptamer Discovery through Apta-Seq and Its Application to ATP Aptamers Derived from Human-Genomic SELEX. *ACS Chem Biol*. 2017;12(8):2149–56.
39. Sharma TK, Bruno JG, Dhiman A. ABCs of DNA aptamer and related assay development. *Biotechnol Adv*. 2017;35(2):275–301.
40. Cube Biotech. (n.d.). PureCube Maleimide Activated MagBeads.
41. Marimuthu C, Tang TH, Tominaga J, Tan SC, Gopinath SCB. Single-stranded DNA (ssDNA) production in DNA aptamer generation. *Analyst*. 2012;137(6):1307–15.
42. Gowland R, Gowers DM. A Lambda-Exonuclease SELEX Method for Generating Aptamers to Bacterial Targets. *Methods Mol Biol*. 2023;2633:145–61.
43. Yeoh TS, Anna A, Tang TH, Citartan M. Development of an optimization pipeline of asymmetric PCR towards the generation of DNA aptamers: a guide for beginners. *World J Microbiol Biotechnol*. 2022;38(2).
44. Liu Q, Zhang W, Chen S, Zhuang Z, Zhang Y, Jiang L, *et al.* SELEX tool: A novel and convenient gel-based diffusion method for monitoring of aptamer-target binding. *J Biol Eng*. 2020;14(1):1–13.

CHAPTER 6. GENERAL CONCLUSIONS

Considering the exposed objectives in Chapter 2 and the obtained results in Chapters 3, 4 and 5, the following conclusion remarks are given:

- The feasibility and efficacy of utilizing aptamer-based LFA for the detection of Phe, an essential marker for monitoring PKU and ACLF patients, was evaluated.
    - The binding affinity, specificity, and sensitivity of Phe aptamers in solution was investigated, and it was found that the aptamer was highly dependent on the binding buffer for effective performance in solution.
    - The aptamers had limited tolerance to the LFA platform, highlighting the need for further research to enhance reproducibility, specificity, and sensitivity.
    - Displacement and competitive assay formats, as well as the diverse range of conformations examined in this study had the potential to address these challenges, but the aptamer's limited tolerance for the LFA platform did not allow the determination of an optimal design for Phe detection.
    - Despite optimization efforts, the performance and sensitivity of the aptamer could not be improved.

- The stability, functionality, and performance of DNA-AuNP conjugates across various conjugation methods and storage conditions, specifically focusing on their application in LFAs was evaluated.
    - Different conjugation methods, such as SA and SA-pH protocols, were found to significantly impact the nucleic acid density and functionality on the AuNP surface, which in turn affected the conjugates' protection against aggregation and overall stability.
    - Conjugates stored in Mg^{2+}-free, low-ionic strength buffers, like deionized water and PBS, showed enhanced stability and reduced aggregation. Conversely, Mg^{2+} and phosphate ions in storage buffers negatively impacted the conjugates, leading to aggregation and reduced functionality over time.
    - The study provided practical recommendations for the use of specific conjugation methods and storage buffers to maintain the stability and functionality of DNA-AuNP conjugates in LFAs.

- Two SELEX processes, including a novel multiplexed approach for the simultaneous isolation of aptamers were designed and evaluated.
    - Both, conventional and Joint One-Pot SELEX processes demonstrated logical responses to selection events and achieved an enrichment tendency by Round 9.

However, despite the incorporation of negative and counter-selection steps, the number of rounds completed was insufficient to achieve sufficient enrichment and identify aptamer candidates.

- MATLAB coding has proven to be a useful alternative in cases where computational power is limited and specific SELEX softwares are therefore out of reach, or when low overrepresentation of the pools limits the practicality of softwares like Galaxy.
- Future work should validate the developed SELEX protocols and MATLAB code to isolate aptamers against ACLF small molecule biomarkers, and explore the efficacy of the isolated aptamer candidates in PoC nanobiosensing platforms for ACLF monitoring.